University of Alberta

The Impact of Multiphase Behaviour on Coke Deposition in Heavy Oil
Hydroprocessing Catalysts

by

Xiaohui Zhang　　©

A thesis submitted to the Faculty of Graduate Studies and Research
in partial fulfillment of the requirements for the degree of

Doctor of Philosophy

in

Chemical Engineering

The Department of Chemical and Materials Engineering

Edmonton, Alberta

Fall 2006

Canada

Abstract

Coke deposition in heavy oil catalytic hydroprocessing remains a serious problem. The influence of multiphase behaviour on coke deposition is an important but unresolved question. A model heavy oil system (Athabasca vacuum bottoms (ABVB) + decane) and a commercial heavy oil hydrotreating catalyst (NiMo/γ-Al$_2$O$_3$) were employed to study the impact of multiphase behaviour on coke deposition.

The model heavy oil mixture exhibits low-density liquid + vapour (L1V), high-density liquid + vapour (L2V), as well as low-density liquid + high-density liquid + vapour (L1L2V) phase behaviour at a typical hydroprocessing temperature (380°C). The L2 phase only arises for the ABVB composition range from 10 to 50 wt %. The phase behaviour undergoes transitions from V to L2V, to L1L2V, to L1V with increasing ABVB compositions at the pressure examined. The addition of hydrogen into the model heavy oil mixtures at a fixed mass ratio (0.0057:1) does not change the phase behaviour significantly, but shifts the phase regions and boundaries vertically from low pressure to high pressure.

In the absence of hydrogen, the carbon content, surface area and pore volume losses for catalyst exposed to the L1 phase are greater than for the corresponding L2 phase despite a higher coke precursor concentration in L2 than in L1. By contrast, in the presence of hydrogen, the carbon content, surface area and pore volume losses for the catalyst exposed to the L2 phase are greater than for the corresponding L1 phase. The higher hydrogen concentration in L1 appears to reverse the observed results. In the presence of hydrogen, L2 was most closely associated with coke deposition, L1 less associated with

coke deposition, and V least associated with coke deposition. Coke deposition is maximized in the phase regions where the L2 phase arises. This key result is inconsistent with expectation and coke deposition models where the extent of coke deposition, at otherwise fixed reaction conditions, is asserted to be proportional to the nominal concentration of coke precursor present in the feed.

These new findings are very significant both with respect to providing guidance concerning possible operation improvement for existing processes and for the development of new upgrading processes.

Acknowledgements

This project would not have been a success without the unselfish contribution and help of many people. Professor John M. Shaw gave me insightful supervision and endless encouragement and support throughout the entire project. Not only is he a fantastic supervisor, but also a good friend in my whole life. Professors Murray R. Gray and Alan E. Nelson gave me most constructive criticism and valuable suggestions, which made this project successful and shining. "Thank you" is far from what I want to say to them.

I would like to thank Drs. Yadollah Maham and Richard McFarlane for their willingness to spend time on polishing and revising my presentations and thesis. Thanks also go to Bei Zhao, Jessie Smith, Martin Chodakowski and Xiangyang Zou for their contribution to this project.

I would like to thank all colleagues in the Petroleum Thermodynamics and Bitumen Upgrading group and all support staff in the Department of Chemical and Materials Engineering. Without your help and cooperation, this undertaking would not have been possible.

I gratefully acknowledge the Scholarship programs at the University of Alberta and research funds from the sponsors of the NSERC Industrial Research Chair in Petroleum Thermodynamics (Alberta Energy Research Institute, Albian Sands Energy Inc., Computer Modelling Group Ltd., ConocoPhillips Inc., Imperial Oil Resources, NEXEN Inc., Natural Resources Canada, Petroleum Society of the CIMM, Oilphase-DBR, Oilphase – a Schlumberger Company, Schlumberger, Syncrude Canada Ltd., NSERC).

No words could describe my debt to my parents and my siblings for their sacrifices and for giving me the opportunity to pursue higher education. My success is attributed to their incessant encouragement and support.

Special thanks to my life's partner, Chongguo, for her love, her sacrifice, her encouragement, ..., to make one of the most important steps in my life successful.

Table of Contents

List of Tables

List of Figures

List of Symbols

A	The light component in a binary mixture
ABVB	Athabasca Bitumen Vacuum Bottoms
AR	Atmospheric residue
A_s	Surface area
A^+	Reactant asphaltenes
A^*	Asphaltene cores
A^*_{max}	Maximum asphaltene cores that can be held in solution
A^*_{ex}	Excess asphaltene cores beyond what can be held in solution
B	The heavy component in a binary mixture
C	Concentration of coke precursor
CCR	Conradson carbon reduction
C_F	Concentration of feed
C_I	Concentration of intermediate
C_{RS}	Surface reactant concentration
CSTR	Continuous-stirred tank reactor
E	Energy of X-ray photons, keV
F	Feed
HDM	Hydrodemetallization
HDN	Hydrodenitrogenation
HDS	Hydrodesulfurization
H^+	Non-volatile heptane soluble reactant

H^*	Non-volatile heptane soluble product
I	Intermediate
I	Intensity of transmitted beam
I_0	Intensity of the incidental beam
k	Constant for mass adsorption coefficient
K point	Point where L_1 and V become critical in the presence of L_2
k_F	Rate constant for parallel fouling
k_I	Rate constant for series fouling
k_a	Adsorption rate constant
K_a	Equilibrium adsorption constant
k_c	Rate constant for catalytic coking
k_t	Rate constant for thermal coking
L point	Point where L_1 and L_2 become critical in the presence of V
L	Liquid phase
L_1	Low-density liquid phase
L_2	High-density liquid phase
LCEP	Lower critical end point
P	Pressure
P_{H2}	Hydrogen partial pressure
q	Coke amount
q_0	Coke amount corresponding to complete fouling
q_c	Carbon amount
$q_{c,max}$	Maximum carbon amount

q_{max}	Maximum estimated coke amount
R	Total rate of coking
R_c	Rate of catalytic coking
R_t	Rate of thermal coking
SARA	Saturates – Aromatics – Resins – Asphaltenes
SAXS	Small Angle X-rays Scattering
T	Temperature
TI	Toluene-insoluble coke
UCEP	Upper critical end point
V	Vapour phase
V	Volatiles
V_p	Pore volume
VR	Vacuum residue
w	Cumulative feed to catalyst ratio, a pseudo time coordinate
w_i	Mass fraction of component i
x	Composition
x	Thickness

Greek Letters

ε_y	Particle porosity
η	Effectiveness factor
λ	Wavelength of X-ray beam

λ_e Effective wavelength of polychromatic X-ray beam

μ Mass absorption coefficient

μ_i Mass absorption coefficient of component i for a monochromatic x-ray beam at wavelength λ.

μ_{ij} Mass absorption coefficient of component i for a polychromatic x-ray beam at a wavelength of λ_j.

ρ Density

ρ_x Microparticle density

1. Introduction

1.1 Background

As the world's supply of conventional light sweet crude oils becomes depleted, the petroleum industry is forced to refine heavy crude oils to supply the increasing demand for transport fuels. These heavy crudes often contain significant amounts of asphaltenes, sulfur, nitrogen and metal-containing organic compounds that foul catalysts used in conventional catalytic cracking and hydrocracking operations. As a consequence, an upgrading process is required to remove most of the sulphur, nitrogen, and metals and to convert part of the heavy ends to lighter distillates before these heavy crudes can be used as feedstocks for existing conventional refinery processes. A number of such upgrading processes have been developed and can be roughly classified into three types: (1) carbon rejection, (2) hydrogen addition and (3) heteroatom removal, with or without catalysts.

Hydropocessing is one of the primary upgrading processes, which is characterized by hydrogen addition, heteroatom removal, minimal carbon rejection, using catalysts. It is widely used as a primary upgrading process in the petroleum industry because this process can obtain a much higher yield and quality of liquid products compared to carbon rejection processes. This feature may make this process more profitable especially in the situation of continuously increasing crude and transport fuel prices and stringent environmental requirements. But there exists a rapid loss of catalyst activity in hydroprocessing of heavy oils due to the significant amounts of asphaltenes, sulphur, nitrogen and metal-containing organic compounds, hence increasing production cost. Therefore, hydroprocessing must achieve a compromise between high yields of light hydrocarbon liquids and catalyst cost and longevity.

The fouling of catalysts still remains a major problem even though extensive studies have been carried out to minimize coking over catalyst, including: catalyst preparation, reactor design, operating condition optimization, processes development. Many methods have been adopted, singly or in combination to deal with the processing problems associated with heavy oils. All of these approaches represent compromises between product yield, quality and catalyst cost, catalyst lifetime, and process equipment cost. And there is room

1

for considerable improvement in the technology for upgrading heavy oils and refinery residues.

Coke formation mechanisms are a key theoretical base for guidance with respect to minimizing coke formation and optimizing hydroprocessing. Although coke formation mechanisms have been investigated intensively, there appear to be inconsistencies between coking kinetics models and observed coke deposition phenomena. In addition, some observed phenomena related to coke deposition occurring in hydroprocessing cannot be explained satisfactorily, while others can be interpreted from several perspectives.

1.2 Coke Deposition Phenomena

1.2.1 Coke Deposition Models on Catalyst

All coke deposition mechanisms on catalyst are classified into three simplified models: uniform surface deposition (Richardson et al. 1996), pore-mouth plugging (Muegge and Massoth, 1991), and bulk phase coke deposition (Richardson et al. 1996). The schematic representation of coke deposition models is shown in Figure 1.1. The Uniform deposition model assumes that coke deposits uniformly on catalyst inner surfaces. The pore-mouth plugging model includes uniform coke deposition on inner surfaces of catalysts but also allows for coke deposition at the small pore mouths within catalysts, leading to local pore blockages. The bulk phase coke deposition model shows that coke will form in the liquid phase and deposit on all surfaces within the reactors and includes both the uniform coke deposition and pore mouth plugging. Detailed descriptions of these three coke deposition models are presented in the literature review.

Uniform surface deposition and pore mouth plugging models are two hotly-debated models because conflicting results were reported on the probable location of coke deposits on hydroprocessing catalyst. Observation of bulk phase coke deposition makes the understanding of coke deposition mechanisms more complex. All models are supported by experimental findings; however, there are no satisfactory theories explaining why coke deposits in three different modes. Since none of the conflicting

2

models has been substantially explained, it is clear that more study is required to shed light on the mechanisms of coke deposition on hydrogenation catalysts.

1. Uniform deposition   2. Pore-mouth plugging   3. Bulk phase coke deposition
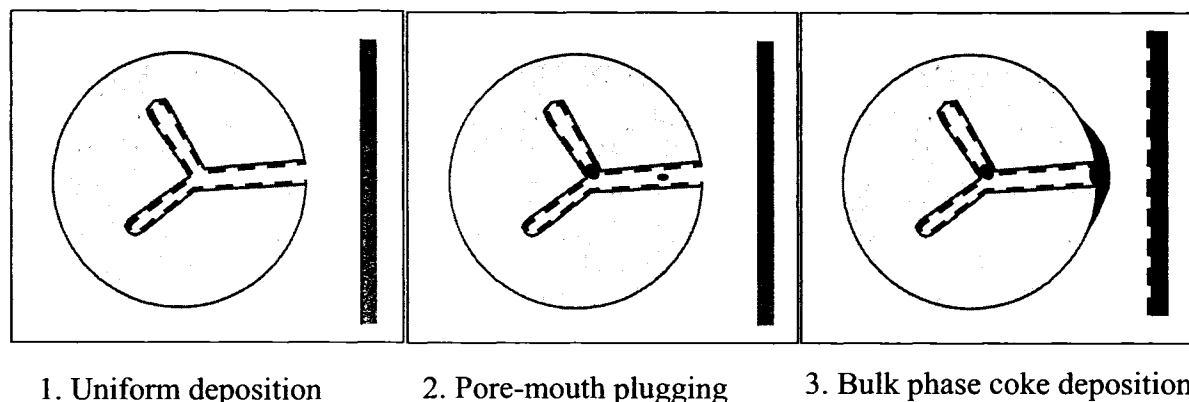
Figure 1.1   Schematic representation of coke deposition models

1.2.2 Coke Deposition along Catalyst Beds in Trickle-Bed Reactors

In order to describe coke formation quantitatively modeling the coke formation process is essential. From the reaction routes perspectives, coke formation models can be classified into three categories: parallel coke formation, series coke formation, and independent coke formation.

In fixed-bed catalytic hydrogenation processes, both parallel coke formation and series coke formation are generally applied. In the parallel model, coke is formed from the feed oil in parallel with light products formation. According to this model, the amount of coke on the catalyst decreases with distance from the reactor inlet (Chang et al., 1982). According to the series model, coke is formed from intermediates and/or products that result in an increase in coking along bed depth (Thakur and Thomas, 1985, Koyama e al. 1996). In some cases, the coke profiles are more complex than that these simple models suggest. For example, Amemiya et al. (2000) and Niu (2001) observed "S" shape coke profiles in terms of catalyst bed depth (Figure 1.2). Neither the parallel, nor the series kinetics model can interpret the "S" shaped curves by themselves. The "S" shaped coke profiles imply that something in addition to the reaction route takes effect in the process, which is not recognized up to now.

3
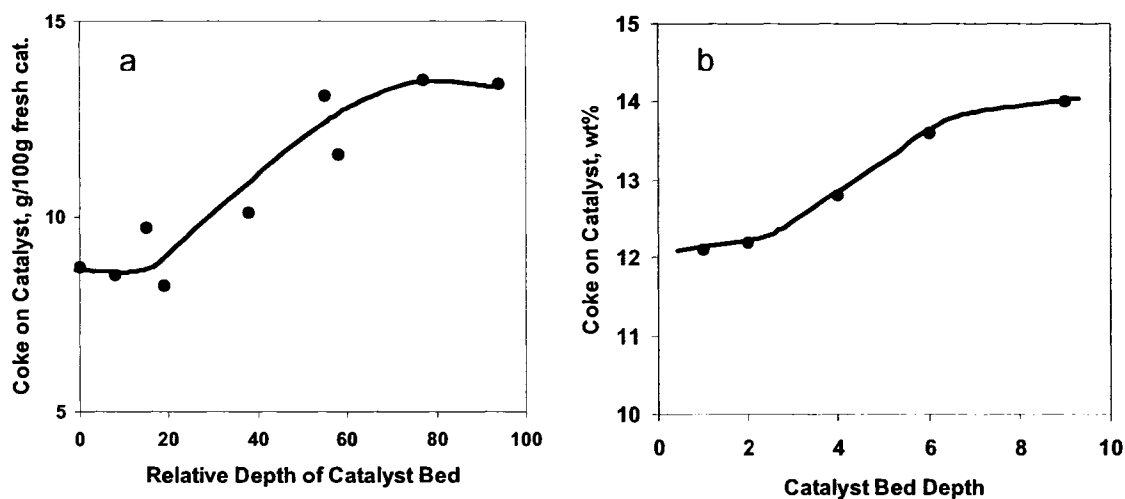
Figure 1.2   Coke profiles along catalyst bed depth. a) Amemiya et al., 2000; b) Niu, 2001

1.2.3 Coke Suppression by Addition of Solvents

Coke deposition during the hydroprocessing of heavy oils over catalysts may be minimized by many methods, one of which is suppressing coke deposition by addition of solvent. One explanation for coke suppression by addition of solvent is the impact of additives on hydrogen transfer from the vapour phase to the oil phase and the high radical scavenging ability of additives (Kubo et al., 1994). Another explanation for coke reduction by adding solvent to the feed is due to the increased dissolution of reaction products (Gray, 1994). Furthermore, supercritical properties caused by adding a solvent to the feed also reduce coke deposition in upgrading of heavy oil (Scotta et al., 2001). For example, diffusion rates of supercritical fluids into catalyst pores are much higher than those for subcritical fluids (Lee, et al. 1991a, 1991b). The reasons for the suppression of coke deposition by addition of solvent are still debated.

1.3 What Can Be Learned from Carbon Rejection Processes?

Coke formation in thermal upgrading with carbon rejection is a complex process involving both chemical reactions and thermodynamic behaviors. For this case, it is widely accepted that coke formation is triggered by liquid-liquid phase separation of the

4

reactant mixture. A kinetic model involving liquid-liquid phase separation developed by Wiehe (Wiehe, 1993) has been successfully applied to explain some phenomena occurring in the coking of heavy oil, such as the existence of an induction period. For delayed coking, the impact of the phase behaviour on the amount of coke produced has been investigated and a relationship between coke yield and phase behaviour was established (Ali, 2002). Under coking conditions, phase behaviour has a dramatic effect on coke yield. With small changes in composition at fixed temperature and pressure, coke yields can be halved or doubled. The dramatic coke yield change is caused by phase behaviour transition from one phase behaviour to another. Low coke yields are expected to be produced in L_1, L_1V region zones, intermediate coke yields in L_1L_2, L_1L_2V zones and high coke yields in L_2, L_2V zones (L1 is the low density liquid phase rich in solvent and L2 is the high density liquid phase rich in the solute). The study of coke formation in thermal processing of heavy oils has been reported by many researchers (Wiehe, 1992, 1993, 1994; Li et al., 1999; Rahmani et al., 2003) and these works show that phase behaviour plays an important role in coke yield during thermal upgrading of heavy oils.

1.4 Preceding Work

The best performance in heavy oil upgrading processes is realized if all operating variables are optimized. Why do heavy oil upgrading processes operate where they do? Preceding work in our group attempted to answer this question from a phase behaviour perspective (Dukhedin-Lalla, 1996; Abedi, 1998; Cartlidge et al. 1996). For example, Abedi (1998) showed a phase diagram for a model heavy oil mixture where the multiphase region of the model mixture intersected the processing region for heavy oil upgrading. Even though the diagram is superimposed on the operating conditions for heavy oil/bitumen upgrading processes, it is satisfactory for qualitative and comparative purposes. The operating parameters for the heavy oil hydroprocessing processes, such as H-Oil, CANMET etc. are chosen such as to avoid the complex phase behaviour zone since coke deposition can be reduced or suppressed. However, small changes in operating conditions can result in operating in multiphase regions that causes severe coke deposition. With the same model heavy oil system, Abedi et al. (1998) observed a link

5

between coke formation and multiphase behaviour. A solid phase separated from the heavy liquid phase L_2 irreversibly at temperatures greater than ~ 650 K. This solid phase did not separate from the light liquid phase L_1 even at temperatures up to 700 K. This result suggests that simple kinetic models alone cannot explain the contrary phenomenon observed when studying coke formation in heavy oil mixtures as the mixtures are more active kinetically at over 700 K than at 655 K in an otherwise similar reaction environment. Clearly, the origin of this contradictory phenomenon is related to phase behaviour. In this work, non-reacting or non-catalyzed systems were examined. Up to now, no direct experimental observation of liquid-liquid phase separation during the hydroprocessing of heavy oil has been reported.

1.5 Hypothesis

Catalytic hydroprocessing of heavy oil is a process that involves both catalytic and thermal processes. The notion of phase separation in hydroprocessing of heavy oil is only mentioned in few papers (Ternan et al., 1994 and Gray, 1994). The authors speculated that phase behaviour would affect coke formation but direct experimental proof was not presented. The thread of their argument follows.

In the hypothetical phase diagram, Figure 1.3 (Gray 1994), the L_1L_2V three phases may coexist in a conventional hydroprocessing slurry reactor when the conversion rate reaches some extent. However, the addition of a solvent may change the phase behaviour from L_1L_2V phase behaviour to L_1V phase behaviour and then suppress the coke formation. This can be readily understood as one would expect higher coke formation rates in the L_2 phase where coke precursors are concentrated than that in the L_1 phase where coke precursor concentration is much lower. In addition, the solubility of hydrogen and hence its concentration in an L_2 phase is much lower than in the L_1 phase, which further increases the likelihood of condensation and polymerization reactions that lead to coke formation (Ternan et al., 1994).

6

Light Ends +H$_2$

L_1V

L_1L_2V

L_2V

Heavy Resid   Middle Distillates
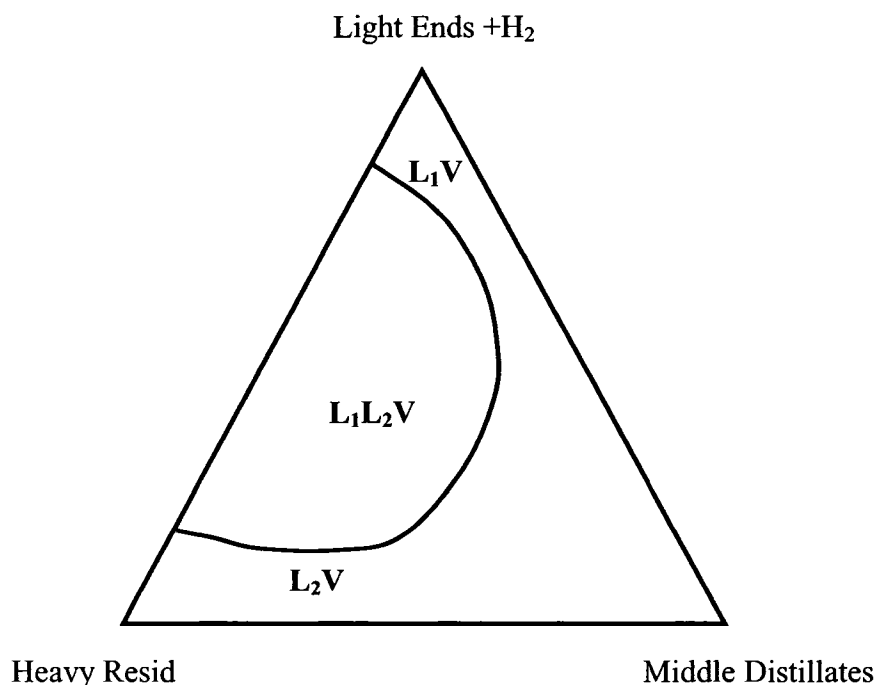
Figure 1.3   Hypothesized ternary phase diagram during hydroprocessing

In batch hydroprocessing reactors one scenario that can arise is that at the beginning the feed falls in an L_1V region. As conversion increases, the mixture shifts to an L_1L_2V region and then back to an L_1V region. If the phase behaviour trajectory follows such a path in a fixed-bed hydrogenation reactor from the inlet to outlet, the "S" shape coke profiles (Amemeya et al., 2000; Niu, 2001) are readily understood. As expected, the coke profile gradient in L_1L_2V region is higher than that in L_1V region.

The three physical models for coke deposition can also be linked to phase behaviour. This idea was initially proposed by Shaw and some fundamental work has been conducted in his group (Miniccuci, 2000; Miniccuci et al., 2002). The idea can be described simply as follows. If operating in an L_1V phase region, the coke deposits uniformly on the inner surface of catalyst. If operating in an L_1L_2V phase region, in which L_1 phase is the continuous phase, pore mouth plugging can also occur as dispersed liquid drops of L_2 phase during coking can become rigid and hence stuck at restrictions within the pore system. If operating in an L_1L_2V phase region, in which L_2 is the

7

continuous phase, or in the L_2V region coke can readily deposit on all surfaces present in a reactor.

If one can prove the occurrence of phase separation in hydroprocessing of heavy oil and that higher coke yields arise in L_2V and L_1L_2V regions than in L_1V regions, and establish a link between the three types of phase behaviour and three coke deposition models, such findings would provide a sound basis for upgrading process development and operation improvement. At the same time, such findings would add an additional dimension to the complexity of hydrogenation catalyst fouling models.

1.6 Objectives

Understanding the link between kinetics and phase behaviour is invaluable when developing kinetic models for coke formation, developing mechanisms for coke deposition, and designing or optimizing hydroprocessing processes. Phase behaviour can change dramatically giving rise to very different phenomena with seemingly very little difference in operating conditions. Knowledge of the location of "danger zones" and operating away from them can dramatically increase the productivity and life of expensive hydrogenation catalysts.

The principal objectives of this study are to establish a relationship between phase behaviour and coke formation kinetics and coke deposition in hydroprocessing processes. Applied issues include elucidation of catalyst fouling mechanisms in hydroprocessing processes. If successful the investigation will become a touchstone for future research in this area. The specific objectives are to:

1. Observe the phase behaviour of selected mixtures in which coke precursors exist and identify a suitable operating condition for coke formation and deposition experiments;

2. Investigate the influence of phase behaviour on the coke deposition in different phase regions;

3. Establish a relationship between the nature of coke deposition (coke deposition model) and phase behaviour.

8

1.7 Thesis Outline

Following this brief introduction, a comprehensive literature review related to this thesis is presented in Chapter 2 to help readers better understand topics addressed subsequently e.g.: heavy oil characteristics, currently commercialized heavy oil catalytic hydroprocessing technologies, coke deposition mechanisms and models. The experimental equipment and procedures are described in Chapter 3. The X-ray transmission view cell was used to explore the phase behaviour of the model heavy oil system, which provided guidance for the catalyst coking experiments and the view cell was also modified and used as a batch reactor for catalyst coking experiments. The coked catalysts were characterized by traditional methods. For clarity, the experimental results and discussions are divided into several chapters with each chapter focusing on a specific topic. Chapter 4 and 5 focus on the phase behaviour study of the model heavy oil system in the presence and absence of hydrogen, respectively. The direct observation of complex phase behaviour in this model heavy oil system is provided and the phase diagrams are constructed. Chapter 6 and 7 provide the results from the investigation of catalyst coking in the presence and absence of hydrogen, respectively, where the impact of phase behaviour and factors associated with phase behaviour on coke deposition are discussed. Chapter 8 and Chapter 9 address the catalyst coking kinetics and industrial process implication, separately. Finally, conclusions are presented in Chapter 10.

2. Literature Review

The origin and focus of the thesis are presented in chapter 1. In this chapter, background materials needed to understand and appreciate the details presented in subsequent chapters are presented. Topics addressed include:

(1) The chemical and physical characteristics of heavy oil/bitumen, especially the troublemaking fraction, asphaltene fraction.

(2) A brief review of current catalytic hydroprocessing technologies for heavy oil/bitumen.

(3) A general description of catalyst fouling, in particular the coke formation which is one of the major causes of catalyst fouling.

(4) A basic introduction to phase diagram theory needed to construct phase diagrams for the model heavy oil system used in this project.

(5) A summary of recent developments related to this project both in thermal upgrading and catalytic hydroprocessing of heavy oil/bitumen.

2.1 Heavy Oils

2.1.1 Heavy Oils/Bitumen-Our Future Energy Resource

With the depletion of conventional crude oils, the heavy oil and bitumen resources are increasingly becoming commercially producible, since the early 80's in the Athabasca, Alberta, Canada and, more recently, in the Orinoco, Venezuela. For example, in Canada, most liquid hydrocarbons are currently produced from bitumen: there is 1.7 to 2.5 trillion barrels of bitumen (one-third of the world's known petroleum reserves) in Alberta, which could meet Canada's energy needs for the next two centuries (Morgan, 2001; Gray and Masliyah, 2004).

As the world's supply of conventional light sweet crude oils becomes depleted, the petroleum industry is forced to refine heavy crude oils and bitumen to supply the increasing demand for transport fuels and petrochemical feeds. Meanwhile the market for

10

heavier fuels is decreasing while that for middle distillates is increasing at a rapid rate, so ideally heavy oils and bitumen recovered in the upstream oil fields, along with residues produced in the downstream refineries, should be upgraded as much as possible into middle distillates.

A key to the full realization of the upgrading potential of these heavy oil reserves and heavy residues will be technology, and more precisely how to find methods allowing to process theses residues at acceptable costs and without excessive energy consumption.

2.1.2 Characteristics of Heavy Oils/bitumen

Understanding of heavy oil/bitumen composition and properties is a prerequisite for investigation of phase equilibrium and kinetics of heavy oil mixtures in upgrading processes. Heavy oils/bitumens include atmosphere residues (AR) and vacuum residues (VR), topped crude oils, coal oil extracts, crude oils extracted from tar sands, etc. (Gray, 1994; Speight, 2002), and in this context, are generally called as heavy oil. Heavy oil is very viscous and does not flow easily. The characteristics of heavy oils are quite different from those of conventional crude oils. They generally have a high specific gravity (>0.95), a low hydrogen-to-carbon ratio (~1.5), and contain large amounts of asphaltenes (>5 wt %), heavy metals (such as vanadium and nickel), heteroatoms (such as sulfur, nitrogen and oxygen) and inorganic fine solids (Speight, 1991). The inorganic fine solids, heavy metals and heteroatoms tend to concentrate in the heaviest fractions, such as resins and asphaltenes (Reynolds, 1994 & 1999; Chung et al. 1997).

The composition and properties of heavy oil have been widely investigated and characterized through fractionation, in particular SARA analysis (ASTM D-2006, ASTM D-2007 and ASTM D-4124). During SARA analysis, heavy oils are fractionated, by selective precipitation (for the asphaltenes) and/or chromatographic techniques, into four classes of compounds: Saturates, Aromatics, Resins, and Asphaltenes (Figure 2.1). Generally, as the boiling point of heavy oil fractions increases, more resins and asphaltenes and less saturates are found.

11
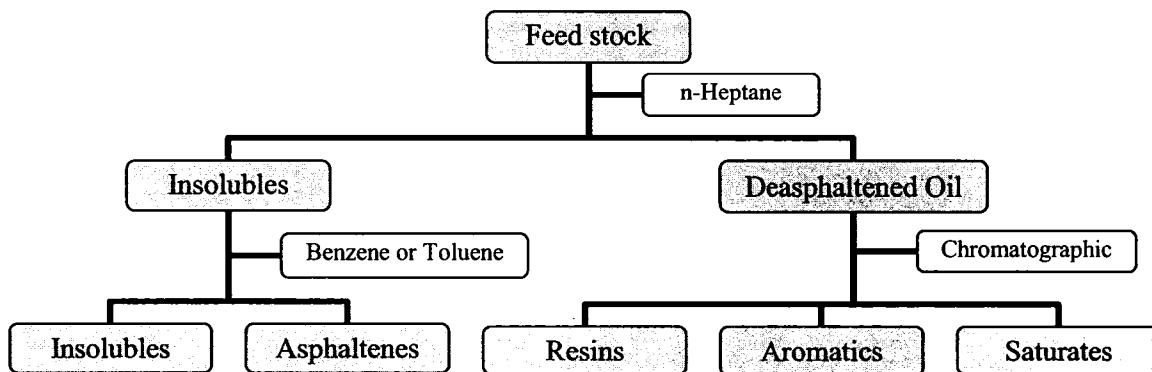
Figure 2.1 Petroleum fractionation

2.1.3 Asphaltenes

Asphaltene represents the most refractory fraction of heavy oils. The importance of asphaltene in the petroleum industry is through its negative impact on various petroleum operations, such as exploration, production, transportation, and refining. One needs to have a good understanding of the chemical properties and colloidal behaviour of asphaltenes in order to avoid or resolve the problems caused by them.

Asphaltenes are identified by SARA analysis as a solubility class which may be composed of molecules that differ significantly in their chemical characteristics (e.g. molar mass, aromaticity, heteroatom and metal content etc.). The chemical composition of asphaltene depends on many variables, including choice of alkane solvent, volume, temperature, and time of mixing, as well as carbonaceous fuel source. Asphaltenes generally have a high content of heavy metals and heteroatoms, which results in a high coking tendency.

Molecular models for asphaltenes are also challenging to validate. Diverse 'average' models for the same or closely related bitumen fractions have been proposed. Pericondensed and archipelago molecular models (Figure 2.2) have both been proposed for Athabasca bitumen fractions (Maham et al. 2005). Pericondensed molecules are characterized by large pericondensed ring structures with short alkyl chains attached to them (Zhao et al. 2001). Archipelago molecules are characterized by small multi-ring structures variably substituted with alkyl chains and interconnected with alkyl chains and

12

heteroatom bridges (Murgich et al. 1999; Strausz et al., 1992; Sheremata et al. 2004). The average molecule structures proposed appear to relate to the relative importance that researchers place on different analytical techniques.
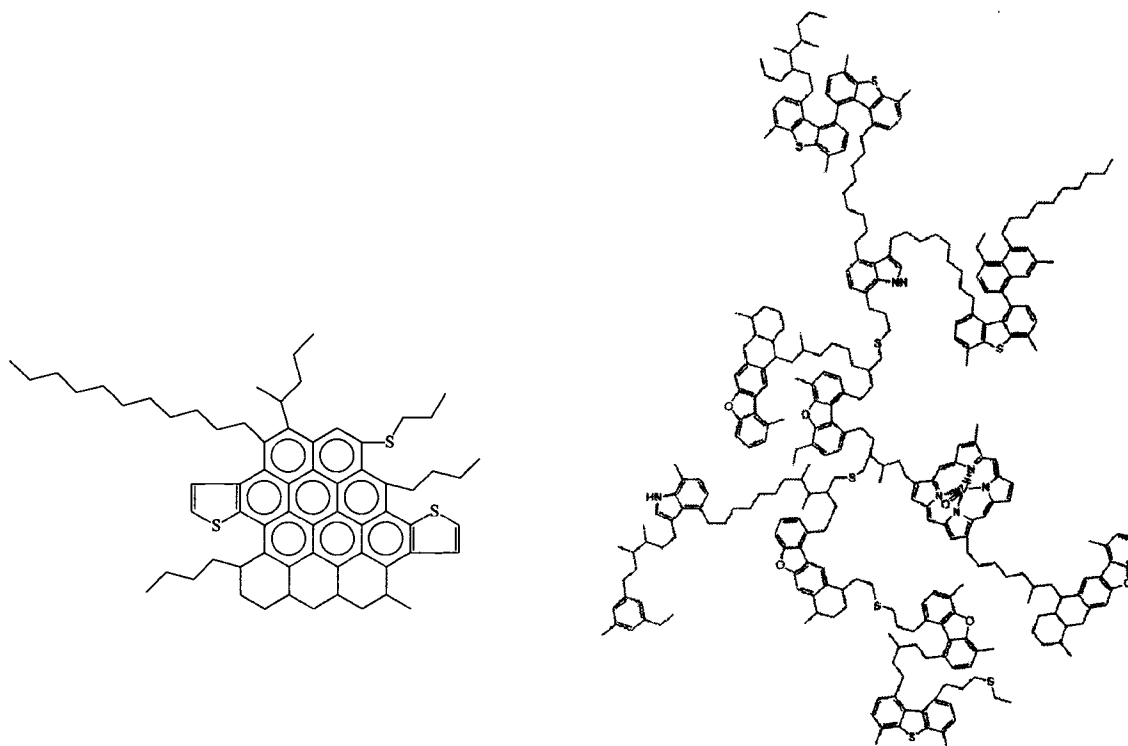
Figure 2.2   Average structure of Athabasca asphaltene molecules. a) pericondensed model (Zhao et al. 2001); b) archipelago model (Sheremata et al. 2004).

The physics and chemistry arising at the supramolecular level are equally unresolved, even though great efforts have been devoted. It has been concluded that heavy oils such as crude oils, residues, bitumen etc. exhibit colloidal behaviour in the presence of asphaltenes, and resin fractions (Li et al. 1996; Bardon et al. 1996; Branco et al. 2001). The asphaltenes are believed to exist in heavy oils partly dissolved and partly in steric-colloidal and/or micellar forms depending on the polarity of their oil medium and presence of other compounds (Priyanto et al. 2001). The asphaltene aggregates dimensions are on the colloidal length scale. Early work showed that the size of asphaltene particles varies between nanometer and micron length scales (Overfield et al., 1989; Yen, 1998). The dimensions of aggregates also depend strongly on the nature of

13

the solvent, asphaltene concentration, and temperature (Espinat et al. 1998). The most characteristic trait of asphaltenes is their strong aggregation propensity in hydrocarbon solution (Overfield et al., 1989). Under unfavorable surrounding conditions, asphaltenes are prone to aggregation by flocculation or micellization, and can precipitate from the oil matrix if the colloid stability of the feed cannot be maintained (Mansoori, 1997).

The conversion of asphaltene is a complex decomposition process (Quann et al. 1988; Dautzenberg and De Deken, 1987). Based on the micelle macrostructures of asphaltene, a generalized sequential asphaltene conversion mechanism was proposed by Takeuchi et al. 1983 and Asaoka et al. 1983 shown in Figure 2.3. Mechanistic studies of asphaltene conversion indicate that metal removal (Vanadium and nickel) plays an important role at the initial step of asphaltene conversion since the metals contained in asphaltene micelles are the bonding constituents to form the asphaltene micelles and the removal of metals destroys the association of asphaltene micelles. Subsequently, further dissociation occurs from depolymerization and thermal cleavage of weak links by weakening of π bond interactions between aromatic sheets and by removal of heteroatoms such as sulphur.

— M — Metal
———— Aromatic sheet
wwww Aliphatic
wwww Week link
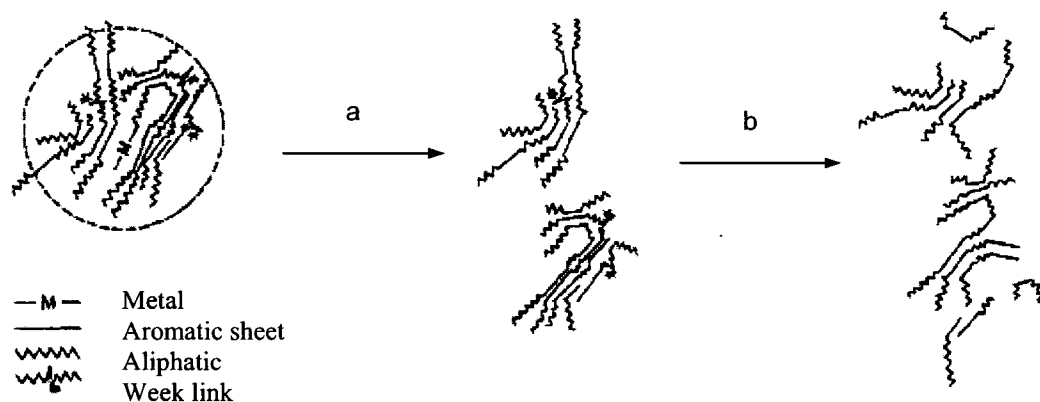
Figure 2.3   Proposed mechanism for asphaltene conversion: a) destruction of asphaltene micelle; b) depolymerization due to heteroatom removal (Asaoka et al. 1983; Takeuchi et al. 1983)

There are diverse views concerning the molecular structure and colloidal behaviour of asphaltenes. Also since the chemistry and physics of asphaltenes are unresolved, the conversion mechanisms of asphaltenes are uncertain. More efforts need to be devoted

14

into the study of both the microscopic and macroscopic structure and conversion mechanisms of asphaltenes. However, there is a growing consensus one way or another on each matter.

2.2 Heavy Oil Catalytic Hydroprocessing

2.2.1 Introduction

Process selection of upgrading technologies depends on the combination of cost, product slate, and byproduct considerations. Since the petroleum is depleting, recently process selection has tended to favour hydroprocessing technologies, which maximize distillate yield and minimize byproducts (especially coke) and generally accomplish significant demetallization and Conradson carbon reduction (CCR), in addition to desulfurization and viscosity reduction. A spectrum of hydroprocessing technologies for heavy oils is available, summarized in several review papers and books including comparison of different technologies (Qabazard et al. 1990; Furimsky, 1998; Dautzenberg and De Deken, 1984; Quann et al. 1988; Gosselink and van Veen, 1999) and a list of technologies available (Absi-Halabi et al. 1997; Speight, 2000; Speight and Ozum, 2002; Dukhedin-Lalla, 1996). This review here is limited to catalytic hydroprocessing technologies used for the treatment of heavy oils and bitumen.

In summary, catalytic hydropocessing is characterized by hydrogen addition, heteroatom removal, minimal carbon rejection, using catalysts (Le Page et al. 1992). In the presence of a hydrogenation catalyst, the hydrogen is able to be added into feed and converts heteroatoms to hydrogen sulphide, water, and ammonia etc. and the coke formation is suppressed at the same time. Not only does the hydrogenation catalyst enhance hydrogenation reactions, but it also serves as a surface for the deposition of metals.

Based on the type of reactor bed employed, commercial catalytic reactors using a granular catalyst can be divided into the three main categories (Le Page et al. 1992; Furimsky, 1998): (a) Fixed-bed processes; (b) Moving-bed processes; (c) Ebullated-bed processes.

15

Traditionally, fixed-bed reactors were used for hydroprocessing of light feeds. Gradually fixed-bed reactors were modified to accommodate heavier feeds. Many fixed-bed reactors can operate reliably on atmospheric residues. However a good operability cannot be achieved with difficult feeds such as vacuum residues. Major concern is the excessive number of catalyst replacement. In contrast, the moving- and ebullated-bed units have demonstrated reliable operations with vacuum residues.

The processes using granular catalyst involve a high cost of the hydroprocessing catalyst caused by the catalyst replacement and disposal, so an alternative process ie. slurry-phase process, is obtaining growing interest. This process employs disposable catalysts, which is added to the feed as finely divided solids. The once-through catalyst will remain in the slag.

Therefore several criteria have to be considered to make choices among these options. But the availability ensures that a wide range of feeds can be processed if an optimal match between the reactor with the catalyst and the feed of interest is made. Figure 2.4 illustrates the relative positions of the various technologies in processing atmospheric and vacuum residues (Scheffer et al. 1998). In the present review, each reactor system except for the homogeneous system is discussed briefly and exemplified with typical processes in commercial operation or near a commercial stage.

Atmospheric residue   Vacuum residue

9%   10%   1%
2%   5%
                                        37%

88%   47%

fixed ebullated slurry moving homogeneous
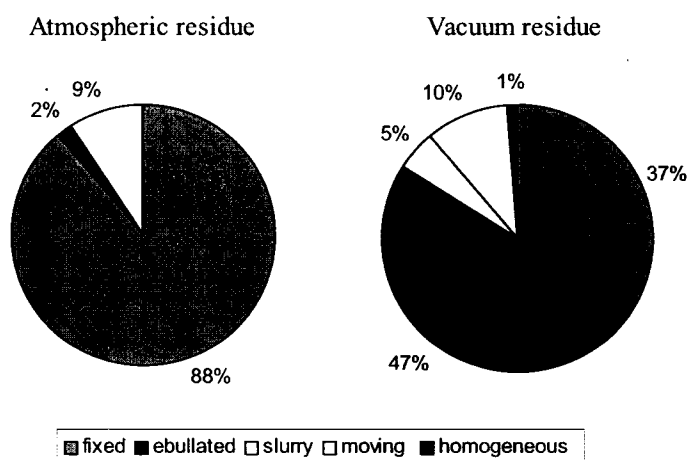
Figure 2.4   Share of the various residue hydroprocessing technologies in upgrading of atmospheric and vacuum residues, respectively.

16

2.2.2 Fixed-Bed Processes

Fixed-bed processes are well developed and have been in commercial use for several decades. The most typical fixed-bed reactor in hydroprocessing is the trickle-bed reactor. The trickle-bed process is relatively easy and simple to operate and scale up. A schematic of the fixed-bed or trickle-bed reactor is shown in Figure 2.5 (Beaton and Bertolacini, 1991). The reactor operates in a downflow mode, with liquid feed trickling downward over the stationary solid catalyst cocurrent with the hydrogen gas. Since the hydrogenation is an exothermal reaction, in some cases, hydrogen is introduced between the beds as a quench to prevent excessive high temperatures within the reactor.

The main limitation of this type of reactor is the gradual accumulation of metals in the pores of the catalyst and the final blockage of access for reactants to catalyst surface when a typical residue is processed. After the catalyst deactivates, the reactor must be shut down and the catalyst bed has to be replaced, which usually takes a longer time around 10-20 days and is uneconomical.
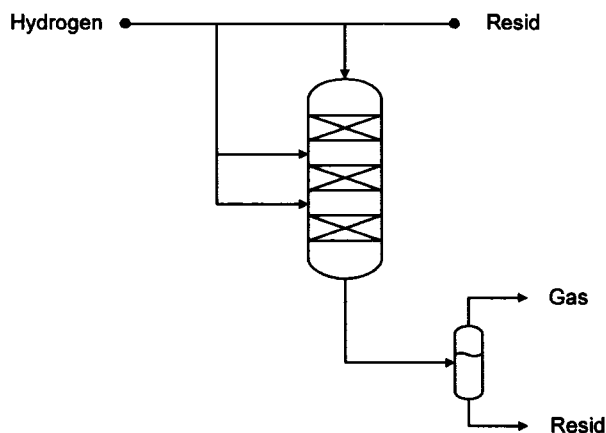
Figure 2.5 Schematic of fixed-bed reactor

Several processes employing fixed-bed reactors for hydroprocessing of heavy feeds are in commercial use. A typical fixed-bed process is the Gulf HDS process (Speight and

17

Ozum, 2002; Speight, 2000; Mckinney and Stipanov, 1971; Yanik et al., 1977), which upgrades residua by catalytic hydrogenation to refined heavy fuel oils or to high quality catalytic charge stocks. In addition, the process can be used, through alternative designs, to upgrade high sulfur crude oils or bitumen that are unsuited for the more conventional refining techniques. A simplified flowsheet of the Gulf resid hydrodesulfuriztion process is shown in Figure 2.6. The feedstock is heated together with hydrogen and recycle gas and charged to the downflow reactor. The liquid product goes to fractionation after flashing to produce the various product streams. On-stream cycles of 4-5 months can be obtained at desulfurization levels of 65-75%, and catalyst life may be as long as 2 years.
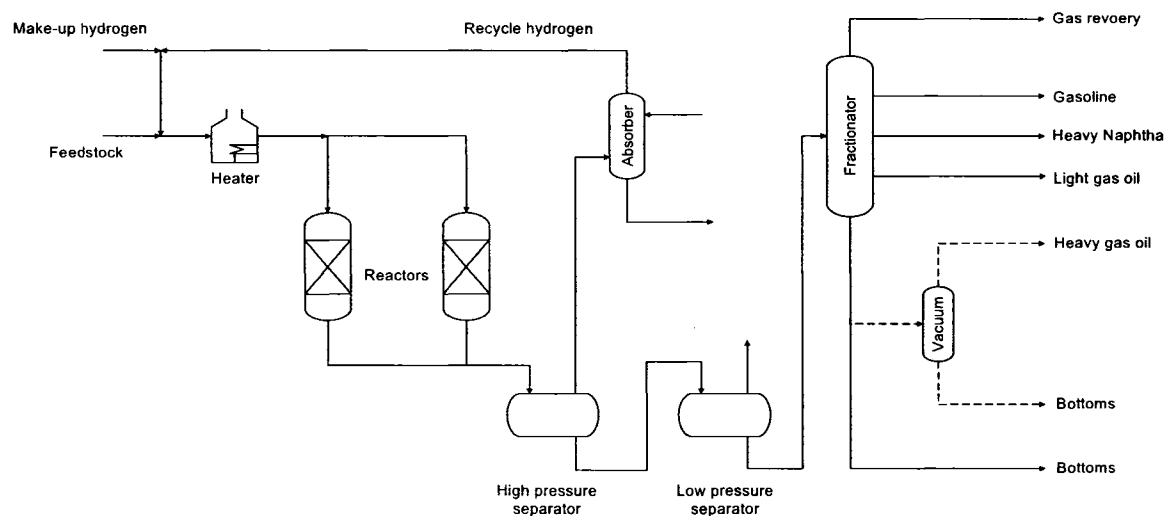
Figure 2.6   The Gulf resid hydrodesulfurization process.

IFP has developed several kinds of fixed-bed processes under the name HYVAHL (Kressmann et al. 1998; Furimsky, 1998; Speight, 2000). The HYVAHL-F process is a classical fixed-bed process using several fixed-bed reactors in series. A recent improvement on the HYVAHL-F process has been made, namely, a swing reactor system is used in front of several fixed bed reactors in series, which is named as HYVAHL-S process. This improvement enables on-stream catalyst replacement. Hydrodemetallation is achieved in the swing reactor system and a relatively high level of conversion is achieved at the same time. Hydrodesulfurization is achieved in the following fixed bed

18

reactors in series. With this arrangement, HDS and HDM levels of 92% and 95% for Arabian light or Arabian heavy vacuum residues, respectively, can be achieved.

A number of other fixed-bed systems are also available in commercial use. The ABC (asphaltenic bottom cracking), licensed by the Chiyoda Chemical Engineering & Construction Co. Ltd., is a fixed-bed catalytic hydrotreating process coupled with a solvent deasphalting unit (Dukhedin-Lalla, 1996; Speight, 2000). The ABC process is suitable for hydrodemetallization, asphaltene cracking and moderate hydrodesulfurization. The RCD (reduced crude to distillate) Unibon process (Dukhedin-Lalla, 1996; Speight, 2000), licensed by UOP Inc., employs a series of fixed-bed reactors to remove contaminants such as nitrogen, sulphur and heavy metals from atmospheric residues at moderately high hydrogen pressures. The BOC (black oil conversion) process, an extension of the RCD process, operates at higher hydrogen pressures for hydroprocessing of vacuum residues (Dukhedin-Lalla, 1996; Speight, 2000).

2.2.3 Moving-Bed Processes

These processes are able to realize continuous catalyst renewal by utilizing moving-bed reactors. The advantage of this moving-bed process is able to process heavy feeds, especially rich in metals. This technology combines the advantage of fixed-bed operation in a plug flow and the ebullated-bed operation in easy catalyst replacement. The well-known example of a moving-bed reactor is the bunker reactor which was successfully developed by Shell and commercialized in 1989 (Scheffer et al. 1998). A schematic diagram of this reactor is shown in Figure 2.7. This trickle-flow system allows discontinuous catalyst replacement without interrupting the operation. During replacement, catalyst movement is slow compared with the linear velocity of the feed. Catalyst addition and withdrawal are performed via the sluice system at the top and bottom of the reactor. The advantage of the bunker reactor is that the top layer of the moving bed consists of fresh catalyst. Thus, metals and salts deposited on the top of the bed move downwards with the catalyst and are released at the bottom. The tolerance to metals and other contaminants is therefore much greater than in a fixed-bed reactor. With

19

this capability, the bunker reactor system may be suitable for hydroprocessing of very heavy feeds, especially when several reactors are combined in series.
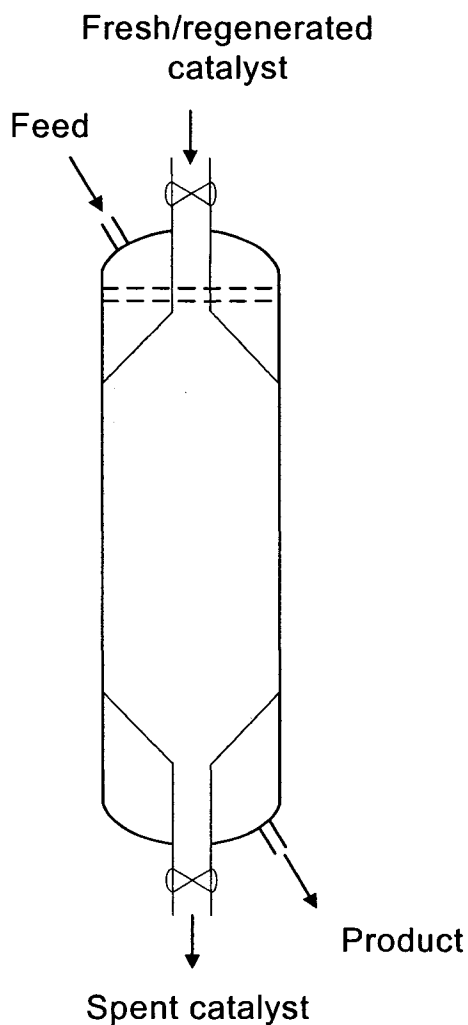
Figure 2.7   Schematic of bunker reactor.

The HYCON process, a first commercial unit using the bunker reactor, consists of five reactors, of which the first three reactors are bunker reactors filled with a silica-based hydrodemetallization (HDM) catalyst. The last two reactors are of the fixed-bed type, filled with the standard hydrodesulfurization (HDS) and hydrocracking catalysts. A simplified flow scheme is shown in Figure 2.8. The feedstock is fed to the HDM section. The catalysts in HDM reactors flow concurrently downward. The demetallized products

20

pass to the fixed bed HCON section where the product is further desulfurized and converted.
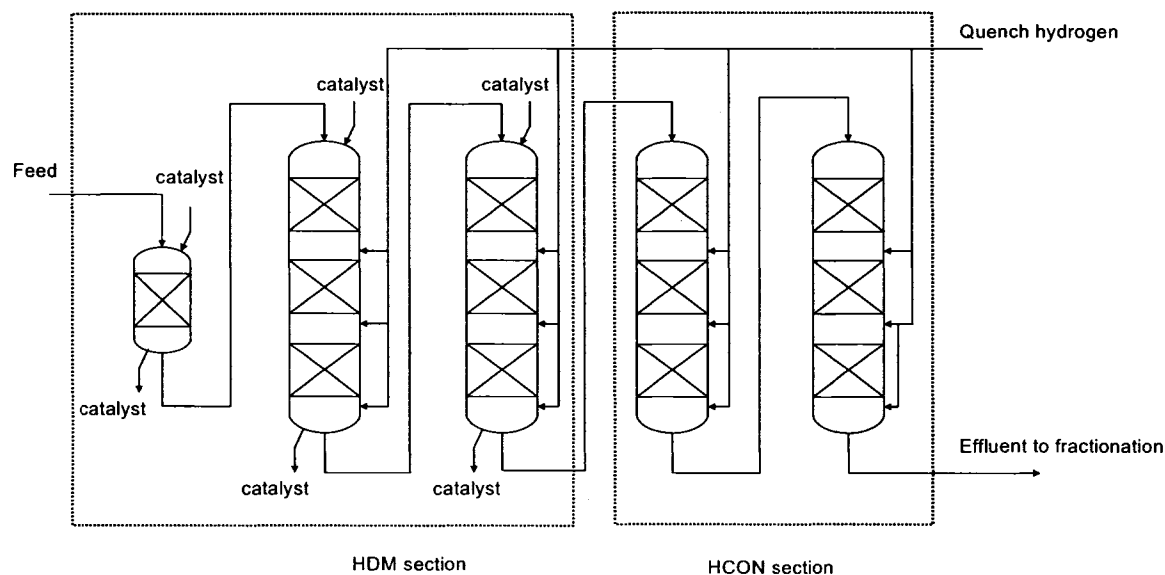
Figure 2.8 Process flow scheme of the HYCON unit.

The other moving bed processes include OCR (On-stream Catalyst Replacement) process licensed by Chevron and HYVAHL-M process licensed by IFP (Morel et al. 1997). Both of these two processes adopt the counter-current moving bed reactor where the catalyst circulates from top to bottom of the reactor while the reaction fluids circulate from bottom to top in counter-current to the catalyst. The counter-current configuration is better than the co-current configuration adopted in the bunker reactor since the spent catalyst saturated by metals meet the fresh feed at the bottom of the reactor whereas the fresh catalyst reacts with an already demetallized feed at the top of the reactor. This configuration results in a lower catalyst consumption.

2.2.4 Ebullated-Bed Processes

The ebullated-bed reactors represent culmination in the development of hydroprocessing reactors. In an ebullated bed reactor (shown in Figure 2.9), the fluids circulate up-flow in the reactor. A recirculating pump expands the catalytic bed and maintains the catalyst in

21

suspension. The expanded bed volume is 30 to 50 % larger than the bed volume at rest. The bed design ensures ample free space between particles allowing entrained solids to pass through the bed without accumulation, plugging or increased pressure drop, and a good mixing between oil and particles behaving like a fully back-mixed reactor. Operation of the ebullated reactor is very flexible. The most important feature of the processes employing ebullated-bed reactors is their capability to periodically withdraw and/or add the catalyst to the reactor without interrupting operation. This is important for hydroprocessing of high asphaltene and metal feeds. The catalysts for ebullated bed operation are equivalent in composition to the catalysts for fixed bed or moving bed operation, but the pellet diameter is usually smaller than 1 mm to facilitate suspension by the liquid phase in the reactor.
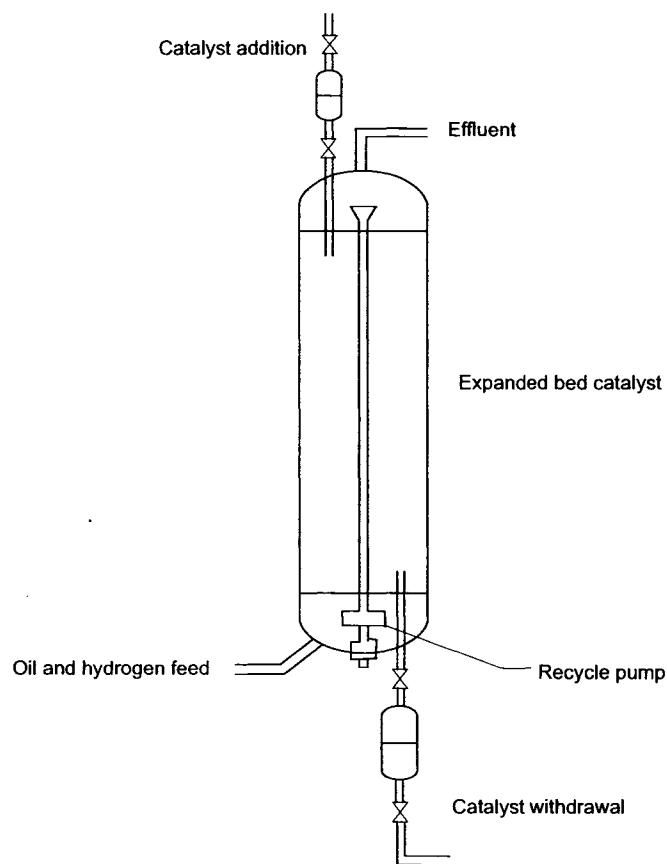
Figure 2.9   Schematic of LC-Fining reactor

The ebullated-bed process was designed to handle the most problematic feeds, such as vacuum residues and heavy oils having a high content of asphaltenes, metals and including sediments. The process is flexible and can be operated either in a high conversion or low conversion mode, i.e., for hydrocracking and HDS, respectively. The first commercial ebullated-bed process was originally known as the H-Oil process licensed by the Hydrocarbon Research Inc. and Texaco. The heart of the H-Oil process is its ebullated bed reactor. In a typical flow scheme (shown in Figure 2.10), feed and hydrogen enter the reactor at the bottom while catalyst is fed from the top. Feed and hydrogen are then pumped upward through the catalyst bed which helps to maintain bed fluidization. Vapour product removed from a vapour space at the top of the reactor is cooled, and condensed partially. The gaseous portion which is mostly hydrogen is purified, reheated and recycled to the reactor. Heavy effluent from the reaction zone is recovered and fractionated. In the case of multi-reactor system, the first reactor is used for HDM and the others for HDS and hydrocracking.
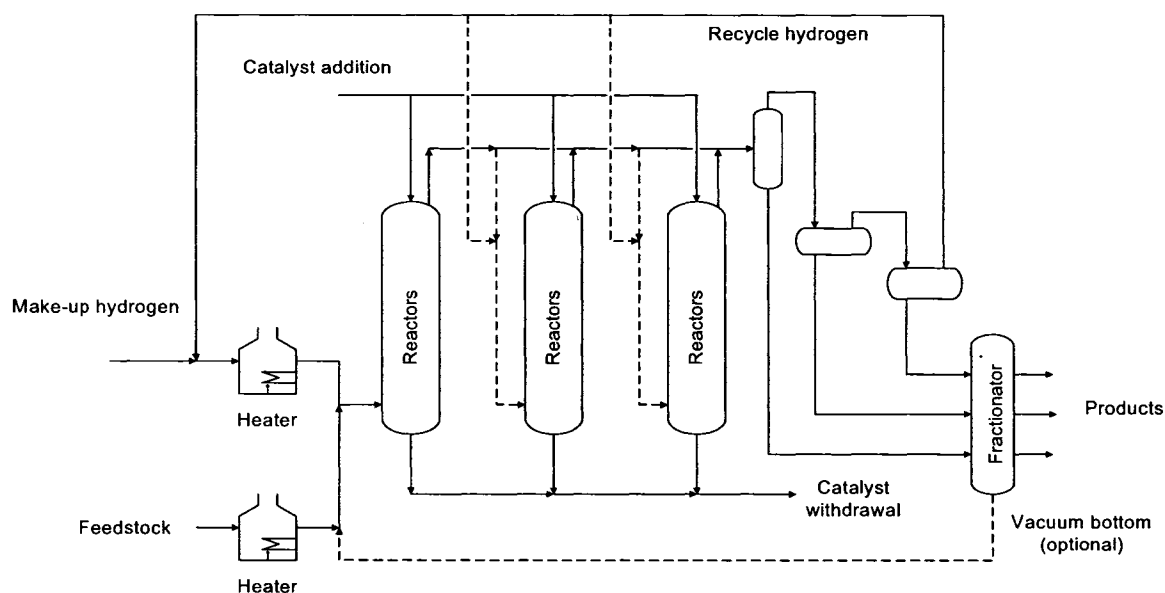
Figure 2.10   The H-Oil process

Another ebullated-bed process is LC-Fining process, licensed by City Services and Lumus and Amoco, which is a continuous and modified process of H-Oil process. Given

23

the history of the development of the ebullated process, the features of both the LC-Fining process and the H-Oil process are very similar. Nevertheless, the information available in the literature is divided as to refer to these processes separately. Several commercial H-Oil and LC-Fining units are in operation in different parts of the world.

2.2.5 Slurry Phase Process

The slurry phase processes, an alternative to fixed-, moving-, and ebullated-bed catalytic processing, employs disposable catalysts such as finely divided solids. The once-through catalyst is slurried with the feed prior to entering the reactor, a free-internal-equipment tubular reactor, where the liquid or liquid suspension of additive flows upward with the hydrogen gas. After reaction, the catalyst remains in the unconverted residue fraction. The recovery of the highly dispersed catalyst is usually not practical and the catalyst is inexpensive such that the catalyst is discarded. Among the most attractive features of slurry-phase operation are the limited amount of catalyst required to achieve the desired conversions, and the simplicity, high efficiency, and improved temperature control possibilities of the reactor vessel. So this process is not attempting simultaneous hydrodesulfurization (HDS), hydrodenitrogenation (HDN), hydrodemetallization (HDM), and cracking conversion in a single reactor. The HDS, HDN is achieved in the downstream reactors. This technology boasts being able to handle a wide feed stock variability, and very high metals, high asphaltene and CCR content.

An example of this approach is the CANMET process (Figure 2.11), developed by the Energy Research Laboratories of Energy Mines and Resources Canada with Petro-Canada in the early 1980's. This scheme is a high conversion, high demetallization residuum hydrocracking process that uses an additive to suppress coke formation and achieves the conversion of heavier fractions. The feed is mixed with a small amount of processing additive (a proprietary iron-coal compound) that is prepared easily and at a low cost. The mixed feed-additive stream is heated and contacted with hydrogen, and then sent to an upflow reactor. Product is removed from the overhead and separated into a hydrogen-rich recycle gas stream, process gas, distillate and a residual pitch fraction with spent additive.

24
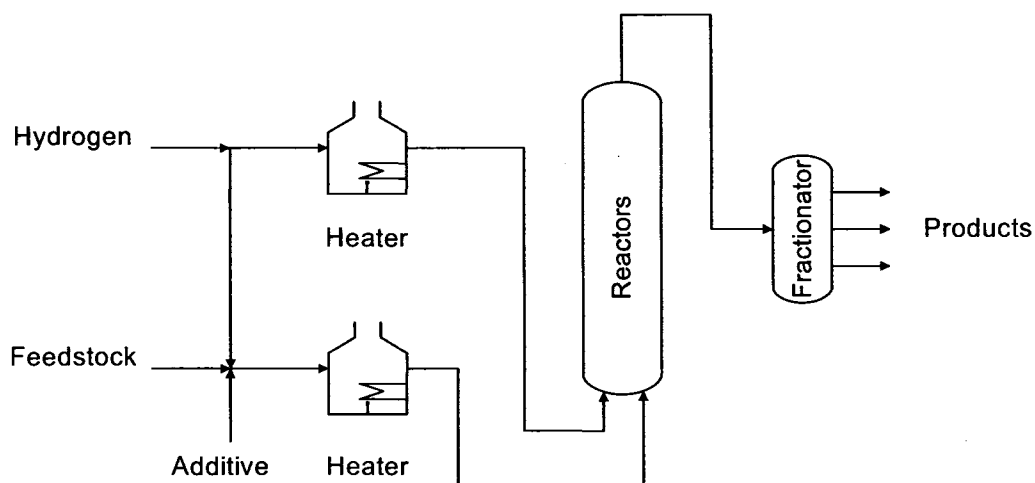
Figure 2.11 The CANMET process

2.2.6 Catalyst Characteristics

Regarding the granular catalysts, a wide range of hydroprocessing catalysts have been developed for commercial applications. The major group includes supported molybdate and tungstate catalysts promoted by either Ni or Co. γ-Alumina is the common support. Since the presence of large quantities of asphaltenes, S, N, and O as well as metals such as Ni, V, Ti, Fe and others in the heavy oils, the catalysts must possess a high activity and at the same time be tolerant to metals. The physical properties of catalysts must be thoroughly considered. Special attention has to be paid to the size of the particles, pore volume and size distribution, pore diameter and the shape of the particles to maximize the utilization of the catalyst. For a heavy oil feed, if the catalyst mean pore diameter is in the neighbourhood of the size of resins and asphaltenes of the feed, the diffusion rate is much slower than the reaction rate, and only part of the catalyst particles is used and metals are deposited on the outside of the catalyst particles. Catalysts with larger pores are required for hydroprocessing of such a feed, but at the expense of the catalyst activity due to the loss of surface area. The influence of pore sizes on radial distribution of metal deposition is illustrated in Figure 2.12. Usually there is an optimum pore size distribution for a given feed to a given process. A proper combination of porosity, surface area and activity becomes an important task in the development of hydroprocessing catalysts for heavy oils.

25
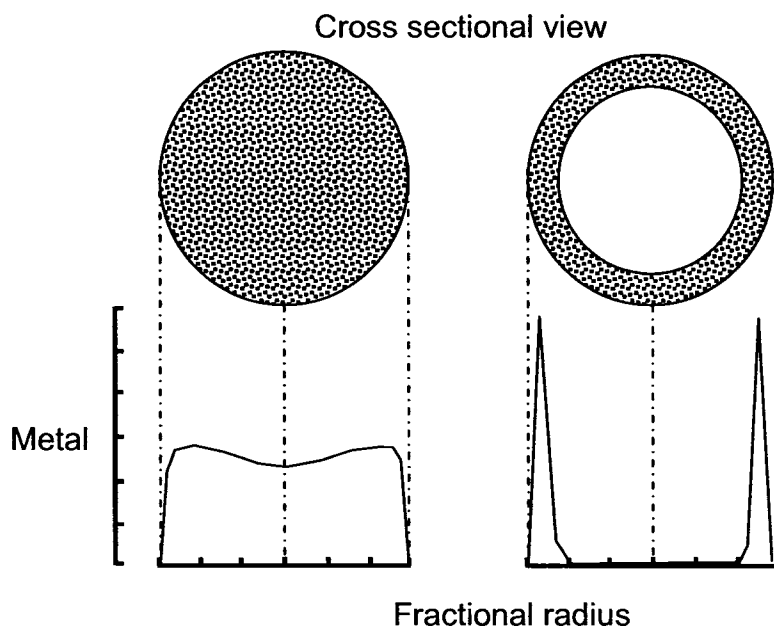
Figure 2.12 Radial distribution of metals on catalyst pellets

For a typical heavy oil, the three types of reactor design using granular catalysts exhibit different coke and metal deposition profiles from the entrance to the exit of the reactor as shown schematically in Figure 2-13. For both fixed bed reactor and moving bed reactor, the coke content of catalysts increases from the entrance to the exit of the reactor. In contrast, the metal content increases for moving bed reactor, while it decreases for fixed bed reactor. Since the catalysts are uniformly distributed in the ebullated bed reactor, the coke and metal contents of catalysts do not depend on their location in the ebullated bed reactor.
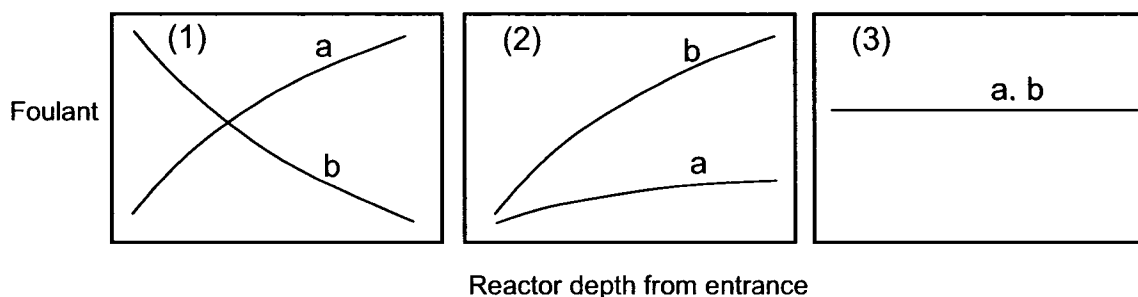
Figure 2.13 Schematic representation of position-dependent foulant deposition profiles. (1) fixed bed; (2) moving bed; (3) ebullated bed. a. coke and b. metals.

26

2.3 Catalyst Coking

2.3.1 Catalyst Fouling Mechanisms

Catalyst fouling can be due to poison adsorption, sintering, and mineral deposition and coke formation (Butt and Petersen, 1988). These may occur singly or in combination. Some impurities can reduce catalyst activity, because they can strongly adsorb at acidic sites on the surface that play important roles in hydroprocessing reactions and block access by the reactants. Poisoning of the hytroprocessing catalyst should be significant only during the first few hours of the startup period and be partially reversible after that period.

Sintering results in change on physical and/or chemical properties of the catalyst, such as surface area, pore volume, pore size and states of the active species. Most commonly this is a thermally activated process and is physical rather than chemical in nature unlike poisoning. However under normal hytroprocessing conditions, this sintering effect is not significant.

Mineral matter from feedstocks can deposit on the catalyst covering the active sites and restricting pore mouths, resulting in permanent loss of catalyst activity. Some of the deposited metals such as iron, nickel, cobalt can even catalyze coking reactions. Only the heavy oils or bitumen, which contains relatively high concentrations of mineral matter, cause significant mineral deposition.

Coke formation is the most significant phenomena causing catalyst fouling. Coke, a kind of carbonaceous material, may be formed from coke precursors on catalyst surfaces by polymerization or condensation and dehydrogenation reactions, which could be caused by any feedstock from light oils such as gasoline to heavy oils such as vacuum residues.

2.3.2 Fouling by Coke

Catalyst fouling in hydrogenation processes is one of the most concerned problems in industry. There have been many reviews attempting to summarize the published information relevant to fouling of hydroprocesing catalysts (Bartholomew, 1994; Absi-Halabi and Stanislaus, 1991; Thakur and Thomas, 1985; Furimsky and Massoth, 1999;

27

Gualda and Toulhoat, 1988; Trimm, 1995). Usually, hydroprocessing catalysts continuously experience some degree of fouling with time on stream at fixed reaction temperature. Catalyst activity, for example HDS conversion for heavy oils, exhibits a typical S-shape curve as illustrated in Figure 2.14c. Under commercial operating conditions, catalyst activity is actually maintained by constantly raising the temperature. Fouling is then manifested by the temperature-rise profile as a function of time on stream, as illustrated by the typical S-curve of Fig. 2.14d. If the feed is heavy oils, catalyst fouling by coke, metal deposits and poisons occurs simultaneously, so it is not easy to distinguish quantitatively between the contributions of all these causes to fouling. The typical coke and metal deposition curves are illustrated in Figure 2.14a and 2.14b. There is a general agreement that initial fouling is caused by coke, which appears to rapidly reach a pseudo steady-state level. The intermediate slow fouling period is usually ascribed to increasing diffusional resistance caused by metal deposition in the pores, whose rate of fouling depends on the metals level in the feed. The final, catastrophic loss in activity is attributed to pore constriction and ultimate pore blockage, which brings the catalyst to the end of its working life.
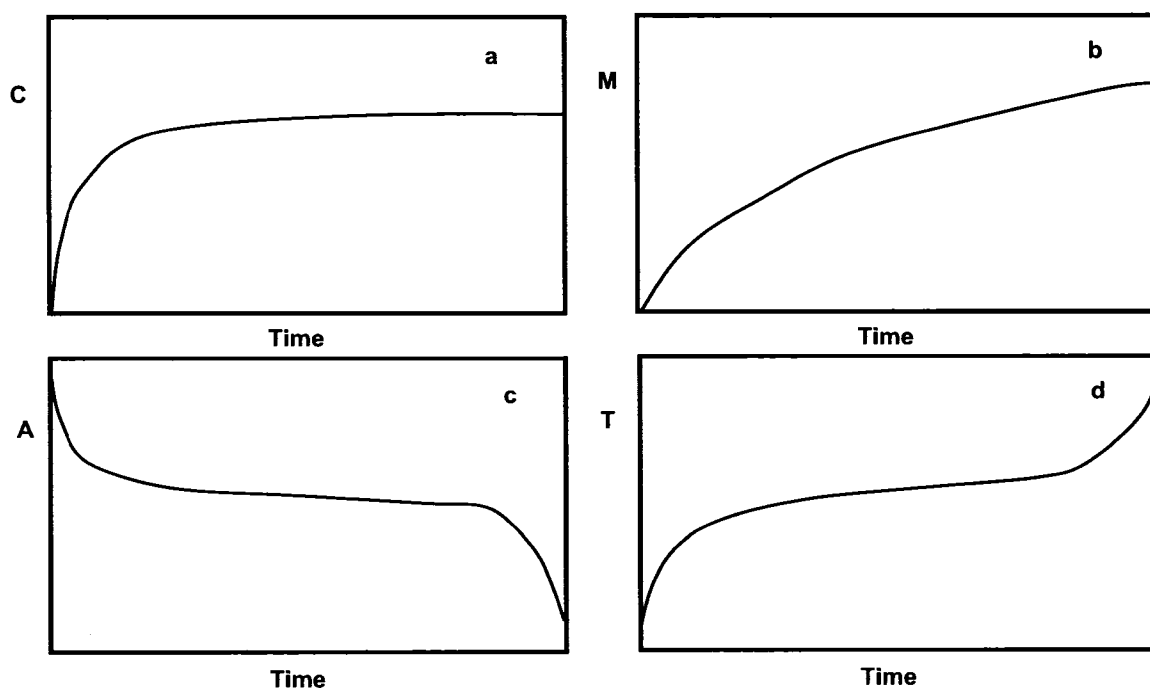
Figure 2.14 Catalyst fouling profiles

28

During the start-up phase in hydroprocessing, initial coke deposition is one of the most significant factors influencing catalyst fouling. Several studies, focusing on the initial catalyst coking, indicate that coke deposition is believed to be very fast in the initial period of operation, particularly, in residual oil hydroprocessing (Marafi and Stanislaus, 2001; Matsushita et al. 2004; Hauser et al. 2005; Richardson et al. 1996; Idei et al. 2002; Gualda and Kasztelan, 1996). Approximately 50 wt% of the total deposited carbon is laid down on the catalyst within the first few days of operation (Hauser et al. 2005). Much of coke formed during the early hours of the run is deposited in micropores of the catalyst leading to a substantial loss in surface area and pore volume (Absi-Halabi et al., 1991; Callejas et al. 2001; Marafi and Stanislaus, 2001). And at the early stage of operation, much of coke on catalyst is reversible species not only in terms of composition but also in terms of quantity (Callejas et al. 2001; Gualda and Kasztelan, 1996). The reversible coke can be easily removed or reversed if a proper operation is applied. The irreversible coke, strongly adsorbed at the support surface, is deposited on catalyst even at the very early state, and the ratio of irreversible coke to reversible coke increases with time on stream. As the time on stream increases, the coke becomes more aromatic, exhibiting in a decrease of H/C ratio.(Matsushita et al. 2004; Hauser et al. 2005; Gualda and Kasztelan, 1996).

2.3.3 Coke Formation Chemistry

The structure of coke and the mechanisms of coke formation are complex and not fully understood. Coke is not a well-defined substance; normally it has an empirical formula approximating CH, but the chemical nature depends very much on how it is formed. Coke is formed via two parallel routes, viz. (i) thermal polymerization or condensation reactions and (ii) catalytic dehydrogenation reactions (de Jong, et al., 1994b). The catalyst composition has a large impact on the amount of catalytic coke whilst physical effects (phase equilibrium) predominate in determining the extent of thermal coke formation. Coke formation on catalysts may take several forms and be caused by different mechanisms. From the nature and shape, coke is normally classified into three main types: amorphous, filamentous and graphite platelets (Hughes, 1984; Butt and

Petersen, 1988; Absi-Halabi et al., 1991). These types would not be distinguished during a routine analysis of the spent catalysts, but merely referred to collectively as "coke". Condensation and polymerization reactions play a major role in amorphous coke formation. Although some hydrogen is removed during condensation, a significant amount still remains in the deposit. As the temperature is raised, dehydrogenation reactions reduce the hydrogen content. Filamentous coke is produced by the catalytic decomposition of carbon containing gases on small metal particles such as iron, cobalt and nickel and their oxides. The graphitic deposit is formed indirectly, at the expense of the other two deposit forms and also requires the participation of a catalyst. The graphite carbon can form only at elevated temperature higher than 1000°C. Therefore, only amorphous and filamentous types of coke deposits are significant in hydroprocessing catalysts.

The species acting as precursors for coke have been the subject of much investigation and speculation. Among hydrocarbons, the alkenes and aromatics (associated with or without heteroatoms) are the generally agreed upon coke precursors. The interaction of aromatics or alkene with the catalyst surface is much stronger than that of saturated hydrocarbons. Therefore they are more likely to convert to higher molecular weight species by polymerization or condensation if sufficient active hydrogen is not available to prevent it. The majority of opinion is in favor of aromatic species as the major coke precursor for heavy oils hydroprocessing (Hughes, 1984). Especially, polar heteroaromatic compounds having strong adsorption tendency and having high cracking and condensation reactivity tend to form more coke, which is evident that the heteroatoms content in coke is higher than in the feed. The aromatics could be present in the feedstock or may form as intermediates in the hydrogenation process.

In the case of heavy feeds where asphaltenes are present, significant coke deposition can be formed on the catalyst and the deposited carbon on spent catalyst is proportional to the concentration of asphaltenes in feed (Gray et al. 1999). Studies have shown that asphaltenes are a major contributor to coke formation in the hydroprocessing of heavy oils (Absi-Halabi et al., 1991; Marafi and Stanislaus, 2001; Gray et al. 1999). They have a higher propensity to form coke by directly depositing on catalyst as coke precursor themselves, or by generating condensed aromatics via cracking off side chains.

30

2.3.4 Coke Deposition Modes

In regard to catalyst fouling mechanisms and catalyst bed fouling, one could apply another classification to interpret coke deposition in hydroprocessing. Uniform surface deposition (Richardson et al. 1996), pore-mouth plugging (Muegge and Massoth, 1991), and bulk phase coke deposition (Richardson et al. 1996) are three observed modes for coke deposition (Figure 1.1). Uniform surface deposition and pore mouth plugging models are two hotly-debated models because conflicting results were reported on the probable location of coke deposits in hydroprocessing catalysts. Richardson et al. (1996) suggest that coke deposits uniformly on catalyst surfaces with monolayer coverage. Deposition beyond a molecular monolayer is not accounted for in this modelling approach. Typical experimental findings that suggest uniform surface deposition show a loss of pore volume for only the smallest pores, a gradual decrease in catalyst surface area, and a gradual decrease in pore volume as overall coke content increases, thus affecting the smallest pores (with highest surface area to volume ratios) before affecting larger pores. The other experimental findings by Ternan et al. (1979), Diez et al. (1990) also support this model.

Muegge and Massoth (1991) studied the effect of coke produced from a model-coke precursor, anthracene, on the physical properties of a catalyst. Examination of pore structures indicated that the loss of pore volume and surface area was due to pore blockage, but the small pores, expected to be blocked, were not preferentially blocked. And the inconsistency between the significant lowering in diffusivity and the small change in average pore radius at higher coke deposition revealed that a wedge-like growth of coke deposit at pore mouth must occur before the pore-mouth plugging. The pore mouth plugging is also experimentally observed at initial rapid coke deposition stage (Absi-Halabi et al. 1991). Lee et al. (1991a) also observed a drastic reduction in diffusivity due to a small amount of coke deposition, indicating that in some cases, the pore network in the catalyst can be blocked at the pore mouth. This model, based on experiments, is consistent with localized multilayer deposition and is inconsistent with

31

the purely catalytic reactions based deposition model (uniform surface deposition). Since neither of the conflicting models has been substantially proven or disproved, it is clear that more study is required to shed light on the mechanisms of coke deposition on hydrogenation catalysts.

The above two models describe how coke forms within the catalyst and affects catalyst activity and imply that no coke forms outside of catalyst pellets. In fact, in some cases, coke also forms on the catalyst pellet exterior surface and inner surface of reactors. Richardson et al. (1996) observed that particulate coke was formed in the liquid phase and plugged the outlet line from their reactor. They suggested that the coking mechanism in the liquid phase was linked to thermal cracking, completely distinct from the coking mechanism on the catalyst surface. Liquid phase coke deposition was also observed in a commercial plant (Nowlan and Srinivasan, 1996). The separators in Syncrude's commercial LC-Finer experienced significant coke deposition in the high temperature separators downstream of the hydrogenation reactors.

2.3.5 Coke Formation Kinetics

Kinetic description of coke formation is significant to predict catalyst fouling i.e. catalyst life. In order to quantitatively describe coke formation i.e. coking kinetics, modeling coke formation process is essential. There is an abundance of information on models for describing the kinetics of coke formation. From the reaction routes perspective, coke formation models can be classified into two categories: parallel coke formation, series coke formation. Coke formation can be viewed as the result of a sequence of side reactions from feedstock, intermediates, products, or any combination of the three. This scheme can be simplified as follows:

Feed (F) $\longrightarrow$ Intermediates (I) $\longrightarrow$ Products

Feed (F) $\longrightarrow$ Coke $\longleftarrow$ Products
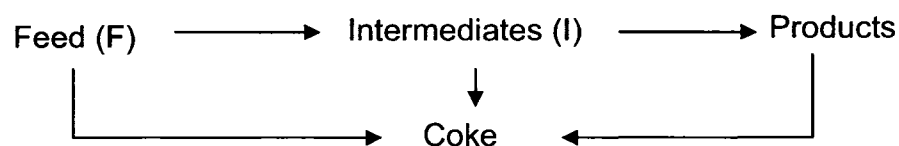
Figure 2.15 Coke formation pathway.

32

If coke forms mainly from feed oil, then this is parallel coke formation; if mainly from intermediates and/ or products, then it is series coke formation; and it is also possible from both. The first-order rate coking kinetics then can be expressed as:

$$\text{Series fouling: } \frac{dq}{dt} = k_I C_I \left(1 - \frac{q}{q_0}\right) \tag{2.1}$$

$$\text{Parallel fouling: } \frac{dq}{dt} = k_F C_F \left(1 - \frac{q}{q_0}\right) \tag{2.2}$$

Where C_F and C_I are concentrations of F and I, k_F, k_I are rate constants for the series, parallel fouling respectively, and q and q_0 are the amount of coke at time t and that corresponding to complete fouling, respectively.

Based on coke monolayer adsorption mechanism, Richardson et al. (1996) obtained a relation:

$$q_C = q_{C,max}\left(1 - e^{-k_a w}\right) \tag{2.3}$$

Where q_c is the actual amount of carbon on the catalyst, $q_{c,max}$ maximum carbon deposition, and w cumulative feed-to-catalyst ratio, a pseudo time coordinate, and k_a an adsorption rate constant. In this model, they assume that most of the coke originates from the asphaltenes in the feed and asphaltenes adsorb on the catalyst surface to form a monolayer and a maximum level for deposition will exist for given conditions.

A more complicated model was developed by de Jong (1994a, b, c) in which both catalytic coke and thermal coke were accounted for. The rate of catalytic coking, following the Langmuir-Hinshelwood type of kinetic equation, is expressed as:

$$R_c = \frac{k_c K_a C}{1 + K_a C} \tag{2.4}$$

where C is the concentration of coke precursor, and K_a equilibrium adsorption constant, and k_c the rate constant dependent on the amount of coke on the catalyst, viz

33

$$k_c = k_{c,0}\left(1 - \frac{q}{q_{max}}\right)$$ (2.5)

in which q is the amount of coke deposited. q_{max} was estimated by extrapolation of the steady-state coke-time curve to zero time. This would imply that catalytic coke is deposited in the early stages. The rate of thermal coke formation was expressed as:

$$R_t = k_t C^2 / P_{H_2}$$ (2.6)

where k_t is the rate constant of thermal reaction and P_{H2} is hydrogen partial pressure.

Then the total rate of coke deposition, R, is

$$R = R_c + R_t$$ (2.7)

This model was successfully tested for predicting the effects of temperature and hydrogen/feed ratio on coke formation.

Both active site blocking and pore plugging by coke was considered in the model developed by Haynes and Leung (1983), the following equation was used to calculate the rate of coking:

$$R = \rho_x\left(1 - \varepsilon_y\right)\eta C_{RS}$$ (2.8)

where ρ_x is the microparticle density, ε_y the particle porosity, η the effectiveness factor, and C_{RS} the surface reactant concentration.

The applicable coke formation model is directly related to the feed properties. Highly aromatic feeds such as coal oil usually exhibit parallel coking; low aromatic feeds such as heavy petroleum exhibit series coking. Therefore, the selection of coking model is usually based on feed aromaticity.

In fixed-bed catalytic hydrogenation processes, both parallel coke formation and series coke formation are generally applied. In the parallel model, coke is formed from the feed oil in parallel with light products formation. According to this model, the amount of coke on the catalyst decreases with distance from the reactor inlet (Chang et al., 1982). According to the series model, coke is formed from intermediates and/or products that result in an increase in coking along bed depth (Thakur and Thomas, 1985, Koyama e al.

34

1996). In regard to catalyst pellets, coke deposition is heavier at the outside of the pellet for parallel coke formation; whereas, deposition inside is heavier for series coke formation. Under severe diffusion limitations, coke deposition is always heavier at the outside of the pellet regardless of the mechanism. Schematic representation of coke profiles for both parallel and series coke formation models in fixed-bed hydrogenation reactors are shown in Figure 2.16. The coke profiles may not necessarily exhibit the shape indicated in Figure 2.16. In many cases, the coke profile is more complex than that these simple models suggest (Bartholomew, 1994).

A. Coke axial distribution of catalyst bed depth   B. Coke radial distribution of a single pellet
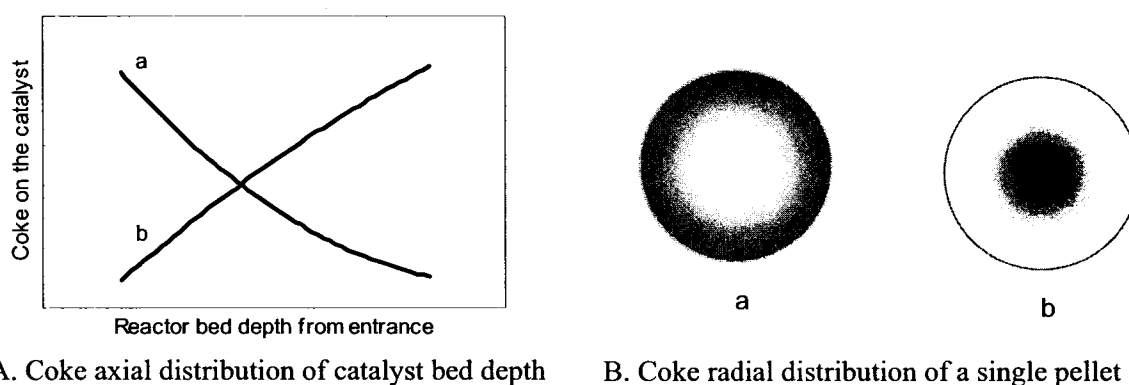
Figure 2.16   A) Schematic representation of position–dependent coke deposition profiles in catalyst beds batch or continuous; B) radial distribution of coke within a single pellet; a) parallel and b) series.

2.3.6 Minimisation of Catalyst Fouling

Catalyst design has been the subject of much study to obtain optimized catalyst properties. In hydroprocessing catalysts, acidic sites crack the reactants to produce low molecular weight of species, but at the same time they also cause coke formation by condensation and polymerization reactions from the unsaturated cracking intermediates. Hydrogenation sites provide the hydrogenation activity to saturate the unsaturated compounds and remove the impurities from the feed. By controlling the ratio of hydrogenation components to the cracking components, the coke may be minimized to a large extent. In addition to catalyst composition, the pore size distribution is found to be another major factor affecting catalyst fouling. Because hydroprocessing of heavy

35

feedstocks is a diffusion-controlled process, micropores are not accessible to large molecules like asphaletenes and are easily blocked by the coke formed at a pore mouth (pore mouth plugging). An optimum catalyst pore structure facilitates access of reactants to the interior of the catalyst and reduces catalyst fouling due to pore mouth plugging and at the same time provides enough catalyst surfaces for reaction. The size of catalyst pellets may also affect the effectiveness of a catalyst. By decreasing particle size, catalyst may be utilized more effectively by avoiding the egg-white coke deposition. However, small particle sizes lead to increased pressure drop and serious bed plugging in a fixed bed reactor. An optimum particle size is a 0.8 to 1.6mm diameter extruded cylindrical pellet (Thakur and Thomas, 1985).

Operating conditions can also be adjusted to minimize coking. Under severe operating conditions such as high space velocities, high temperature and low hydrogen pressure, coke forms much faster thereby resulting in rapid catalyst fouling. It is very easy to understand why high space velocities cause high coking rates in that the coke precursor amount passing through the catalyst is higher for high space velocities than at low space velocities. High reaction temperatures yield higher free radical concentrations which may cause high coking rates if they are not saturated. An increase in hydrogen pressure has a favourable effect if catalyst fouling is caused by coke formation, because the free radical intermediates which form coke can be saturated by hydrogen before coke can form. The hydrogen to oil ratio is another important parameter in hydroprocessing. Coke extents pass through a maximum going from low to high ratios. This is due to the existence of a critical condition, that is, a dew point for the fluid inside the reactor (de Jong et al., 1994). Catalyst fouling increases with the molecular weight/boiling point of the feedstock. By controlling the feed into a reactor, coke formation may be reduced. For example, high molecular weight of asphaltene is the major source of coke, and pre-treatment of the feed by solvent deasphalting leads to a major reduction in coke formation.

Another approach to reduce coke formation is by modifying the composition of the feed mixture or the recycle (Gray, 1994). The addition of hydrogenated heavy aromatic petroleum fractions or heavy aromatic petroleum fractions suppresses coke formation by providing a medium with high hydrogen solubility and which reduces hydrogen consumption (Kubo et al., 1994 and 1996). The success of this approach is normally

36

attributed to enhanced hydrogen transfer from the vapour phase to the oil phase and the high radical scavenging ability of additives (Kubo et al., 1994). Another explanation for coke reduction by adding solvent to a feed is the solubility increase due to the solvent addition makes the more solid soluble in the fluid and therefore suppresses the coke formation (Gray, 1994). Supercritical conditions caused by adding a solvent to the feed also reduce coke formation in upgrading of heavy oil (Scotta et al., 2001). Diffusion rates of supercritical fluids into catalyst pores are much higher than those for subcritical systems (Lee, et al. 1991a, 1991b), and an optimum fluid density which minimizes coke deposition and mass transfer limitations can be expected to exist at supercritical or near-supercritical conditions (Baptist-Nguyen, and Subramanjam, 1992).

2.4 The Role of Phase Behaviour in Coke Formation

2.4.1 Introduction

Phase diagram and phase behaviour are often the starting point and base for designing or developing many industrial processes. One of the most typical examples is the heavy oil solvent deasphalting process (McHugh and Krukonis, 1994), which operates in the LLV or LL multiphase phase region and produces purified light oil by getting rid of L2 - the asphaltene rich phase. Liquid-liquid phase separation created by mixing light solvent and heavy oil is a key to achieve upgrading of heavy oils. Some industrial processes such as coking processes and solvent deasphalting processes try to take advantage of this kind of phase separation, while some other processes such as visbreaking process have to avoid the occurrence of phase separation. In heavy oil hydroprocessing, phase separation may occur and cause serious coke formation. Phase diagrams and the evolution of phase diagrams as reactions progress in heavy oil hydroprocessing may provide key insights into the coke formation mechanism. Therefore, understanding phase behaviour is crucial to the design and development of industrial processes.

2.4.2 Some Basic Theories of Phase Behaviour

2.4.2.1 Fluid Phase Behaviours

37

In addition to the V, L1 or L2 phase behaviour, the petroleum fluids in upstream production and downstream transportation and upgrading system may exhibit a variety of phase behaviours and critical phenomena as noted in Figure 2.17, including L1V or L2V, L1L2, and L1L2V phase behaviour and associated critical phenomena. The designations L=V or L1=L2 in Figure 2.17 mean that the two phases in question are critically identical. They possess the same values for density, composition, molar volume, viscosity and all other physical properties and the boundary between the phases, designated as a dashed line in Figure 2.17, disappears. Two phases can also become critically identical in the presence of a third phase giving rise to so-called K and L points. A K point arises when an L1 becomes critically identical to an V in the presence of an L2 and is designated as L1=V + L2. An L point arises when an L1 and an L2 become critically identical in the presence of an V phase and is designated as L1=L2 + V. Tricritical point means that three phases (V, L1 and L2 phases) are critically identical, and are designated as L1=L2=V. Such tricritical points, while present in phase diagrams and phase projections, are rarely observed in practice. The multiphase behaviours illustrated in Figure 2.17 are often observed for the asymmetric mixtures in which one component dominates on a mole fraction basis and others dominate on a mass fraction basis. Many operating fluids in petroleum production and upgrading processes such as reservoir gas injection recovery and solvent deasphalting can be classified as asymmetric mixtures.
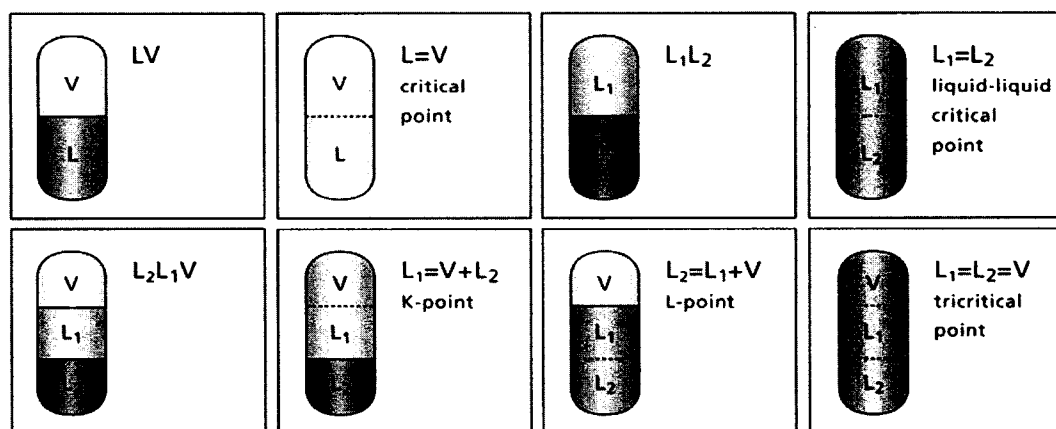
Figure 2.17   Phase behaviours exhibited by hydrocarbon mixtures. Dashed phase boundaries indicate critically identical phases.

2.4.2.2 Binary Mixtures

Even though the binary mixtures are scarce and almost every process involves multicomponents in chemical engineering application, the investigation of binary mixtures phase behaviour is of great importance. Because the study of binary mixtures provides a sound basis for understanding the phase behaviour of more complex mixtures and play a key role in the development of models that describe the phase equilibrium and phase state.

Van Konynenburg and Scott (1980) classified the fluid phase behaviour of binary mixtures into six types according to the shape of the mixture critical line and in the absence or presence of three-phase lines. Below is a brief description of the various types. For more detailed discussion of the classification, one is referred to Van Konynenburg and Scott (1980) and Prausnitz et al. (1999).

Figure 2.18a is a P-T projection of Type I phase behaviour. A continuous L=V critical locus joins the vapour pressure lines of each pure component. The critical locus goes through a maximum; thus, vapour can exist at higher pressures for the mixtures than for either of the pure components at the same temperature. The continuous vapour-liquid critical line is often observed for mixtures where the two components are chemically similar and/or their critical properties are comparable.

Type II, presented in figure 2.18b, is similar to Type I except for a line of liquid-liquid immiscibility at low temperatures (below the critical temperature of the light component). The L1=L2 critical locus begins at the upper critical endpoint (UCEP) of the three phase equilibrium curve (L1L2V) and extends to very high pressures. The UCEP in this case is a liquid-liquid critical point in the presence of a vapour (L point). The essential feature of this type is the continuous vapour-liquid critical line that is distinct from the liquid-liquid critical line. The liquid-liquid immiscibility of Type II phase behaviour typically occurs at intermediate compositions. The L1L2V phase line may in some cases reside above the vapour pressure curve of lighter component.

Different from type II, type III (Figure 2.18c) connects the liquid-liquid critical line and vapour-liquid critical line together. For mixtures with higher immiscibility, the locus of the liquid-liquid critical lines moves to higher temperatures and then interfere with the

39

vapour-liquid critical curve; at the same time the vapour-liquid critical line is separated into two branches. One branches goes from the vapour-liquid critical point of the lighter component to UCEP where the L1L2V line begins and extends to low temperature. The UCEP in this case is a vapour-liquid critical point in the presence of second equilibrium liquid phase (K point).

As seen in Figure 2.18d, Type IV phase behaviour retains the low temperature liquid-liquid immiscibility line found in Type II; and the L=V critical locus discontinuity like type III. The binary critical curve is divided into two parts: first, beginning at the critical point of the pure light component, the L1=V critical curve extends similar to Type I or Type II; however, in this case it terminates at the UCEP of a second (high pressure, high temperature) L1L2V phase equilibrium curve. This UCEP is a liquid-vapour critical point in the presence of a second heavier liquid (K point). From the lower critical endpoint (LCEP) of this second L1L2V curve, which is also an L point, the critical curve continues as a L1=L2 critical locus and will transform into L2=V critical locus at temperatures above the K point. The L2=V critical locus continues, joining the heavy component vapour pressure curve at its pure component critical point. This is similar to type III in that there is a connected critical curve of liquid-liquid critical line and vapour-liquid critical line. The L1=L2 critical locus is also divided into two parts, the first part has been described just above; the second part is that it begins at the upper critical endpoint (UCEP) of the three phase equilibrium curve (L1L2V) and extends to very high pressures, similar to type II.

Type V (Figure 2.18e) is different from type IV only in that Type V has no the low temperature liquid-liquid immiscibility region, that is, below LCEP the liquids are completely miscible. Type V phase behaviour is not really a separate classification from that of Type IV, and merely is Type IV where the low temperature L1L2V equilibrium curve is obscured by solidification of the heavier component. The same argument applies to Type I and Type II. More discussion on the role of solidification follows.

Type VI phase behaviour (Figure 2.18f) has two critical curves: one connects the critical points of two pure components while another connects UCEP and LCEP to form a closed-loop liquid-liquid equilibrium.
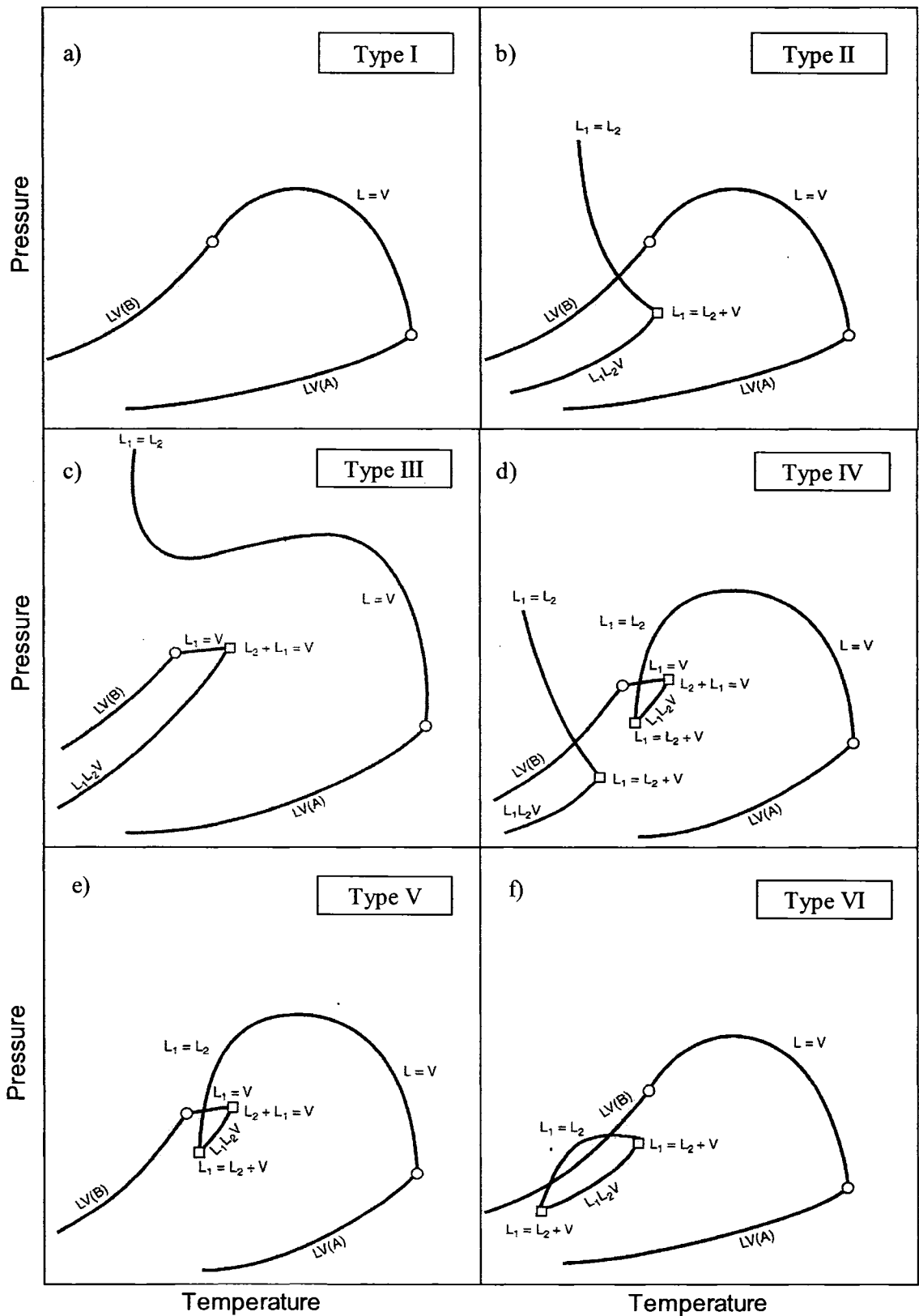
Figure 2.18 Phase behaviour classification for binary mixtures

41

2.4.2.3 Ternary Mixtures

As the number of components is increased from two to three, LLV phase behaviour extends over a region in pressure temperature space for any given ternary. Phase diagrams for ternary systems are at least 4-dimensions. In practice, construction and interpretation of phase diagrams of ternary systems are similar to and based on those of binary systems.

Gregorowicz et al. (1993) reported detailed discussions on how to expand phase diagrams of binary mixtures to phase diagrams of ternary mixtures. As an example, Type V phase diagrams of a binary mixture shown in Figure 2.19 are expanded to ternary mixture phase diagrams shown in Figure 2.20 when a miscible component for both components is added.
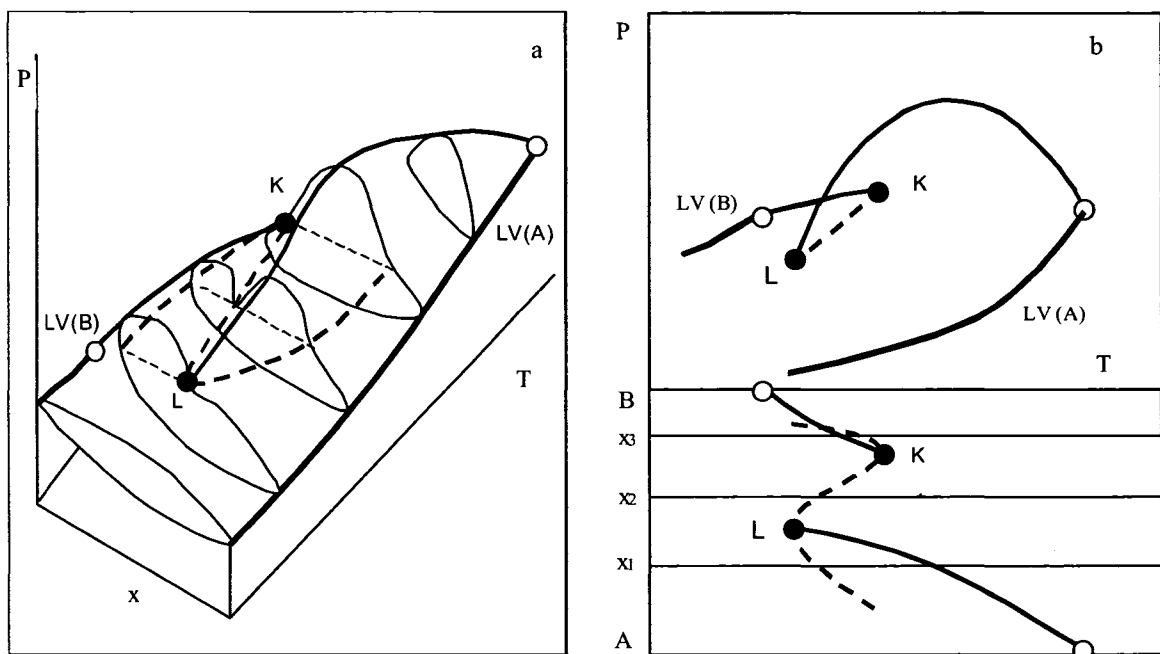
Figure 2.19 Schematic Type V phase behaviour for a binary system. a: PTx three-dimensions; b: PT and Tx projections of the PTx three-dimensions

Figure 2.20a, b, c show the phase behaviour at mole fraction x1, x2, x3 as indicated in Figure 2.19b, where x is the mole fraction of heavy component (A) and x1>x2>x3. For

42

the highest concentration of the heavy component, x1, the three phase curve starts at the point where the line x1=constant intersects the L2 branch of the L1L2V curve and ends at the K point. In this case only part of the L1L2V curve can be observed. For the mole fraction x2 the whole L1L2V curve can be seen, which begins from L point to K point with a point where the line x2=constant intersects the L1 branch separating it into two parts and for the mole fraction x3 a part of the L1L2V curve can be seen, which starts at the point where the line x3=constant intersects the V branch of the L1L2V curve and ends at the L point. Addition of a third component to this binary mixture increases the number of degrees of freedom by one, and thus expands the three-phase phase behaviours from curves to regions in the PT section as shown in Figure 2.20, i.e. from 2.20a to 2.20d, 2.20b to 2.20e, and 2.20c to 2.20f respectively. LLV three phase regions can make an important phenomenon occur in reservoir engineering, so-called unusual retrograde condensation (Shaw et. al, 1993), i.e. retrograde condensation of heavy liquid (L2) in the three-phase region. In Figure 2.20f, as pressure is increased at fixed temperature, one can observe sequences such as V→ L1 + V → L1+ L2 +V→ L1 + V →V (D.B. Robinson, 1989) and in Figure 2.20e, another sequence like V→ L1 + V → L1+ L2 +V→ L1 + V → L1 (Gregorowicz et al. 1993). These findings among others are of great significance in solving industrial problems and in developing new industrial processes.
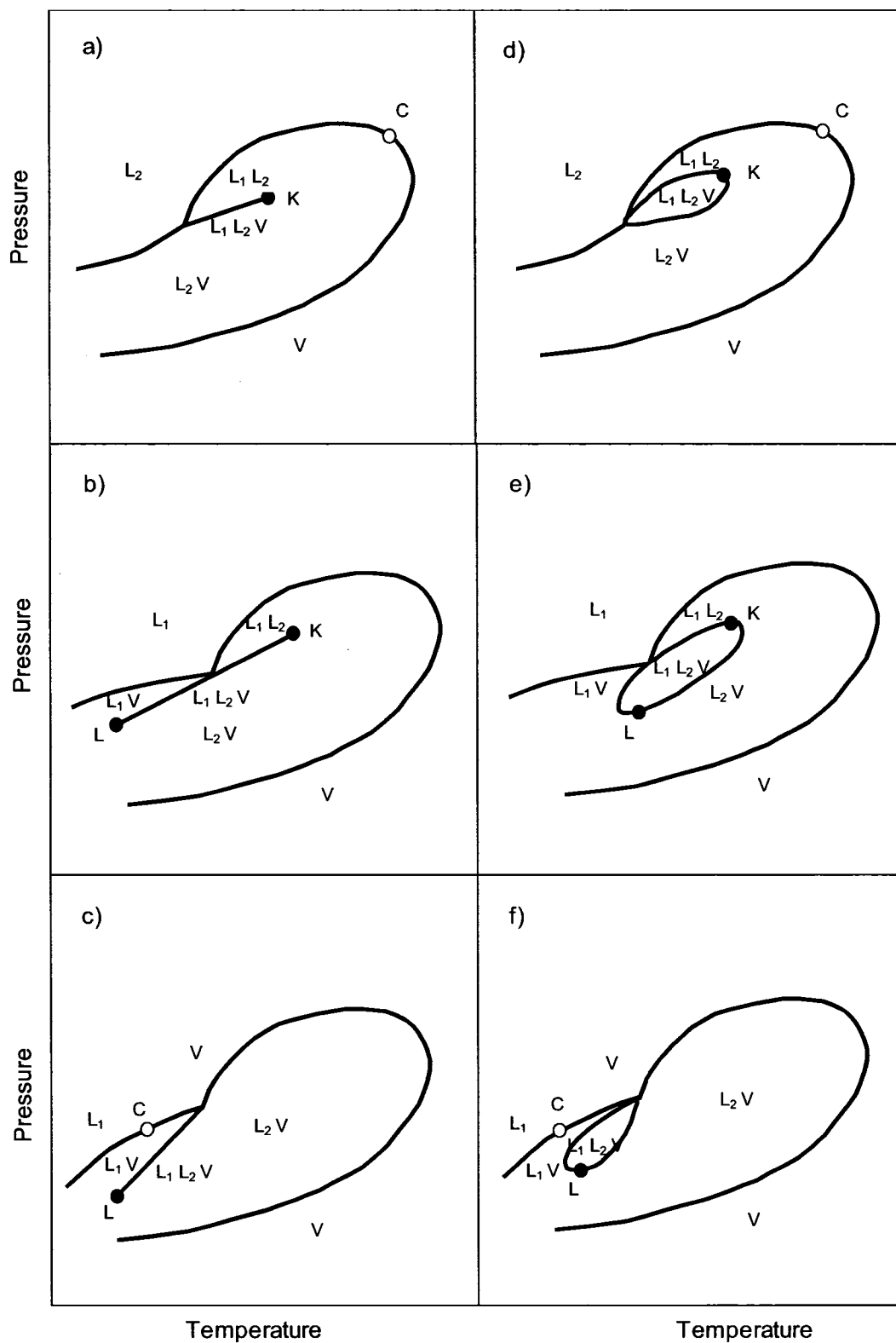
Figure 2.20   Expansion of P-T diagrams of Type V phase behaviour from binary mixtures to ternary mixtures

2.4.2.4 Pseudocomponents and Their Multiphase Behaviour in Oil Industry

The phase behaviour exhibited in oil industry is very useful to exploit process development and design. But the demonstration of phase diagram for oil systems is not as easy as for defined components. For crude oil and bitumen, the number of components is far too great to uniquely identify each of them. So the general approach is to simplify phase behaviour representations by grouping components with similar behaviour together in terms of their normal boiling point, molecular weight and/ or density at standard conditions into hypothetical or pseudo-components.

At constant composition for undefined systems, the construction of P-T phase diagrams (Radosz, 1987) is the same as described for defined systems without concerns about the pseudocomponent definition. But the construction of phase diagrams in terms of composition must be based on the pseudocomponent determination. According to the properties of systems investigated and the purposes of the phase diagrams, the system investigated may be defined as pseudo-binary system (Radosz, 1987; Pollack and Enick, 1988), pseudo-ternary system (Wilson et al., 1936), and even pseudo-quaternary system (Shaw, 2002).

Pseudo-binary phase diagrams in the form of pressure-composition (P-x) are often utilized to illustrate the phase behaviour of oil mixture + light solvents. In such a diagram, the oil mixture is defined as a single pseudocomponent. Due to the asymmetry of such system, phase diagrams for such systems have often been found to exhibit multiple phase behaviour at temperature and pressures near the critical point of the solvent. One example is the P-x phase diagram of a solvent (CO_2) + crude oil system at constant temperature (Figure 2.21). In this diagram the LLV three phase region is bounded by a lower liquid-vapor region (L2V) and an upper liquid-liquid region (L1L2) and a K point exists on the three phase boundary at the intersection of L1L2 region and L2V region. Even though the phase diagram is expressed in terms of composition, it is still difficult to indicate the composition in each phase of LLV region.

45
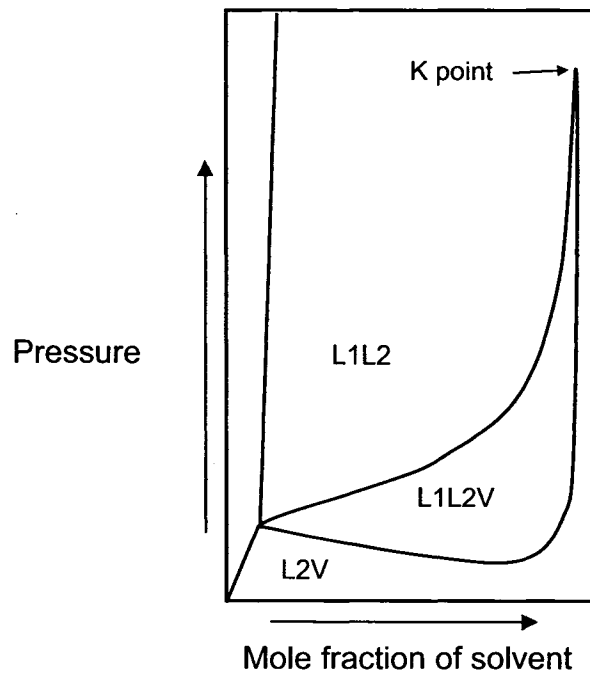
Figure 2.21   P-x phase diagram of a solvent (CO₂) + crude oil system (Pollack and Enick, 1988)

Usually the components in oil mixture cover over a wide range of molecular weight and size. Sometimes it is inconvenient to illustrate the phase behaviour and phase diagrams by considering the whole oil mixture as only one pseudocomponent. To give a fairly clear picture of the rather complex behaviour of some oil systems, the separation of the oil mixture into two or three pseudocomponents sometimes seem more reasonable and illustrative. For example, a ternary phase diagram will be more helpful for understanding the propane deasphalting process in which the asphalt is removed from the oil mixture by addition of a solvent, that is, propane. Figure 2.22 is the ternary phase diagrams showing the multiphase behaviour in which propane, oil, and asphalt are considered to be three single components. In this diagram the LLV three-phase region is bounded by two liquid-vapor regions (L1V and L2V) and one liquid-liquid region (L1L2). The region enclosed by a triangle represents a three-phase zone. The compositions of these three phases are fixed and represented by the three vertexes of the triangle, respectively. The relative amount of each coexisting phase is determined from the mass balances. A more detailed

46

description of the pseudo ternary phase diagram for such system can be found in the paper published by Wilson et al. (1936).
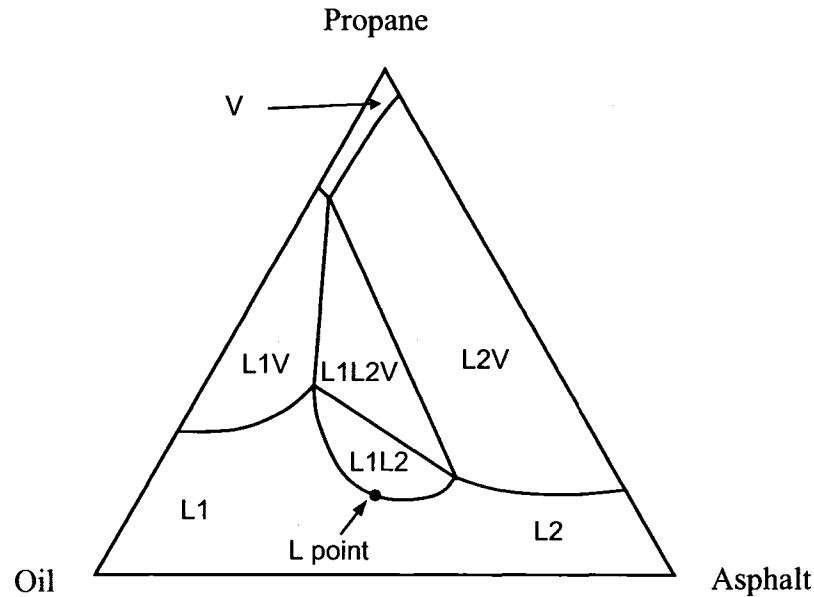
Figure 2.22   Ternary phase behaviour of the asphalt-oil-propane mixture at a temperature close to the critical temperature of propane (Wilson, Keith and Haylett, 1936).

Equilateral pyramids with a triangular base are widely used as phase diagrams for quaternary or pseudo quaternary mixtures at fixed temperature and pressure. Recently Shaw (2002) discussed the possibilities and necessities of using pyramid diagrams as shown in Figure 2.23 to describe the complex behaviour of asphaltene containing heavy oil mixtures. Asphaltene containing heavy oil mixtures may be lumped into four pseudo components, i.e., light gases, oil I, oil II, and asphaltenes, which are designated as the apexes of the pyramid. This four pseudocomponents lumping method unify the lumping methods of two or three pseudo components employed in the literature. For reservoir fluids, the typical scheme is to construct ternary diagrams using the pseudocomponents light gases, maltenes and asphaltenes at fixed temperature and pressure. For bitumen and heavy oil systems, the light components are typically ignored and one encounters pseudo

47

binary and more typically ternary diagrams where the composition variables are asphaltenes, and one or two oil fractions.
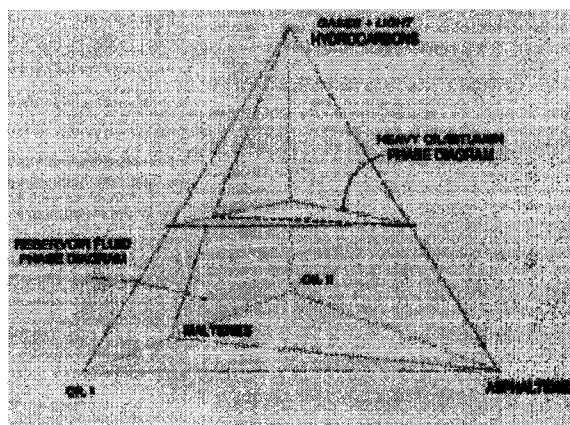
Figure 2.23 Generalized phase diagram at constant temperature and pressure for reservoir fluids, and heavy oil and bitumen + diluent mixtures.

2.4.3 The Role of Phase Behaviour in Thermal Cracking

2.4.3.1 Liquid-Liquid Phase Separation Coke Formation Mechanism

Coke formation during the thermal treatment of petroleum residue is postulated to occur by a mechanism that involves liquid-liquid phase separation. This is accepted by most researchers (Wiehe, 1993; Li et al., 1999; Rahmani, 2003). The initial reactions in the coking of petroleum feedstocks involve the thermolysis of large aromatic-alkyl molecules to produce volatile species (paraffins and olefins) and non-volatile species (primarily aromatics). In addition, the formation of liquid hydrocarbon products creates regions of instability causing the highly aromatic and highly polar refractory products to separate from the surrounding oil medium as an insoluble phase and proceed to form coke. This concept of co-existence of two liquid phases at reaction condition has been suggested by Dukhedin-Lalla, et al. in 1989. And the existence of two liquid phases was justified by their experimental data. A schematic representation of coke formation is shown in Figure 2.24 (Speight, 1998 and 1999). A similar schematic representation of coke formation was

48

proposed by Gray and Masliyah (2004), but exhibited by a reaction route of a large model compound.

This mechanism can be satisfactorily utilized to elucidate kinetic phenomena. Many investigators (Takatsuka et al., 1989; Sasaki et al., 1993) have experimentally observed an induction period before coke formation. But they did not include this step in their kinectic models for coke formation. A detailed description about coke formation from petroleum residua was given by Wiehe (1993). Aspaltenes in petroleum residua cracks to form asphaltene cores which are primarily aromatics. These asphaltene cores are unreactive as long as they remain dissolved in heptane solubles that provide abstractable hydrogen. As the conversion is increased, the asphaltene core concentration increases and the non-volatile heptane solubles concentration decreases until the solubility limit of asphaltene cores in heptane solubles is exceeded. At that point asphaltene cores separate to form a second liquid phase that is lean in abstractable hydrogen. The asphaltene cores in the second liquid phase are cracked off non-volatile heptane-soluble fragments and then recombine to form toluene-insoluble, solid coke. From this mechanism, one may conclude that the induction period can be considered as the time the residuum thermolysis takes before phase separation occurs.
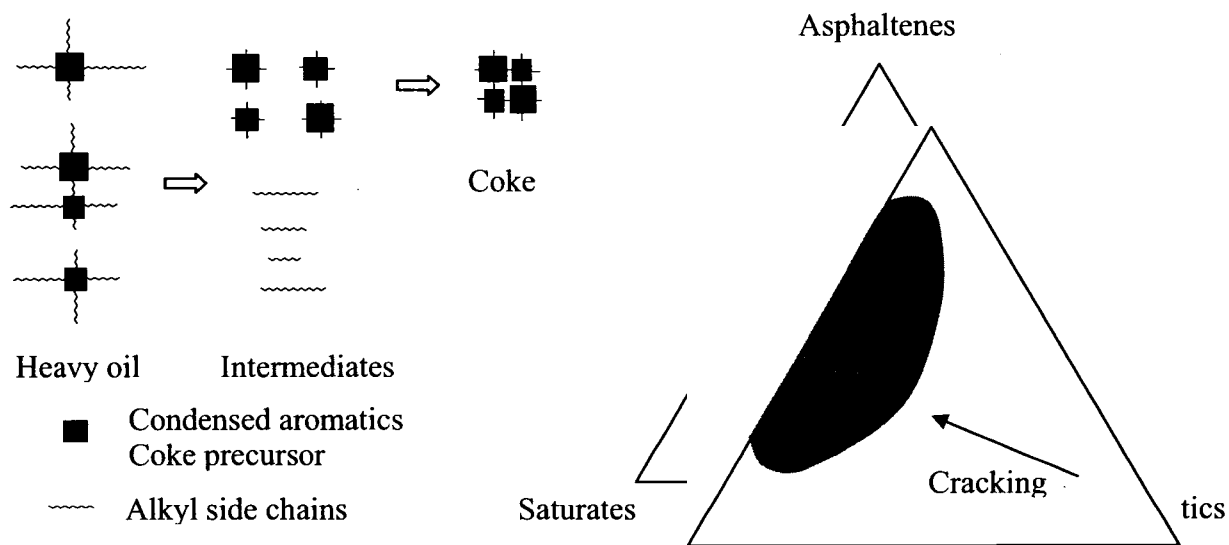
Figure 2.24 Schematic representation of coke formation

49

Weihe also summarizes four common features of residuum conversion kinetics: an induction period prior to coke formation; a maximum concentration of asphaltene at the end of induction period; an approach to a constant ratio of the concentration of asphaltenes to the concentration of non-volatile heptane solubles at long reaction times; the high reactivity of the unconverted asphaltenes. Based on the above mechanism, a kinetic model (from Equation 2-9 to 2-13) was proposed in which an infinite reaction rate for this coke-forming reaction is used to show that this reaction rate is phase equilibrium controlled. So a detailed investigation in the phase equilibrium of petroleum residuum thermolysis processes is very useful to understand the whole process and improve kinetic models.

$$H^+ \xrightarrow{\ K_H\ } aA^* + (1-a)V \tag{2-9}$$

$$A^+ \xrightarrow{\ K_A\ } mA^* + nH^* + (1-m-n)V \tag{2-10}$$

$$A^*_{max} = S_L(H^+ + H^*) \tag{2-11}$$

$$A^*_{ex} = A^* - A^*_{max} \tag{2-12}$$

$$A^*_{ex} \xrightarrow{\ \infty\ } (1-y)TI + yH^* \tag{2-13}$$
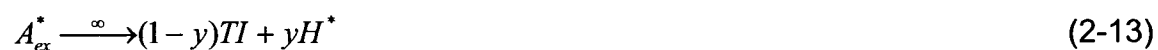
where A^+ is reactant asphaltenes; A^*, asphaltene cores; A^*_{max}, maximum asphaltene cores that can be held in solution; A^*_{ex}, excess asphaltene cores beyond what can be held in solution; H^+, reactant, non-volatile heptane solubles; H^*, product, non-volatile heptane solubles; TI, toluene-insoluble coke; and V, volatiles.

For coking processes such as delayed coking, fluid coking, flexicoking, coke is accepted as a solid by-product in order to allow for higher conversion of feedstock to distillate liquid products. As analyzed above, a second liquid phase is developed just before the coke is formed. Contrary to coking processes, visbreaking process does not accept coke formation, so the conversion has to be held below the onset of phase separation, in another word, conversion time within the induction period.

50

2.4.3.2 Impact of Phase Behaviour on Coke Formation

For delayed coking, the impact of the phase behaviour on the amount of coke produced has been investigated and a relationship between coke yield and phase behaviour was established (Ali, 2002). Under coking conditions, phase behaviour has a dramatic effect on coke yield. With small changes in composition at fixed temperature and pressure, coke yields can be halved or doubled. The dramatic coke yield change is caused by phase behaviour transition from one phase behaviour to another. Low coke yields are expected to be produced in L_1, L_1V region zones, intermediate coke yields in L_1L_2, L_1L_2V zones and high coke yields in L_2, L_2V zones. The study of coke formation in thermal processing of heavy oils has been reported by many researchers (Wiehe, 1992, 1993, 1994; Li et al., 1999; Rahmani et al., 2003) and these works show that phase behaviour plays an important role in coke yield during thermal upgrading of heavy oils.

2.4.4 The Role of Phase Behaviour in Hydroprocessing

2.4.4.1 Phase Behaviour in Heavy Oil Hydroprocessing

There exist difficulties to observe phase behaviour of opaque heavy oil systems, so few multiphase equilibrium data are available for such system in the literature. The X-ray view-cell technique allows one to observe the phase behaviour of opaque mixtures, such as heavy oils, bitumen, etc. Abedi et al. (1998) observed L_1L_2V phase behaviour in a model heavy oil system at elevated temperatures in the presence of hydrogen (Figure 2.25). They also observed that a solid phase separated from the heavy liquid phase L_2 irreversibly at temperatures greater than ~ 650 K. This solid phase did not separate from the light liquid phase L_1 even at temperatures up to 700 K. In their work, non-reacting or non-catalyzed systems were examined. Up to now, no direct experimental observation of LL phase separation during the hydroprocessing of heavy oil has been reported.

Gray (1994) hypothesized and depicted the phase behaviour in hydroprocessing of heavy residue in terms of a ternary composition phase diagram with light component, middle distillates and heavy resids as three pseudocomponents (Figure 1.3). This ternary phase diagram indicates an immiscible region with two liquid phases exists at the typical

operating conditions. In fixed bed reactors, a liquid phase that was initially homogeneous at the reactor inlet could develop a second liquid phase as the reactions progress. Phase splitting would be most likely to occur at high conversion levels, where some heavy fractions become chemically dissimilar from the bulk composition of the oil. In batch hydroprocessing reactors, one scenario that can arise is that at the beginning feed falls in an L_1V region. As conversion increases, the mixture may shifts to an L_1L_2V region. One would expect coke deposition to increase along the bed length. For CSTR/slurry bed operation the reactors may operate in L1L2V region or L1V region depending on the conversion rate. The L_2 phase is a heavy liquid that has relatively larger concentrations of polar compounds and condensed ring compounds; L_1 phase is a light liquid that has relatively larger concentrations of saturated and non-polar compounds. The hydrogen solubility in L_2 phase would be much lower than in L_1 phase (Dukhedin-Lalla et al., 1989; Shaw, 1987; Shaw et al., 1988), thereby leading to poorer hydrogen transfer and an increase in condensation and aromatization reactions and rapid coke formation within the reactor.
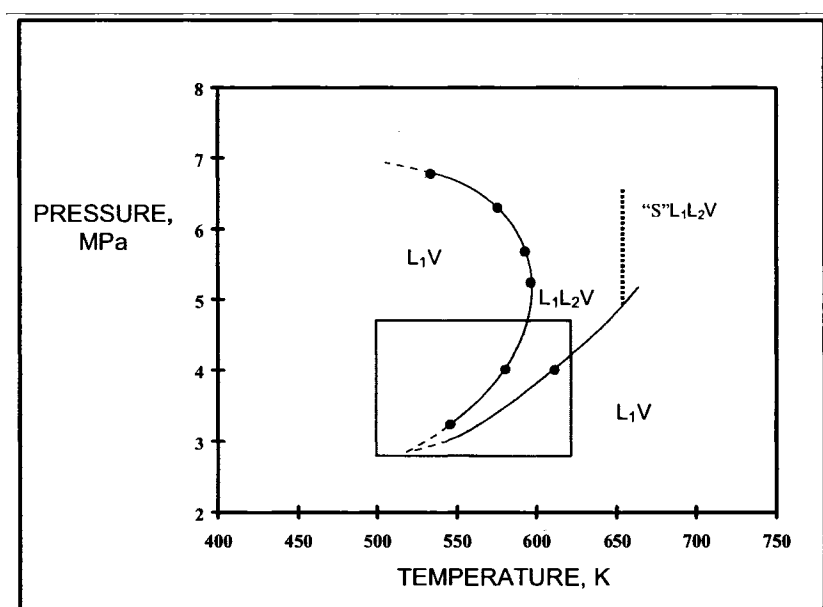
Figure 2.25   Partial phase diagram for the model heavy oil ABVB 25 wt % + dodecane 73 wt % + hydrogen 2 wt %.

52

2.4.4.2 Coke Deposition Mechanism Involving Phase Separation

Phase separation may also occur in hydroprocessing of heavy oil (Ternan et al., 1994), which is supposed to affect coke formation on catalyst. A detailed reaction mechanism (Figure 2.26) in hydrogenation environment was reported by Ternan et al. in 1994. At reaction condition, there exist two liquid phases in the reactor. One phase is polar liquid that has relatively larger concentrations of polar compounds and condensed ring compounds, plus a comparatively smaller solubility of hydrogen. The other phase, a non-polar liquid, has relatively larger concentrations of both naphthenic compounds and hydroaromatic compounds, plus a comparatively larger hydrogen concentration. Since hydrogen has greater solubility in the nonpolar phase (Cai et al., 2001), it is more likely that molecules in that phase ($(CM)_{np}$) will be hydrogenated (HYD) and subsequently cracked (CRACK) to form distillable liquids and gases. The same molecule in the polar phase ($(CM)_p$) would not have as much hydrogen available. Either no reaction or dehydrogenation (DEHYD) via hydrogen-transfer reactions should occur. This could be followed by condensation (CONDENS) reactions to form larger carbonaceous molecules, eventually coke. A similar description related to phase separation in hydroprocessing was published by Gray (1994). This is also consistent with the studies by Wiehe (1992, 1993) on coke formation due to phase separation. But catalytic reactions make this process more difficult to model. Unlike Wiehe (1993), Ternan did not build a kinetic model that describes the reaction and phase separation.
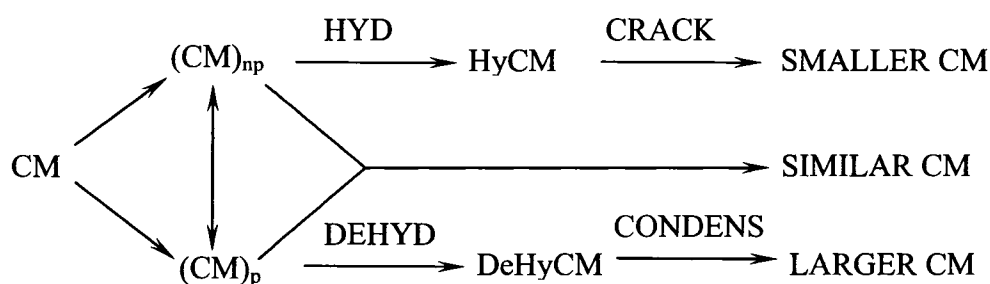
Figure 2.26   Residuum Hydrocracking Reaction Mechanism

2.4.5 Coke Formation Mechanism Involving Colloidal Phenomena

As discussed above, the phase separation is caused by asphaltenes exceeding the solubility limit of the oil as reactions proceed, while the formation of asphaltene rich phases discussed by Storm et al. (1995; 1996; 1998) is purely physical – flocculation and precipitation. It has been concluded that heavy oils such as crude oils, residues, bitumen etc. exhibit colloidal behaviour in the presence of asphaltenes, and resin fractions (Li et al. 1996; Bardon et al. 1996; Branco et al. 2001). The asphaltenes are believed to exist in heavy oils partly dissolved and partly in steric-colloidal and/or micellar forms depending on the polarity of their oil medium and presence of other compounds (Priyanto et al. 2001). But asphaltenes and heavier species can precipitate from the oil matrix if the colloid stability of the feed cannot be maintained. Storm et al. (1995; 1996; 1998) observed that asphaltenes could flocculate and precipitate to form another asphaltenic phase at elevated temperature even well below the temperature at which chemical reactions occur. They suggested that the asphaltenic phase is the precursor to the coke-producing phase in the reacting residue. Under catalytic hydroprocessing conditions, this colloidal structure is more likely disrupted and asphaltenes and heavier species can precipitate on the catalyst surface because of instabilities caused by thermal and hydrogenation reactions, which may enhance coke formation (Furimsky and Massoth, 1999). The incompatibility is partly due to the competing thermal and catalytic reactions, but mainly due to the difference in the reactivity of the components of the residual oil, namely, oils, resins, and asphaltens (Matsushita et al. 2004). Under such conditions, the naphthenic groups and alkyl side chains in the asphaltene molecules will be cracked off. The remaining polynuclear aromatic core of the asphaltene molecules will be less soluble in the oil medium since the resins, which act as a solubilizing agent, are also hydrogenated and cracked in the process. The cracking rate of resins is faster than the asphaltenes. All of these cause the asphaltenes sedimentation, which enhances coke deposition on the catalyst. The instability of hydrotreated heavy oil products was recently proved using a flocculation onset titration method (Bartholdy et al. 2000; 2001).

54

2.5 Summary

With the depletion of conventional crude oils, the rocketing rise of petroleum price, and more and more stringent environmental regulations, refiners must convert the "bottom of barrel" into "light, clean fuels". Consequently, heavy oil hydroprocessing plays an increasingly key role as a primary upgrading process. Diverse processes are in industrial use or nearing commercialization. In all cases, catalyst fouling is a major concern. Considerable effort has been devoted to this research area. Although significant progress has been made, many issues are still debated in the literature. There is no general agreement on coke deposition modes, coke deposition mechanisms and related issues from industrial perspectives and more effort needs to be devoted to the study of coke deposition. Some observed phenomena such as irregular coke deposition profiles, coke suppression by addition of solvents, indicate that phase behaviour may be an important factor influencing coke deposition. But many of the following questions regarding this area have not been answered in the literature. Does a second liquid phase exist or develop under typical hydroprocessing conditions and does resid conversion extent affect the nature of the phase behaviour? What is the impact of phase behaviour on coke deposition both with respect to coke content and coke deposition modes? How does phase behaviour affect coke deposition through the significant difference in properties of the co-existing phases? Due to prior experimental technique limitations, there is no direct proof of the role played by phase behaviour in the literature. The experimental technique employed in this study and the planned experiments are expected to provide significant insights into the research on coke deposition in catalytic heavy oil hydroprocessing.

55

3. Experimental

3.1 Materials

Athabasca vacuum bottoms, ABVB, is the 525 °C + boiling fraction of Athabasca Bitumen, and was supplied by CANMET. A detailed composition analysis and physical properties for ABVB are listed in Table 3.1. The chemicals used in this project and their grade, purity and suppliers are given in Table 3.2. The catalyst, commercialized for ebullated-bed hydrogenation reactors, is a 1 mm diameter cylindrical extrudate NiMo/γ-Al$_2$O$_3$ catalyst with 10 to 15 wt % MoO$_3$ and 2 to 4 wt % NiO. The catalyst has a BET surface area of 220 m^2/g, and a pore volume of 0.59 cm^3/g. The sulfidized catalyst has a BET surface area of 179 m^2/g and a pore volume of 0.55 cm^3/g. The pore size distribution of this catalyst in oxide and sulphide form is shown in Figure 3.1 and the sorption isotherm for this catalyst is shown in Figure 3.2.

Table 3.1   Physical and chemical properties of ABVB (Zou, 2003)

Density, g/cm^3	1.045
Saturates, wt%	6.80
Aromatics, wt%	41.99
Resins, wt%	19.04
Asphaltenes, wt%	32.18
Carbon, wt%	81.66
Hydrogen, wt%	9.54
Sulfur, wt%	6.87
Nitrogen, wt%	0.65
Nickel, ppm	137
Vanadium, ppm	344

56

Table 3.2 Chemicals used and their purity, suppliers.

Chemicals	Grade purity	Supplier
Hydrogen	Research, 99.999 %	Praxair
Nitrogen	Research, 99.998 %	Praxair
n-Decane	Research, 99.5 + %	Aldrich
n-Dodecane	Research, 99.5 + %	Aldrich
1-Methylnaphthalene	Research, 97 + %	Fluka
Carbon Disulfide	Research, 99.8 + %	Aldrich
Toluene	Research, 99.9 + %	Aldrich
Tetrahydrofuran	Research, 99.9 + %	Aldrich
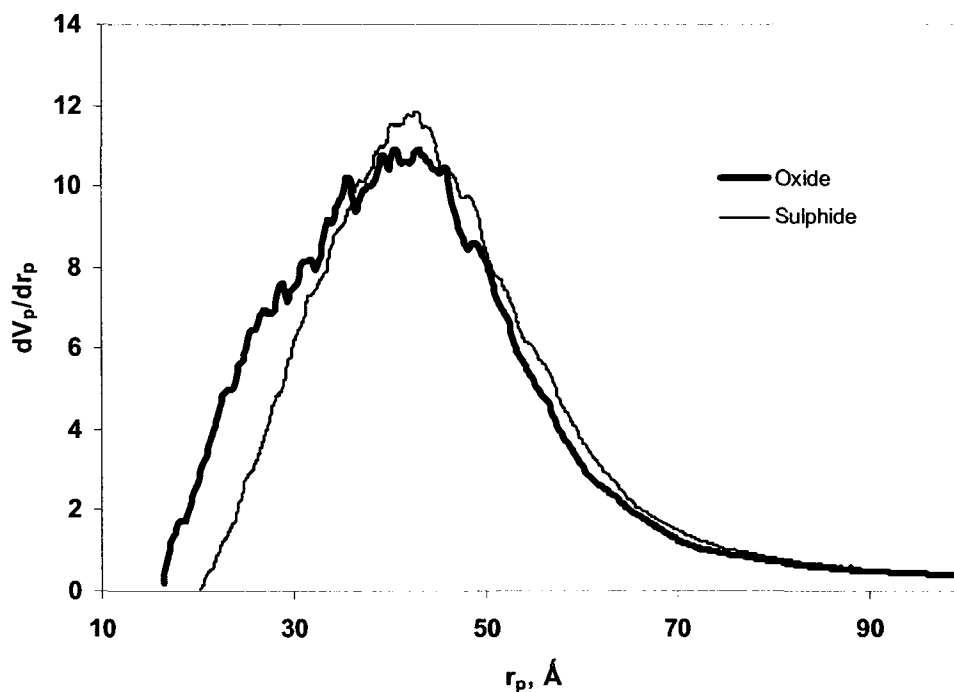
Figure 3.1 Pore size distribution of catalyst

57
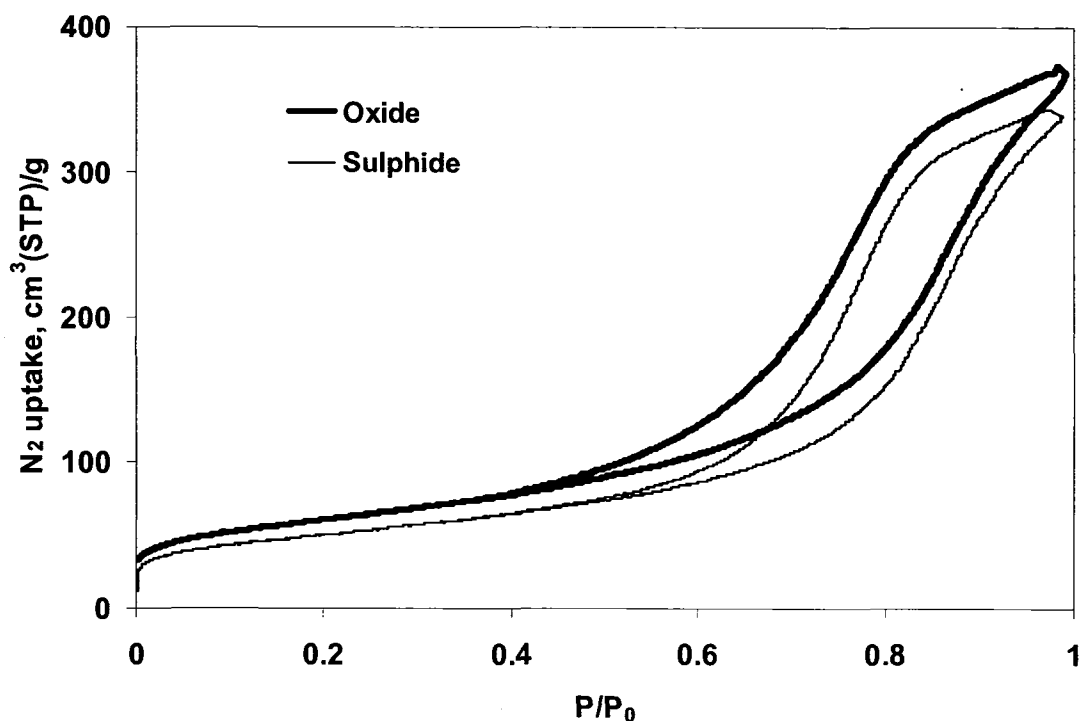
Figure 3.2 Isotherms of catalyst

3.2 X-ray View Cell

3.2.1 Experimental Set-up

The general experimental set-up and basic components of the X-ray view cell (Figure 3.3) used in this study are the same as those reported by Abedi, 1998 and a detailed description of this equipment is available elsewhere (Dukhedin-Lalla, 1996 and Abedi, 1998, Zou, 2003). Only a brief introduction of the arrangement of X-ray view cell is described here. A high voltage power supply is connected to Phillips MCN-165, tungsten-target bremsstrahlung X-ray gun with spectral endpoint energies between 5 and 160 keV. X-rays, stimulated by high voltage, are emitted from the X-ray tube gun. Since the view cell is made of beryllium, a metal relatively transparent to X-rays, X-rays are partially transmitted through the view cell. The transmitted X-rays are then directed to the image intensifier located just behind the view cell where the X-rays can be amplified and converted to an optical image. The optical image is then captured by a camera connected

58

to a live video monitor. The optical image can also be recorded by "frame grabber" software as a digital image for further image analysis and intensity measurement. The view cell is fitted with a stainless steel bellows attached to the top cap of the view cell and the internal volume of the view cell can be reduced by expanding the bellows, permitting investigation of a wide range of pressures at fixed temperatures. The view cell can be operated from vacuum to 27.5 MPa and from room temperature to 725 K, covering most of the reservoir and refining conditions. This technology can give rich and valuable information such as the number of phases present, their individual volumes, densities and elemental compositions without sampling for opaque heavy oil systems, for which visible light view cell technologies are not applicable.
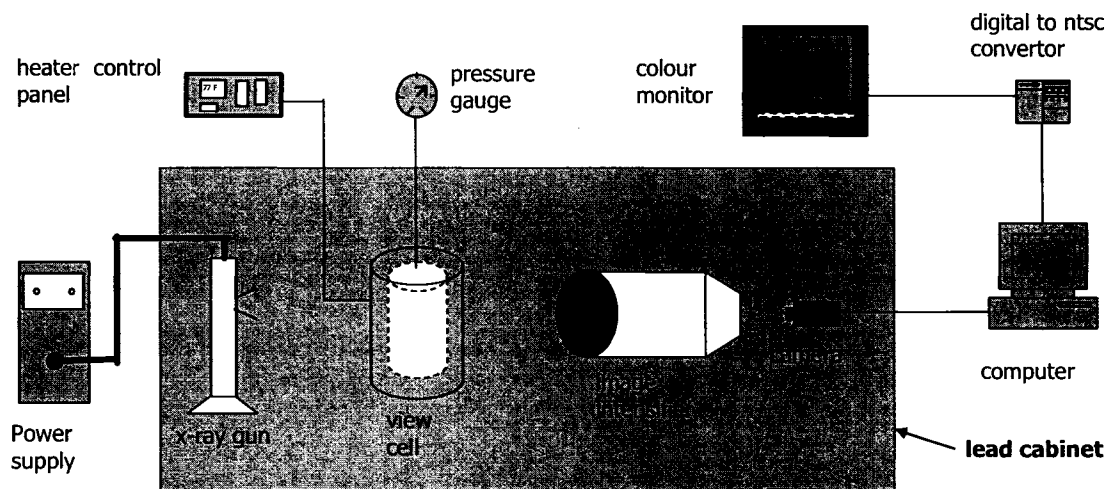
Figure 3.3   Schematics of X-ray view cell

3.2.2 Working Principles

On passing through a medium, X-ray beams may lose energy by photoelectric absorption and scattering by elements. The sum of photoelectric absorption and scattering by elements is often called X-ray absorption or attenuation. Phase behaviour investigation is based on the X-ray absorption or attenuation phenomena, which is also widely used in other radiographic technologies, such as for chest X-rays. The amount of absorption of the X-ray beam provides information about the sample regarding its composition,

59

homogeneity, and thickness or density. As shown in Figure 3.4, when a monochromatic beam of X-rays with wavelength λ and intensity I_0 falls onto an homogeneous medium with density ρ and thickness x, only a fraction (I/I_0) of the X-ray beam passes through the medium due to the absorption of X-rays by the medium. The balance is absorbed. The absorption is governed by

$$I(\lambda) = I_0(\lambda)e^{-\rho x \mu(\lambda)}$$

(3.1)

where μ is the mass absorption coefficient of the medium. The mass absorption coefficient depends on the elemental composition and the wavelength of the X-ray beam. For a chemical compound, a solution or a mixture, the mass absorption coefficient is simply the weighted average of the mass absorption coefficients of its constituent elements:

$$\mu(\lambda) = \sum_{i=1}^{n} \mu_i(\lambda)w_i$$

(3.2)

where w_i is the mass fraction of element i and $\mu_i(\lambda)$ is the mass absorption coefficient of element i at wavelength λ and n is the number of elements.

If the X-ray beam is polychromatic instead of monochromatic, the intensity of transmitted X-rays (I) is the sum over all wavelengths:

$$\sum_j I(\lambda_j) = \sum_j I_0(\lambda_j)\exp[-\rho x \sum_{i=1}^{n} w_i \mu_{ij}(\lambda_j)]$$

(3.3)

where $\mu_{ij}(\lambda_j)$ is the mass absorption coefficient of element i at wavelength λ_j.

Equation 3.3 is applied when composition analysis is required, but it is complex to apply for routine experiments as multiple excitation voltages must be applied, etc. For other applications, equation 3.3 can be simplified.

60

X

Incidental X-rays

$I_0(\lambda)$

Other photons
(photoelectric effect)

Transmitted X-rays

$I(\lambda)$

, μ

Coherent and incoherent
scattering
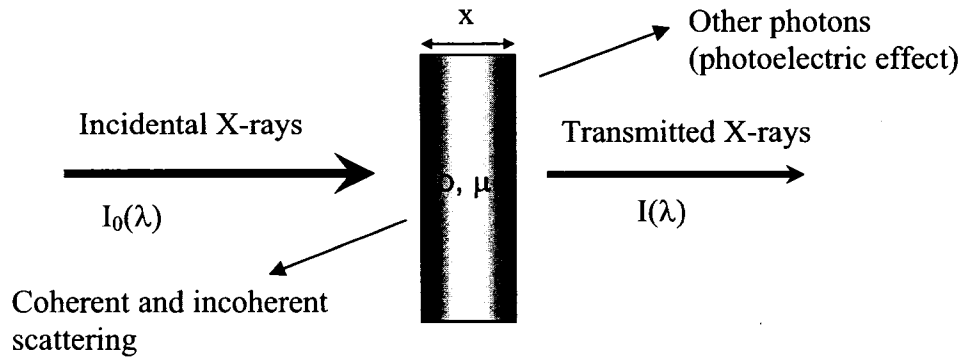
Figure 3.4   Schematic of X-ray absorption

As the number of the wavelengths emitted by the tungsten filament is large, the wavelength distribution can be approximated as continuous. Consequently the mass absorption coefficients can also be approximated as a continuous distribution and an effective wavelength concept is introduced to simplify equation 3.3. The effective wavelength (λ_e) of a polychromatic X-ray beam is defined as the wavelength of a monochromatic beam which has an equivalent behaviour in an absorption measurement. By introducing the effective wavelength concept, equation 3.3 becomes:

$$I(\lambda_e) = I_0(\lambda_e)\exp[-\rho x \sum_{i=1}^{n} w_i \mu_i(\lambda_e)]$$

(3.4)

Both the intensities of transmitted and incidental X-rays can be obtained from X-ray images. The mass absorption coefficient varies with the atomic number of elements present and X-ray wavelength and for a pure element,

$$\mu(\lambda) \approx k\lambda^{2.83}$$

(3.5)

where k is a constant. The wavelength is directly related to the energy of X-ray photons (E):

$$\lambda(nm) = \frac{1.24}{E(keV)}$$

(3.6)

61

Experimental absorption coefficient data can be found in literature (de Bore, 1989). The unknowns in equation 3.4 are density and elemental composition, which could be obtained if transmitted X-ray images at different excitation conditions are available.

In this study, the elemental composition of each phase is not obtainable due to X-ray scattering by asphaltene particles (Zou, 2003). Only an apparent fluid density is obtained. A detailed deconvolution procedure for transmitted X-ray images used to calculate the apparent density is presented in Zou's thesis (2003). The same procedure is applied in this study. The accuracy of density measurement for light hydrocarbons is ± 12 kg/m^3.

The phase volumes can be simply obtained by determining the interface heights and bellows positions with the aid of a cell volume calibration. Volume calibration is taken from Zou's thesis (2003). The minimum detectable volume is 0.61 ml and the minimum detectable volume difference is 0.12 ml - equivalent to the height of one pixel.

3.2.3 Illustration of a Single X-ray Transmission Image

From equation 3.1, the intensity of an X-ray transmission video image decreases exponentially with density. Higher density materials appear darker since more X-rays are absorbed or scattered, while lower density materials appear lighter since more X-rays pass through. Figure 3.5 is an example of X-ray transmission image. This single image was recorded at 360 °C and 24.26 bar for the 10% ABVB + decane mixture. Based on visual observation, this image shows LLV phase behaviour. In this image, the bellows is pulled back to the top of the view cell. The lower density liquid phase (L1) is represented by the middle grey area. The vapour phase, represented by the light grey area, is above, and the higher density liquid phase (L2), represented by the darker area, is below. From images like this, it is easy to discern the existence of separate phases, the relative amount of each phase, and the direction a phase boundary moves with changing process conditions. This real-time, qualitative information is useful when attempting to determine the type of phase behaviour a system exhibits. One can also process the images to provide the quantitative information of a system, such as phase volume, and density. The intensity and density profiles for the image shown in Figure 3.5 are shown in Figure 3.6. Even though the intensity profile is not flat across a single phase, the density profile after

62

calibration is flat. The final density for each phase is calculated by averaging the density profile across each phase. In order to calculate the volume for each phase, the phase boundary must be determined first. The numbers shown on the intensity-pixel plot are the pixel position labelling the phase boundaries and bellows position. Then, the phase volumes can be simply calculated with the aid of volume calibration curve.
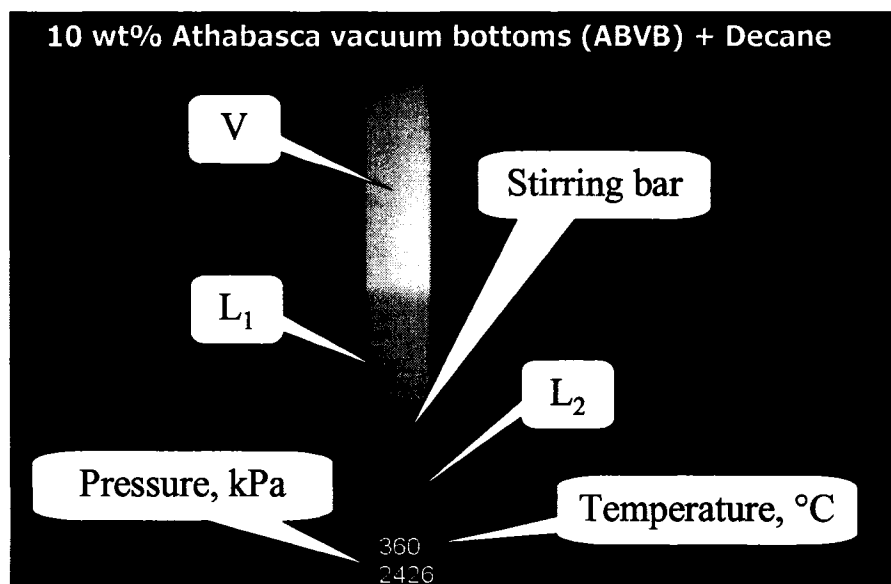
Figure 3.5 Illustration using a single X-ray transmission image

3.2.4 Flow Diagram

The flow diagram used in this study is shown in Figure 3.7. The equipment and plumbing connections were designed and built to facilitate leak testing, protection of the bellows, and safety.

63
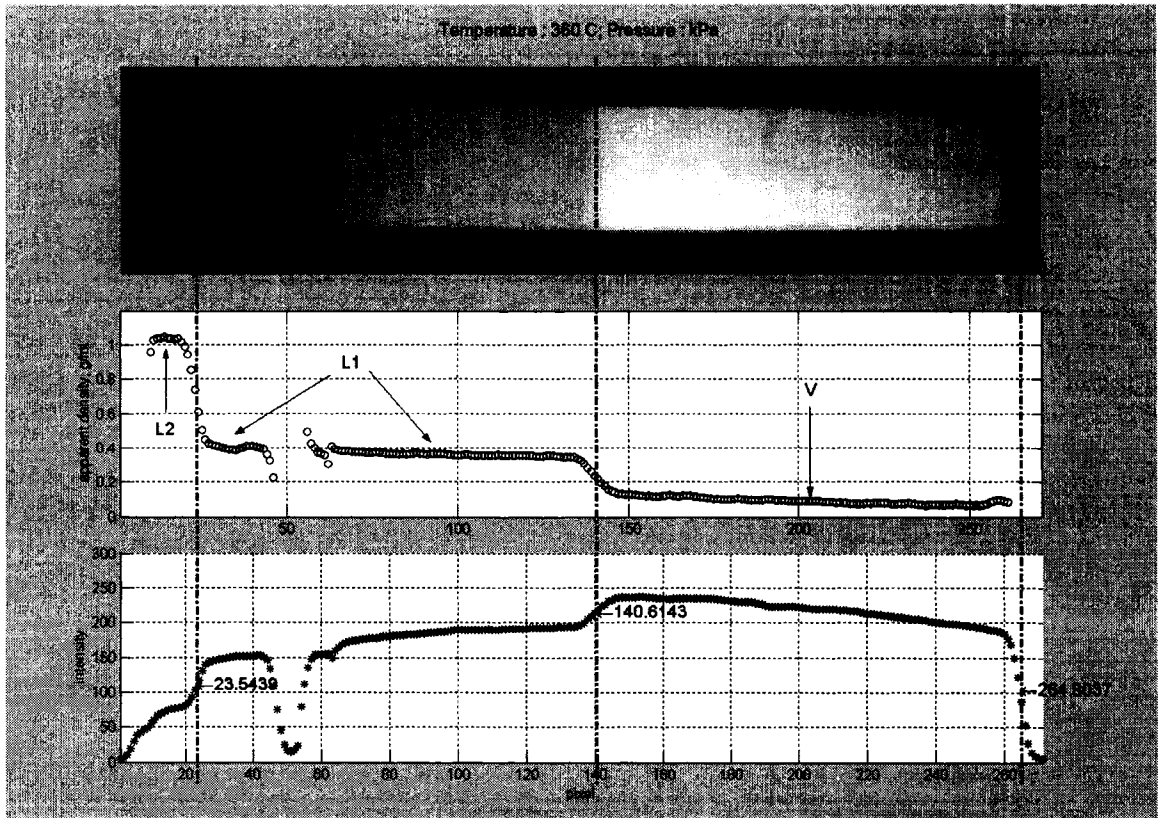
Figure 3.6 Intensity and density profile corresponding to the single X-ray image in
Figure 3.5
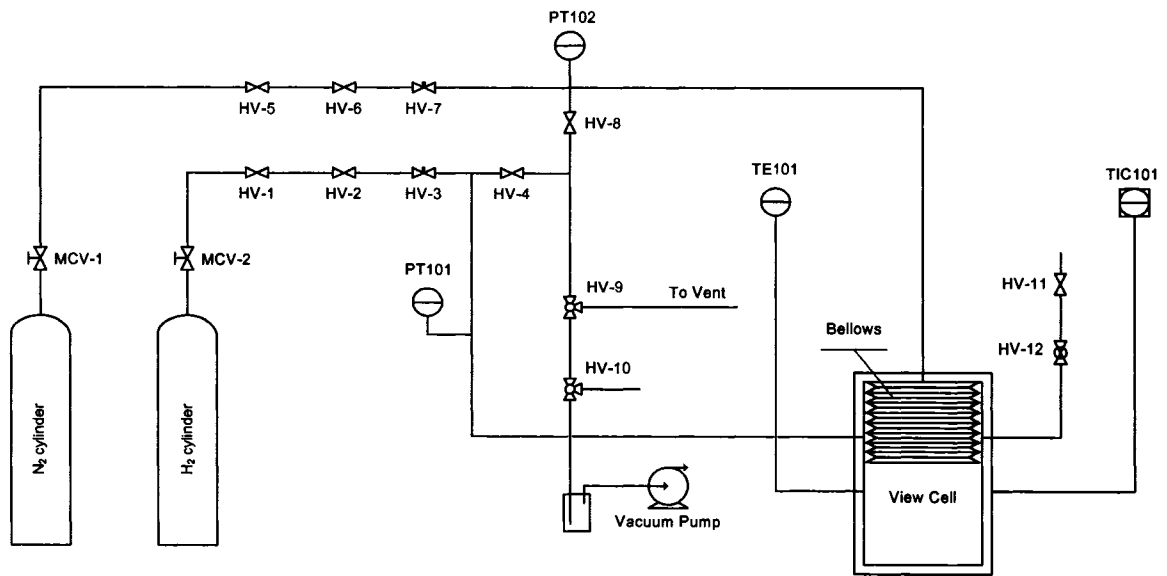
Figure 3.7 View cell flow diagram

3.3 The Selection of Model Fluid System

The objective of this project is to test the impact of various phase behaviour regimes on catalyst coking. The first priority was to identify a model system which exhibits multiphase behaviour. From a phase behaviour prospective, light alkanes + ABVB (Athabasca Bitumen Vacuum Bottom) mixtures are highly asymmetric since asphaltenes in ABVB are much larger than light alkanes and possess different polarities, structures and physical properties. Previous work in our group (Zou, 2003) showed that ABVB + n-alkane mixtures exhibit the multiphase behaviour over a broad range of conditions. In the presence of hydrogen, dodecane + ABVB mixture still possesses the multiphase behaviour at the typical hydroprocessing temperature conditions. For pentane and heptane + ABVB mixtures, multiphase behaviour arises at temperatures much lower than those associated with typical hydroprocessing conditions; dodecane + ABVB mixtures have only a small amount of L2 under hydroprocessing conditions. Based on this previous work, we anticipated that mixtures with decane would be suitable for this project. Subsequent phase behaviour experiments with ABVB + decane mixtures confirmed this choice.

3.4 Phase Behaviour Experiments

The X-ray view cell technology has been applied to observe the phase behaviour for more than 10 years. Experimental strategies and procedures associated with the synthetic method are outlined in Appendix I.

The phase behaviour of ABVB + decane mixtures both with and without addition of hydrogen was investigated. The experiments for ABVB + decane mixtures can follow the same general procedure in Appendix I. The experiments were conducted for 10%, 20%, 25%, 30%, 35%, 40%, 50%, 70%, 90% and 100% ABVB for the temperature range from room temperature to 380 °C.

The experiments for ABVB + decane + hydrogen mixtures followed the same general procedure in Appendix I. The phase behaviour experiments with hydrogen were conducted with a mass ratio of hydrogen to ABVB + decane of 0.0057. The phase

65

behaviour experiments with hydrogen case were conducted only for 10, 20, 30 and 40 wt % ABVB.

At each examined condition, X-ray transmission images were recorded. Based on the observation of a series of images and the systematic analysis of phase density and volume, the phase diagrams were constructed. The image processing and data analysis method was adopted from Zou, 2003 to calculate the densities, volumes of different phases, but with modifications to the image processing and data analysis software. The X-ray images and raw data from image analysis are summarized in Appendix II and Appendix III respectively.

Since thermal cracking occurs at temperatures above 340 °C (Cai et al. 2001 a and b), the samples were exposed to temperatures above 340 °C for less than one hour to avoid significant cracking. Even so, phase diagrams at temperatures greater than 340 °C are only approximate.

3.5 Catalyst Presulfidation

The catalyst presulfidation experiments were performed with 15-mL microbatch reactors constructed from stainless-steel tubing and Swagelok fittings (Kanda et al. 2004). The hydrogen and carbon disulfide amount, which is needed to presulfide the catalyst, is calculated based on the following chemical reactions:

$$CS_2 + 4H_2 = 2H_2S + CH_4 \qquad (3.7)$$

$$MoO_3 + 2H_2S + H_2 = MoS_2 + 3H_2O \qquad (3.8)$$

$$3NiO + 2H_2S + H_2 = Ni_3S_2 + 3H_2O \qquad (3.9)$$
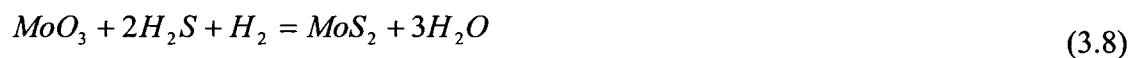
Prior to presulfidation, 350-mg catalyst was desiccated in an oven at 200 °C for 2 h. Then the catalyst was transferred to a microbatch reactor, followed by injection of 70-μL liquid carbon disulfide at room temperature, which is approximately twice the amount required stoichiometrically to sulfidize the catalyst. After purging several times with hydrogen, the sealed microbatch reactors were pressurized to 750 kPa, at room temperature, with

66

hydrogen. The amount of hydrogen added is equivalent to that consumed to convert the added carbon disulfide to produce hydrogen sulphide. The reactor was then placed in an air-fluidized sand bath at 350 °C for 2 hours and vibrated at the same time to obtain good mixing. After catalyst presulfidation, the reactor was removed from sand bath and quenched in a water bath. Presulfided catalyst was used in the catalyst coking experiments.

3.6 Catalyst Coking Experiments

Catalyst coking experiments were also performed in the X-ray view cell. The advantage of using the view cell as a batch hydroprocessing reactor is that one can monitor and control the phase to which catalyst pellets are exposed. Individual phase volumes were also monitored concurrently. In order to ensure that the catalyst stays in a designated phase, a variable position catalyst holder was designed and installed (Appendix IV).

All catalyst coking experiments were conducted at 380 °C, a typical heavy oil hydrotreating temperature. This temperature is far below the thermal cracking temperatures associated with hydroconversion, since one of the objectives for these experimental designs was to minimize composition change during the experiments, so that the impact of phase behaviour per se could be investigated. The catalyst charge was also kept low, ~0.3 g, compared to the liquid charge (60 g). Even for experiments with the lowest ABVB composition (5 wt%), the catalyst charge is still less than 10% of ABVB content. Again, this is intended to minimize composition change caused by catalytic hydroprocessing reactions and to minimize hydrogen consumption for cases where hydrogen is present. Experimental validation is provided in Chapter 7.

In order to exemplify the general arrangements for experiments, two X-ray transmission video images taken during experiments, one for catalyst placed in both L1 and L2 phases; another for catalyst placed in L1 + L2 dispersed, are shown in Figure 3.8. For clarification, schematic representations are also shown in Figure 3.8. In Figure 3.8a, catalyst pellets were placed in both the L1 and the L2 phases. In Figure 3.8b, catalyst pellets were placed in the continuous L1 phase with L2 phase dispersed in the L1 phase. The catalyst charge placed in both L1 and L2 phases is 0.15 g; while the catalyst charge

67

in L1 + L2 dispersed experiment is 0.3 g. Care was taken to ensure that catalyst was exposed to only one bulk phase. The bulk phase to which catalyst pellets were exposed was monitored and controlled by manipulating cell volume and stirring rates. For catalyst placement in both L1 and L2 phases, catalyst pellets were placed in the catalyst holders that were suspended in the view cell. The catalyst holder for the L1 phase was suspended at an elevation above ABVB at room temperature and the anticipated L1-L2 interface at reaction conditions. The catalyst holder for the L2 phase was suspended at an elevation within ABVB at room temperature and below the anticipated L1-L2 interface at reaction temperature. Then ABVB was added into the view-cell and heated up to 200 °C under vacuum. The view cell was then cooled to room temperature (below the glass transition temperature of ABVB). The decane was then added into the view cell. For catalyst placement in the L1+ dispersed L2 experiments, first ABVB was added to the view cell and the catalyst holder was suspended in the view-cell at an elevation above ABVB and the anticipated L1-L2 interface at reaction conditions. Then the view cell was heated to 200 °C under vacuum. The decane was added into the view cell after the view cell was cooled to room temperature.
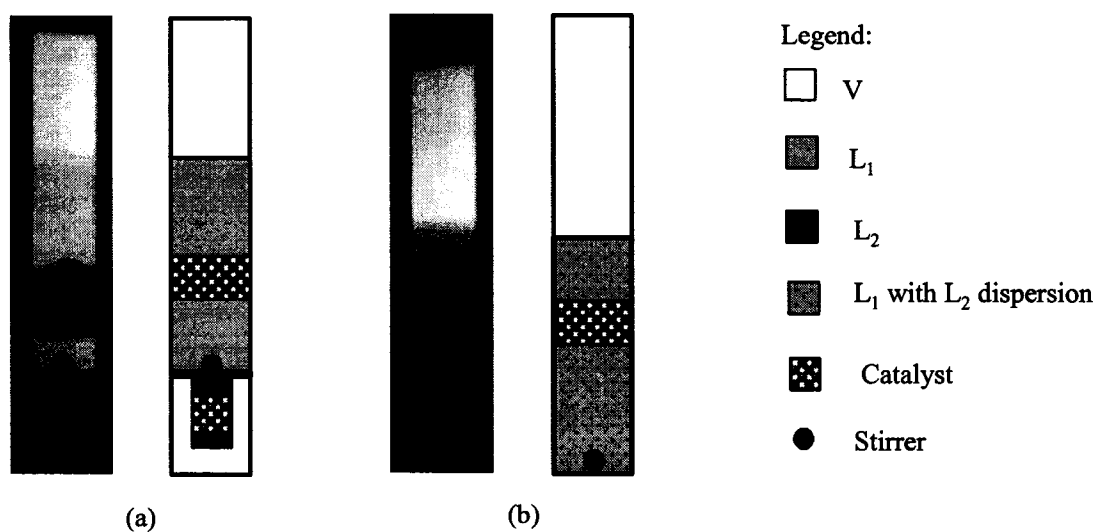
Figure 3.8   X-ray transmission images and schematic representations for: a) showing catalyst held in the L1 and L2 phases of a mixture; and b) showing catalyst held in the L1 phase with the L2 phase dispersed.

The catalyst coking experiments both with and without hydrogen were performed. Once the catalyst and all fluids were in place, the reactor was degassed under mild vacuum (~30 kPa) for 30 minutes prior to heating. For the case with hydrogen, the view cell was pressurized with hydrogen to a calculated pressure equivalent to 0.342 g of hydrogen. The temperature profiles for heating, reaction, and cooling are shown in Figure 3.9. The reaction times at 380 °C were 2 hours and 5 hours. As reaction rates are negligible at temperatures below ~ 300 °C (Cai et al. 2001a, b), there is sufficient time, during the three-hour heating period for diffusion processes to approach completion prior to the occurrence of chemical reaction. At the end of an experiment, the reactor was cooled to room temperature over a three-hour period.
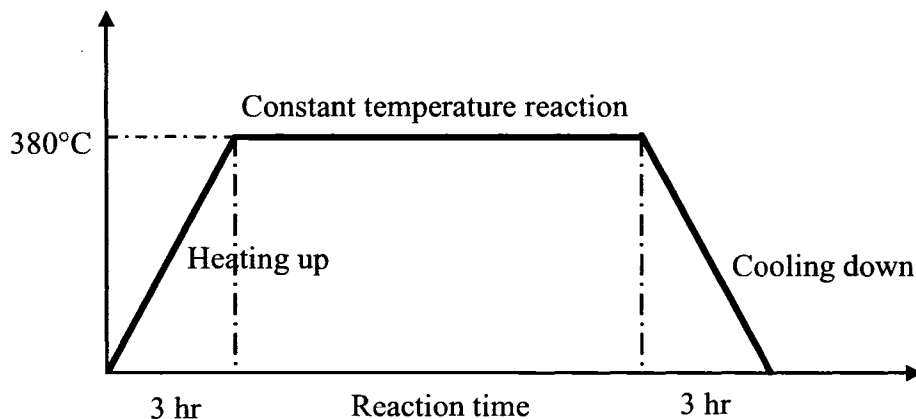
Figure 3.9 Temperature profile for catalyst coking experiments.

A portion of catalyst coking experiments was also conducted in a batch reactor – the same reactor as for the catalyst presulfidation. The procedure for catalyst coking experiments in the batch reactor can be simply described as follows. About 150 mg of presulfided catalyst was transferred to the batch reactor, followed by adding correct amount of ABVB and solvent (decane or 1-methyl naphthalene) according to the compositions (the total feed charge is 4.5 g). Then the batch reactor was sealed. After purging several times with hydrogen, the sealed batch reactor was pressurized with hydrogen to the expected pressure at room temperature with a mass ratio of hydrogen to feed at 0.00057 – the same ratio as for the coking experiments in view cell reactor. The

69

reactor was then placed in an air-fluidized sand bath at 380 °C for 2 hours and vibrated at the same time. After coking experiment, the reactor was removed from sand bath and quenched in a water bath. The experiments conducted by batch reactors were tried to be kept comparable with the experiments by view cell. The results of coking experiments with batch reactors were indicated in the text.

3.7 Catalyst Characterization

Prior to characterizing the coked catalyst, the coked catalyst was extracted with toluene. For the first set of experiments (without hydrogen), the coked catalyst pellets were extracted for 24 hours in excess toluene and then dried for 2 hours at room temperature under vacuum. For the second set of experiments (with hydrogen), the pellets were Soxhlet extracted for 2 hours in hot toluene and then vacuum dried for 30 minutes at room temperature, followed by drying for 2 hours at 120 °C under flowing nitrogen. Each set of experiments was treated consistently, and the impact of the extraction procedure difference on results is shown in Appendix V.

Bulk elemental analyses for carbon, hydrogen, and nitrogen were obtained using a Carlo Erba Strumentazione Elemental Analyzer 1108. Sulphur content was measured using Schoniger method. The bulk elemental analysis was conducted by elemental analysis laboratory in the Chemistry Department at the University of Alberta. In order to ensure representative sampling, 150 mg of coked catalyst was ground to fine powder and then 2-mg samples were used for elemental analysis. A summary of the elemental analyses for all coking experiments is provided in Appendix V.

The local quantitative elemental analysis of the cross sections of whole coked catalyst pellets were conducted using a JEOL 8900 electron microprobe in the Department of Earth and Atmospheric Sciences at the University of Alberta. Pellets were sectioned radially at the mid-point, and then mounted in a mould with epoxy resin. Exposed surfaces were dry polished using 3-μm diamond as the final abrasive. Finally, the polished surfaces were evaporatively coated with a thin layer of carbon. Local composition measurements were obtained at 35-μm intervals from the centre to the

70

exterior surface of the particles.

The cross sections of catalyst pellets were also observed using visible light microscopy coupled with a digital camera which is connected to a computer, located in an undergraduate's laboratory in the Department of Chemical and Materials Engineering at the University of Alberta. The photomicrographs were recorded as digital computer files.

The surface area, pore volume, and pore size distribution of the catalysts were determined using an Omnisorb 360 in the Department of Chemical and Materials Engineering at the University of Alberta and were measured in powder form unless specified in context. Nitrogen adsorption measurements were used to calculate surface areas, using the BET equation. Pore size distributions and pore volume were determined using nitrogen desorption data and the Kelvin equation (Gregg and Sing, 1982). A summary of the BET measurements for all coking experiments is also provided in Appendix V.

71

4. Phase Behaviour of ABVB + Decane Mixtures

4.1 Introduction

From a phase behaviour prospective, ABVB + decane mixtures are highly asymmetric since ABVB consists of asphaltenes and other molecules that are much larger than decane and possess different polarities, structures and physical properties. Classical phase behaviours of binary asymmetric mixtures, such as type III, type IV or type V phase behaviour were expected for these mixtures. However since ABVB itself is a mixture containing numerous components, the phase behaviour of decane + ABVB mixture was found to be more complicated than that of binary mixtures. ABVB appears to be a glass or solid at low temperature, but here it was treated as a liquid in order to simplify phase diagram construction. In this thesis, ABVB + decane system is modelled as a pseudo-binary mixture.

4.2 Pressure-Temperature and Pressure-Composition Phase Diagrams

From single images, apparent densities and volumes of phases can be determined based on the visual observation and image processing. Systematic analysis of a series of images at different experimental conditions places individual observations in context and allows one to place phase boundaries and phase behaviour boundaries in phase diagrams. However, as the number of conditions observed is limited, it is only possible to construct partial phase diagrams with a focus on the pressure, temperature and composition ranges of interest. Other phase boundaries and phase behaviours are inferred on the basis of theory. In the figures which follow, well-defined phase boundaries are shown as solid curves and tentative boundaries are shown as dashed curves.

4.2.1 P-T Phase Diagram

To help readers understand the phase diagram construction approach in this thesis, the P-T phase diagram construction for 10% ABVB + decane mixture is used to exemplify the

72

construction of P-T phase diagrams for ABVB + decane mixtures. The X-ray images showing phase transitions for 10% ABVB + decane from 20 to 380 °C are presented in Figure 4.1. Except for at 20 °C, there were at least two images taken at different pressures but the same temperature (aligned vertically in Figure 4.1). For the image taken at the lowest pressure, the bellows are pulled back as close as possible to the top of the view cell. The images showing the same phase behaviour are grouped together within a border. The X-ray images indicate multiphase behaviour over a broad range of temperature and pressure including L1L2V, L2V, and L1L2. Sometimes it is difficult to observe phase boundaries in an image if two phases are close to a critical point (the image for 370 °C and 27.02 bar), or the volume of a phase is very small. However by analyzing the X-ray images using software developed in this thesis, most of phase boundaries were identified unambiguously. The information from the experiments such as pressure and temperature is mapped to corresponding phase diagram in Figure 4.2. According to the types of phase behaviour observed, the experimental data points falling into different phase behaviour regions are presented by different symbols. The experimentally determined phase boundaries are placed in the phase diagram as solid curves. Due to the fragmentary nature of the experimental data obtained, it is impossible to have a complete phase diagram. However, according to the phase behaviour theories coupled with the experimental data, at least a partial phase diagram can be constructed with tentative and approximate phase boundaries shown as dashed curves. Also indicated in Figure 4.2 are the phase behaviour zones. In this thesis, the phase diagrams focus on only the LLV multiphase regions and neighbouring phase regions. The pressure-temperature at constant composition phase diagrams for the mixtures decane + 20, 25, 30, 35, 40, 50, 70, 90 and 100 wt% ABVB are presented in Figure 4.3 to 4.11 respectively.

73
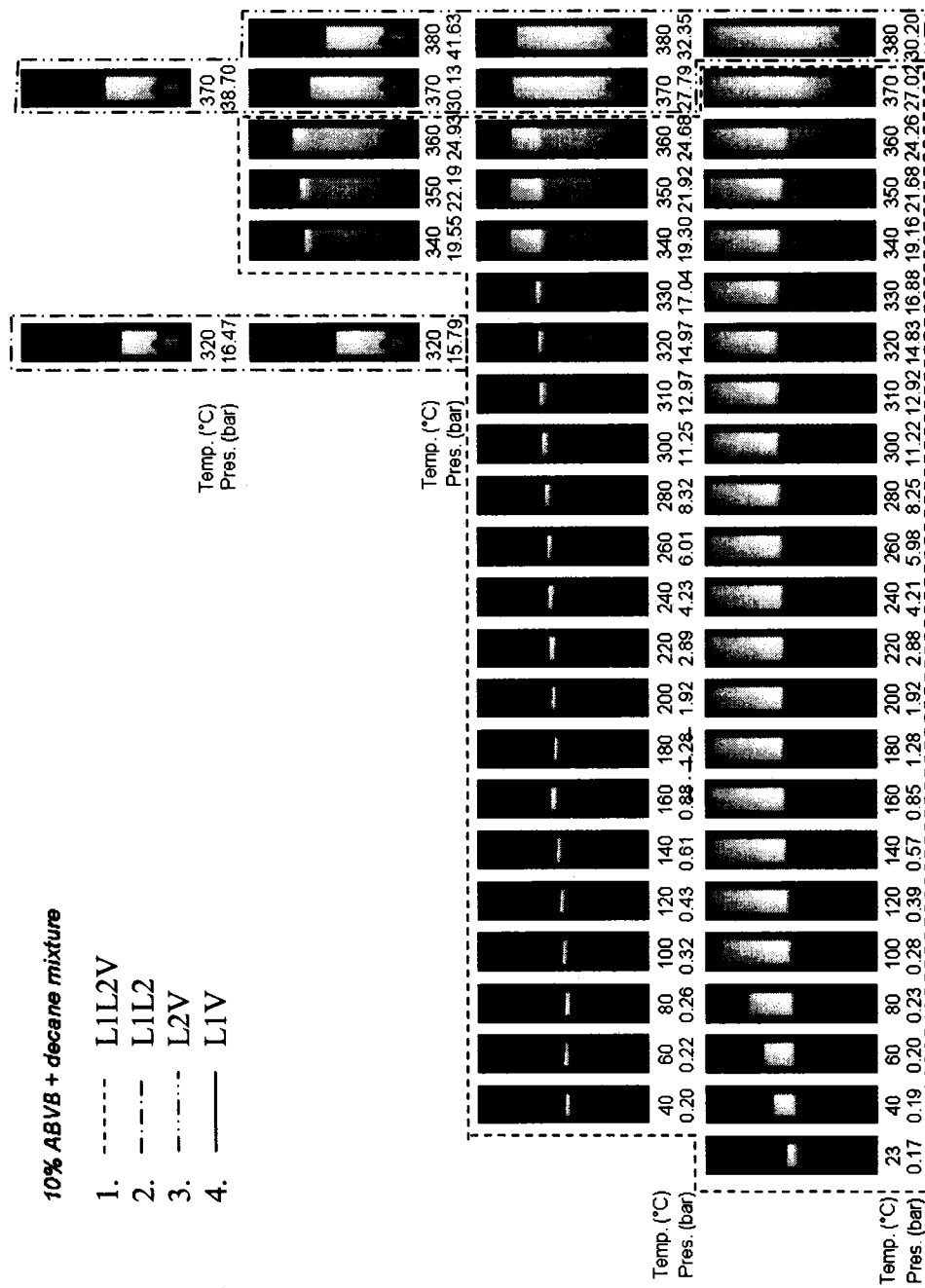
Figure 4.1 X-ray images of ABVB (10 wt %) + decane mixture.
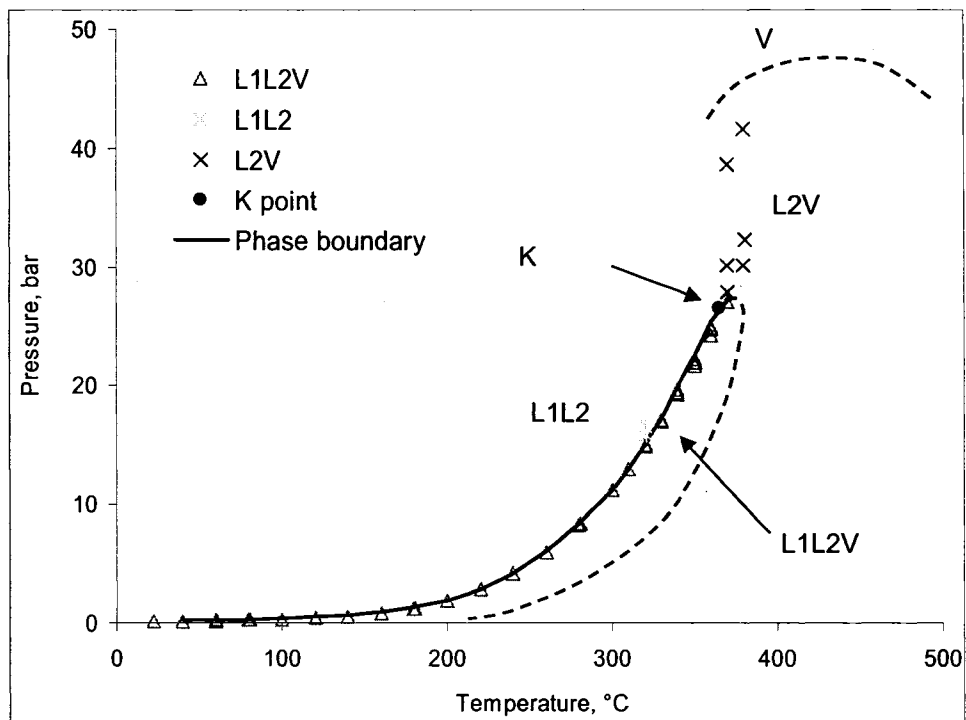
Figure 4.2   P-T phase diagram of 10% ABVB + decane mixture
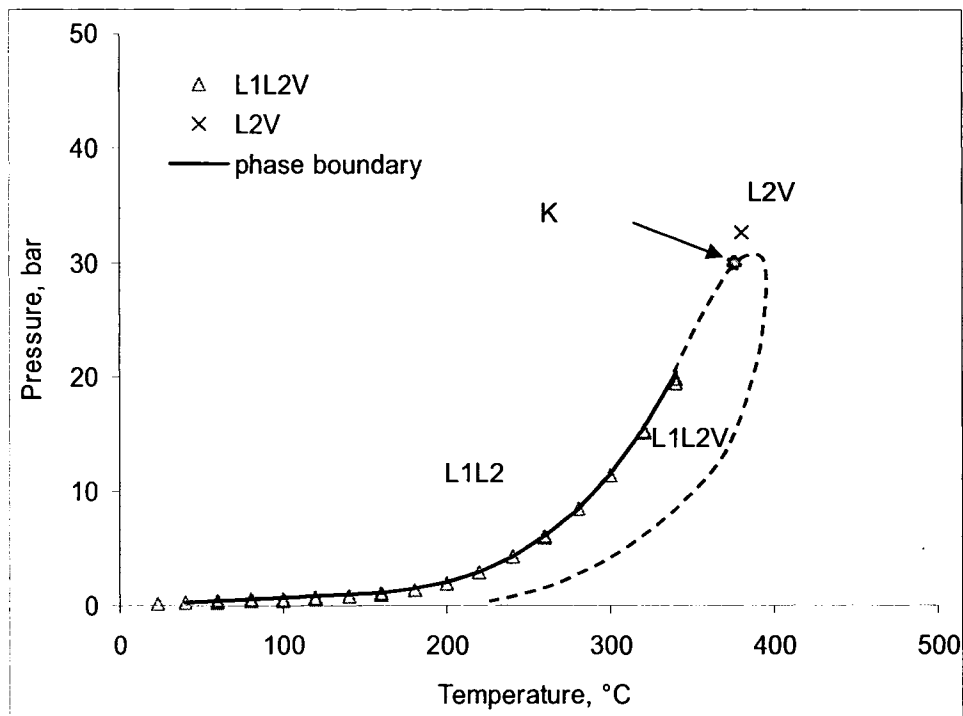
Figure 4.3   P-T phase diagram of 20% ABVB + decane mixture

75
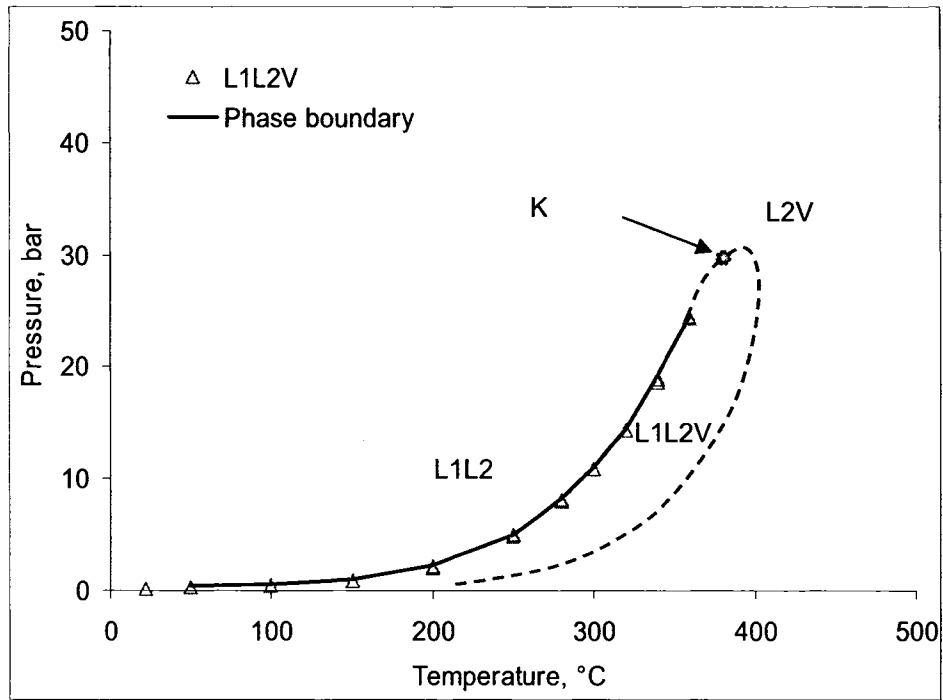
Figure 4.4   P-T phase diagram of 25% ABVB + decane mixture
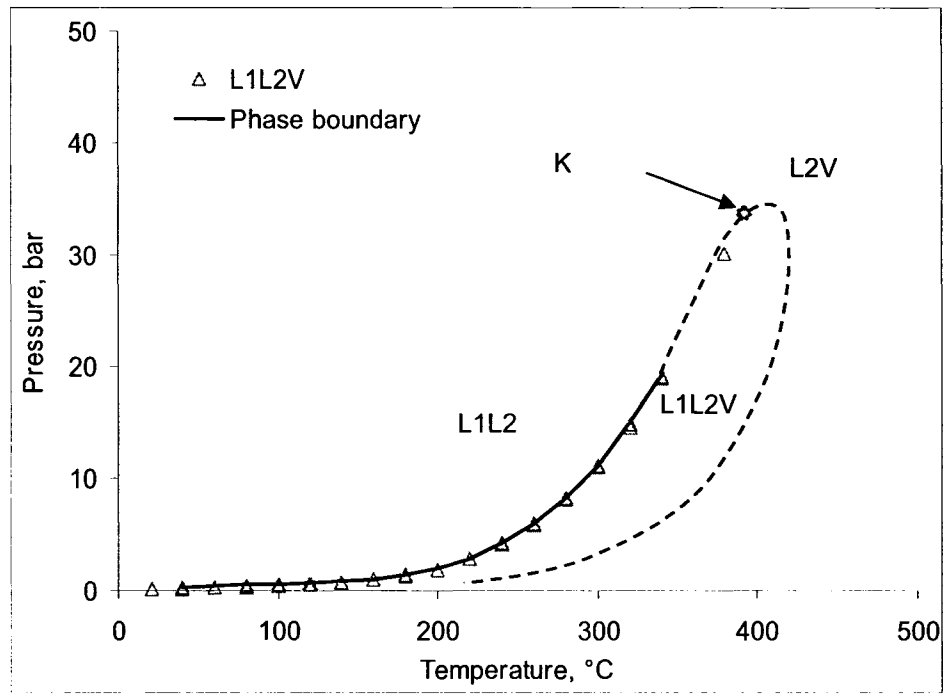
Figure 4.5   P-T phase diagram of 30% ABVB + decane mixture
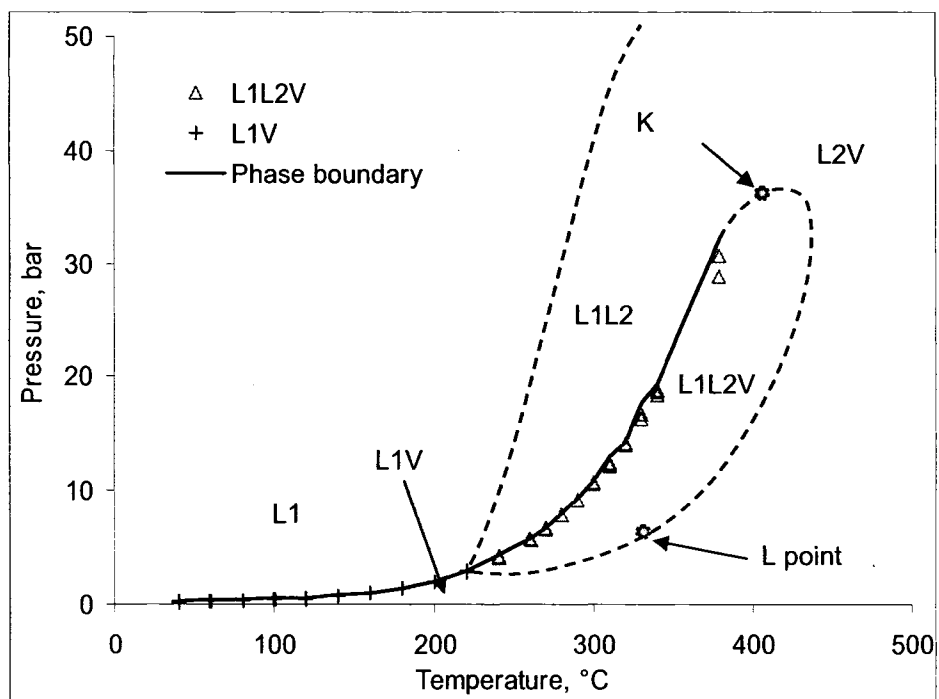
Figure 4.6   P-T phase diagram of 35% ABVB + decane mixture
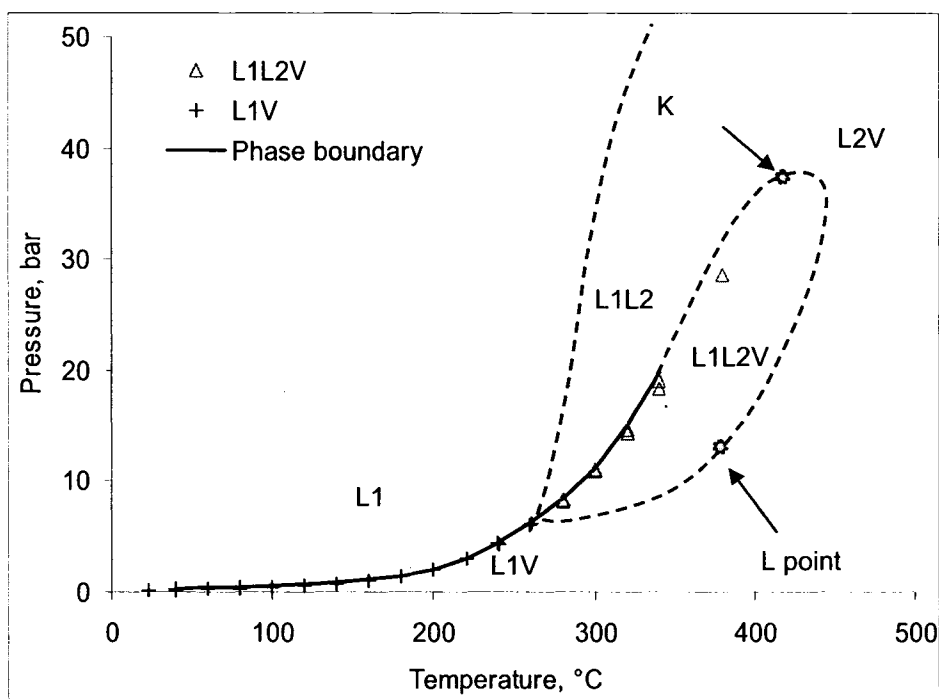
Figure 4.7   P-T phase diagram of 40% ABVB + decane mixture
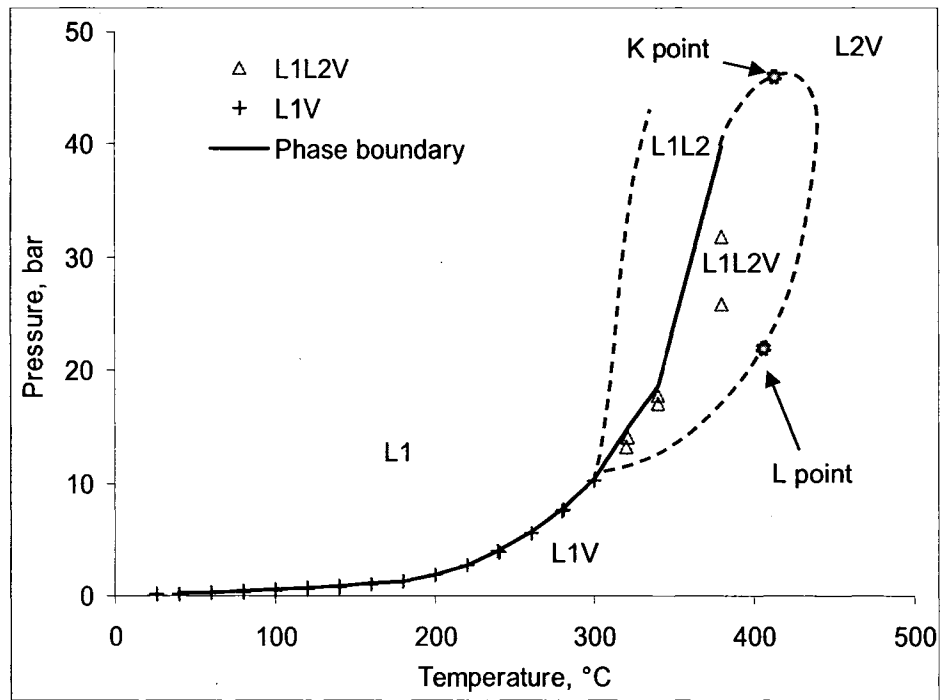
Figure 4.8   P-T phase diagram of 50% ABVB + decane mixture
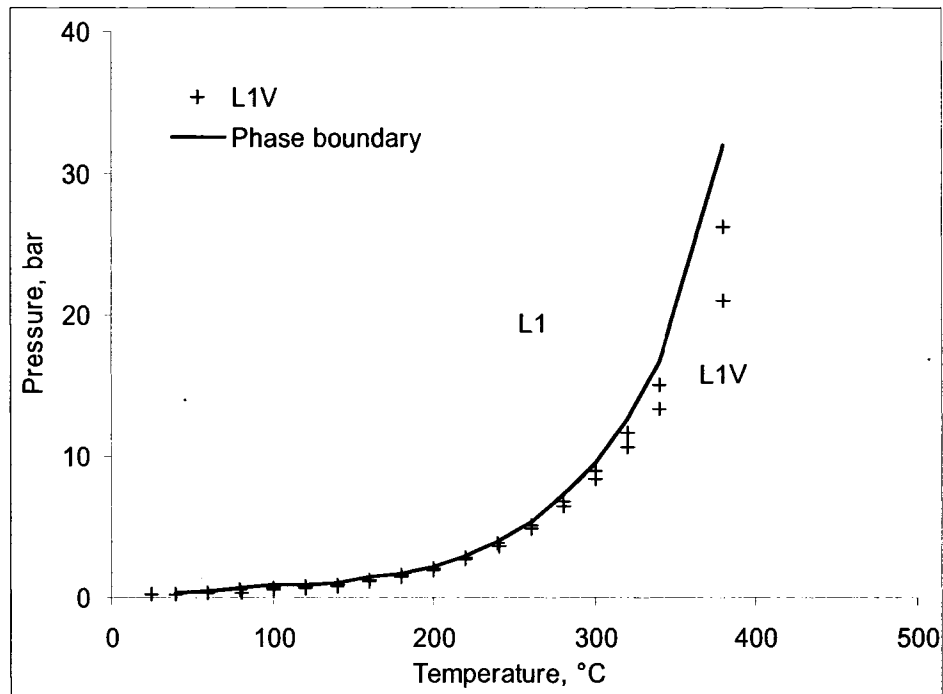
Figure 4.9   P-T phase diagram of 70% ABVB + decane mixture
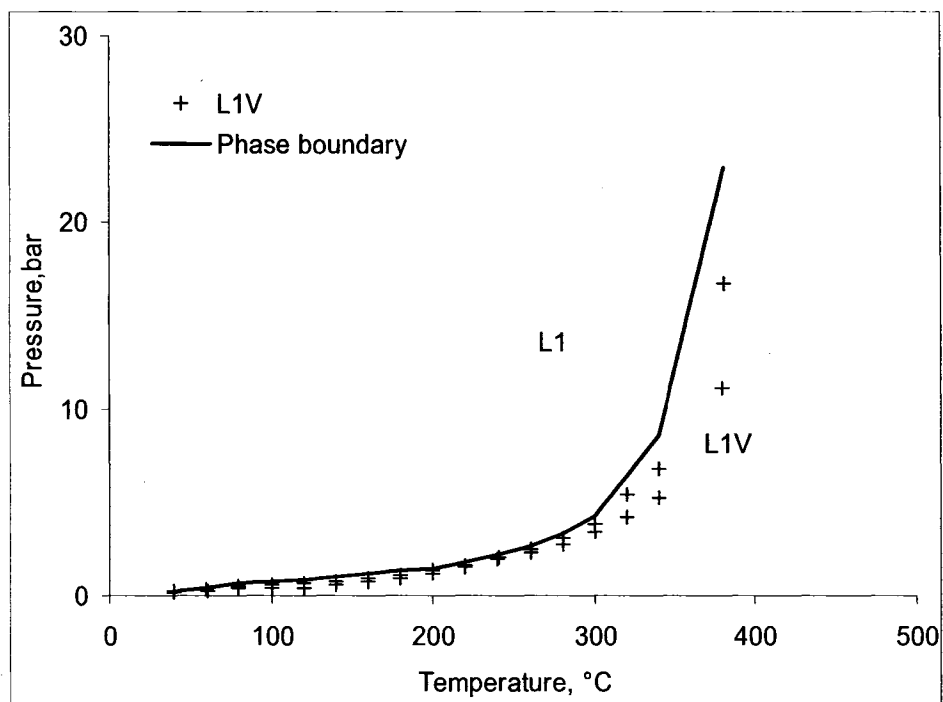
Figure 4.10   P-T phase diagram of 90% ABVB + decane mixture
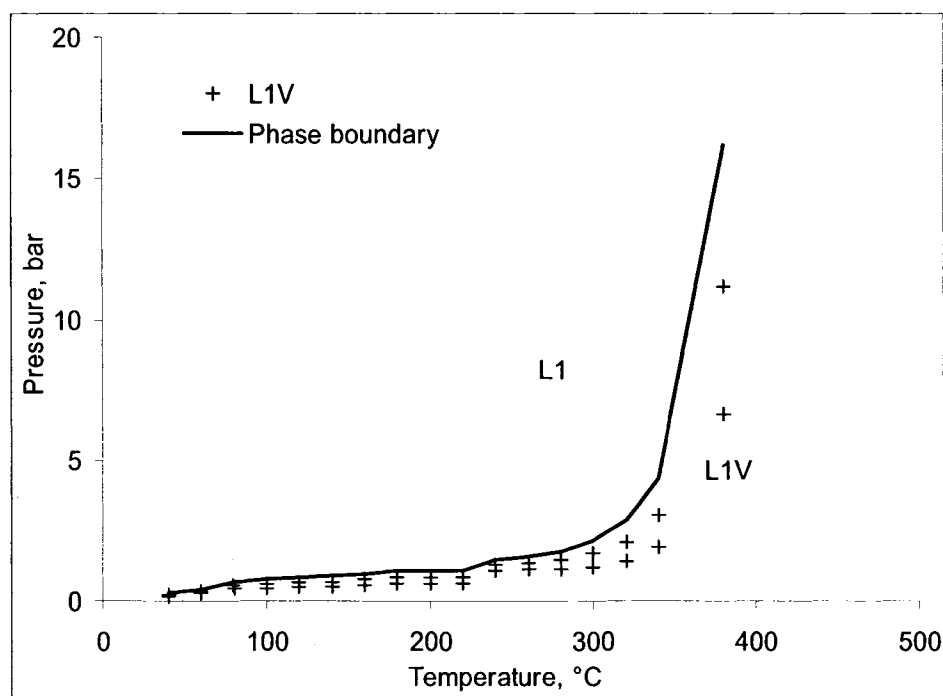
Figure 4.11   P-T phase diagram of 100% ABVB + decane mixture

4.2.2 P-x Phase Diagram

As phase equilibrium and phase boundary data were obtained at 20 °C intervals for 10 compositions from room temperature to 380 °C, a large number of constant temperature phase diagrams could in principal be constructed as cross plots. To avoid repetition, only key diagrams were constructed. First, the construction of a pressure-composition diagram at 380 °C is presented as an example. The images at 380 °C for different compositions are shown in Figure 4.12. The images show that for decane + 10, 20, 30, 35, 40, and 50 wt. % ABVB mixtures, an L2 phase is present. But for the decane + 70 to 90 wt. % ABVB mixtures and for ABVB itself, only L1V phase behaviour was observed. L1L2V phase behaviour was observed for 30, 35, 40, and 50 wt % ABVB mixtures. For 10 and 20 wt % ABVB mixtures, only L2V phase behaviour was observed. As 380 °C is above the critical temperature of decane (344.6 °C), the mixture exhibits vapour phase behaviour at low ABVB mass fractions. Therefore, based on the observations, the phase behaviour undergoes transitions from V for pure decane to L2V, to L1L2V, to L1V with increasing ABVB content at 380 °C. The same construction strategy for pressure–composition phase diagrams as for pressure-temperature phase diagrams was employed to construct the partial P-x phase diagram shown in Figure 4.13. Again the solid curves are experimentally determined phase boundaries and dashed curves are employed to approximate phase boundaries which were not observed but could be inferred.

Since the 380 °C pressure-composition phase diagram is a key phase diagram throughout this thesis, it is described here in detail. As the mass fraction of ABVB is raised a dense liquid (L2) appears at low pressures. If the pressure is raised, this liquid becomes miscible with the gas phase. In the centre of the diagram one of three phenomena are observed depending on the mass fraction of ABVB:

1. Low density liquid (L1) appears above the L2 phase as pressure is increased and then disappears as pressure is further increased.

2. Low density liquid (L1) appears above the L2 phase as pressure is increased and then the vapour phase (V) disappears as pressure is increased further revealing the presence of an K point in the diagram, i.e.: where a low density liquid and a vapour become critically identical in the presence of another liquid phase (L1=V + L2).

80

3. High density liquid (L2) appears beneath a low density liquid (L1) as pressure is increased, revealing the presence of an L point in the diagram, i.e.: where two liquids become critically identical in the presence of a vapour phase (L1=L2 + V).

At high ABVB mass fractions, L1V phase behaviour is observed at low pressure. As the pressure is increased, a bubble pressure is encountered and at higher pressures L1 phase behaviour is observed.

The pressure-composition phase diagram at 380 °C is a typical phase diagram with K and L points on the LLV region boundary. However, at a temperature below the critical temperature of decane, the pressure-composition phase diagram does not include an K point. The 320 °C pressure-composition phase diagram shown in Figure 4.14 belongs to this category. In Figure 4.14, only an L point exists on the lower boundary of the LLV three phase region. The LLV phase region is bounded by four two-phase regions, L1L2, L2V and two L1V. Even though not observed experimentally, the L1V phase region at low ABVB compositions must exist according to phase behaviour theory. It is included in the phase diagram for completeness.

4.3 Evolution of P-x Phase Diagrams with Temperature

Two typical but partial pressure-composition phase diagrams at constant temperatures of 320 and 380 °C have been presented. However, the phase behaviour of a binary as a whole is best presented as a limited series of sketches that capture key features of the phase space. These are shown in Figure 4.15. At temperatures less than the critical temperature of decane, phase diagrams qualitatively similar to Figure 4.15a are expected. At a temperature slightly higher than the critical temperature of decane, the L1V phase region detaches from the pressure axis and closes at a L1V critical point - Figure 4.15b. Transitional phase diagrams like Figure 4.15b, which only arises over a narrow temperature range are difficult to observe experimentally. The small L1V phase region at low ABVB compositions vanishes at higher temperatures and the phase diagram is shown in Figure 4.15c in which the L1V critical point disappears and an K point arises. For all three cases, an L point exists on the LLV three phase region boundary.

81

ABVB + Decane mixture at 380 °C

1. ------ L1L2V
2. –·–·– L1L2
3. –··–··– L2V
4. ——— L1V

Comp.(wt% ABVB): 10
Pres.(bar): 41.63

Comp.(wt% ABVB): 10   35   50   70   90   100
Pres.(bar): 32.35   30.59   31.81 26.21 16.72 11.15

Comp.(wt% ABVB): 10   20   30   35   40   50   70   90   100
Pres.(bar): 30.20   32.55 30.19 28.79 28.59 25.91 21.01 11.08 6.63
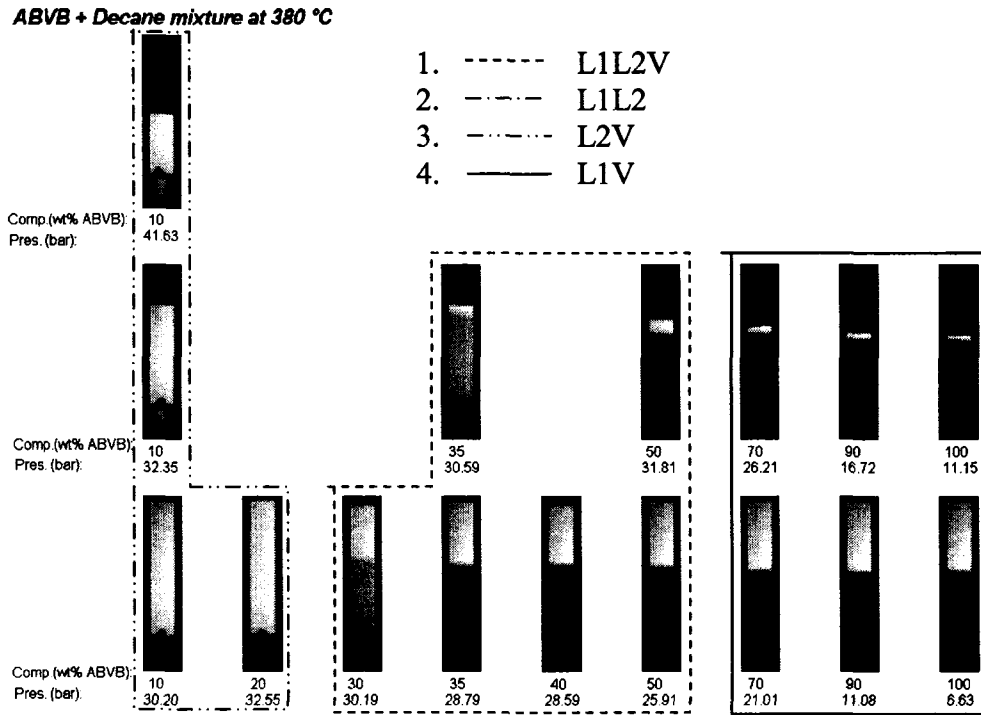
Figure 4.12   X-ray images of 10% to 100% ABVB + decane mixtures at 380 °C
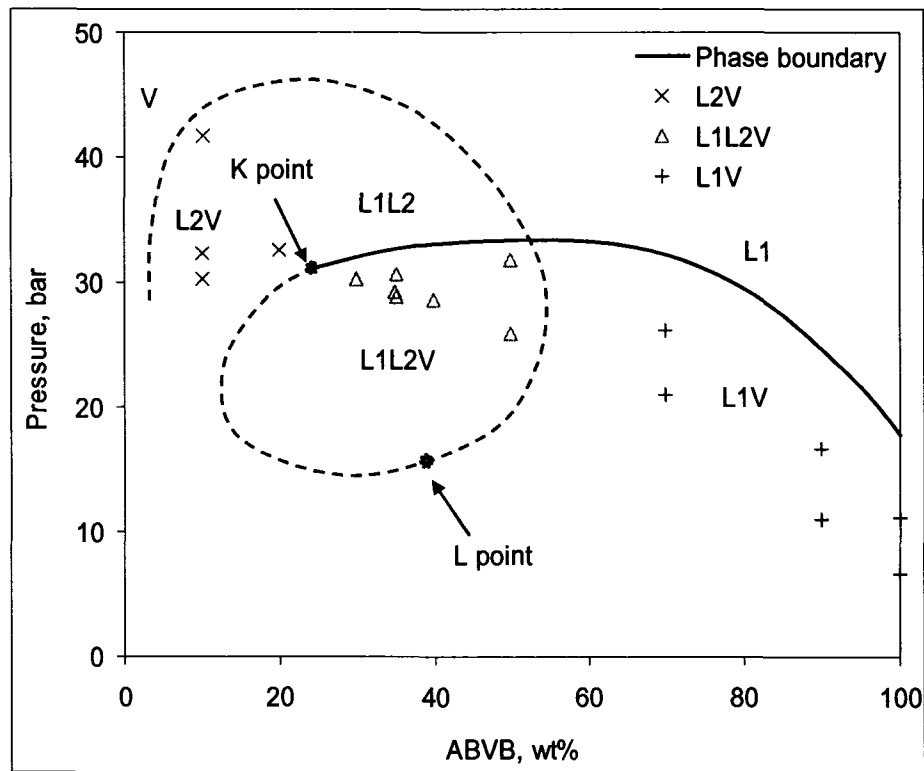
Figure 4.13   P-x phase diagram at 380 °C
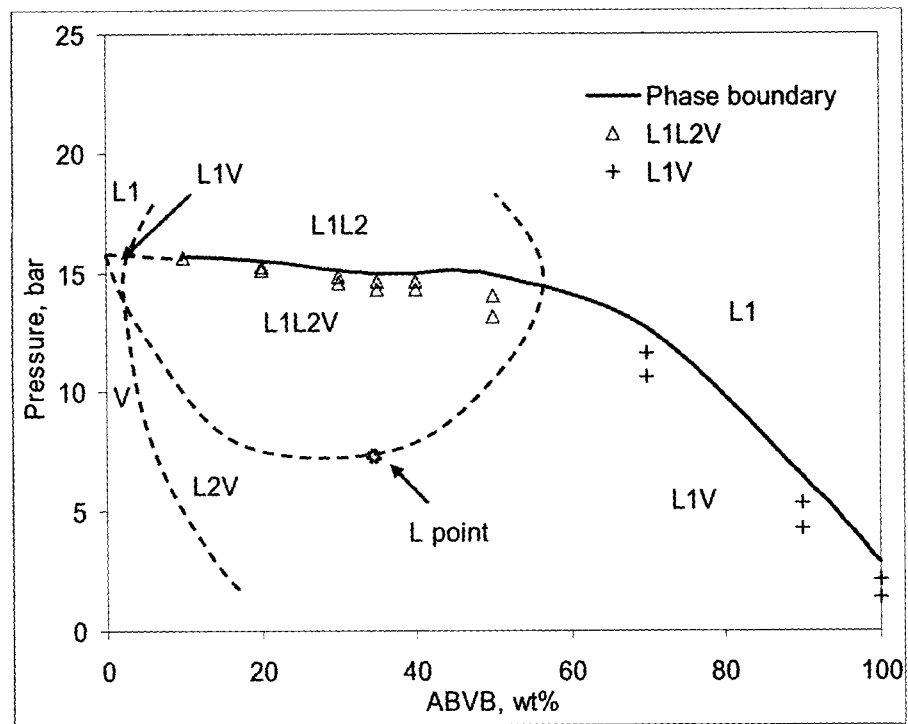
Figure 4.14   P-x phase diagram at 320 °C

83
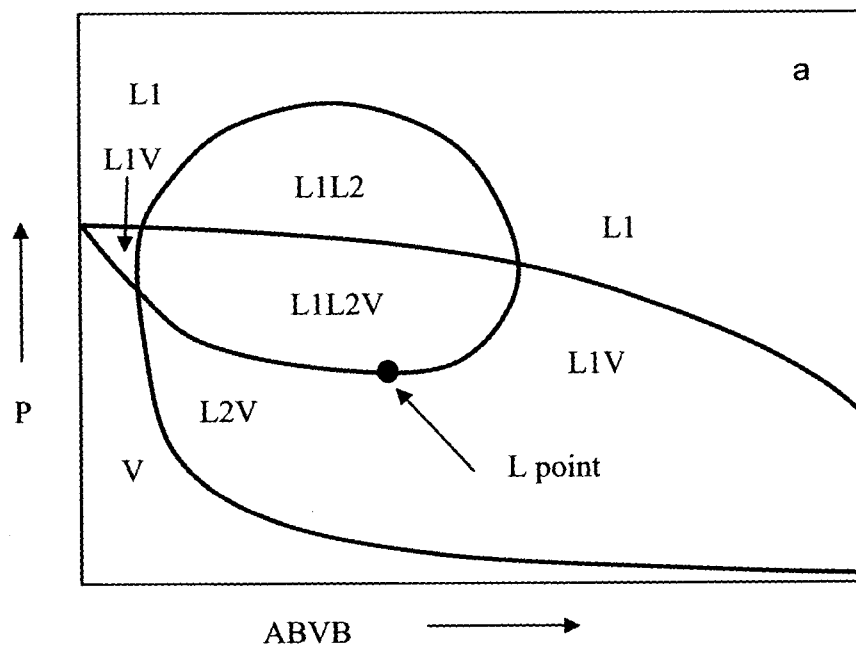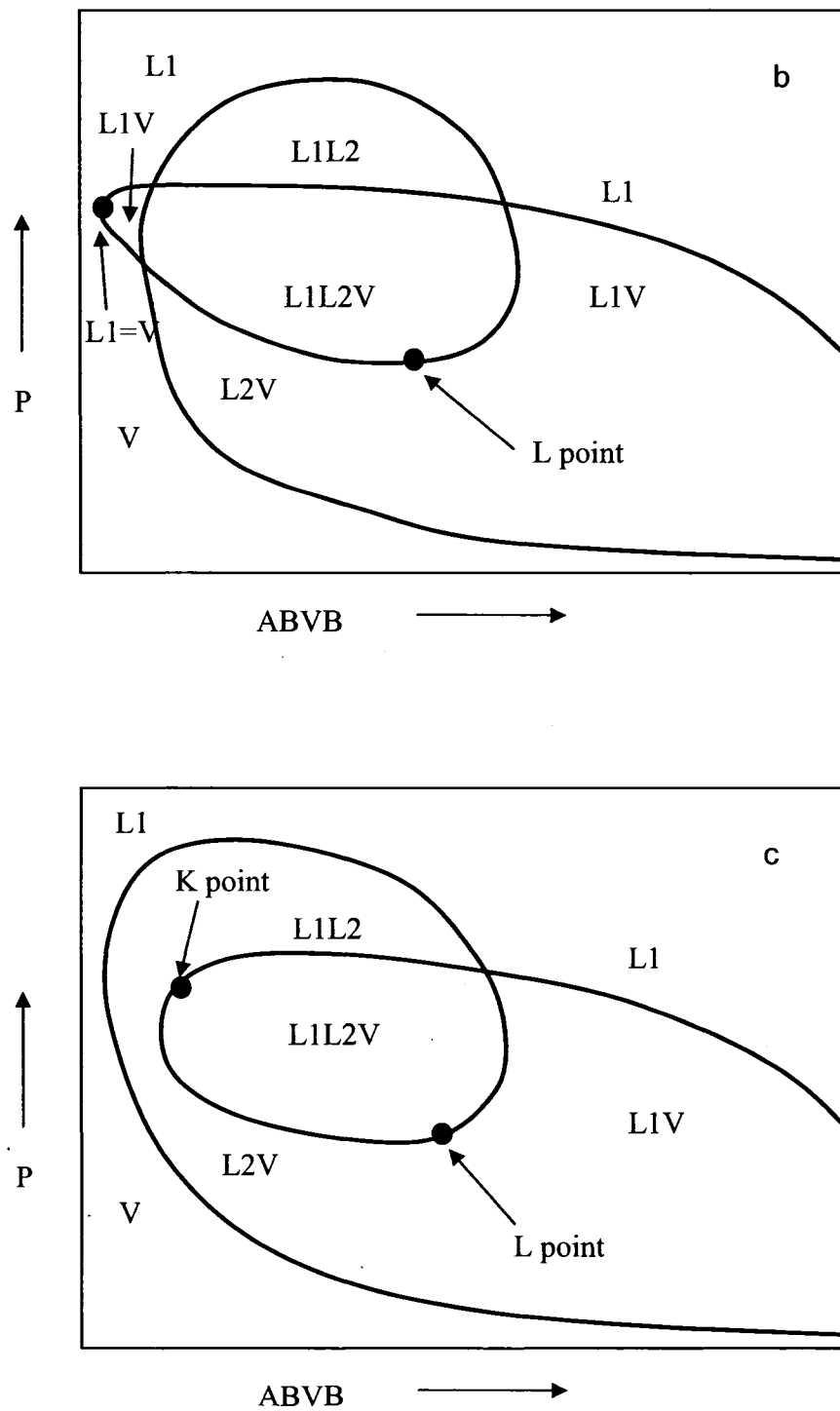
Figure 4.15   Sketches of P-x phase diagrams evolution for ABVB+decane mixtures at three characteristic temperatures. a) T < decane critical temperature; b) T just greater than decane critical temperature; c) T > the temperature at which the left hand L1V zone collapses into the LLV zone.

84

5. Phase Behaviour of ABVB + Decane + Hydrogen Mixtures

5.1 Introduction

In heavy oil hydroprocessing, the impact of hydrogen on phase behaviour is of great theoretical and practical significance. Does hydrogen change the phase behaviour per se or just increase the pressure associated with phase boundaries? How does hydrogen solubility in liquids increase with system pressure? The solubility of hydrogen in several model compounds and petroleum fractions has been measured previously by our group (Cai et al. 2001). For example, hydrogen solubility increases linearly with hydrogen partial pressure for hydrogen + ABVB and hexadecane binaries. This chapter focuses on the impact of hydrogen on phase behaviour.

5.2 The Impact of Hydrogen on the Phase Behaviour of ABVB + Decane mixtures

The phase behaviour of ABVB + decane + hydrogen mixtures was observed as per ABVB + decane mixtures. Since there was no significant difference in phase behaviour between the with and without hydrogen cases at the same ABVB composition, phase behaviour experiments with hydrogen were only conducted for 10, 20, 30 and 40 wt% ABVB + decane mixtures. Pressure-temperature at constant composition phase diagrams for ABVB + decane + hydrogen mixtures with a mass ratio of hydrogen to ABVB + decane of 0.0057:1 are presented in Figure 5.1 to 5.4. The phase behaviour of 10% ABVB + decane + hydrogen mixture was only examined at elevated temperature. The pressure-composition phase diagram was only constructed for 380 °C (Figure 5.5), since it is the key phase diagram for catalyst coking experiments. Comparison between Figure 4.13 and Figure 5.5 clearly indicates that there is no significant difference in overall phase behaviour, i.e., these two phase diagrams show similar phase behaviours. However, the addition of hydrogen shifts the phase behaviour regions and boundaries vertically from low pressure to high pressure, and expands the multiphase regions. Since hydrogen is the lightest component and immiscible with both decane and ABVB, the shift and

85

expansion of the multiphase regions were expected.
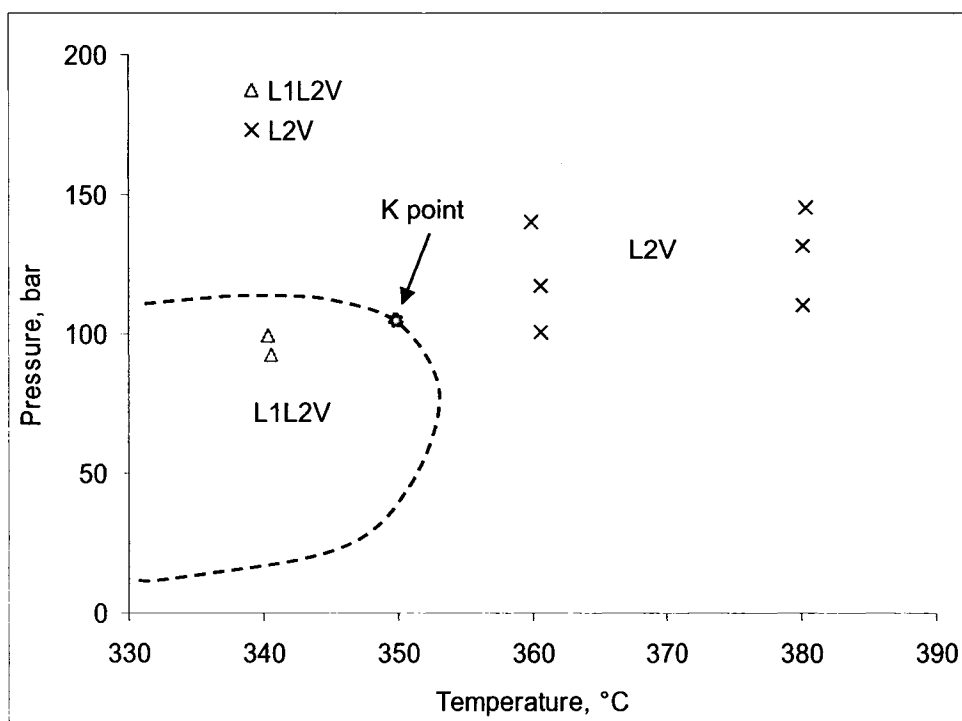
Figure 5.1   P-T phase diagram of 10% ABVB + decane + hydrogen mixture
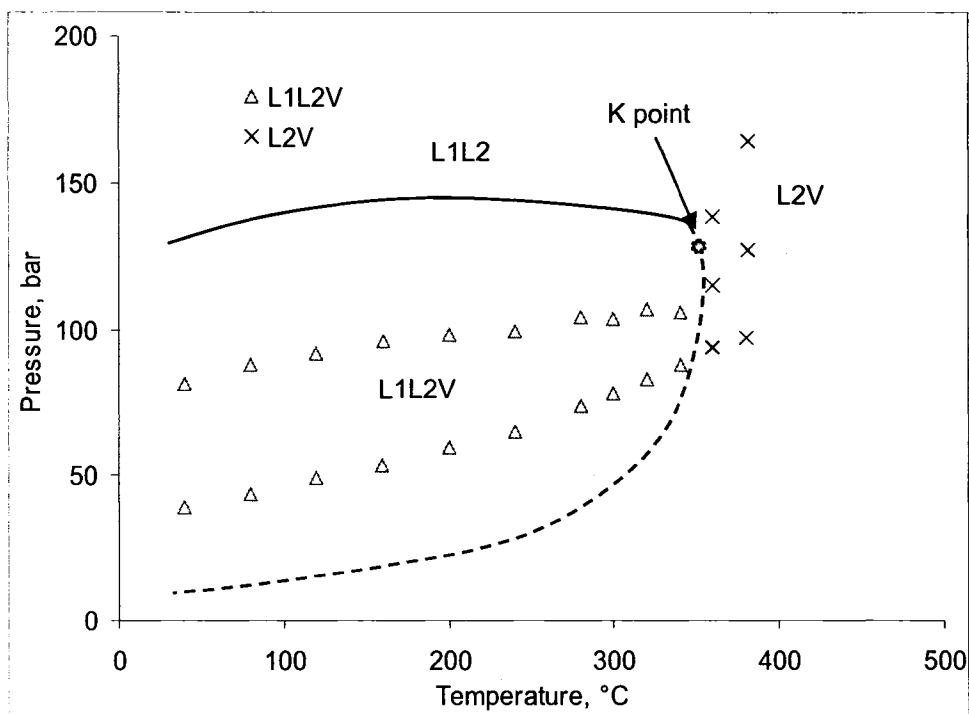
Figure 5.2   P-T phase diagram of 20% ABVB + decane + hydrogen mixture
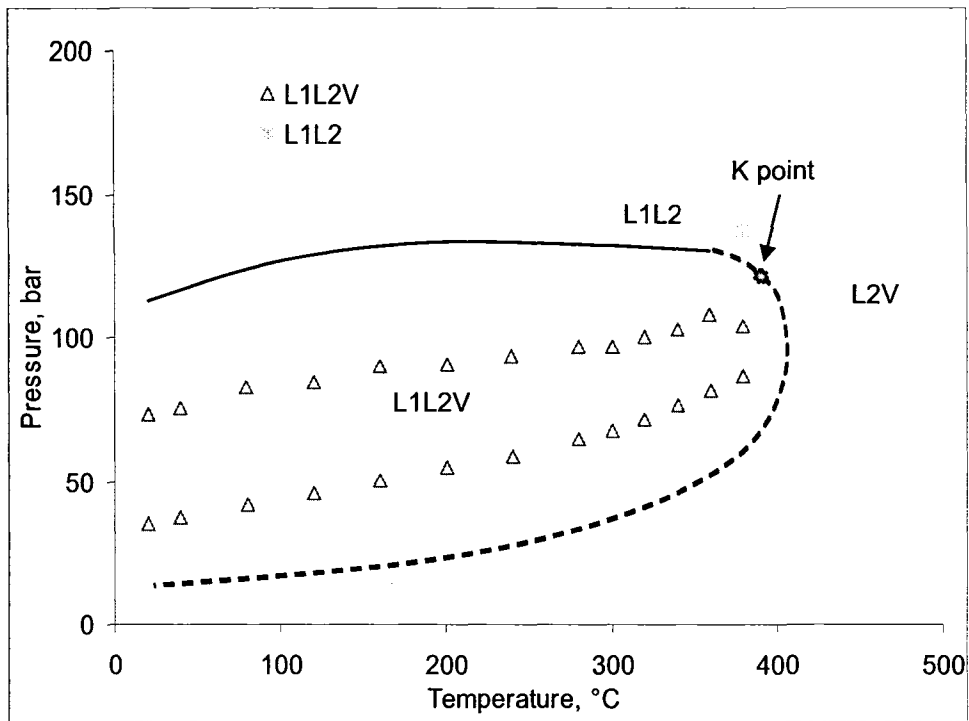
Figure 5.3   P-T phase diagram of 30% ABVB + decane + hydrogen mixture
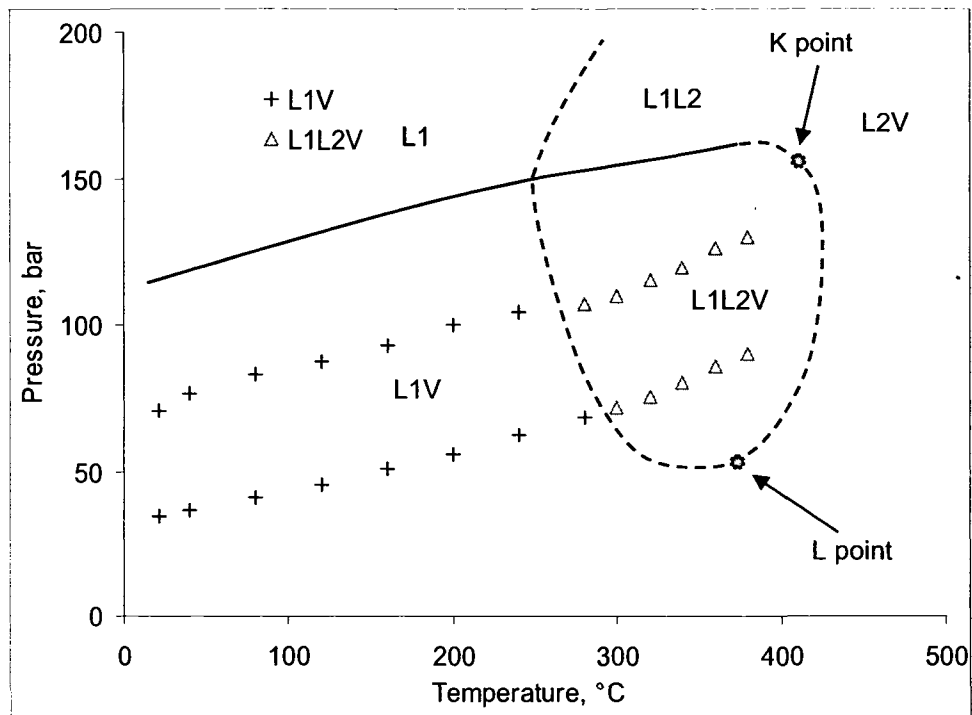
Figure 5.4   P-T phase diagram of 40% ABVB + decane + hydrogen mixture

87
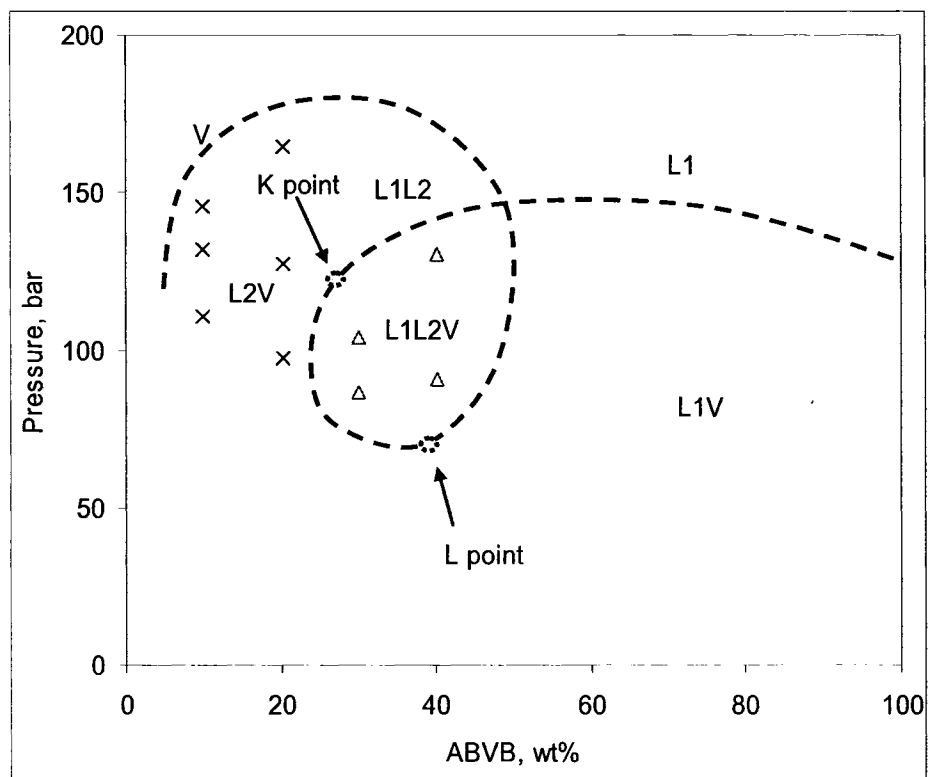
Figure 5.5   P-x phase diagram at 380 °C

6. The Impact of Multiphase Behaviour on Coke Deposition in Catalysts Exposed to ABVB + Decane Mixtures*

6.1 Introduction

The phase behaviour exhibited by mixtures of ABVB + decane and ABVB + decane + hydrogen is complex and from the perspective of assessing the impact of multiphase behaviour on coke deposition outcome this poses a number of challenges. In particular, we must be aware of hydrodynamic effects. If two liquid phases are present, to which is the catalyst exposed? Is one phase dispersed as drops in the other? If so, which phase is continuous and which is dispersed? We must also recognize that pressure is a composite variable: phase behaviour is a function of composition at fixed pressure. Within a multiphase region, the absolute and relative amounts of phases change with pressure at fixed composition. It is difficult to probe the effect of pressure per se while keeping the values of other variables fixed. Many of these issues are addressed directly in chapters 6 and 7 of this thesis.

In this chapter, we focus on the impact of phase behaviour on coke deposition in porous catalyst pellets in the absence of hydrogen. Catalyst coking experimental results in the absence of hydrogen provide baseline data as well as valuable understanding concerning the coke deposition mechanism, under sedimentation conditions.

6.2 Catalyst Coking Experimental Design.

For these coking experiments, the catalyst was used in its oxide form, and the global composition of the mixture was fixed (30 wt % ABVB + 70 wt% decane). The reaction times were set at 2 hrs and 5 hrs, at 380 °C and ~30 bar where the mixture exhibits L1L2V phase behaviour - Figure 6.1. The densities of the L1 and L2 phases at this condition are approximately 470 and 870 kg/m^3, respectively and the volumes for the L1 and L2 phases for a total charge of 60 g are ~ 93.7 and ~ 8.8 cm^3, respectively (from the related phase behaviour experiment). For 2 hrs reaction time, the catalyst was coked in

89

both L1 and L2 phases separately as shown in Figure 3.8a. For 5 hrs reaction time, this experiment was repeated and in addition, an experiment was conducted where the catalyst was placed in the L1 phase and the L2 phase was dispersed, as shown in Figure 3.8b.
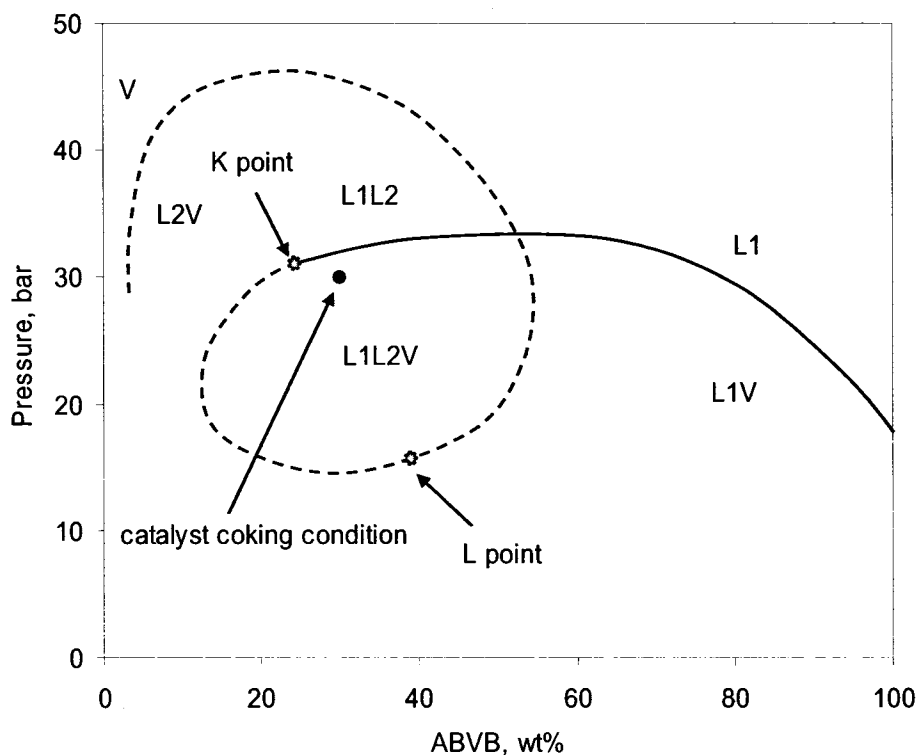
Figure 6.1   Phase behaviour for catalyst coking experiments with the mixture 30 wt% ABVB + decane.

6.3 Bulk Properties of the Coked Catalyst Pellets.

Elemental analyses for coked catalyst samples are reported in Table 6.1. The carbon content reflects the coke content of coked catalyst where the wt % values include the mass of the catalyst. The carbon content of the coked catalysts increases with coking time as expected (Gualda and Kasztelan, 1996; Marafi and Stanislaus, 2001; Matsushita et al. 2004). The standard error for carbon content is less than 1 % of the reported values, as shown in Appendix V Table A-4. Clearly, the carbon contents for catalyst exposed to the

90

L1 phase are higher than for the corresponding, L2, or L1+L2 dispersed cases. It was unexpected that the coke content of catalyst in the L2 phase would be less than that in the L1 phase. According to the coke deposition models more coke would be formed in the L2 phase than in the L1 phase, since the coking reaction rates are assumed to be proportional to the coke precursor concentration and the precursor concentration in the L2 phase is nominally much greater than in the L1 phase. The reason for this unexpected result is addressed in section 6.5.

Table 6.1   Elemental analysis of coked catalysts

Coking time	5 hrs			2 hrs	
Catalyst exposed to:	L1	L2	L1+L2	L1	L2
C, wt%	27.6	26.1	26.4	23.3	20.7
H, wt%	2.15	2.04	2.11	1.94	1.82
H/C, mole/mole	0.93	0.94	0.96	1.00	1.05
S, wt%	5.1	5.2	4.7	2.9	3.6
N, wt%	0.60	0.60	0.58	0.48	0.46

The surface area, pore volume and derivative properties of the coked catalysts are reported in Table 6.2. The pore volume and surface area loss of coked catalysts for 5 hrs coking time are substantially greater than for 2hrs coking time, which are consistent with the coke content result of coked catalysts. The pore volume losses for catalyst pellets exposed to L1 are greater than for the corresponding L2 or L1+L2 dispersed cases. The surface area loss is substantially less for the L1 + L2 dispersed case than for the others.

By comparing the surface area loss and pore volume loss, one finds that the surface area loss is less than the pore volume loss. The difference between these two losses can been interpreted given an uniform coke deposition for which the pore volume would decrease with the square of the thickness of the coke deposit and surface area would decrease linearly with the thickness of coke deposit (Gray et al. 1999).

91

Table 6.2 BET analysis of coked catalysts

Coking time	5 hrs			2 hrs	
Catalyst exposed to:	L1	L2	L1+ L2 (dispersed)	L1	L2
Catalyst form during analysis	Powder	powder	pellet	Powder	
Surface area, m²/g	112	113	127	126	157	165
Surface area loss, %	48	48	42	42	28	25
Pore volume, cm³/g	0.14	0.17	0.17	0.17	0.24	0.29
Pore volume loss, %	76	71	71	72	59	50
Mean pore radius, Å	25.0	29.0	26.9	26.4	30.8	35.4

Figures 6.2 and 6.3 show the pore size distributions of coked catalysts following 5 hrs and 2 hrs of coking time as well as the pore size distribution of fresh catalyst. The fresh catalyst has only one broad peak with a mean pore radius of ~ 40 angstroms. But after coking, the catalysts possess bimodal pore size distributions (Richardson, 1996). The median pore sizes for the principal broad peaks which originate from catalyst were reduced. Generally the more coke forms, the smaller the median pore size of the principal peak.

The adsorption/desorption isotherms of fresh catalyst and coked catalyst for 2 hrs and 5 hrs of coking time are shown in Figures 6.4 and 6.5, respectively. The shift of the adsorption/desorption hysteresis curves for coked pellets compared with fresh pellets results from the lower relative intrusion pressure required to reach similar relative pore volumes in the coked pellets. The coked pellets appear to contain smaller pores than the fresh pellets resulting from preferential coke deposition in larger pores rather than in smaller ones. This effect is shown directly in Figures 6.2 and 6.3. The similarity of the hysteresis curves for coked catalyst and fresh catalyst suggests that the coked catalyst pores retain shapes similar to those of fresh catalyst and that pore narrowing rather than pore mouth plugging occurs during coke deposition. Both the pore size distribution

(Figure 6.2 and 6.3) and adsorption/desorption hysteresis curves (Figures 6.4 and 6.5) show that the catalyst pores coked in the L1 phase were narrowed more, on average, than in the L2 phase.
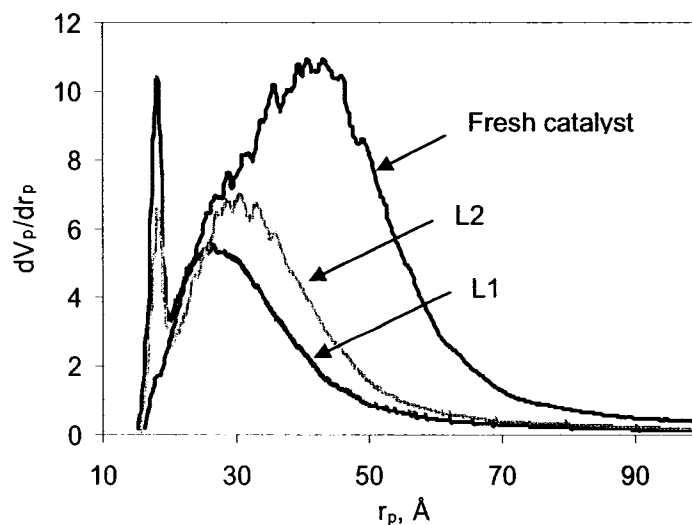
Figure 6.2 Pore size distributions of coked catalysts for 2 hrs of coking.
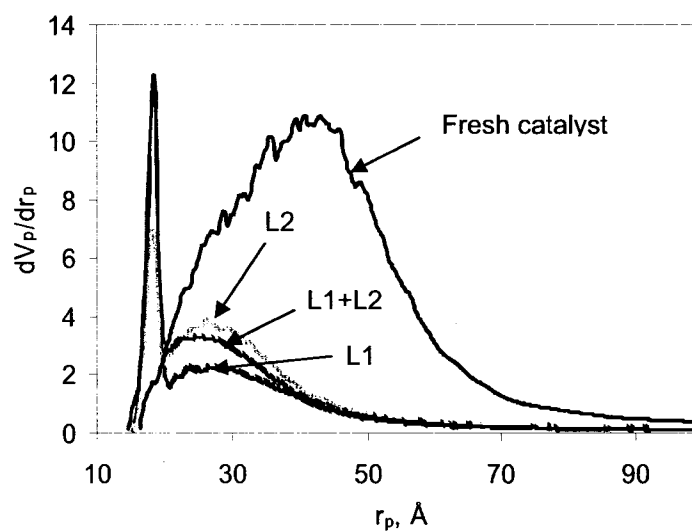
Figure 6.3 Pore size distributions of coked catalysts for 5 hrs of coking.

93
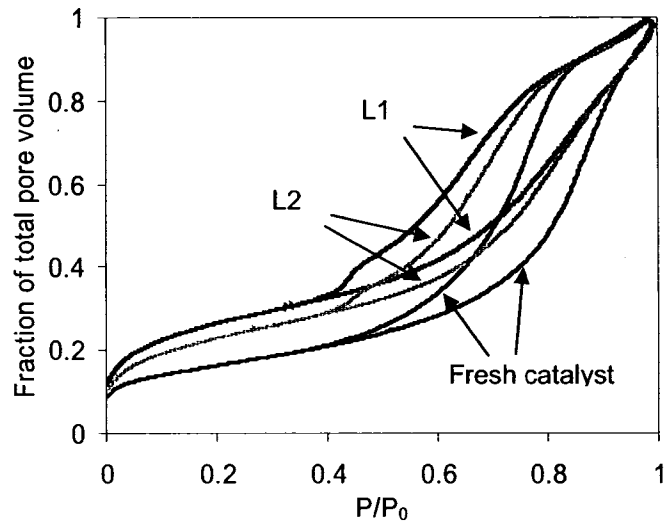
Figure 6.4 Adsorption/desorption isotherms of coked catalyst following 2 hrs of coking.
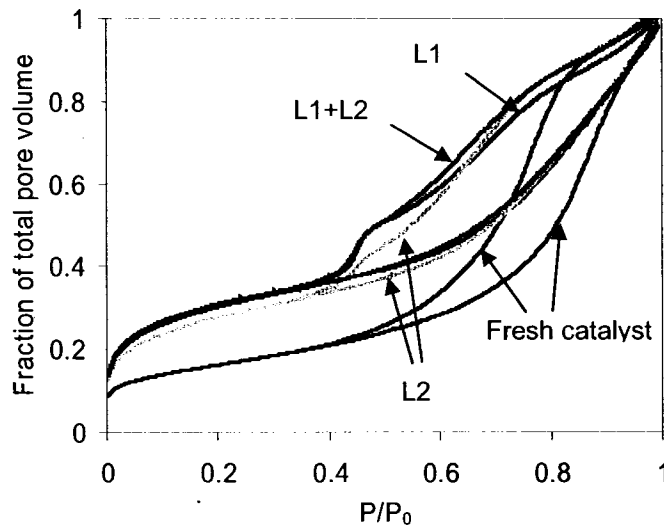
Figure 6.5 Adsorption/desorption isotherms of coked catalyst following 5 hrs of coking

6.4 Characteristics of Cross Sections of Coked Catalyst Pellets.

It is difficult to section and analyze interior surfaces of catalyst pellets without introducing artifacts and care must be taken to avoid over interpretation of data obtained. For example, some smearing of all elements arises on exposed surfaces during polishing. This is unavoidable. Fortunately, the microprobe sample volume extends well below the

94

surface, and the smearing represents only a small fraction of the volume sampled. Similarly, it is difficult to analyze for carbon in gold coated samples, due to the relative weakness of the signal from carbon, and one must accept that the carbon content of carbon coated samples is relative. Element distributions within mounted and polished catalyst pellets following 5 hours of coking, as well as for a control sample (mounted and carbon coated fresh catalyst) are reported in Figure 6.6. For the coked catalyst, the average value for carbon is ~ 20 wt %, for sulphur ~ 6.5 wt % and for vanadium ~ 0.03 wt % (6 times the detection limit). The average value for carbon in the control is ~ 10 wt %. The basis for the local composition measurements includes the carbon coating, the organic deposit and catalyst. Clearly, the coating represents only a small fraction of the volume sampled. The carbon content of the control would otherwise be higher. The mass fraction for carbon in deposits is overstated whereas the mass fraction of vanadium in deposits is understated due to the carbon coating. The local mass fraction for sulphur includes sulphur in the sulfidized catalyst (nickel sulphide and molybdenum sulphide) and the organic deposit. These cannot be discriminated based on the measurements. Despite these artifacts, it is clear that carbon, comprising ~ 27 wt % for the spent catalyst as a whole (obtained from bulk measurements and reported in Table 6.1) is deposited preferentially on exterior as opposed to interior surfaces of the catalyst irrespective of which of the two phases, L1 or L2, wets the catalyst. The carbon content within the pellets is significantly lower in all cases ~ 10 to 20 wt % than the bulk measurement. Unfortunately, since the data are very scattered, it is impossible to discriminate the difference among three cases. The results confirm that carbon, vanadium and sulphur are well distributed throughout the pellets, as one would expect for catalysts possessing a network of macropores. All of these are consistent with the results in the literature (Higashi et al. 2004).

The coke layer thicknesses for the cases investigated are presented in Figure 6.7 and range from 10 to 20 microns. The coke did not deposit on the outer surface of catalyst uniformly. A fresh catalyst pellet, Figure 6.7 a, acts as a control. If one assumes that the carbon content in coke is 85 wt%, the external coke layer accounts for 15-20 wt% of the total coke present. It is evident that coke layer thickness is variable at fixed reaction time regardless of the phase to which the catalyst was exposed. Coke was also deposited on

vessel surfaces. Such deposits are thought to arise from asphaltene precipitation during thermal reaction (Gray et al. 1999). If so, asphaltenes are clearly precipitating from both L1 and L2 phases and the catalyst pellets act as traps for asphatenes, as the liquid circulates among the pellets.
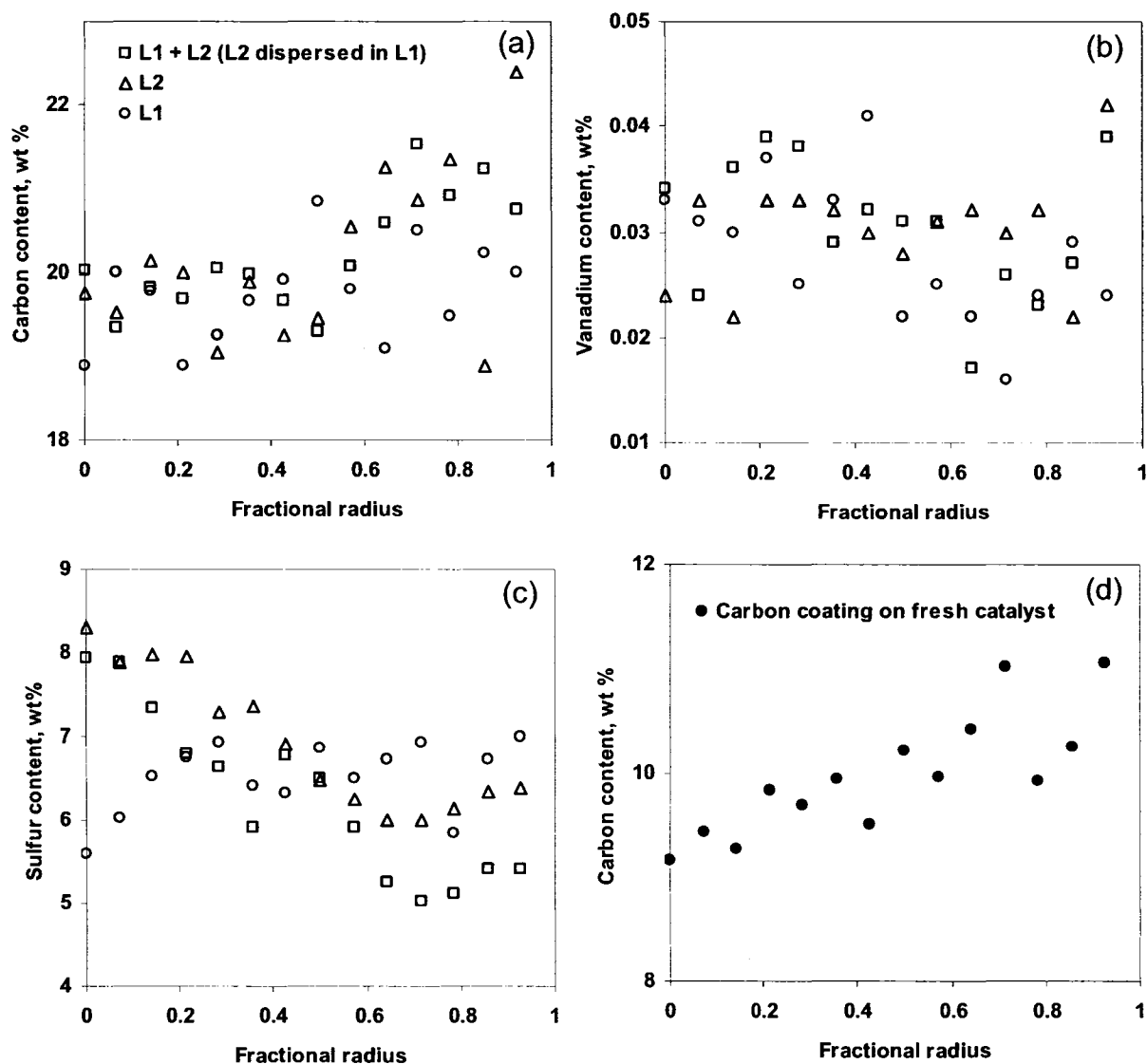
Figure 6.6   Element distributions within catalyst pellets for a) carbon (including carbon coating), b) vanadium, c) sulphur for 5 hours of coked catalyst and d) for the carbon coating on fresh catalyst.

The mechanism appears to be the same in both L1 and L2 – a surprising result given the composition differences between two phases. According to the catalyst characterization, the coke deposition observed in these experiments is similar to the bulk phase coke deposition model schematically represented in Figure 1.1c. However, since the coke

96

deposited preferentially in larger pores than in smaller ones, coke did not uniformly deposit on the catalyst inner surface. And pore-mouth plugging was not observed as well. A modified coke deposition model is schematically represented in Figure 6.8.
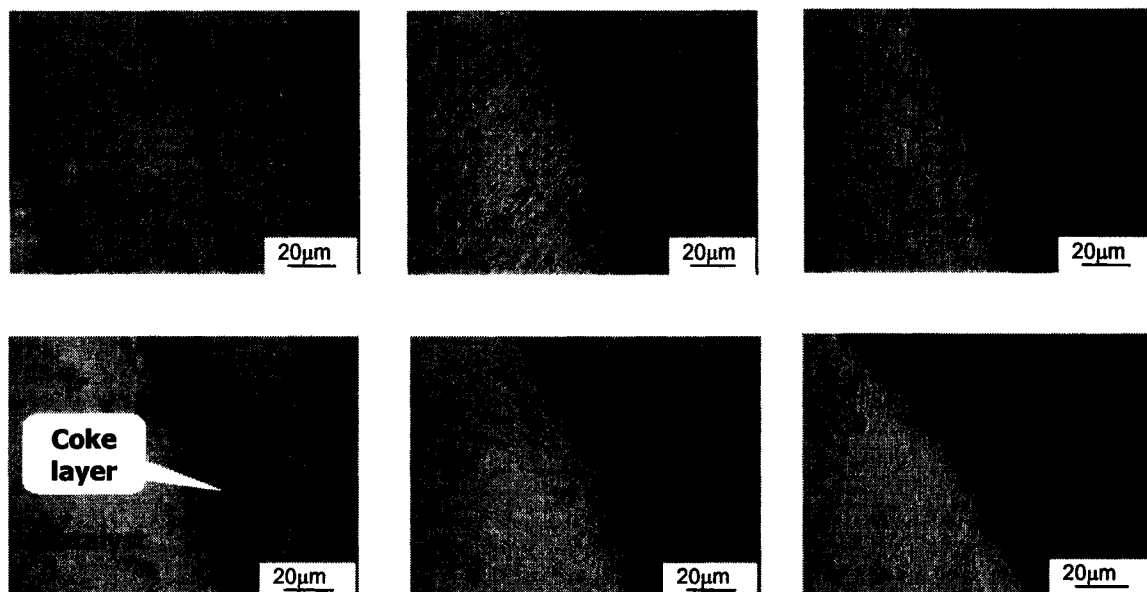
Figure 6.7 Photomicrographs of catalyst cross-sections for a) fresh catalyst; b) 2hr coked catalyst in L1; c) 2hr coked catalyst in L2; d) 5hr coked catalyst in L1+ L2 dispersed; e) 5hr coked catalyst in L1; f) 5hr coked catalyst in L2.
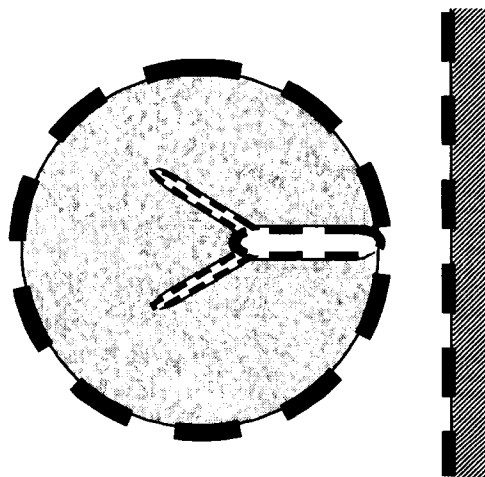
Figure 6.8 Modified bulk phase coke deposition model

97

6.5 Possible Explanations for Greater Deposition in Catalysts Exposed to L1 vs L2

The carbon contents, surface area and pore volume losses for catalyst pellets exposed to L1 are greater than for the corresponding L2 case. As the mass of the catalyst is small compared to the mass of the bulk phases and the mass of coke precursors present in each phase, and the residence times are relatively long, one may examine transport processes for an explanation of the above results. The viscosity of the L1 phase (a solvent-rich phase) is less than the viscosity of the L2 phase (an asphaltene-rich phase). One is tempted to assert that therefore L1 circulates more readily within the macropores of the pellets facilitating asphaltene transport and hence coke deposition. High-temperature viscosity data for bitumen combined with a variety of alkane solvents does not support this assertion as the viscosities of both phases at 380 °C are low – less than 2 mPa-s (Seyer and Gyte, 1989). An alternative explanation must be sought for these results.

Asphaltene aggregates size may play an important role at the beginning of coking. A fraction of asphaltene aggregates present in heavy oils are small enough to be observed by SAXS measurements. Figure 6.9 shows scatterer size distribution data for ABVB and ABVB (5 wt %) + dodecane. The method is limited to scatterers with leading dimensions in the 10 Å to 1000 Å size range. While the conditions are not identical to the ones employed in the coking experiments, it is clear that a greater fraction of smaller scatterers is present in ABVB diluted in dodecane over a broad range of temperatures than in the parent oil under similar conditions. Further, the leading dimensions of these small scatterers fall well within the size range of catalyst pores. Thus, the average scatterers present in L1 (the dilute ABVB phase) may penetrate the catalyst more readily than the average ones present in L2 (the more concentrated ABVB phase). This difference readily accounts for the greater pore area and pore volume loss, and coke content within pellets for the L1 vs. L2 cases. After a coke layer is formed on the catalyst outer surface, the asphaltene aggregates do not further affect coking in the pellet interior. It is also well known that the deposit at the early stage of the catalyst fouling process is deposited reversibly and desorbs under favourable operating conditions. Thus the solubility of initial deposits in the surrounding liquid phase may also play a role. Since the L2 phase

98

has a higher solubility for the asphaltenes and sediments than the L1 phase, one could argue that less material and possibly different material deposits on the catalyst. Both of the latter explanations are tenable, based on experimental evidence.
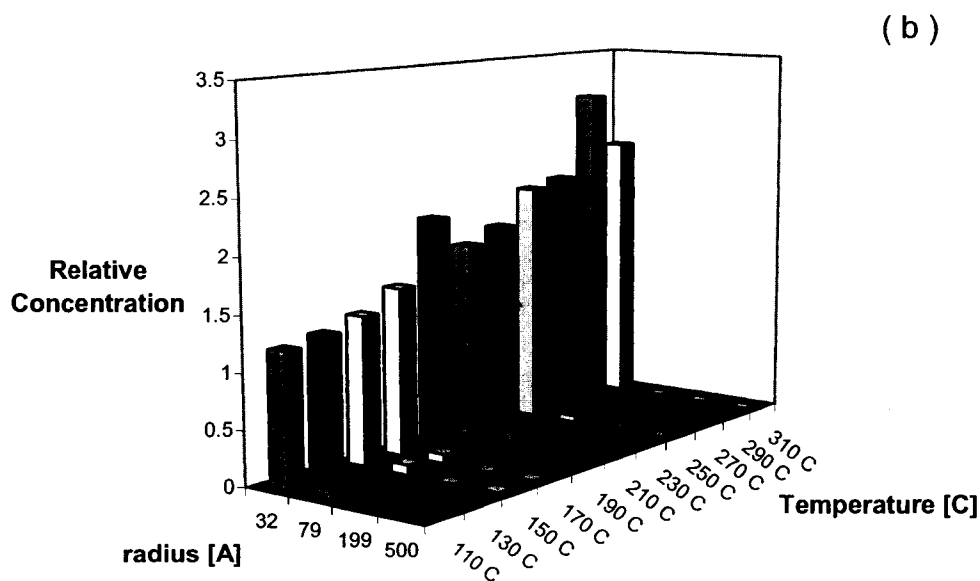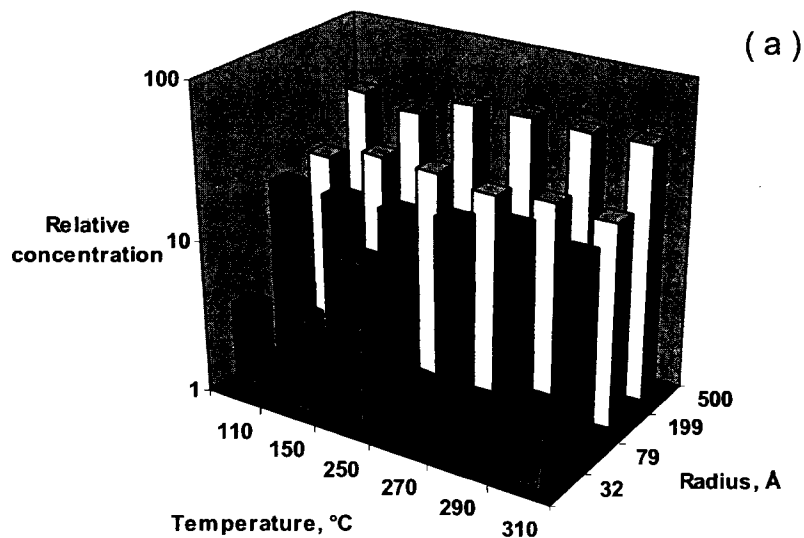
Figure 6.9   Asphaltene aggregate size distribution for a) ABVB (32 wt % asphaltenes); b) 5% ABVB in dodecane (1.6 % asphaltenes).

99

6.6 Origin of the Bimodal Pore Size Distribution

There is no significant difference between the reported surface areas and pore volumes when spent catalyst powder or pellets from the 5 hr L1 +L2 dispersed case are analyzed – Table 6.2 and Figure 6.10 a. However, nitrogen uptake in catalyst pellets at low pressure (P/P0 < 0.3) is significantly less for the whole pellets than for powdered catalyst – Figure 6.10 b, and the sorption isotherms are functionally different. According to the classification of isotherm types (Gregg and Sing, 1982), the isotherm for the powder is a type II isotherm, while the isotherm for the pellets shows type III isotherm behaviour. Clearly, the external coke layer possesses a small mean pore size that hinders but does not prevent nitrogen diffusion into the catalyst. The secondary peak at 18 angstroms, only present in the coked pellets, is therefore attributed to coke and not the catalyst per se.

(a)   (b)
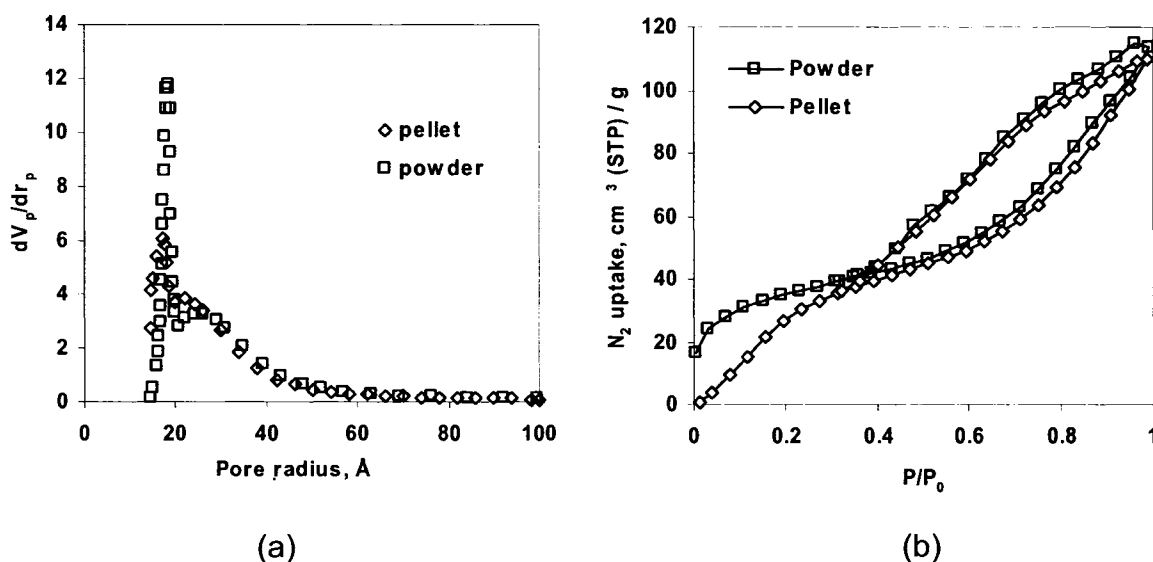
Figure 6.10   A comparison of (a) the pore size distribution and (b) sorption isotherm for powdered and pellet coked catalyst samples from the 5 hr, L1 + L2 dispersed case.

6.7 Summary

The influence of multiphase behaviour on coke deposition on and within commercial hydrotreating catalyst pellets in the absence of hydrogen was explored using the model

100

mixture Athabasca vacuum bottoms (ABVB) + decane. Under these conditions, the impact of phase behaviour on the amount of coke deposited on and within catalyst pellets and the distribution of coke within catalyst pellets was found to be a secondary one despite the differences in the physical properties of the solvent rich L1 phase and asphaltene rich L2 phase. In all cases, the exterior surfaces of pellets were coated with a thick nanoporous deposit layer. Observed differences in mean pore size, pore surface area and pore volume of coked catalyst exposed to the L1 and L2 phases and to multiphase environments are consistent with observed differences in the asphaltene aggregate size distribution and asphaltene solubility in the two phases.

7. The Impact of Multiphase Behaviour on Coke Deposition in Catalyst Exposed to ABVB + Decane + Hydrogen Mixtures*

7.1 Introduction

As noted in Chapter 5, hydrogen addition does not change the nature of the phase behaviour of the model system (ABVB + decane), but does shift the phase behaviour regions of interest from lower to higher pressure. It is well known that hydrogen significantly reduces coke deposition on catalysts, but it is not clear how hydrogen affects coke deposition when multiple phases are present. In this chapter, the impact of hydrogen, total pressure, and phase behaviour on coke deposition in catalyst pellets is investigated and discussed.

7.2 Catalyst Coking Experimental Design.

The catalyst coking experiments with ABVB + decane + hydrogen mixtures were conducted at 380 °C for 2hrs. The catalyst charge was 0.3 g in its sulphide form and the liquid charge was 60 g. All of the experiments were conducted at a hydrogen/liquid mass ratio of 0.0057, except for one where the ratio was 0.0086. Not only was the effect of phase behaviour per se addressed, as discussed in the previous chapter, pressure and composition effects were investigated as well. The conditions for all experiments, except for the higher hydrogen/feed mass ratio (0.0086), are labeled with solid circles in the P-x phase diagram (Figure 7.1). The conditions examined include the phase regions L2V, L1L2V, L1V, and at low ABVB compositions (10, 20, 30 wt %) at least two pressures were examined. The catalyst coking experiment for the higher hydrogen/feed mass ratio (0.0086) was conducted at only 30 wt% ABVB where the mixture exhibits L1L2V phase behaviour. In this latter case, the pressure was 144.5 bar. Again, catalyst was placed as shown in Figure 3.8 where the L1L2V phase behaviour arose. If the L2 phase was absent at the experimental conditions (> 50 wt % ABVB), the catalyst was placed as shown in Figure 3.8b. At low ABVB composition (< 30 wt %) where only L2V phase behaviour

was observed, the catalyst was placed in the V and L2 phases.
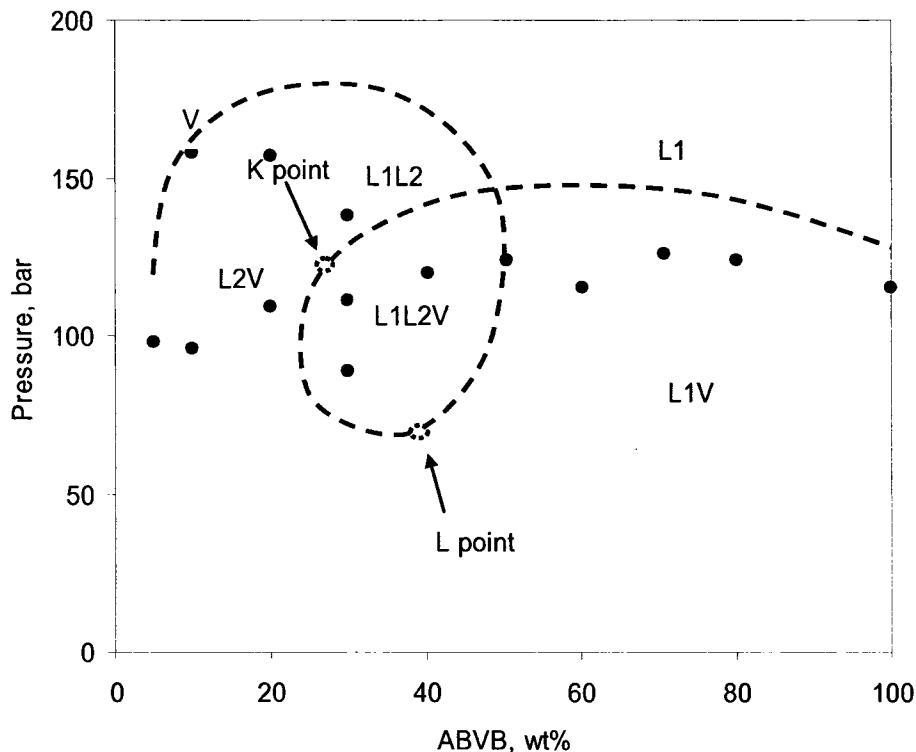
Figure 7.1   The conditions for the catalyst coking experiments with ABVB + decane + hydrogen. The hydrogen to feed mass ratio was fixed at 0.0057.

7.3 The Impact of Hydrogen Addition on Coke Deposition

With catalyst placed as in Figure 3.8a, the impact of hydrogen addition on coke deposition is illustrated by comparing the carbon content of coked catalyst exposed to the L1 and L2 phases in the presence of hydrogen with the results obtained in the absence of hydrogen (Table 7.1). The experimental conditions with hydrogen case both from a thermodynamic and hydrodynamic perspective are similar to those for the hydrogen free case except for pressure (Table 7.2). As expected, hydrogen significantly reduces coke deposition in catalyst pellets exposed to both the L1 and L2 phases. Since less coke is formed in the presence of hydrogen, pore volume and surface area losses are correspondingly lower. In the absence of hydrogen, the carbon content of the catalyst exposed to L1 is greater than for the corresponding L2 phase, contributing to greater pore volume and surface area loss in the L1 than in the L2 phase. This result was attributed to

103

differences in the mean asphaltene aggregate size and asphaltene solubility in the two phases. In the presence of hydrogen, the carbon content of the catalyst exposed to the L2 phase is greater than for the corresponding L1 phase. Hydrogen solubility in the L1 phase is greater than in the L2 phase. This facilitates hydrogenation preferentially in the L1 phase compared to the L2 phase, thus reducing coke deposition, as well as pore volume and surface area losses for catalyst exposed to the L1 versus L2 phase. By increasing the hydrogen/feed mass ratio from 0.0057 to 0.0086, the carbon content was further reduced but not as significant as from 0 to 0.00057 ratio and the statistical analysis of error of experimental data (95% confidence) shows the difference is at margin. It is anticipated that when more hydrogen is added into a reactor with a fixed volume within a certain hydrogen/feed ratio, the pressure, as well as the hydrogen solubility in liquid phases, increases, thus reducing coke deposition.

The catalysts coked in the presence of hydrogen also possess a bimodal pore size distribution (Figures 7.2), similar to those coked in the absence of hydrogen. However, the secondary peak at 18 Å, attributed to coke, is less pronounced. The sorption/desorption isotherms for fresh and coked catalysts are shown in Figures 7.3. The hysteresis curves for these coked catalysts are similar to that for fresh catalyst, indicating that pore narrowing rather than pore mouth plugging occurred during coke deposition. Thus, the coke deposition mechanism is unaffected by the presence of hydrogen.

Table 7.1   The impact of hydrogen addition on coke deposition.

Hydrogen/feed, g/g	0.0000		0.0057		0.0086	
Phase	L1	L2	L1	L2	L1	L2
C, wt %	23.3	20.7	14.5	16.4	13.9	15.6
H, wt%	1.94	1.82	1.61	1.75	1.68	1.62
H/C, mole/mole	1.00	1.05	1.34	1.28	1.45	1.25
S, wt%	2.9	3.6	5.6	5.2	5.9	5.9
N, wt%	0.48	0.46	0.47	0.44	0.50	0.47
surface area, m^2/g	157	165	162	156	151	163
pore volume, cm^3/g	0.24	0.29	0.35	0.32	0.35	0.34

Table 7.2 Experimental conditions for experiments associated with Table 7.1

Hydrogen/feed g/g	ABVB content wt%	Pressure Bar	Phase	Volume cm^3	Density g/cm^3
0.000	29.9	30.0	L1	93*	~ 0.47
			L2	9*	~ 0.87
0.0057	30.0	110.0	L1	80*	~ 0.44
			L2	16*	~ 0.80
0.0086	30.0	144.5	L1	~90	--
			L2	~10	--

* Phase volume and density were obtained from the phase behaviour experiments
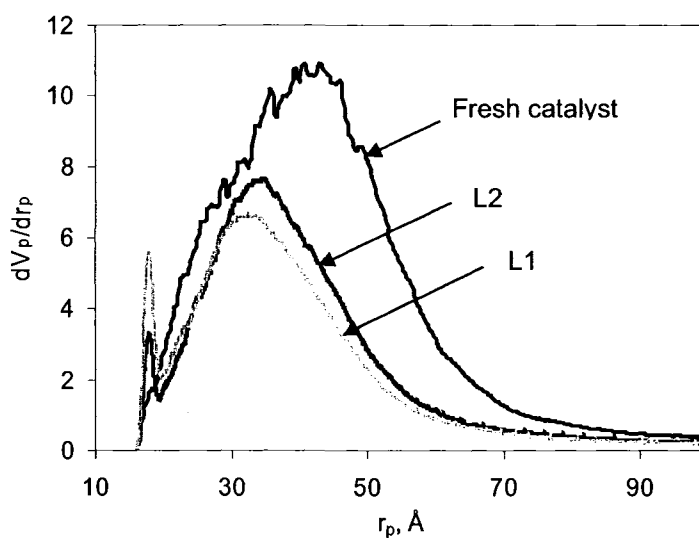
Figure 7.2   Pore size distributions of fresh catalyst and coked catalyst for a hydrogen/feed ratio of 0.0057.
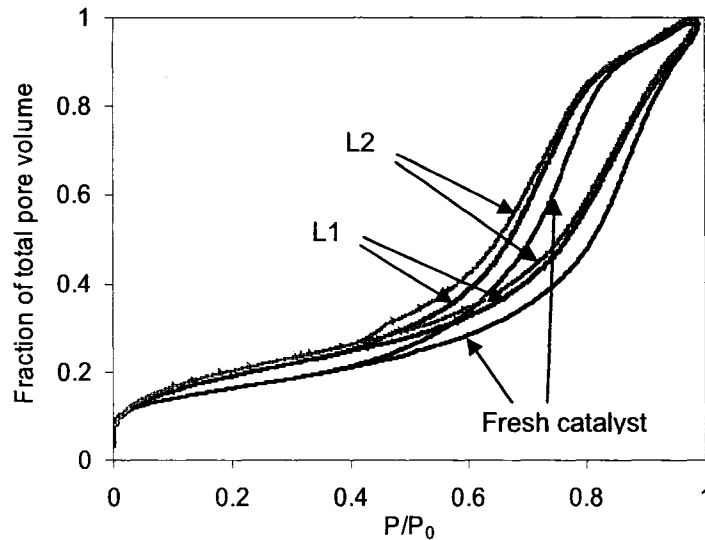
Figure 7.3 Adsorption/desorption isotherms of fresh catalyst and coked catalyst for a hydrogen/feed ratio of 0.0057.

7.4 The Impact of Pressure on Coke Deposition

The effect of pressure on coke deposition was investigated at three different fixed global compositions. The results, which illustrate the composite nature of pressure as a variable, are shown in Figure 7.4. The phase behaviours included V+L2 dispersed (10 wt % and 20 wt % ABVB) and L1+L2 dispersed +V and L1+L2 dispersed (30 wt % ABVB). For the 10 % and 20 % ABVB + decane + hydrogen mixtures, the carbon content of the catalyst decreased as pressure was increased. For these two cases, the mass fraction of the L2 phase decreased in favour of the vapour phase. The hydrogen concentration in the vapour phase and the hydrogen solubility in the L2 phase increased concurrently. For 30 % ABVB, the mass fraction in the vapour phase decreased as pressure was increased; the mass fraction in the L2 phase increased then decreased vis a vis the L1 phase as pressure was increased, while hydrogen solubility increased with pressure. For this latter case, the impact of pressure is much less pronounced for a comparable pressure change. Clearly, transfer of feed to the vapour phase as pressure is increased has a greater impact on reducing coke deposition than shifting feed from L2 to L1 or the impact of pressure on hydrogen solubility in either of the liquid phases. This result is consistent with both thermodynamic and kinetic arguments for why increasing pressure reduces coke deposition. However, pressure is a composite variable and changes in phase behaviour

106

with pressure can largely negate this effect. Further, dense vapours are preferred over liquids from the perspective of avoiding coke deposition on catalyst pellets.

ABVB, wt%:	10	20	20	30	30	30
Pressure, bar: 96	158	109	157	89	111	138
L2 volume, cm³: 3	~1*	8	~1*	12	23	6
L1 volume, cm³: --	--	--	--	77	117	143
V volume, cm³: 197	153	166	146	112	26	--

(Chart y-axis: Carbon, wt% from 12.0 to 15.0)
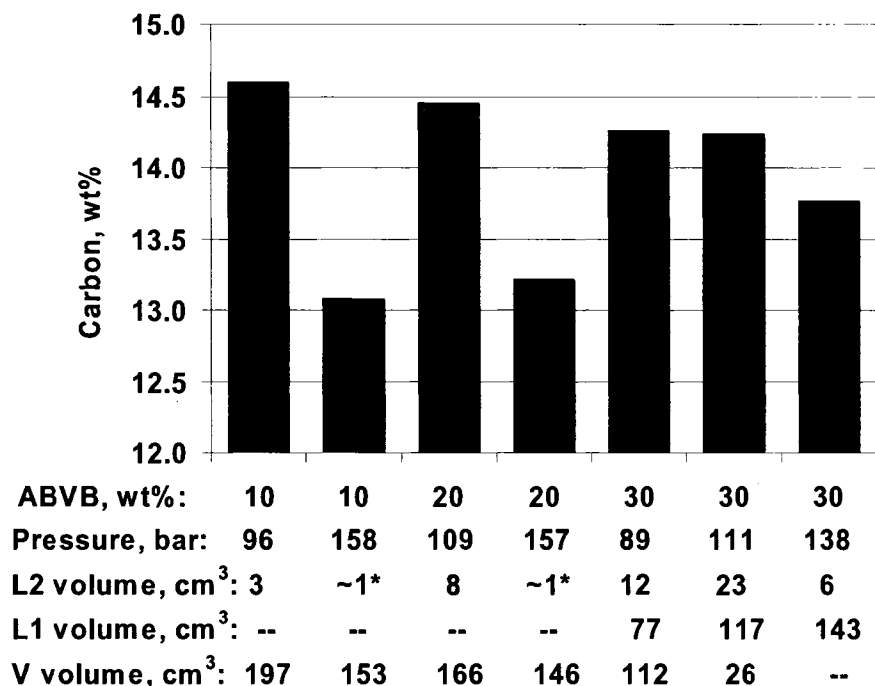
Figure 7.4   The effect of pressure on coke deposition on catalysts under the hydrodynamic regime illustrated in Figure 3.8b. Except as noted, phase volumes are measured ~ 15 minutes after coking reaction at 380 °C. * Phase volume is estimated from phase behaviour experiments.

7.5 The Effect of Composition on Coke Deposition

Coke deposition at compositions ranging from 5 % ABVB to 100% ABVB was evaluated in order to examine the effect of composition coupled with phase behaviour on coke deposition. Hydrogen consumption during coking experiments is very low, i.e. is less than 3 % of the hydrogen present for the 20% ABVB case, assuming that most of the hydrogen is consumed for sulphur removal. Thus the mass ratio of hydrogen to oil remains nearly constant through a 2-hour experiment. Catalyst placement was as shown in Figure 3.8b. Global compositions, approximate phase volumes, pressures and other experimental details are shown in Table 7.3. From the coke deposition vs. composition

107

profile, Figure 7.5a, the maximum carbon content arises at low ABVB mass fraction ~ 10 wt % ABVB. The carbon content drops sharply with either an increase or a decrease in ABVB mass fraction from this composition. Above 50 wt % ABVB, the carbon content of the coked catalyst appears to increase again slightly. With reference to the phase diagram shown in Figure 7.1, coke deposition is greatest in the L2V region, tapers to lower values within the L1L2V region and is least in the L1V region even though nominal coke precursor concentration increases monotonically with ABVB mass fraction and the L2 volume peaks at ~ 30 wt % ABVB. Clearly, the L2 phase is most closely associated with coke deposition irrespective of the global composition of coke precursor.

BET surface areas (Figure 7.5 b), pore volumes (Figure 7.5 c), sorption/desorption isotherms (Figure 7.5 d) and pore size distributions (Figure 7.5 e) were obtained from samples of the coked catalyst. At low ABVB content, the surface area and pore volume of the coked catalyst drop rapidly with concentration but above 10 wt % ABVB, neither the surface area nor the pore volume change significantly. As well, the effect of composition on sorption/desorption isotherms and the pore size distributions, Figures 7.5 d and e, are not significant. Even though the effect of phase behaviour on coke deposition for BET analysis is not as obvious as for coke content, this does not mean the phase behaviour has no effect on the pore structures of coked catalysts. The BET method may not be sensitive enough to detect the slight differences caused by composition variation. With reference to Figure 7.5, results from repeated experiments reported in Appendix V show that the error in the BET measurements is relatively high compared to the analysis of carbon content.

7.6 Summary

Hydrogen plays a very important role in suppressing coke deposition, leading to less pore volume and surface area loss. At the same global composition, coke deposition in the L2 phase is greater than in the L1 phase since hydrogen solubility in L2 phase is much lower than in the L1 phase. The more dense liquid phase, L2, was most closely associated coke deposition, the less dense liquid phase, L1, was less associated with coke deposition, and the vapour phase, V, least associated with coke deposition. Coke deposition is greatest in the L2V region, tapers to lower values within the L1L2V region and is least in the L1V

108

region even though nominal coke precursor concentration increases monotonically with ABVB mass fraction and the L2 volume peaks at ~ 30 wt % ABVB. Clearly, all of the above observations indicate the L2 phase is most closely associated with coke deposition irrespective of the global composition of coke precursor.

Table 7.3 Experimental conditions for the experiments associated with Figure 7.5.

ABVB Composition wt%	Pressure Bar	Phase behaviour	Phase volume cm^3
5.0	98	V	199
		L2	N/d
10.0	96	V	197
		L2	3
20.1	109	V	166
		L2	8
30.0	111	V	26
		L1	117
		L2	23
40.3	120	V	36
		L1	106
		L2	9
50.4	124	V	42
		L1	101
		L2	n/d or no L2 phase
60.1	115	V	36
		L1	103
70.6	126	V	76
		L1	58
80.0	124	V	43
		L1	85
100	115	V	48
		L1	76
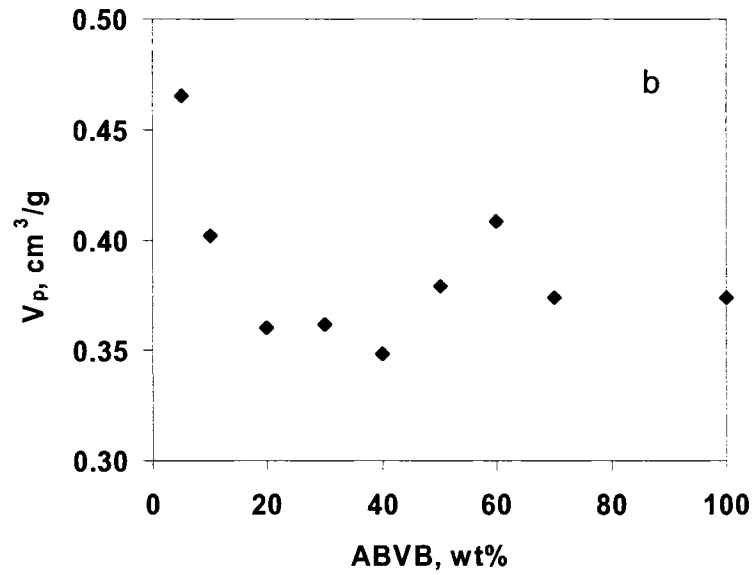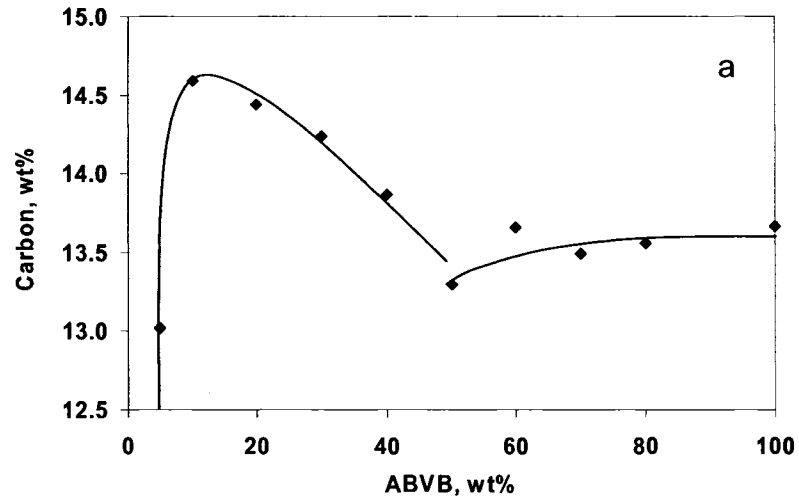
Figure 7.5   The effect of phase behavior on coke deposition at 0.57 wt % hydrogen. a) carbon content in coked catalyst; b) coked catalyst pore volume; c) coked catalyst surface area; d) adsorption/desorption isotherms and e) pore size distributions.

110
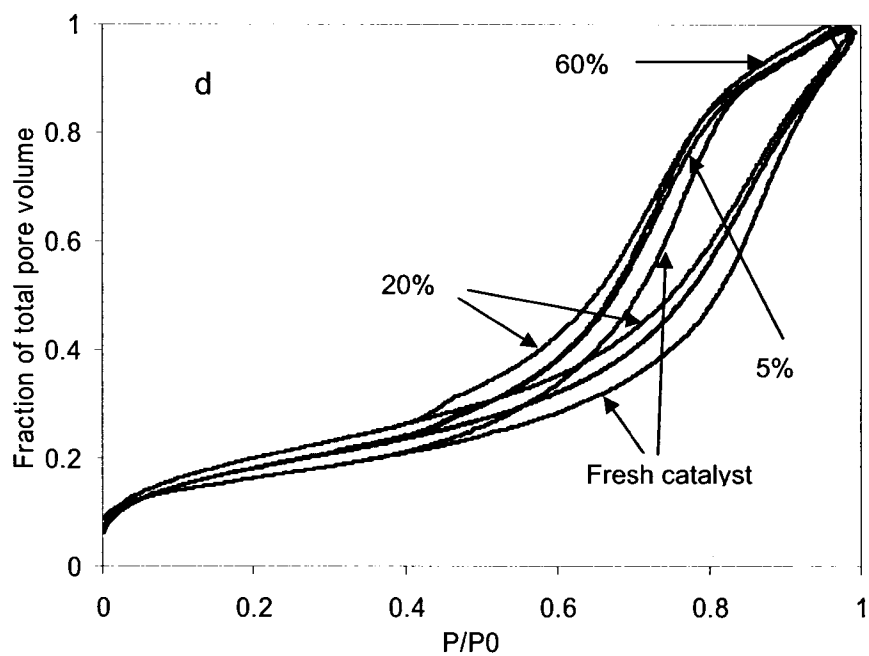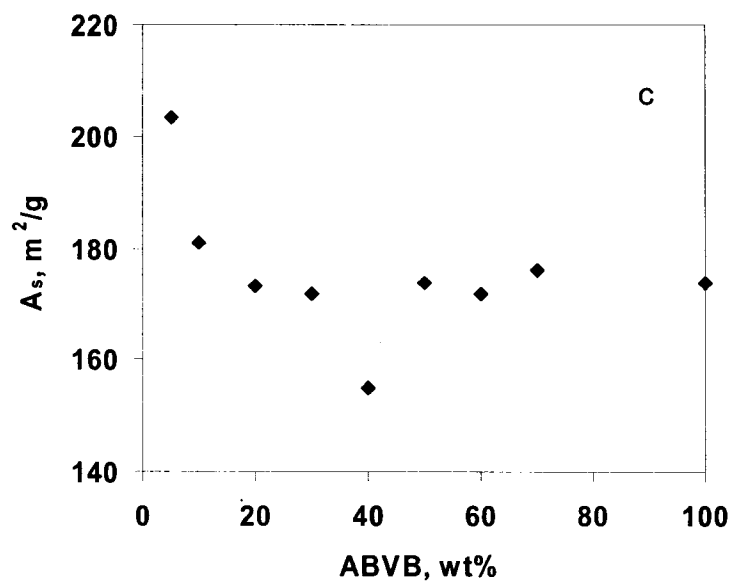
Figure 7.6 The effect of phase behavior on coke deposition at 0.57 wt % hydrogen. a) carbon content in coked catalyst; b) coked catalyst pore volume; c) coked catalyst surface area; d) adsorption/desorption isotherms and e) pore size distributions.

111

e

dV$_p$/dr$_p$

100% ABVB
70% ABVB
60% ABVB
50% ABVB
40% ABVB
30% ABVB
20% ABVB
10% ABVB
5% ABVB
Fresh catalyst

10   30   50   70   90

r$_p$, Å
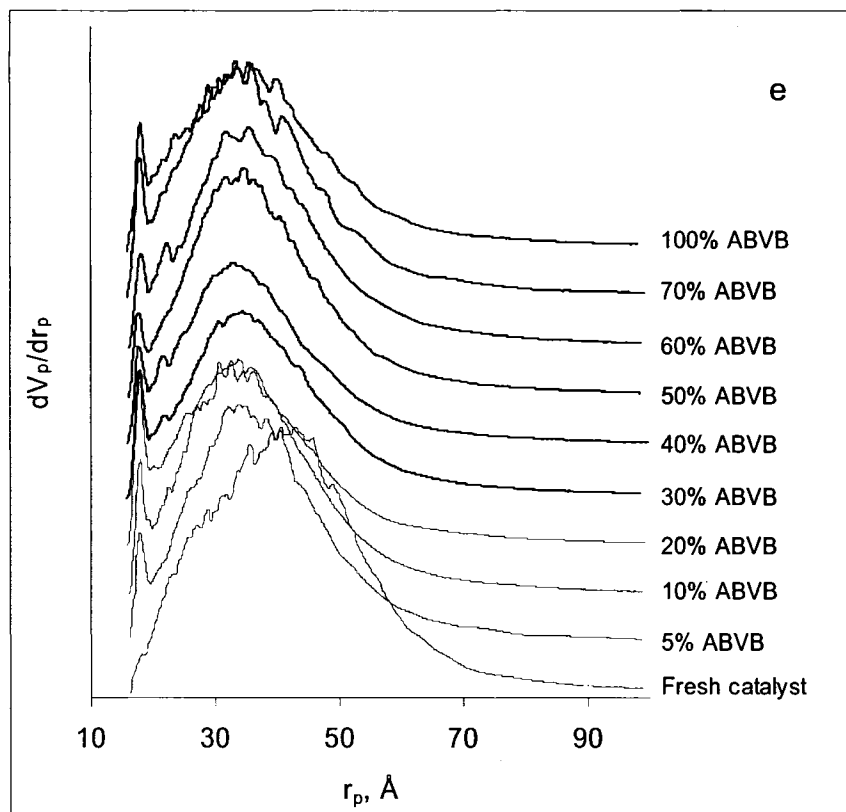
Figure 7.7   The effect of phase behavior on coke deposition at 0.57 wt % hydrogen. a) carbon content in coked catalyst; b) coked catalyst pore volume; c) coked catalyst surface area; d) adsorption/desorption isotherms and e) pore size distributions.

112

8. Coke Deposition Models

8.1 Coke Deposition Variation with Comparison

Development of quantitative models describing the rate of coke deposition on catalyst as a function of coke precursors is frequently one of the aims of catalytic hydroprocessing investigations. Such kinetic models are difficult to formulate. Coking kinetic equations, whether based on empirical correlations or mechanistic models (Furimsky and Massoth, 1999; Froment and Bischoff, 1979), usually predict a smooth curve for coke deposition versus coke precursor concentration for a fixed reaction time, temperature, and pressure. If one assumes that an ABVB constituent is a coke precursor, the predicted coke deposition profile should increase starting from a minimum, at 0 wt. % ABVB, to a maximum at 100 percent ABVB in the feed. Catalyst coking experiments (batch reactor) for 1-methyl naphthalene + ABVB + hydrogen mixtures appear to have exactly this trend – Figure 8.1. The carbon content increases monotonically with ABVB content. From previous work in our group, the 1-methly naphthalene + ABVB + hydrogen mixtures exhibit only L1V phase behaviour. However, mixtures of decane + ABVB + hydrogen exhibit complex multiphase behaviour under similar reaction conditions. The results from the catalyst coking experiments (batch reactor) for decane + ABVB + hydrogen show a pronounced maximum in the carbon content of the coked catalysts in the L2V phase region at low ABVB concentration. The coke deposition profiles by view cell and batch reactor have the same trend.

A sketch of coke deposition profiles, Figure 8.2, illustrates the difference between the expected coke deposition profile and the profile observed in this work. The expected profile follows the curve including segments I, III and II. The observed profile follows curve segments I, IV and II. The two profiles overlap in segments I and II, i.e., in the V and L1 or L1V phase regions and diverge for the L2V, L1L2V or L1L2 phase regions (segment IV). This observed behaviour is inconsistent with expectation and with coke deposition models where the extent of coke deposition, at otherwise fixed reaction conditions, is proportional to the nominal concentration of coke precursor present in the feed. The present results suggest that the nature of phases present must be included in coke deposition models in order to capture key deposition phenomena. Coke deposition

113

models must also allow for phase behaviour variation with composition in order to predict or correlate multiphase behaviour effects even if, for example, only one of the liquid phases is encountered, at a time, in related experiments.
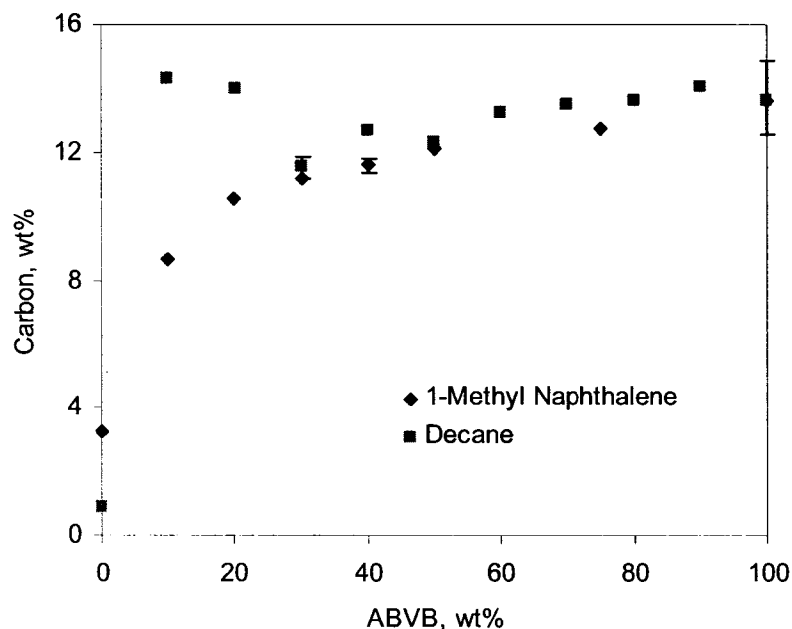
Figure 8.1   Comparison of coke deposition profiles for ABVB + decane + hydrogen mixtures which exhibit multiphase behaviour and ABVB + 1-methyl naphthalene + hydrogen mixtures which exhibit two phase behaviour. (All data from batch reactor)

8.2 Thoughts on Coke Deposition Models

In catalytic processes, we assume as most researchers do, that the coke forms at a catalyst surface by polymerization and condensation. It is known that aromatics are the major coke precursor, therefore in this model the aromaticity of the heavy oils can be taken as the concentration of coke precursors. If only one liquid phase is present, it is relatively easy to quantitatively formulate the coke deposition by simply following Langmuir-Hinshelwood type of kinetic equation. But if a second liquid phase coexists or develops during reaction, the following additional variables are introduced:

1. The L1 and L2 phase volumes

114

2. Coke precursor concentration, and size distribution in the case of asphaltenes in the L1 and L2 phases

3. Hydrogen solubility in the L1 and L2 phases

4. Catalyst contact probability with the L1 and L2 phases

These variables are not readily measured and much less modeled or predicted. Resolving the above issues involves great efforts.
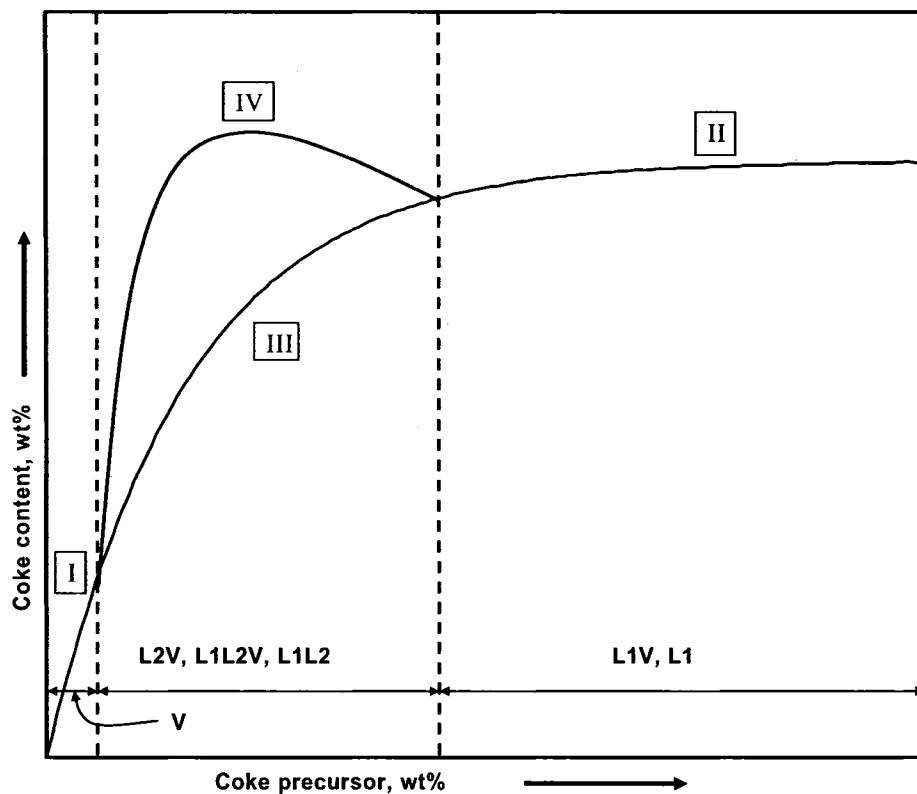
Figure 8.2   A sketch of comparing the experimental coke deposition profile involving multiphase behaviour and the predicted coke deposition profile with simple conventional kinetics at a fixed reaction time.

8.3 Summary

Inclusion of phase behaviour into catalyst fouling models is a complex task that requires significant process knowledge coupled with accurate phase behaviour prediction under process conditions and detailed understanding of the nanoscale associative phenomena arising in heavy oils. Development of quantitative inclusive models is premature.

115

9. Process Implications

9.1 Introduction

Based on the findings in this thesis, there are a number of implications for existing and potential processes associated with petroleum refining processes. As the heavy liquid phase causes more coke deposition, operators of existing processes should try to avoid operating under conditions where the heavy liquid phase is present or to minimize the amount of such phase; developers of new processes should select operating conditions where heavy liquid phase formation is avoided. Specific process implications are addressed below.

9.2 Trickle-Bed Reactor

Trickle-bed reactors are one of the most widely used reactor configurations in heavy oil hydroprocessing. The reactor comprises a fixed bed of catalyst particles contacted by a cocurrent downward gas-liquid flow carrying both reactants and products (Al-Dahhan et al. 1997). According to the definition of trickle flow, the liquid flows down the column from particle to particle on the surface of the catalyst particles while the gas phase flows through the void space among the catalyst particles as shown in Figure 9.1a (Ng and Chu, 1987). From the coke deposition data presented here, over dilution of feeds with lighter liquids or significant reaction leading to the production of lighter products, may push the whole bed or the lower part of the bed from the L1V region into the L1L2V region. Transfer to the L2V region would require significant dilution and is unlikely to arise in industrial practice. If even a small mass fraction of the feed or the liquid in the reactor is present as a dispersed L2 phase, then the flow regime and enhanced coke deposition associated with the presence of L2 arises (Figure 9.1 b), and catalyst life is shortened. The magnitude of this effect is uncertain at this time. From a practical perspective, trickle-bed reactors for the hydroprocessing of heavy oils should be operated in the L1V phase behaviour region to minimize coke deposition on catalyst. While dilution of heavy feed is not normally practiced, it is important to note that such dilution employed in the face of operating problems may exacerbate coke deposition for this application.

116
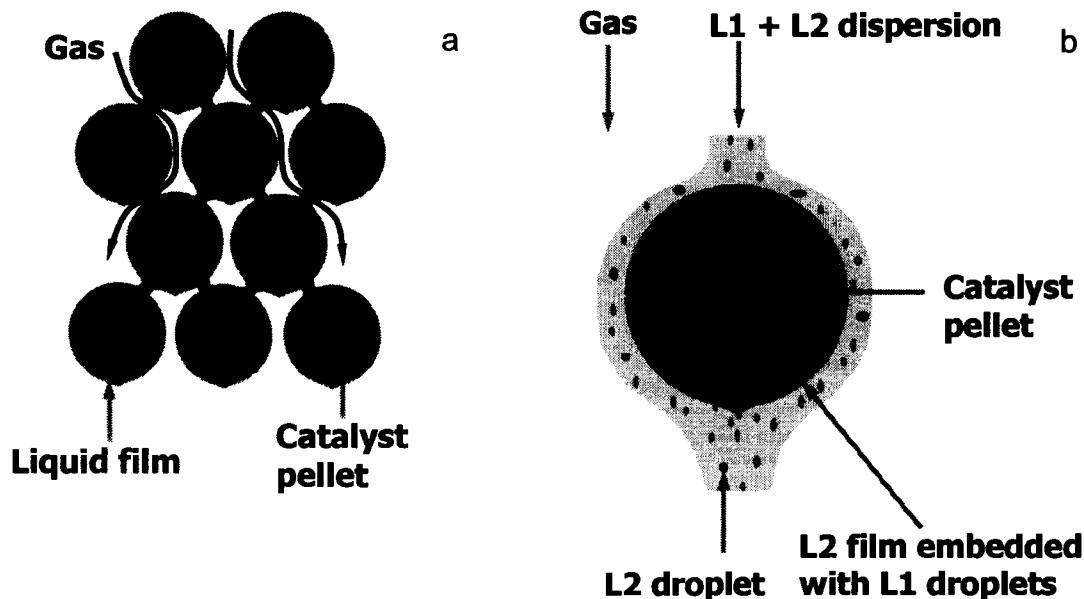
Figure 9.1 **Schematics of flow pattern in trickle-bed hydroprocessing reactor. a) a trickling flow pattern; and b) the flow pattern around a single pellet, in the presence of two liquid phases.**

9.3 Solvent Addition Processes and Supercritical Hydrogenation Processes

The more dense liquid phase, L2, is most closely associated coke deposition, the less dense liquid phase, L1, is less associated with coke deposition, and the dense vapour phase, V, is least associated with coke deposition. Therefore, operating conditions should be carefully controlled in order to avoid the L2 phase. Due to limitations imposed by the feedstock composition and desired conversion, sometimes it is not practical to adjust the operating conditions to remain within the L1V phase region. Dilution with highly aromatic cuts obtained from elsewhere in the refinery is an option, but ideally the reactors should be operated in a single dense V phase region to minimize coke deposition. This can be achieved by adding a suitable supercritical fluid to the system (Scotta et al., 2001). Here for example, when enough decane (> 80 wt %) is mixed with ABVB, the mixture becomes a single dense vapour phase at elevated temperature and pressure. In addition, in supercritical fluids, the diffusion coefficients are higher than in typical liquids and this

117

can enhance the desired hydrogenation reaction rates.

9.4 Summary

A practical approach to suppress coke deposition is by operating hydroprocessing reactors in phase regions where no L2 phase exists. However, an optimized process involves a lot of other considerations such as conversion rate, product qualities and so on. Therefore, when a current process reaches its best optimization, the only way for improvements is by modifying the current process or developing a new process. Solvent addition process is an example of modification of previous conventional processes. By fully understanding the new findings in this thesis from different perspectives, the current industrial processes can be improved or new processes can be developed.

118

10. Conclusions

The impact of multiphase behaviour on coke deposition in commercial hydrotreating catalyst pellets under typical catalytic hydrotreating conditions was explored using a model heavy oil mixture. Prior to the catalyst coking experiments, the phase behaviour of the model heavy oil system was first explored. The phase behaviour and catalyst coking experiments were conducted both in the presence of hydrogen and in the absence of hydrogen. The key conclusions are listed below:

1. The heavy oil model mixture Athabasca vacuum bottoms (ABVB) + decane exhibits low-density liquid + vapour, L1V, high-density liquid + vapour, L2V, as well as low-density liquid + high-density liquid + vapour, L1L2V, phase behaviour at typical hydroprocessing conditions. This multiphase behaviour facilitates the study of the impact of multiphase behaviour on coke deposition on $NiMo/Al_2O_3$ catalyst pellets.

2. As 380 °C is above the critical temperature of decane (344.6 °C), ABVB + decane mixtures exhibit vapour phase behaviour at low ABVB mass fractions at this temperature. For decane + 10, 20 wt % ABVB mixtures, L2 and L2V phase behaviour is observed, depending on pressure. For decane + 70, 90, and 100 wt % ABVB mixtures, only L1 and L1V phase behaviour was observed. L1L2V three phase equilibrium was observed at intermediate compositions: 30, 35, 40, and 50 wt % ABVB. Phase behaviour transitions from V for pure decane to L2V, to L1L2V, to L1V with increasing ABVB content are readily observed.

3. The addition of hydrogen to ABVB + decane mixtures does not change the nature of the phase behaviour significantly, but shifts the phase behaviour regions and boundaries from lower pressures to higher pressures.

4. The catalyst coking experiments in the absence of hydrogen show that the carbon content, surface area and pore volume losses for catalyst pellets exposed to the L1 phase are greater than for the corresponding L2 cases despite a higher coke precursor concentration in the L2 phase than in the L1 phase. This result may be attributed to differences in the asphaltene aggregates size distribution and asphaltene solubility in these two phases.

119

5. In the presence of hydrogen, the carbon content of the catalyst exposed to the L2 phase is greater than for the corresponding L1 phase. Hydrogen solubility in the L1 phase is greater than in the L2 phase. This facilitates hydrogenation preferentially in the L1 phase, thus reducing coke deposition, as well as pore volume and surface area losses for catalyst exposed to the L1 versus the L2 phase.

6. A comparison between experiments where no hydrogen is added and ones where it is added shows that hydrogen solubility plays a very important role in suppressing coke deposition in both L1 and L2 phases. And the hydrogen addition has a higher influence on the L1 phase in coke suppression than on the L2 phase due to the higher hydrogen solubility in L1 phase than in L2 phase.

7. In the presence of hydrogen, the more dense liquid phase, L2, was most closely associated coke deposition, the less dense liquid phase, L1, was less associated with coke deposition, and the vapour phase, V, is least associated with coke deposition.

8. Coke deposition is greatest in the L2V region, tapers to lower values within the L1L2V region and is least in the L1V region even though nominal coke precursor concentration increases monotonically with ABVB mass fraction and the L2 volume peaks at ~ 30 wt % ABVB.

9. The results from catalyst coking experiments with decane + ABVB + hydrogen show that the coke deposition variation with composition exhibits a maximum carbon content in the L2V phase region. This observed result is inconsistent with expectation and with coke deposition models where the extent of coke deposition, at otherwise fixed reaction conditions, is proportional to the nominal concentration of coke precursor present in the feed. The nature of phases present must be included in coke deposition models in order to capture key deposition phenomena. Coke deposition models must also allow for phase behaviour variation with composition in order to predict or correlate multiphase behaviour effects even if, for example, only one of the liquid phases is encountered, at a time, in experiments.

These findings have important implications for upgrading process development and operation improvement even though the results negate some aspects of the hypothesis proposed in Chapter 1. From a practical perspective, trickle-bed reactors for the

120

hydroprocessing of heavy oils should be operated in the L1V phase behaviour region to minimize coke deposition on catalyst. Adding solvents with high solubility of heavy hydrocarbons or supercritical fluids to heavy oil hydroprocessing reactors can also reduce the coke deposition.

121

References

Abedi, S. J., "Unusual Retrograde Condensation and Asphaltene Precipitation in Model Heavy Oil Systems Using X-ray Imaging", PhD thesis, University of Toronto, 1998.

Abedi, S. J.; Seyfaie, S.; Shaw, J. M., "Unusual Retrograde Condensation and Asphaltene Precipitation in a Model Heavy Oil System", Petroleum Science and Technology, 16 (3&4), 209-226 (1998).

Absi-Halabi, M.; Stanislaus, A.; Trimm, D.L., "Coke Formation on Catalysts during the Hydroprocessing of Heavy Oils", Applied Catalysis, 72, 193-215 (1991).

Absi-Halabi, M.; Stanislaus, A.; Qabazard, H., "Trends in Catalysis Research to Meet Future Refining Needs", Hydrocarbon Processing, 76 (2), 45 (1997).

Al-Dahhan, M.H.; Larachi, F.; Dudukovic, M.P.; Laurent, A., "High-Pressure Trickle-Bed Reactors: A Review", Industrial & Engineering Chemistry Research, 36(8), 3292-3314 (1997).

Ali, V., "The Impact of Phase Behaviour on Coke Formation in Delayed Cokers", MSc thesis, University of Toronto, 2002.

Amemiya, M.; Suzuka, T.; Korai, Y.; Mochida, I., "Catalyst Deactivation in Distillate Hydrotreating (Part 1): Catalyst Deactivation in The Commercial Vacuum Gas Oil Hydrotreating Unit", Sekiyu Gakkaishi, 43(1), 52-58 (2000).

Asaoka, S.; Nakata, S.; Shiroto, Y.; Takeuchi, C. "Asphaltene Cracking in Catalytic Hydrotreating of Heavy Oils. 2. Study of Changes in Asphaltene Structure during Catalytic Hydroprocessing", Industrial & Engineering Chemistry Process Design and Development, 22, 242-248 (1983).

Baptist-Nguyen, S.; Subramanjam, B., "Coking and Activity of Porous Catalysts in Supercritical Reaction Media", AIChE Journal, 38(7), 1027-1037 (1992).

Bardon, C.; Barre, L.; Espinat, D.; Guille, V.; Li, M. H.; Lambard, J.; Ravey, J.C.; Rosenberg, E.; Zemb, T., "The Colloidal Structure of Crude Oils and Suspensions of Asphaltenes and Resins", Fuel Science and Technology International, 14(1&2), 203-242 (1996).

Bartholdy, J.; Andersen, S. I., "Changes in Asphaltene Stability during Hydrotreating", Energy & Fuels, 14, 52-55 (2000).

Bartholdy, J.; Lauridsen, R.; Mejlholm, M.; Andersen, S. I., "Effect of Hydrotreatment on Product Sludge Stability", Energy & Fuels, 15, 1059-1062 (2001).

Bartholomew, C.H., "Catalyst Deactivation in Hydrotreating of Residua: A Review", in: M.C. Oballa, S.S. Shih (Eds.), Catalytic Hydroprocessing of Petroleum and Distillates, Marcel Dekker, New York, 1994.

Beaton, W.I.; Bertolacini, R.J., "Resid Hydroprocessing at Amoco", Catalysis Reviews-Science and Engineering, 33 (3-4), 281-317 (1991).

Branco, V.A.M.; Mansoori, G.A.; Xavier, L.C.D.A.; Park, S.J. Manafi, H., "Asphaltene Flocculation and Collapse from Petroleum Fluids", Journal of Petroleum Science and Engineering, 32, 217-230 (2001).

Butt, J.B.; Petersen, E.E., Activation, Deactivation, and Poisoning of Catalysts, Academic Press Inc., San Diego, California, 1988, p 3-26.

Cai, H.Y.; Shaw, J.M.; Chung K.H., "Hydrogen Solubility Measurements in Heavy Oil and Bitumen Cuts", Fuel, 80(8), 1055-1063 (2001a).

Cai, H.Y.; Shaw, J. M.; Chung, K. H., "The Impact of Solid Additives on the Apparent Solubility of Hydrogen in Petroleum Fractions and Model Hydrocarbon Liquids", Fuel, 80, 1065-1077 (2001b).

Callejas, M.A.; Martínez, M.T.; Blasco, T.; Sastre, E., "Coke Charaterisation in Aged Residue Hydrotreating Catalysts by Solid-State 13C-NMR Spectroscopy and Temperatrue-Programmed Oxidation", Applied Catalysis A: General, 218, 181-188 (2001).

Cartlidge, C. R.; Dukhedin-Lalla, L.; Rahimi, P.; Shaw, J. M., "Preliminary Phase Diagrams for ABVB+n-Dodecane+Hydrogen", Fluid Phase Equilibria, 117, 257-264 (1996).

Chang, H.J.; Seapan, M.; Crynes, B.L., "Catalyst Decay during Hydrotreatment of a Heavy Coal Oil", ACS Symposium Series, 196, 309-320 (1982).

123

Chung, K.H.; Xu, Chunming; Hu, Yunxiang; Wang, R., "Supercritical Fluid Extraction Reveals Resid Properties", Oil and Gas Journal, 95(3), 66-69 (1997).

Dautzenberg, F. M.; De Deken, J.C., "Modes of Operation in Hydrodemetallization", ACS symp. series 344, ACS, Washington, DC. 1987, p233-256.

Dautzenberg, F.M.; De Deken, J.C., "Reactor Developments in Hydrotreating and Conversion of Residues", Catalysis Reviews-Science and Engineering, 26 (3&4), 421-444 (1984).

De Boer, D.K.G., "Fundamental Parameters for X-ray Fluorescence Analysis" Spectrochimica Acta, 44B (11), 1171-1190 (1989).

De Jong, K.P.; Reinalda, D.; Emeis, C.A., "Coke Deposition in Trickle-Bed Reactors during Heavy Oil Processing – Catalytic and Physical Effects", Studies in Surface Science and Catalysis, 88, 155-166, Catalyst Deactivation (1994a).

De Jong, K.P. "Effects of Vapour-Liquid Equilibria on Coke Deposition in Trickle-Bed Reactors during Heavy Oil Processing. 1. Experimental Results", Industrial & Engineering Chemistry Research, 33, 821-824 (1994b).

De Jong, K.P. "Effects of Vapor-Liquid Equilibria on Coke Deposition in Trickle-Bed Reactors during Heavy Oil Processing. 2. Modeling", Industrial & Engineering Chemistry Research, 33, 3141-3145 (1994c).

Diez, F.; Gates, B.C.; Miller, J.T.; Sajkowski, D.J.; Kukes, S.G., "Deactivation of a Ni-Mo/γ-Al$_2$O$_3$ Catalyst: Influence of Coke on the Hydroprocessing Activity, Industrial & Engineering Chemistry Research, 29, 1999-2004 (1990).

Dukhedin-Lalla, L., "A Study of Complex Phase Behaviour Arising in Heavy Oil/ Bitumen Mixtures Using X-ray Imaging", Ph.D. Thesis, University of Toronto, 1996.

Dukhedin-Lalla, L.; Sun, Y.S.; Shaw, J.M., "Phase Splitting of Complex Hydrocarbon Mixtures", Fluid Phase Equilibria, 53, 415-422 (1989).

Espinat, D.; Rosenberg, E.; Scarsella, M.; Barre, L.; Fenistein, D.; Broseta, D. "Colloidal Structural Evolution from Stable to Flocculated State of Asphaltene Solutions and Heavy Crudes", in Mullins O.C.; Sheu, E.Y., Structures and Dynamics of Asphaltenes, Plenum

124

press, New York, 1998, p145-201.

Froment G.F.; Bischoff, K.B., Chemical Reactor Analysis and Design, John Wiley & Sons: New York, 1979.

Furimsky, E., "Selection of Catalysts and Reactors for Hydroprocessing", Applied Catalysis A: General, 171, 177-206 (1998).

Furimsky, E.; Massoth, F.E., "Deactivation of Hydroprocessing Catalysts", Catalysis Today, 52, 381-495 (1999).

Gosselink, J.W.; van Veen, J.A.R., "Coping with Catalyst Deactivation in Hydrocarbon Processing", in Delmon B. and Froment, G.F. eds. Catalyst Deactivation, 1999, p3-16.

Gray, M.R., Upgrading Petroleum Residues and Heavy Oils, M. Dekker, New York, 1994.

Gray, M.R. and Masliyah, J.H., Extraction and Upgrading of Oil Sands Bitumen: Intensive Short Course, Edmonton, Alberta. University of Alberta, 2004.

Gray M.R.; Zhao, Y; McKnight, C.M.; Komar, D.A.; Carruthers, J.D., "Coking of Hydroprocessing Catalyst by Residue Fractions of Bitumen", Energy & Fuels, 13, 1037-1045 (1999).

Gregg, S. J.; Sing, K. S., Adsorption, Surface Area and Porosity; Academic Press: London and New York, 1982.

Gregorowicz, J.; de Loos, T.W.; de Swaan Arons, J., "Liquid-Liquid-Vapour Phase Equilibria in the System Ethane+ Propane+ Eicosane: Retrograde Behaviour of the Heavy Liquid Phase", Fluid Phase Equilibria, 84, 225-250 (1993).

Gualda, G.; Kasztelan, S., "Initial Deactivation of Residue Hydrodemetallization Catalysts", Journal of Catalysis, 161, 319-337 (1996).

Gualda, G.; Toulhoat, H., "Study of the Deactivation of Hydrotreating Catalysts by Coking", Revue De L Institut Francais du Petrole, 43(4), 567-594 (1988).

Hauser, A.; Stanislaus, A.; Marafi, A.; Al-Adwani, A., "Initial Coke Deposition on Hydrotreating Catalysts. Part II. Structure Elucidation of Initial Coke on Hydromatallation Catalysts", Fuel, 84 (2-3), 259-269 (2005).

Haynes Jr., H.W.; Leung, K., "Catalyst Deactivation by Pore Plugging and Active-Site Poisoning Mechanisms", Chemical Engineering Communications, 23 (1-3), 161-179 (1983).

Higashi, H.; Takahashi, T.; Kai, T., "Involvement of Asphaltene Decomposition in the Rapid Deactivation of Hydrodesulfurization Catalysts under Conditions for Deep Desulfurization of Atmospheric Residue", Journal of the Japan Petroleum Institute, 47 (4), 297-302 (2004).

Hughes, R., Deactivation of Catalysts, Academic Press, Orlando, Florida, 1984, p 7-28.

Idei, K.; Takahashi, T.; Kai, T., "Effect of Coke and Metal Deposition on Catalyst Deactivation at Early Stages of Resid Hydrodesulfurization Operation", Journal of the Japan Petroleum Institute, 45(5), 295-304 (2002).

Kanda, W.; Siu, I; Adjaye, J.; Nelson, A.E.; Gray, M.R., "Inhibition and Deactivation of Dydrodenitrogenation (HDN) Catalysts by Narrow-Boiling Fractions of Athabasca Coker Gas Oil", Energy & Fuels, 18, 539-546 (2004).

Koyama, H.; Nagai, E.; Kumagai, H., "Catalyst Deactivation in Commercial Residue Hydrodesulfurization", Deactivation and Testing of Hydrocarbon-Processing Catalysts, ACS Symposium Series 634, 1996.

Kressmann, S.; Morel, F.; Harle, V.; Kasztelan, S., "Recent Developments in Fixed-bed Catalytic Residue Upgrading", Catalysis Today, 43, 203-215 (1998).

Kubo, J.; Higashi, H.; Ohmoto, Y.; Arao, H., "The Additive Effects of Hydrogen-Donating Hydrocarbons Derived from Petroleum in Hydrotreating of Heavy Oils", Prepr. ACS, 39(3), 416-421 (1994).

Kubo, J.; Higashi, H.; Ohmoto, Y.; Arao, H., "Heavy Oil Hydroprocessing with the Addition of Hydrogen-Donating Hydrocarbons Derived from Petroleum", Energy & Fuels, 10, 474-481 (1996).

Le Page, J.F.; Chatila, S.G.; Davidson, M., Resid and Heavy oil Processing, Editions Technip, Paris, 1992.

Lee, S. Y.; Seader, J. D.; Tsai, Chung H.; Massoth, F. E., "Restrictive Diffusion under

Catalytic Hydroprocessing Conditions", Industrial & Engineering Chemistry Research, 30, 29-38 (1991a).

Lee, S. Y.; Seader, J. D.; Tsai, Chung H.; Massoth, F. E., "Solvent and Temperature Effects on Restrictive Diffusion under Reaction Conditions", Industrial & Engineering Chemistry Research, 30, 607-613 (1991b).

Li, S. H.; Liu, C. G.; Que, G. H.; Liang, W. J.; Zhu, Y. J., "Colloidal Structures of Three Chinese Petroleum Vacuum Residues", Fuel, 75, 1025-1029 (1996).

Li, S.; Liu, C.; Que, G.; Liang, W.; Zhu, Y., "Phase Separation Behaviours and Their Relations with Coke Formation in Thermal Reaction Systems of Vacuum Residue", Petroleum Science and Technology, 17(7&8), 693-709 (1999).

Maham, Y.; Chodakowski, M.G.; Zhang, X.H.; Shaw, J.M., "Asphaltene Phase Behavior: Prediction at A Crossroads", Fluid Phase Equilibria, 227, 177–182 (2005).

Mansoori, G.A., "Modeling of Asphaltene and Other Heavy Organic Depositions", Journal of Petroleum Science and Engineering, 17, 101-111 (1997).

Marafi, M.; Stanislaus, A., "Influence of Catalyst Acidity and Feedstock Quality on Hydrotreating Catalyst Deactivation by Coke Deposition", Petroleum Science and Technology, 19(5&6), 697-710 (2001).

Matsushita, K.; Hauser, A.; Marafi, A.; Koide, R.; Stanislaus, A., "Initial Coke Deposition on Hydrotreating Catalysts. Part 1. Changes in Coke Properties as a Function of Time of Stream", Fuel, 83, 1031–1038 (2004).

Matsushita, K.; Marafi, A.; Hauser, A.; Stanislaus, A., "Relation between Relative Solubility of Asphaltenes in the Product Oil and Coke Deposition in Residue Hydroprocessing", Fuel, 83, 1669–1674 (2004).

McHugh, M.A.; Krukonis, V.J., Supercritical Fluid Extraction: Principles and Practice, 2nd ed. Boston : Butterworth-Heinemann, 1994.

Mckinney, J.d.; Stipanov, J., "Gulf HDS Handles Resids", Hydrocarbon Processing, 50 (5), 97 (1971).

Minicucci, D., "The Impact of Liquid-Liquid-Vapour Phase Behaviour on Coke

127

Formation from Model Coke Precursors", MSc thesis, University of Toronto, 2000.

Minicucci, D.; Zou, X.Y.; Shaw, J.M., "The Impact of Liquid-Liquid-Vapour Phase Behaviour on Coke Formation from Model Coke Precursors", Fluid Phase Equilibria, 194-197, 353-360 (2002).

Morgan, G., "An Energy Renaissance of Oil Sands Development", World Energy, 4, 46-53, (2001).

Morel, F.; Kressmann, S.; Harle, V.; Kasztelan, S., "Processes and Catalysts for Hydrocracking of Heavy Oil and Residues", in Froment, G.F.; Demon, B.; Grange, P. editors, Hydrotreatment and Hydrocracking of Oil Fractions, 1997, p1-16.

Muegge, B. D.; Massoth, F. E., "Basic Studies of Deactivation of Hydrogenation Catalysts with Anthracene", Fuel Processing Technology, 29, 19-30, (1991).

Murgich, J.; Abanero, J.A.; Strausz, O.P., "Molecular Recognition in Aggregates Formed by Asphaltene and Resin Molecules from the Athabasca Oil Sand", Energy & Fuels, 13(2), 278-286 (1999).

Ng, K.M.; Chu, C.F., "Trickle-Bed Reactors", Chemical Engineering Progress, 83(11), 55-63 (1987).

Niu, C.F., PhD thesis, Research Institute of Petroleum Processing, 2001.

Nowlan, V.J.; Srinivasan, N.S., "Control of Coke Formation from Hydrocracked Athabasca Bitumen", Fuel Science and Technology International, 14(1&2), 41-54 (1996).

Overfield, R.E.; Sheu, E.Y.; Sinha, S.K.; Liang, K.S., "SANS Study of Asphaltene Aggregation", Fuel Science & Technology International, 7 (5-6), 611-624 (1989).

Pollack, N.; Enick, R., "The Mapping of Three Phase Volumetric Behaviour of Pseudo-Binary", Fluid Phase Equilibria, 39, 325-332 (1988).

Prausnitz, J.M.; Lichtenthaler, R.N.; Edmundo Gomes de Azevedo, Molecular Thermodynamics of Fluid-Phase Equilibria, Upper Saddle River, New Jersey, 1999.

Priyanto, S.; Mansoori, G.A.; Suwono, A., "Measurement of Property Relationships of Nano-Structure Micelles and Coacervates of Asphaltene in a Pure Solvent", Chemical Engineering Science, 56, 6933–6939 (2001).

128

Qabazard, H.; Adarme, R.; Crynes, B.L., in: D.L. Trimm et al. (Eds.), Catalysts in Petroleum Refining 1989, Elsevier, Amsterdam, 1990.

Quann, R.J.; Ware, R.A.; Hung, C.W.; Wei, J., "Catalytic Hydrodemetallation of Petroleum", Advances in Chemical Engineering, 14, 95-259 (1988).

Radosz, M., "Multiphase Behaviour of Supercritical Fluid Systems: Oil Solutions in Light Hydrocarbon Solvents", Industrial & Engineering Chemistry Research, 26, 2134-2139 (1987).

Rahmani, S.; McCaffrey, W.; Elliott, J.A.W.; Gray, M.R., "Liquid-Phase Behaviour during the Cracking of Asphaltenes", Industrial & Engineering Chemistry Research, 42, 4101-4108 (2003).

Reynolds, J.G., "Effects of Asphaltene Precipitation on the Size of Vanadium-, Nickel- and Sulfur-Containing Compounds in Heavy Crude Oils and Residua", in Yen, T. F.; Chilingarian, G.V. (eds), Asphaltenes and Asphalts, 1, Elsevier Science Press, New York, 1994.

Reynolds, J.G., "Metals and Heteroatoms in Heavy Oils" in Speight, J.G. (eds), Petroleum Chemistry and Refining, Taylor& Francis Press, Washington DC, 1999.

Richardson, S. M.; Nagaishi, H.; Gray, M. R., "Initial Coke Deposition on a NiMo/γ-Al$_2$O$_3$ Bitumen Hydrogenation Processing Catalyst", Industrial & Engineering Chemistry Research, 35, 3940-3950 (1996).

Robinson, D.B., "The Interface between Theory and Experiment", Fluid phase Equilibria, 52, 1-14 (1989).

Sasaki, T.; Jenkins, R.G.; Eser, S.; Schobert, H.H., "Carbonization of Anthracene and Phenanthrene. 1. Kinetics and Mesophase Development", Energy & Fuels, 7(6), 1039-1046 (1993).

Scheffer, B.; van Koten, M.A.; Robschlager, K.W.; de Boks, F.C., "The Shell Residue Hydroconversion Process: Development and Achievements", Catalysis Today, 43, 217-224 (1998).

Scotta, D. S.; Radleinb, D.; Piskorzb, J.; Majerskib, P.; deBruijn, Th. J. W., "Upgrading

of Bitumen in Supercritical Fluids", Fuel, 80(8), 1087-1099 (2001).

Seyer, F. A.; Gyte, C. W. AOSTRA Oilsands Handbook, Loren G. Hepler and Chu Hsi, Eds. AOSTRA, 1989; Chapter 7: Viscosity.

Shaw, J.M., "A Correlation for Hydrogen Solubility in Alicyclic and Aromatic Solvents", The Canadian Journal of Chemical Engineering, 65, 293-298 (1987).

Shaw, J.M.; Gaikwad, R. P.; Stowe, D. A., "Phase Splitting of Pyrene-Tetralin Mixtures under Coal Liquefaction Conditions", Fuel, 67, 1554-1559 (1988).

Shaw, J.M., "Toward Common Generalized Phase Diagrams for Asphaltenes Containing Hydrocarbon Fluids," ACS Petroleum Chemistry Div. Preprints, 47 (4), 338-342 (2002).

Shaw, J.M.; de Loos, Th.W.; de Swaan Arons, J., "Prediction of Unusual Retrograde Condensation in Model Reservoir Fluids", Fluid Phase Equilibria, 84, 251-266 (1993).

Sheremata, J.M.; Gray, M.R.; Dettman, H.D.; McCaffrey, W.C., "Quantitative Molecular Representation and Sequential Optimization of Athabasca Asphaltenes", Energy & Fuels, 18 (5), 1377-1384 (2004).

Speight, J.G., The Chemistry and Technology of Petroleum, Marcel Dekker, New York, 1991.

Speight, J.G., "The Chemistry and Physics of Coking", Korean Journal of Chemical Engineering, 15(1), 1-8 (1998).

Speight, J.G., The Chemistry and Technology of Petroleum, New York, 1999.

Speight, J.G., The Desulfurization of Heavy Oils and Residua, Marcel Dekker, New York, 2000.

Speight, J.G.; Ozum, B., Petroleum Refining Process, Marcel Dekker, New York, 2002.

Storm, D. A.; Barresi, R. J.; Sheu, E. Y., "Rheological Study of Ratawi Vacuum Residue in the 298-673 K Temperature Range", Energy & Fuels, 9, 168-176 (1995).

Storm, D. A.; Barresi, R. J.; Sheu, E. Y., "Flocculation of Asphaltenes in Heavy Oil at Elevated Temperatures", Fuel Science and Technology International, 14(1&2), 243-260 (1996).

Storm, D. A.; Barresi, R. J.; Sheu, E. Y.; Bhattacharya, A.K.; DeRosa, T.F., "Microphase Behaviour of Asphaltic Micelles during Catalytic and Thermal Upgrading", Energy & Fuels, 12, 120-128 (1998).

Strausz, O.P.; Mojelsky, T.W.; Lown, E.M., "The Molecular Structure of Asphaltene - an Unfolding Story", Fuel, 71 (12), 1355-1363 (1992).

Takatsuka, T.; Kajiyama, R.; Kashimoto, H.; Matsuo, I.; Miwa, S., "A Practical Model of Thermal Cracking of Residual Oil", Journal of Chemical Engineering of Japan, 22, 304-310 (1989).

Takeuchi, C.; Fukui, Y.; Nakamura, M.; Shiroto, Y., "Asphaltene Cracking in Catalytic Hydrotreating of Heavy Oils. 1. Processing of Heavy Oils by Catalytic Hydroprocessing and Solvent Deasphalting", Industrial & Engineering Chemistry Process Design and Development, 22, 236-242 (1983).

Ternan, M.; Furimsky, E.; Parsons, B.I., "Coke Formation of Hydrodesulfurization Catalysts", Fuel Processing Technology, 2, 45-55 (1979).

Ternan, M.; Rahimi, P.M.; Clugston, D.M.; Dettman, H.D., "The +525 C Residue before and after Hydrocracking with Bimodal Catalysts of Varying Macropore Volume", Energy & Fuel, 8(3), 518-530 (1994).

Thakur, D.S.; Thomas, M.G., "Catalyst Deactivation in Heavy Petroleum and Synthetic Crude Processing: A Review", Applied Catalysis, 15, 197-225 (1985).

Trimm, D.L., "Catalyst Deactivation", in: Absi-Halabi, M. et al. (eds), Catalysts in Petroleum Refining and Petrochemical Industries, 1995.

Van Konynenburg, P.H.; Scott, R.L., "Critical Lines and Phase Equilibria in Binary van der Waals Mixtures", Philos. Trans. R. Soc. London, 298, 495-540 (1980).

Wiehe, I.A., "A solvent-Resid Phase Diagram for Tracking Resid Conversion", Industrial & Engineering Chemistry Research, 31(2), 530-536 (1992).

Wiehe, I.A., "A Phase-Separation Kinetic Model for Coke Formation", Industrial & Engineering Chemistry Research, 32(11), 2447-2454 (1993).

Wiehe, I.A., "The Pendant-Core Building Block Model of Petroleum Residua", Energy &

Fuels, 8(3), 536-544 (1994).

Wilson, R.E.; Keith, P.C.; Haylett, R.E., "Liquid Propane: Use in Dewaxing, Deasphalting, and Refining Heavy Oils", Industrial and Engineering Chemistry, 28(9), 1065-1078 (1936).

Yanik S.J.; Frayer J.A.; Huling G.P.; Somers A.E., "Latest Data on Gulf HDS Process", Hydrocarbon Processing, 56 (5), 97-104 (1977).

Yen, T.F., "Asphaltenes: Types and Sources", in Mullins O.C.; Sheu, E.Y.(eds), Structures and Dynamics of Asphaltenes, Plenum press, New York, 1998, p145-201.

Zhao, S., Kotlyar, L.S., Woods, J.R., Sparks, B.D., Hardacre, K., Chung, K.H., "Molecular Transformation of Athabasca Bitumen End-Cuts during Coking and Hydrocracking", Fuel, 80, 1155–1163 (2001).

Zou, X.Y., "Selective Removal of Inorganic Fine Solids, Heavy Metals and Sulfur from Bitumen/Heavy Oils", PhD thesis, University of Toronto, 2003.

Appendix I. General Experimental Procedure Using X-ray View Cell

The following experimental procedure should be followed when experiments are conducted on the X-ray view cell apparatus:

1. Load the solid component;
2. Pressure test;
3. Vacuum test;
4. Load the liquid component;
5. Degas the system;
6. Load the gas component;
7. Preheat the sample;
8. Conduct formal experiment;
9. Discharge and dissemble

1. Load the solid component

Following the installation instructions for the view cell assembly from the D.B. Robinson Company, install the view cell bottom cap, gaskets, beryllium insert and the Beryllium cylinder. Load all solid components and the magnetic stirrer into the view cell. Following the installation instructions for the view cell assembly from the D.B. Robinson Company, install the view cell top cap and seal it. (Refer to Beryllium X-ray View Cell Operating and Maintenance Guide, DB Robinson Design and Manufacturing Ltd. 1997)

Start up the X-ray machine and the image system following their established procedures respectively. Make sure you can see a clear image on the TV and find the position of the bellows.

2. Pressure test

1. Open HV4 and HV8 to keep the pressure of both bellows side and view cell side identical; slowly open HV1, HV2 and HV3 and load the view cell with hydrogen until the pressure of view cell reaches over 10% higher than the maximum experimental pressure; close HV1, HV2 and HV3.
2. Use combustible gas detector to find the leaks and fix them.
3. After no leaks are detected with combustible gas detector, a 24-hrs pressure test is performed. Before the long run of pressure test, record the temperature and

133

pressure of the view cell, and after 24 hrs later record the temperature and pressure of the view cell again and do necessary calculations to find any leakage.

4. Slowly switch HV9 to the vent position and release the gas inside the view cell to atmosphere.

3. Vacuum test

1. Switch HV9 and HV10 to the vacuum position. Turn on the vacuum pump and evacuate the view cell for 20 minutes and close HV9 and HV10. Record the temperature and pressure of the view cell.

2. Record the temperature and pressure of the view cell 24 hours later; do necessary calculations to find any vacuum leakage.

3. Find the leak and correct for it.

4. Load the liquid component

1. Close HV4 and HV8.

2. Use a clean syringe and weigh the desired amount of a liquid component; connect the syringe to HV11.

3. Slowly open HV11 and HV12, and allow the liquid sample to be sucked into the view cell; then close HV11 and HV12.

4. Open HV9 and HV10 to the vacuum position and vacuum evacuate the liquid and solid components by turning on the vacuum pump; then close HV9 and HV10 after vacuum evacuation.

5. Degas the system

1. Heat the view cell up to 200 °C and keep constant temperature at 200 °C for 1 hour while turn on the stirrer as long as it is movable.

2. Cool down to room temperature; open HV4 and HV8, and switch HV9 and HV10 to vacuum position; turn on the vacuum pump to degas for 20 minutes.

Caution: Some light hydrocarbon solutions could be very volatile and poisonous. Safety precautions are mandatory. Also do not evacuate the view cell too long since it may result in imnegligible change to the sample composition due to the loss of volatile solvent.

6. Load the gas component

1. Open HV4 and HV8; then open HV1, HV2 and HV3 to load hydrogen into the system.

134

2. Close HV1, HV2, HV3, HV4 and HV8, and open HV9 to vent position; then slowly open HV8 until the bellows reaches the top of the view cell, but do not generate a pressure difference, then close HV8. Record the pressure and temperature and do the necessary calculation to check whether the mass of gas is equivalent to the expected value.

3. If more than the expected value, then release by slowly open HV4 and HV9; if lower than the expected value, then load the system to even higher pressure than before and repeat the step 1 to 3.

7. Preheat the sample

Preheating is a key step to ensure consistent experimental data for the asphaltenes-containing heavy oil samples. Heavy oil sample, such as ABVB, are often solid or semi-solid, which make it very hard to completely mix with light hydrocarbon solvents at room temperatures. Besides Asphaltenes are prone to form aggregates in solution, and these aggregates need to be broken so that asphaltene "monomer" have sufficient opportunities to interact with solvent molecules. These problems are solved by preheating the asphaltenes-containing heavy oil. Typically in experiment, the heavy oil + light hydrocarbon solvent mixtures are heated to 300 °C and the mixer is switched to high speed and kept running for 30 minutes at this temperature. Turn off the heating system but keep the mixer on, and let the mixture cool down to room temperature.

8. Conduct formal experiment

According to the experimental plan, conduct the formal experiment. During the formal experiment, all valves connecting to the view cell side should be closed. When there is a need to adjust the pressure of view cell, slowly open HV5, HV6, HV7 to load the nitrogen into the bellows if increasing the view cell pressure; slowly open HV8, HV9 to vent position to release the gas in the bellows if decreasing the view cell pressure.

9. Discharge and dissemble

Cool down the view cell to room temperature. If the system pressure is higher than atmosphere, slowly release the gas in both bellows side and view cell side and always keep the bellows close to the top of the view cell by controlling the release rate of two sides and disconnect the tubing connecting the bellows first and plug the bellows side. If the system pressure is lower than atmosphere, disconnect the tubing connecting to the view cell side first to push the bellows up to the top of the view cell and plug the view cell side. Then disconnect another side and plug it. Dissemble the view cell and discharge

135

the sample. (Refer to Beryllium X-ray View Cell Operating and Maintenance Guide, DB Robinson Design and Manufacturing Ltd. 1997)

136

Appendix II. X-ray Transmission Images

20% ABVB + decane mixture

Temp. (°C)	40	60	80	100	120	140	160	180	200	220	240	260	280	300	320	340
Pres. (bar)	0.24	0.37	0.50	0.58	0.70	0.85	1.08	1.44	2.01	2.92	4.27	6.08	8.44	11.43	15.27	19.88

1.	------	L1L2V
2.	—·—·—	L1L2
3.	—··—···	L2V
4.	———	L1V

Temp. (°C)	23	40	60	80	100	120	140	160	180	200	220	240	260	280	300	320	340	380
Pres. (bar)	0.18	0.21	0.32	0.40	0.48	0.60	0.77	1.03	1.41	1.99	2.91	4.25	6.04	8.43	11.36	15.12	19.54	32.55
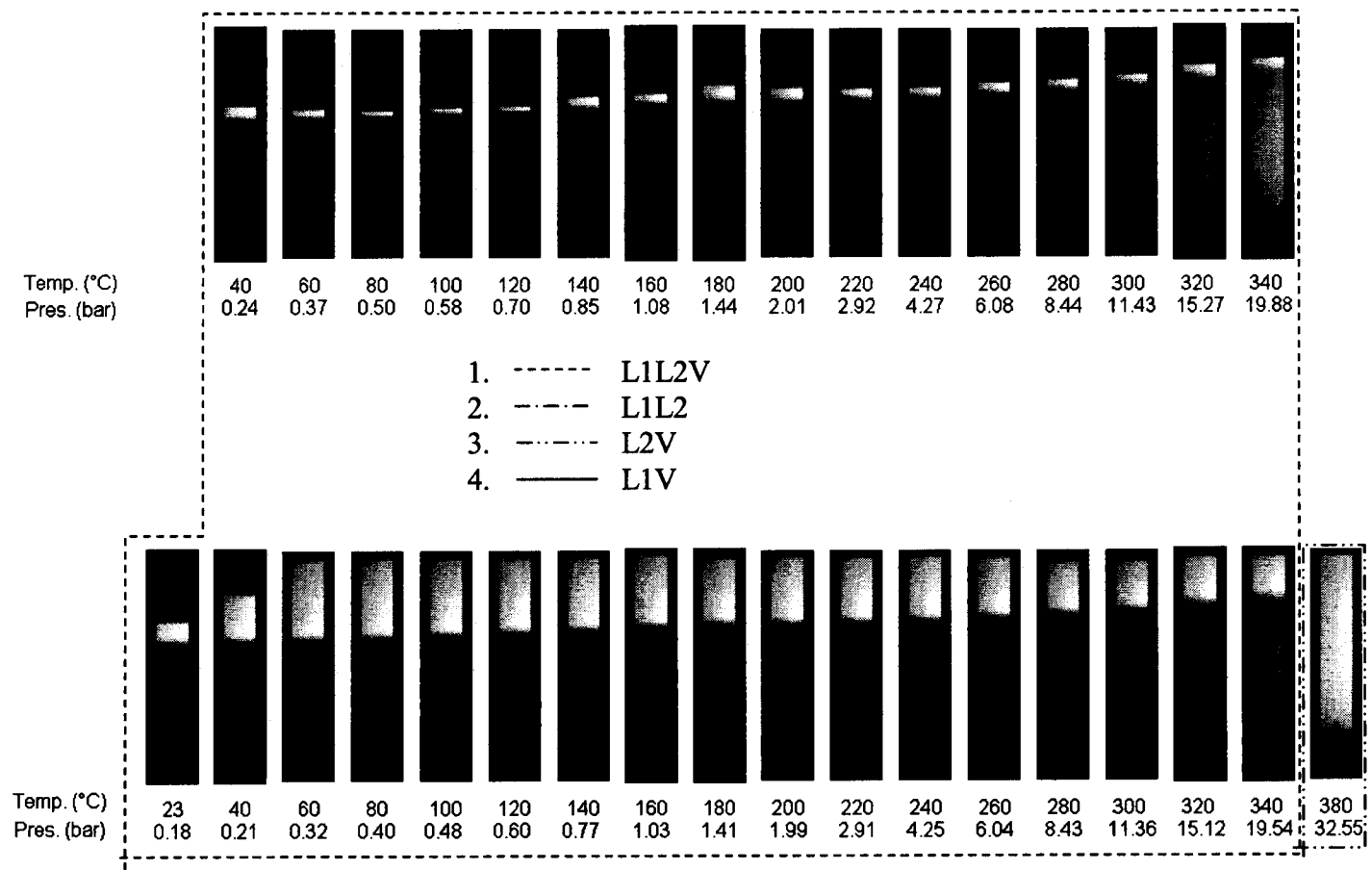
Figure A-1a X-ray images of decane + ABVB (20 wt %) mixture

137

25% ABVB + decane mixture   L1L2V

| Temp. (°C) | 50 | 100 | 150 | 200 | 250 | 280 | 300 | 320 | 340 | 360 |
| Pres. (bar) | 0.31 | 0.49 | 0.93 | 2.13 | 4.96 | 8.13 | 10.91 | 14.37 | 18.92 | 24.44 |

| Temp. (°C) | 22 | 50 | 100 | 150 | 200 | 250 | 280 | 300 | 320 | 340 | 360 |
| Pres. (bar) | 0.20 | 0.26 | 0.42 | 0.86 | 2.03 | 4.94 | 8.06 | 10.88 | 14.30 | 18.66 | 24.39 |
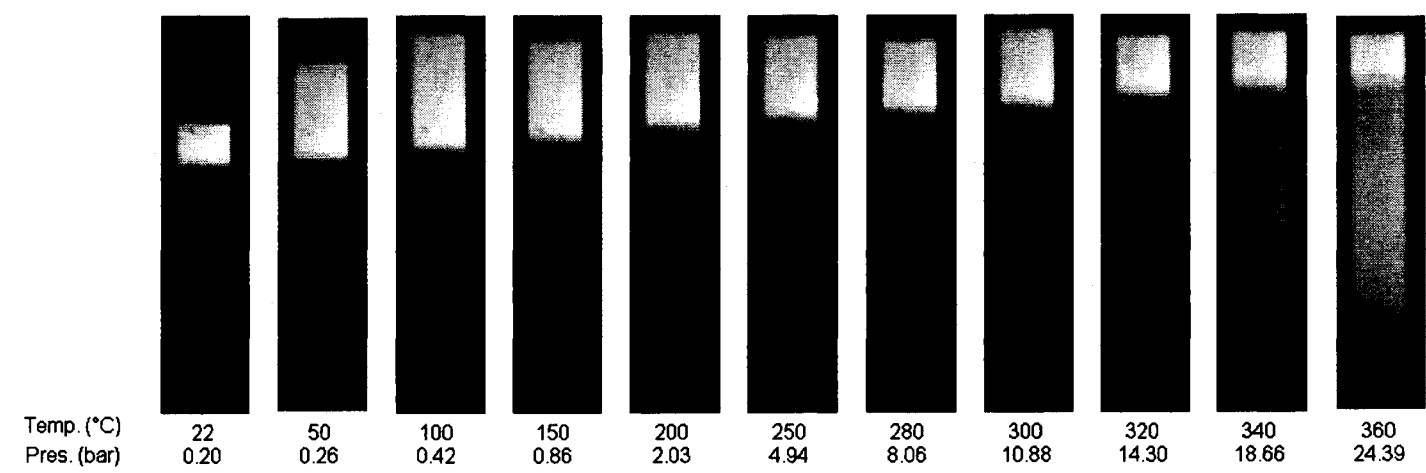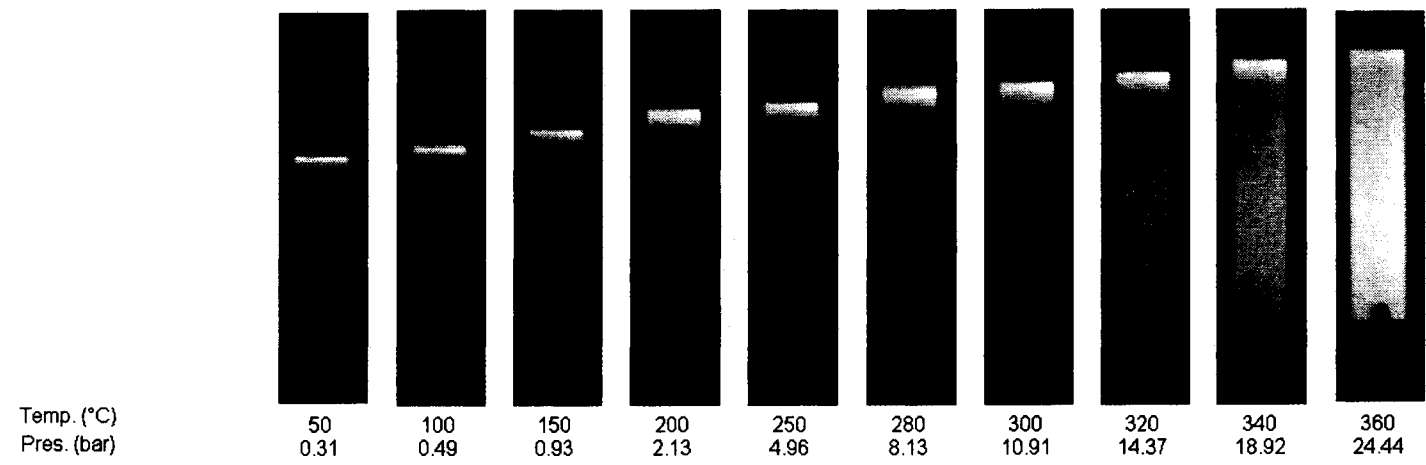
Figure A-1b X-ray images of decane + ABVB (25 wt %) mixture

138

30% ABVB + decane mixture   L1L2V

Temp. (°C)	40	60	80	100	120	140	160	180	200	220	240	260	280	300	320	340
Pres. (bar)	0.23	0.32	0.41	0.50	0.61	0.77	1.01	1.37	1.92	2.82	4.22	5.93	8.23	11.10	14.83	19.17

Temp. (°C)	21	40	60	80	100	120	140	160	180	200	220	240	260	280	300	320	340	380
Pres. (bar)	0.16	0.21	0.26	0.33	0.41	0.53	0.70	0.97	1.33	1.91	2.81	4.19	5.90	8.18	11.05	14.59	18.95	30.19
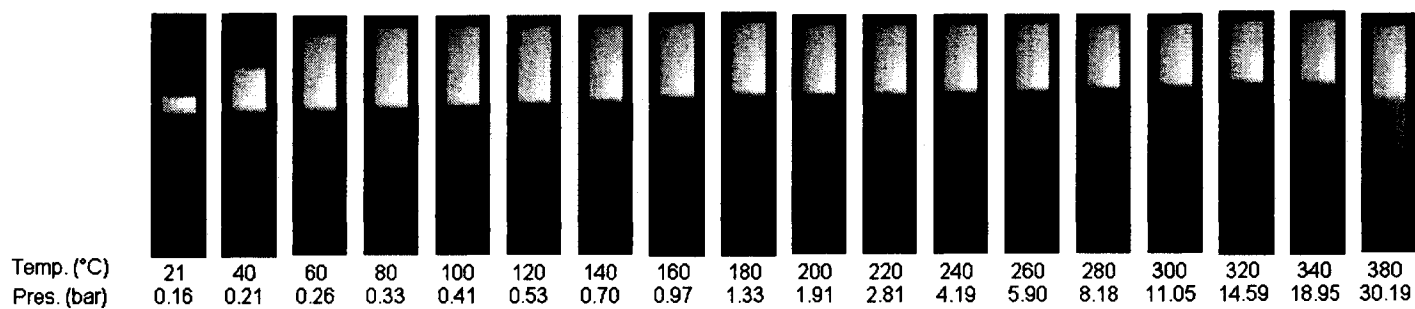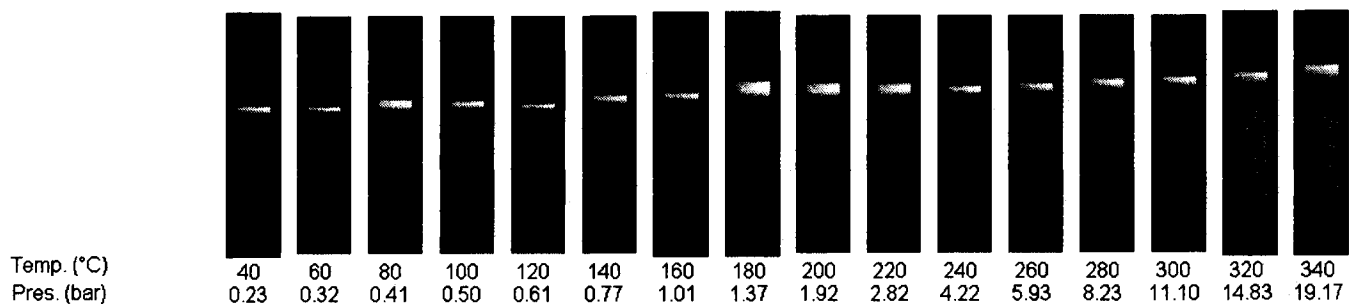
Figure A-1c X-ray images of decane + ABVB (30 wt %) mixture

139

35% ABVB + decane mixture

Temp. (°C)	40	60	80	100	120	140	160	180	200	220	240	260	270	280	290	300	310	320	330	340	380
Pres. (bar)	0.23	0.28	0.34	0.43	0.55	0.72	0.99	1.39	1.96	2.92	4.23	5.73	6.75	7.92	9.25	10.72	12.43	14.17	16.61	18.77	30.59

1. ----- L1L2V
2. —·—·— L1L2
3. —··—··— L2V
4. ——— L1V

Temp. (°C)	310	320	330	340
Pres. (bar)	12.28	14.12	16.28	18.58

Temp. (°C)	40	60	80	100	120	140	160	180	200	220	240	260	270	280	290	300	310	320	330	340	380
Pres. (bar)	0.21	0.24	0.28	0.36	0.48	0.66	0.94	1.36	1.94	2.86	4.17	5.70	6.70	7.84	9.18	10.63	12.21	13.94	16.19	18.34	28.79

140

Figure A-1d X-ray images of decane + ABVB (35 wt %) mixture
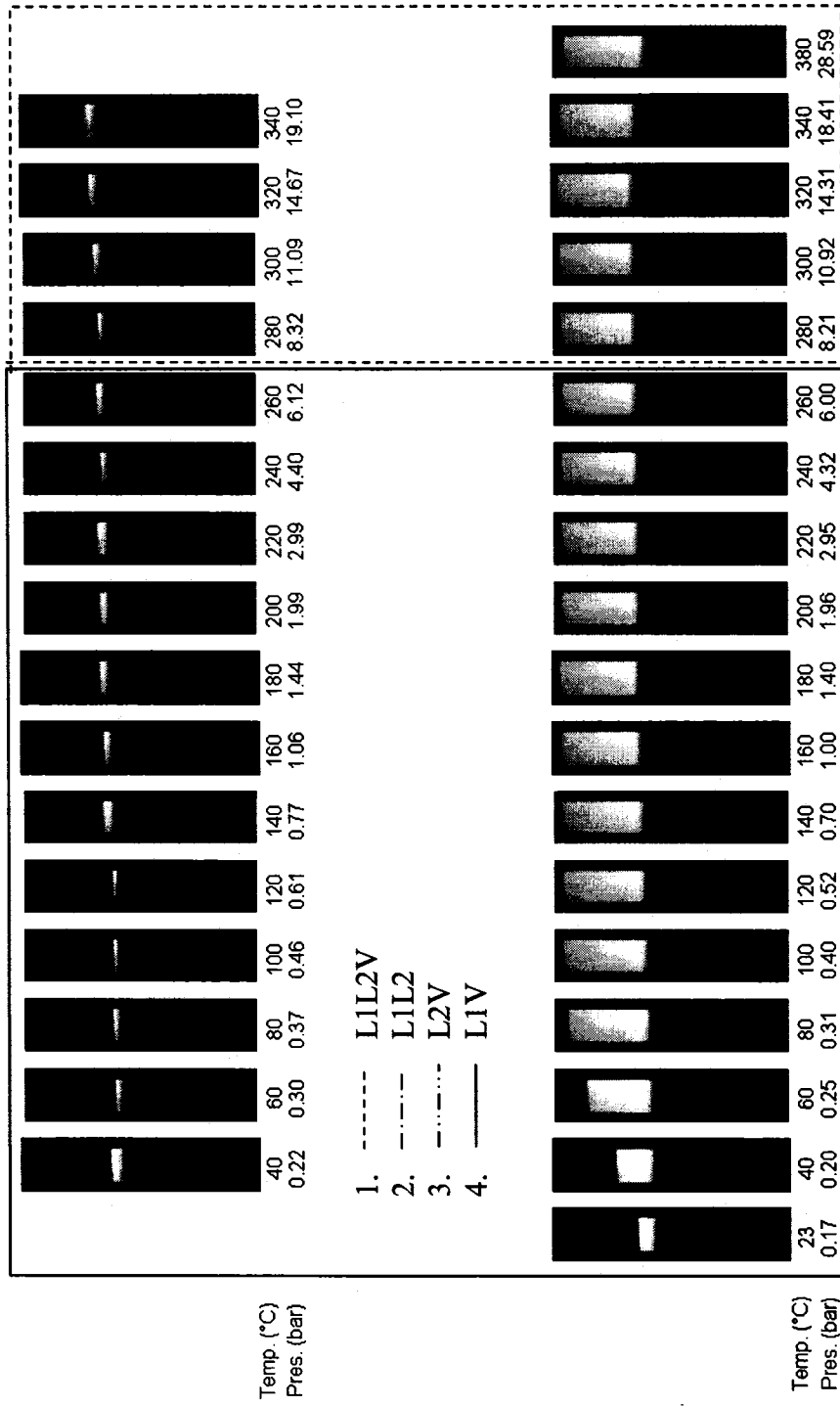
Figure A-1e X-ray images of decane + ABVB (40 wt %) mixture

141

50% ABVB + decane mixture

Temp. (°C)	40	60	80	100	120	140	160	180	200	220	240	260	280	300	320	340	380
Pres. (bar)	0.21	0.30	0.42	0.51	0.66	0.82	1.01	1.26	1.81	2.69	3.93	5.54	7.70	10.28	14.05	17.77	31.81

1. ------ L1L2V
2. —·—·— L1L2
3. —··—··· L2V
4. ——— L1V

Temp. (°C)	26	40	60	80	100	120	140	160	180	200	220	240	260	280	300	320	340	380
Pres. (bar)	0.16	0.20	0.27	0.35	0.44	0.59	0.77	0.97	1.25	1.83	2.64	3.88	5.47	7.57	10.20	13.20	17.04	25.91
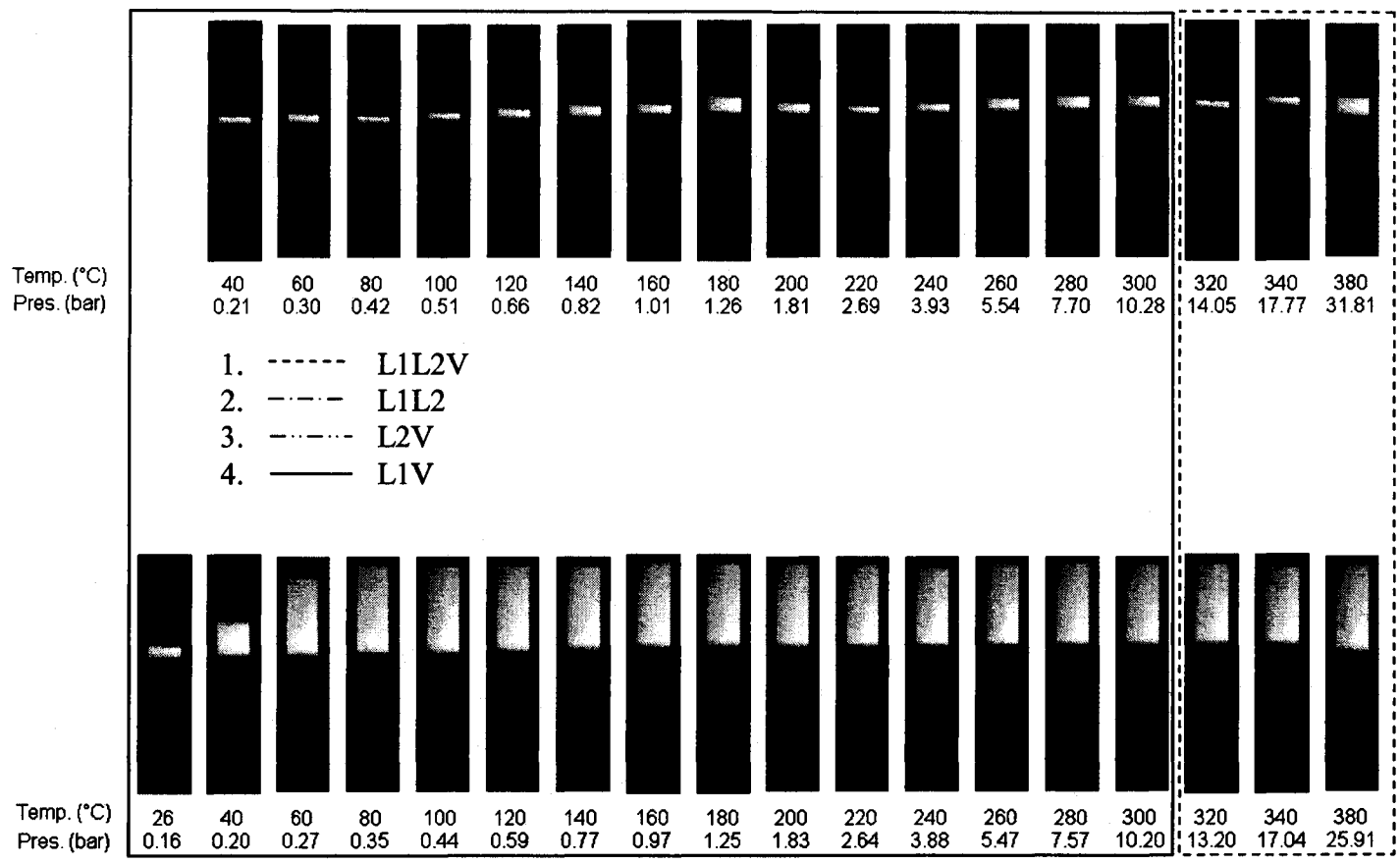
Figure A-1f X-ray images of decane + ABVB (50 wt %) mixture

142

70% ABVB + decane mixture   L1V

Temp. (°C)	40	60	80	100	120	140	160	180	200	220	240	260	280	300	320	340	380
Pres. (bar)	0.26	0.39	0.54	0.68	0.76	0.92	1.28	1.58	2.03	2.81	3.79	5.10	6.79	8.92	11.61	14.98	26.21

Temp. (°C)	25	40	60	80	100	120	140	160	180	200	220	240	260	280	300	320	340	380
Pres. (bar)	0.17	0.21	0.30	0.38	0.51	0.64	0.81	1.12	1.48	1.92	2.66	3.63	4.86	6.41	8.38	10.61	13.39	21.01
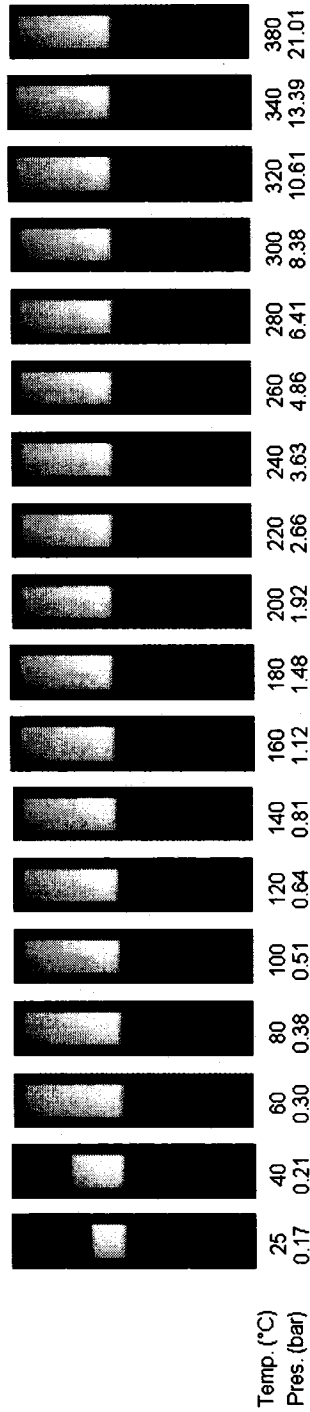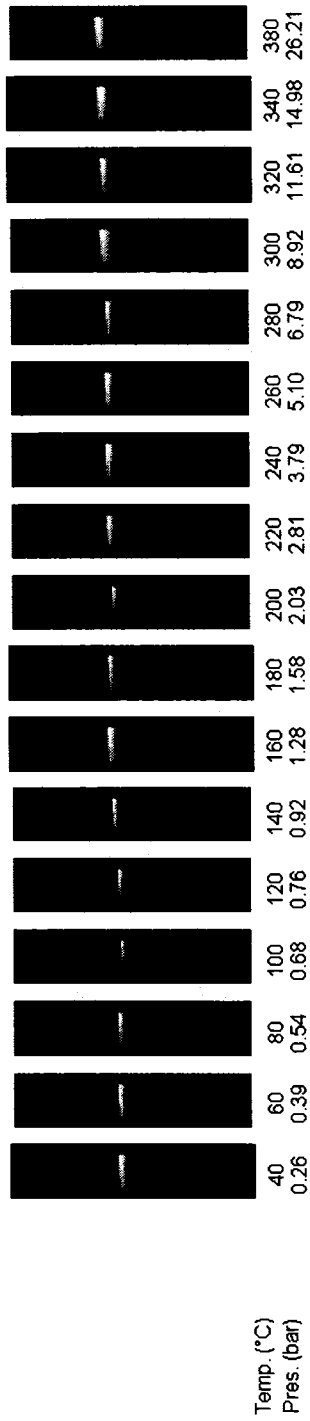
Figure A-1g X-ray images of decane + ABVB (70 wt %) mixture

143

90% ABVB + decane mixture   L1V

Temp. (°C)	40	60	80	100	120	140	160	180	200	220	240	260	280	300	320	340	380
Pres. (bar)	0.23	0.35	0.54	0.61	0.66	0.81	0.97	1.14	1.37	1.66	2.07	2.48	3.07	3.88	5.38	6.83	16.72

Temp. (°C)	40	60	80	100	120	140	160	180	200	220	240	260	280	300	320	340	380
Pres. (bar)	0.21	0.28	0.39	0.43	0.47	0.61	0.74	0.94	1.24	1.56	1.94	2.30	2.79	3.46	4.25	5.23	11.08
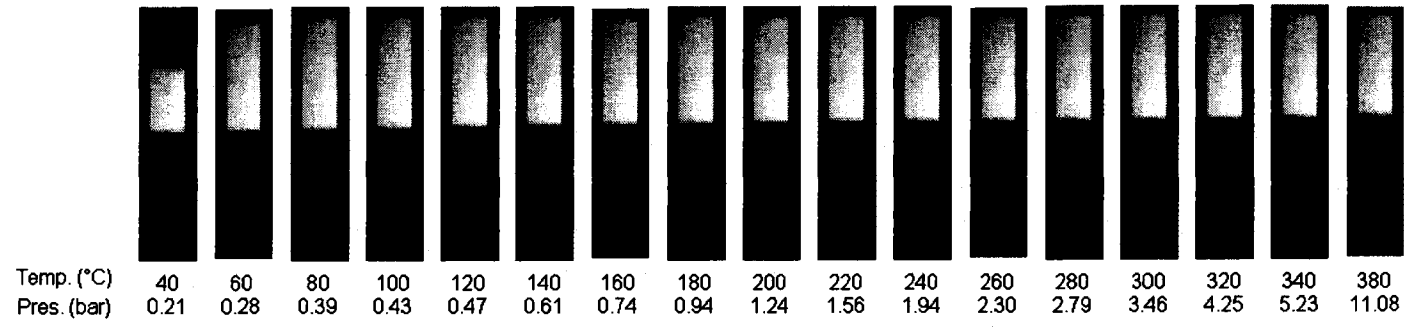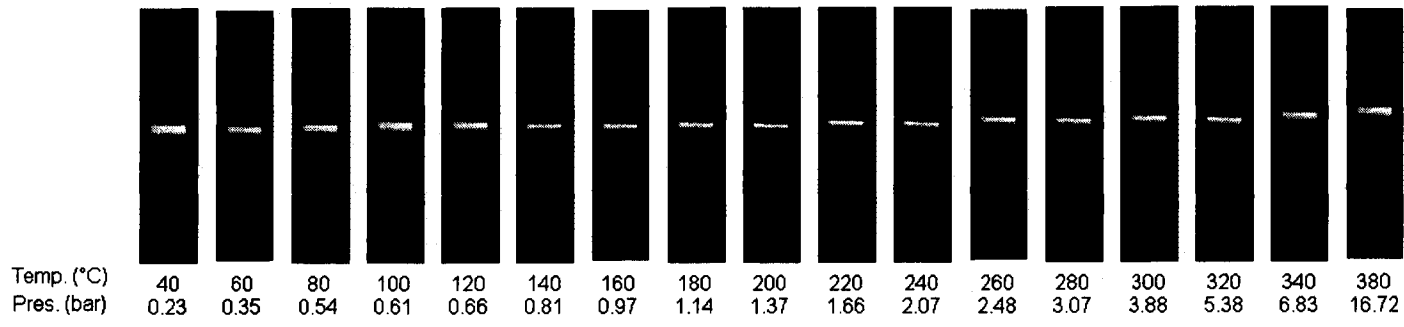
Figure A-1h X-ray images of decane + ABVB (90 wt %) mixture

100% ABVB　L1V

Temp. (°C)	40	60	80	100	120	140	160	180	201	220	240	260	280	300	320	340	380
Pres. (bar)	0.21	0.32	0.55	0.61	0.66	0.70	0.77	0.84	0.87	0.86	1.28	1.37	1.46	1.68	2.12	3.05	11.15

Temp. (°C)	40	60	80	100	120	140	160	180	200	220	240	260	280	300	320	340	380
Pres. (bar)	0.19	0.27	0.44	0.45	0.49	0.52	0.58	0.63	0.64	0.62	1.10	1.12	1.15	1.21	1.41	1.92	6.63
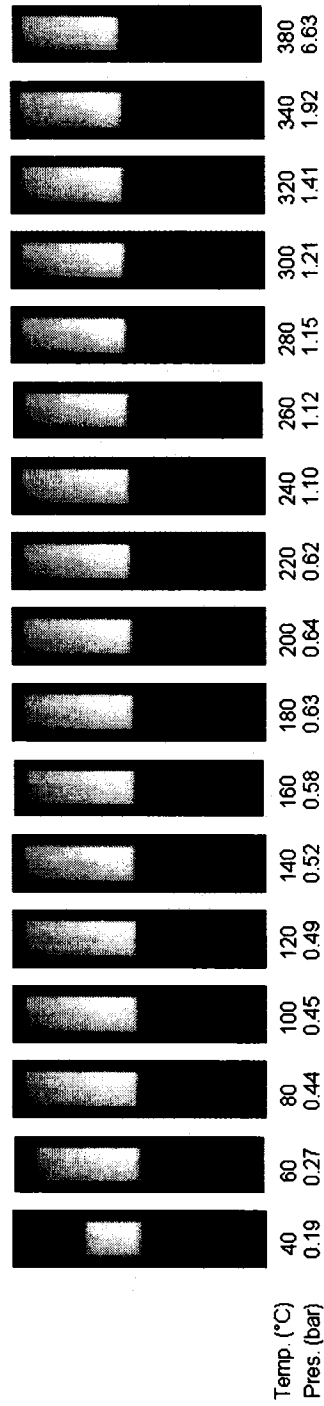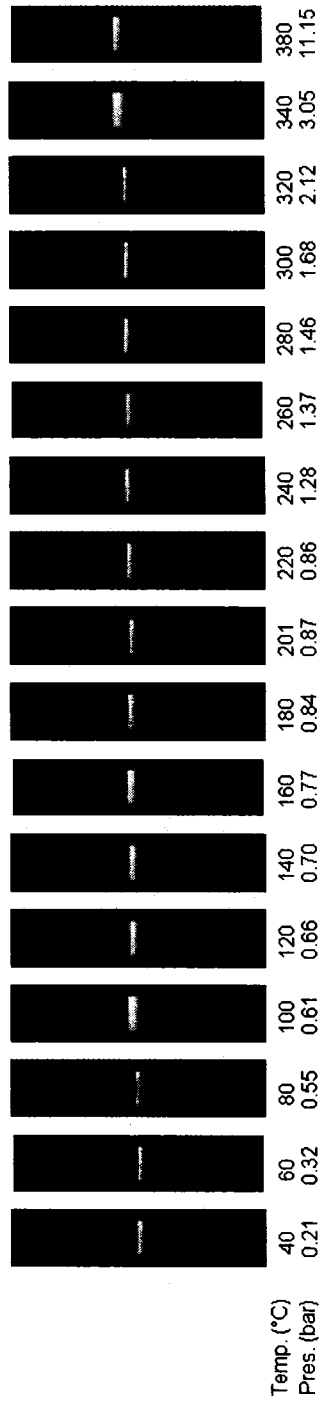
Figure A-1i X-ray images of ABVB

145
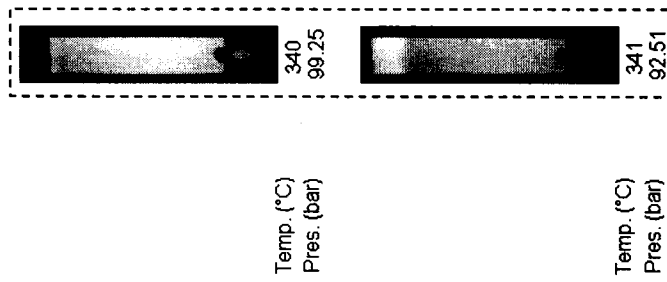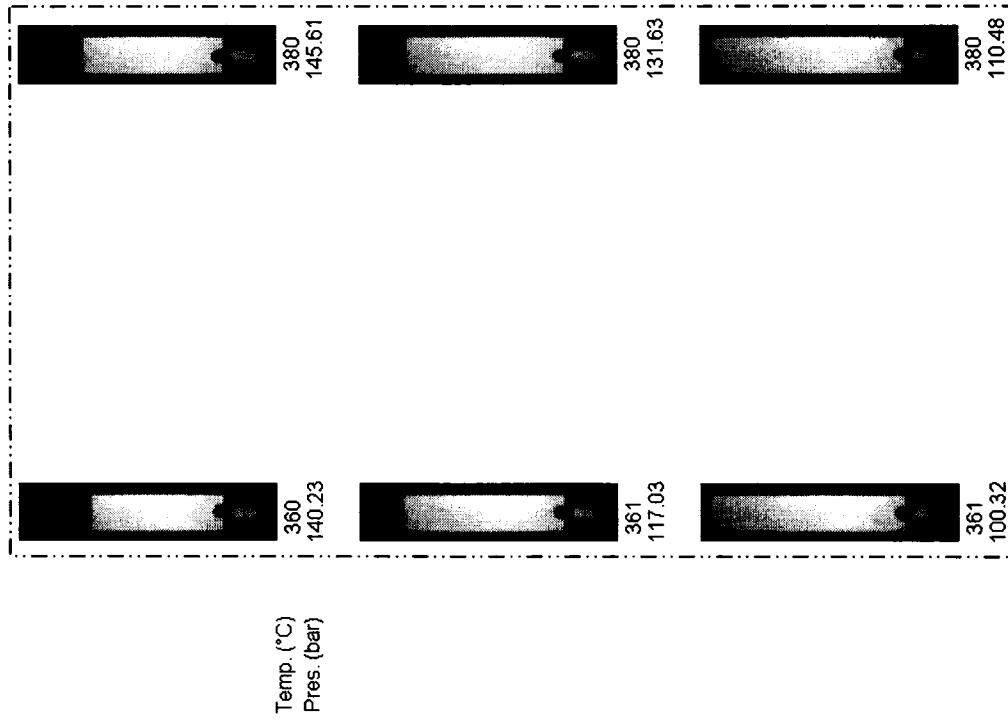
Figure A-2a X-ray images of decane + ABVB (10 wt %) + hydrogen (0.57 wt %) mixture

146
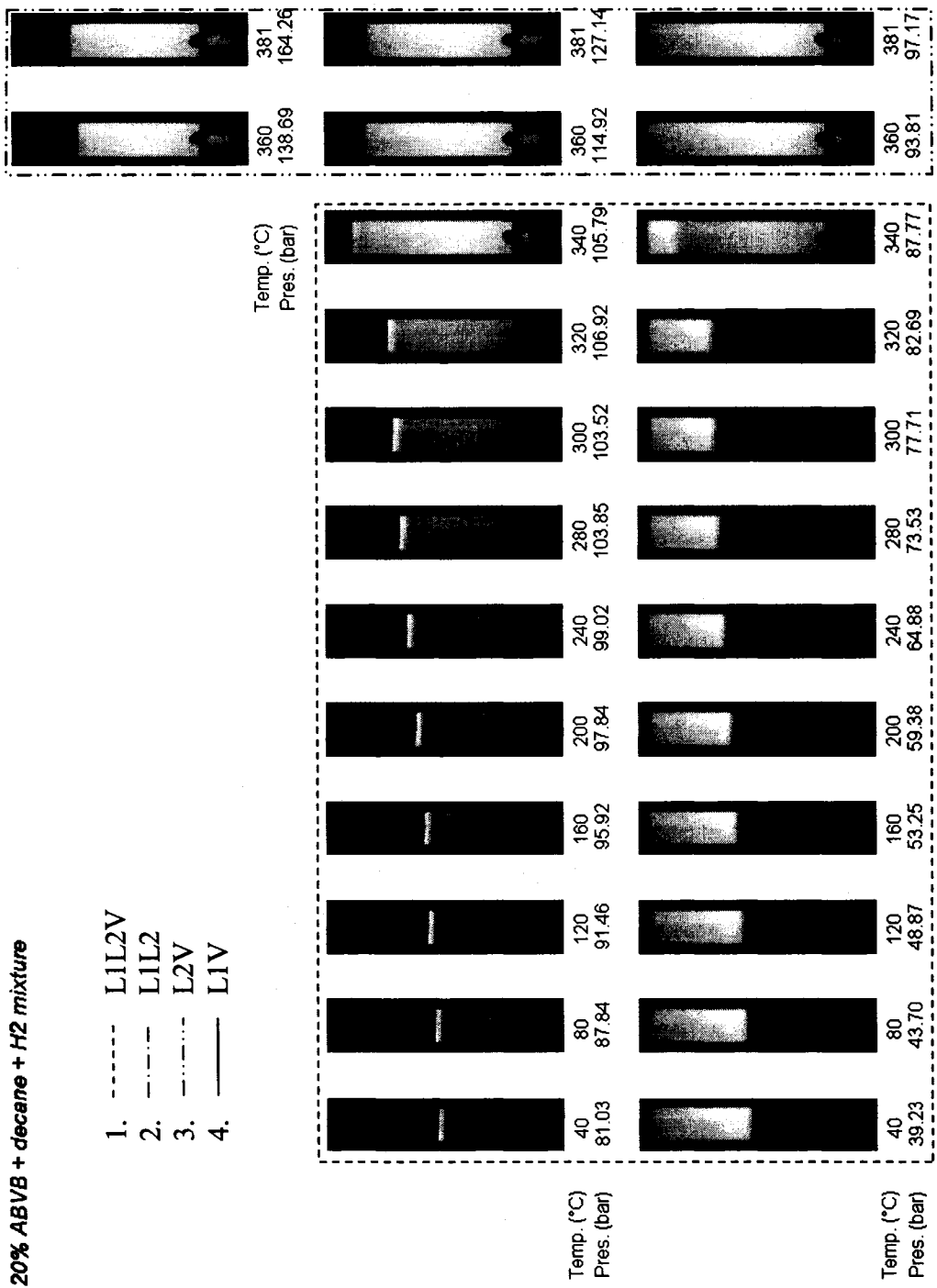
Figure A-2b X-ray images of decane + ABVB (20 wt %) + hydrogen (0.57 wt %) mixture

147

Figure A-2a X-ray images of decane + ABVB (30 wt %) + hydrogen (0.57 wt %) mixture

148
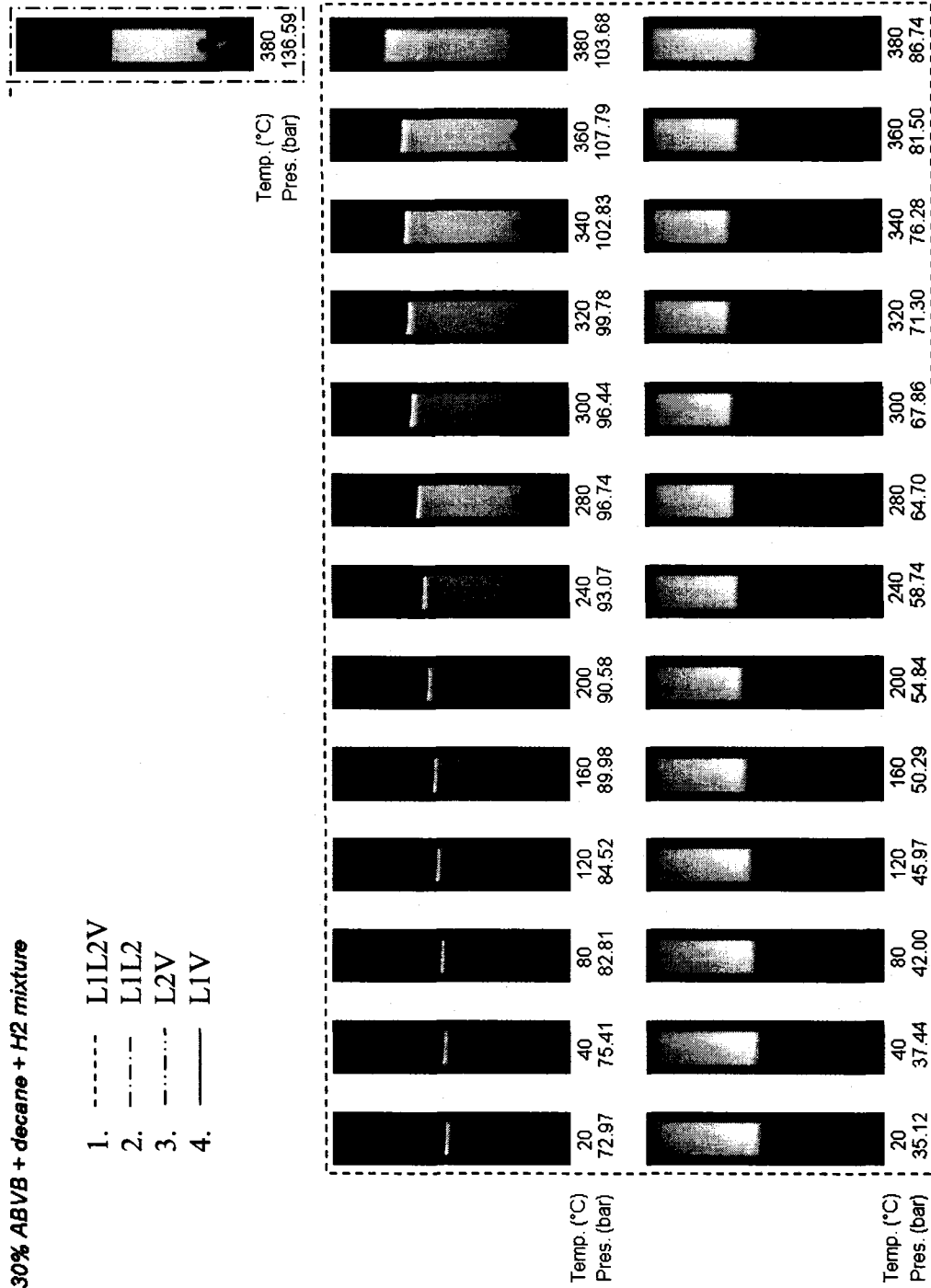
40% ABVB + decane + H2 mixture

Temp. (°C)	21	40	80	120	160	200	240	280	300	320	340	360	380
Pres. (bar)	70.72	76.37	82.80	87.57	92.80	100.23	104.46	107.34	110.03	115.32	119.55	126.14	130.05

1. ------ L1L2V
2. — ·— ·— L1L2
3. — ··— ··· L2V
4. ———— L1V

Temp. (°C)	21	40	80	120	160	200	240	280	300	320	340	360	380
Pres. (bar)	34.63	36.39	40.94	45.52	50.57	55.65	62.43	68.44	71.59	75.67	80.60	85.56	90.41

Figure A-2a X-ray images of decane + ABVB (40 wt %) + hydrogen (0.57 wt %) mixture

149
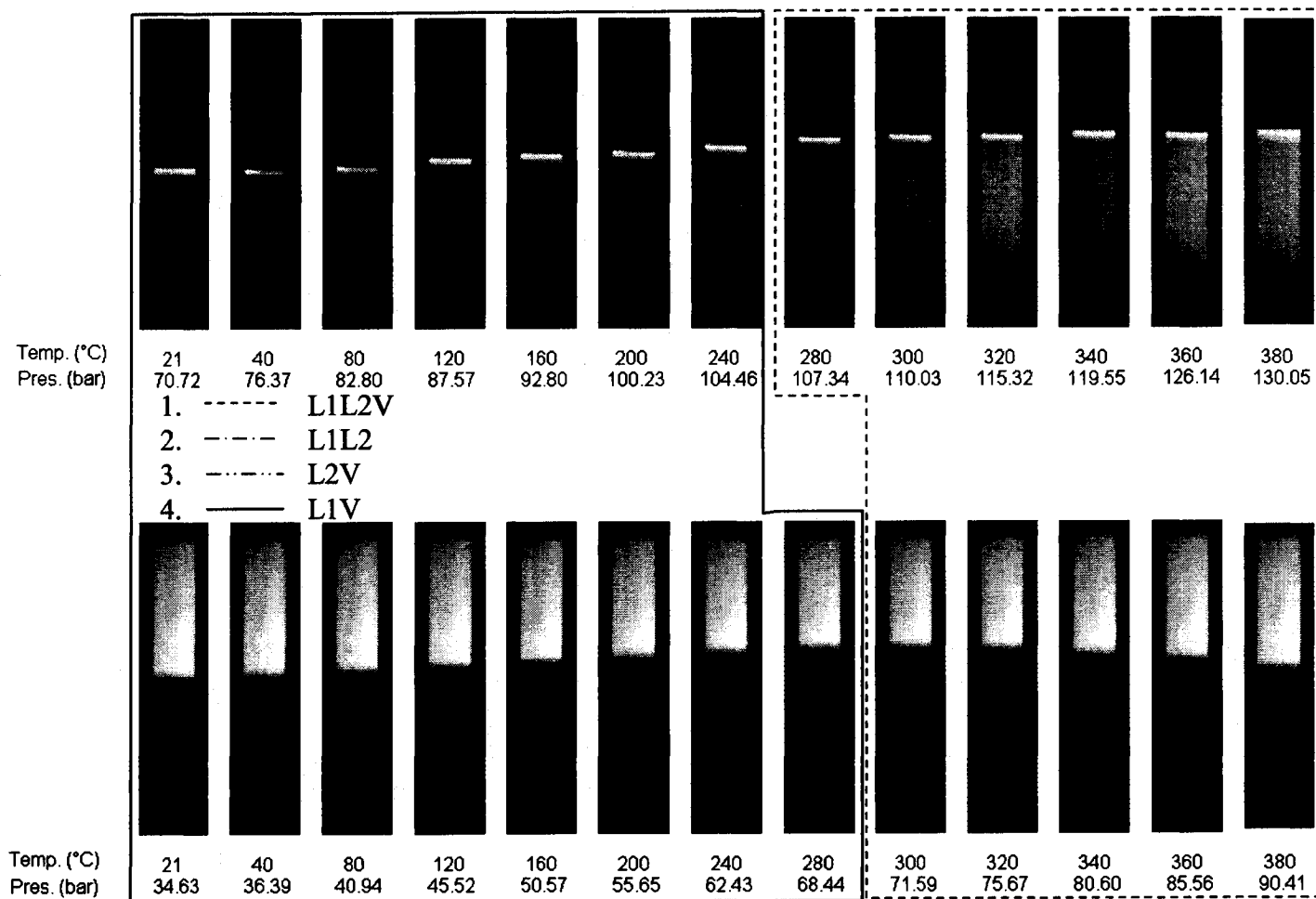
Appendix III. Phase Equilibrium Raw Data

Table A-1a. Phase equilibrium raw data of decane + ABVB (10 wt%) mixture

DATE	29-Aug-03						
System	ABVB	n-C10					
Composition, wt%	10.09	89.91					
Feed (g)	5.06	45.07					
Experimental Conditions		**Density for different phases(g/cm3)**			**Volume for different phases(cm3)**		
Temperature, °C	Pressure, bar	L2	L1	V	L2	L1	V
22.72	0.17		0.82	0.07		62.04	66.89
40.18	0.19		0.81	0.03		63.60	75.24
40.06	0.20		0.86	0.39		66.23	57.51
60.19	0.20		0.82	0.01		67.79	76.24
59.89	0.22		0.83	0.35		66.23	58.45
79.85	0.23		0.77	0.00		69.73	85.62
80.10	0.26		0.78	0.44		66.60	57.14
100.12	0.28	0.80	0.72	0.01	1.85	72.56	103.11
100.16	0.32	0.82	0.75	0.54	2.23	67.50	56.37
120.04	0.39	0.84	0.72	0.01	1.11	73.06	110.44
119.98	0.43	0.84	0.75	0.40	0.86	71.49	55.16
140.05	0.57	0.80	0.70	0.00	0.86	77.74	104.11
140.14	0.61	0.80	0.73	0.35	0.86	74.74	54.27
160.09	0.85	0.78	0.66	0.01	0.86	79.55	104.66
160.00	0.88	0.76	0.70	0.14	0.98	79.43	54.18
180.12	1.28	0.71	0.65	0.01	0.98	79.43	104.19
180.00	1.28	0.76	0.68	0.38	0.86	79.55	51.82
200.10	1.92	0.70	0.63	0.00	0.86	81.12	101.21
200.11	1.92	0.75	0.65	0.20	0.73	79.68	50.88
220.03	2.88	0.72	0.61	0.01	0.73	79.68	104.66
219.99	2.89	0.68	0.63	0.15	0.86	81.12	54.03
240.09	4.21	0.66	0.59	0.01	0.73	80.46	103.88
240.11	4.23	0.66	0.61	0.14	0.73	82.80	52.94
259.97	5.98	0.61	0.55	0.00	0.73	84.37	98.09
260.09	6.01	0.62	0.58	0.17	0.73	84.37	52.32
279.96	8.25	0.61	0.54	0.01	0.73	84.37	99.97
280.19	8.32	0.61	0.55	0.19	0.73	89.05	49.05
300.08	11.22	0.65	0.49	0.00	0.73	86.46	95.52
300.03	11.25	0.70	0.52	0.20	0.73	91.93	48.06
310.15	12.92	0.79	0.49	0.01	0.73	88.80	95.54
309.85	12.97	0.70	0.51	0.10	0.86	94.93	44.47
320.12	14.83	1.03	0.46	0.02	0.98	87.90	96.66
320.15	14.97	1.06	0.51	0.26	0.98	95.71	45.92
320.10	15.79	1.03	0.52		0.86	122.41	
320.14	16.47	1.01	0.50		0.86	112.03	
330.10	16.88	1.02	0.45	0.03	0.98	85.43	98.19
329.99	17.04	1.01	0.46	0.21	0.98	97.27	47.19
339.90	19.16	1.01	0.43	0.05	0.98	83.21	98.99
340.08	19.30	0.98	0.46	0.13	0.98	95.71	67.62
340.19	19.55	0.96	0.44	0.25	0.86	100.52	46.42
350.11	21.68	1.02	0.39	0.06	1.60	80.62	100.96
350.14	21.92	1.02	0.41	0.12	1.11	97.15	64.17
350.09	22.19	1.01	0.41	0.19	1.23	101.71	46.75
360.16	24.26	0.96	0.37	0.11	1.85	75.03	105.83
359.93	24.68	0.95	0.37	0.19	1.85	96.12	62.57
360.25	24.93	0.93	0.36	0.22	1.85	105.49	47.06

150

370.08	27.02	0.82	0.32	0.21	3.10	51.00	130.51
370.00	27.79	0.90		0.29	2.35		158.19
370.00	30.13	0.97		0.37	1.85		140.76
370.15	38.70	0.98		0.43	0.98		124.64
380.00	30.20	0.99	0.64	0.23	1.11	4.40	176.74
380.20	32.35	0.96	0.84	0.33	0.73	0.87	154.22
380.00	41.63	0.97		0.43	0.60		129.61

Table A-1b. Phase equilibrium raw data of decane + ABVB (20 wt%) mixture

DATE	5-Jun-03						
System	ABVB	nC10					
Composition, wt%	20.08	79.92					
Feed, g	14.08	56.05					
Experimental Conditions		**Density for different phases(g/cm3)**			**Volume for different phases(cm3)**		
Temperature, °C	Pressure, bar	L2	L1	V	L2	L1	V
23.49	0.18	0.86	0.82	0.03	1.23	89.71	57.80
39.95	0.21	0.85	0.79	0.01	1.36	91.27	71.22
40.00	0.24	0.85	0.80	0.07	1.23	91.27	52.47
60.08	0.32	0.88	0.76	0.01	1.48	92.71	89.94
60.05	0.37	0.88	0.79	0.10	1.85	90.65	51.52
79.95	0.40	0.89	0.76	0.01	1.73	95.46	87.41
80.00	0.50	0.91	0.79	0.24	1.60	94.02	46.98
100.09	0.48	0.90	0.75	0.01	1.60	97.15	85.85
99.95	0.58	0.93	0.77	0.13	1.60	95.58	46.84
120.02	0.60	0.89	0.73	0.01	1.60	99.49	83.51
120.03	0.70	0.91	0.77	0.25	1.60	98.71	44.19
139.99	0.77	0.91	0.72	0.01	1.36	103.40	79.85
140.06	0.85	0.94	0.75	0.04	1.36	101.83	46.97
159.94	1.03	0.89	0.70	0.01	1.36	106.52	77.20
160.10	1.08	0.89	0.72	0.10	1.36	104.96	45.26
179.98	1.41	0.88	0.68	0.01	1.23	108.21	73.28
180.07	1.44	0.87	0.71	0.03	1.36	108.08	46.86
200.00	1.99	0.86	0.66	0.01	1.23	109.77	74.55
200.13	2.01	0.86	0.70	0.08	1.23	108.21	45.91
219.97	2.91	0.81	0.66	0.01	0.98	111.45	71.69
220.06	2.92	0.80	0.68	0.06	0.86	111.58	42.44
240.04	4.25	0.73	0.64	0.01	0.98	111.45	72.64
240.04	4.27	0.88	0.66	0.14	0.86	113.27	41.23
259.97	6.04	0.76	0.62	0.01	0.98	114.58	69.04
260.08	6.08	0.77	0.63	0.13	0.98	116.14	40.58
280.14	8.43	0.95	0.57	0.03	1.48	117.46	62.84
280.02	8.44	0.97	0.59	0.06	1.48	119.02	39.10
300.14	11.36	1.00	0.54	0.03	2.23	121.40	58.62
300.09	11.43	0.98	0.56	0.18	2.47	124.27	35.68
320.23	15.12	0.97	0.49	0.01	3.47	124.84	53.46
320.10	15.27	0.97	0.51	0.08	3.97	127.47	34.77
340.15	19.54	0.94	0.44	0.02	5.22	127.78	50.19
340.09	19.88	0.94	0.45	0.25	5.72	131.96	30.88
380.02	32.55	0.79		0.36	12.71		172.84

151

Table A-1c. Phase equilibrium raw data of decane + ABVB (30 wt%) mixture

DATE	12-Jun-03						
System	ABVB	nC10					
Composition, wt%	30.05	69.95					
Feed, g	21.05	49.01					
Experimental Conditions		**Density for different phases(g/cm3)**			**Volume for different phases(cm3)**		
Temperature, °C	Pressure, bar	L2	L1	V	L2	L1	V
21.01	0.16	0.95	0.90	0.05	1.11	86.05	57.81
40.00	0.21	0.95	0.88	0.01	1.23	87.49	71.35
40.10	0.23	0.95	0.89	0.17	1.23	87.49	51.06
60.09	0.26	0.94	0.85	0.01	1.11	89.05	89.25
59.99	0.32	0.96	0.88	0.21	1.48	90.12	48.66
80.07	0.33	0.94	0.83	0.01	1.36	93.37	88.47
79.97	0.41	0.93	0.86	0.17	1.36	90.49	51.24
100.08	0.41	0.91	0.82	0.01	1.36	94.93	86.90
100.00	0.50	0.93	0.84	0.22	1.36	93.37	47.89
120.01	0.53	0.90	0.81	0.01	1.36	96.49	85.34
119.97	0.61	0.91	0.82	0.56	1.23	95.05	43.50
139.98	0.70	0.88	0.78	0.01	1.36	98.05	83.78
140.00	0.77	0.89	0.80	0.14	1.36	98.05	46.03
159.96	0.97	0.86	0.76	0.01	1.48	101.05	80.65
160.00	1.01	0.88	0.79	0.21	1.48	99.49	45.42
180.00	1.33	0.87	0.74	0.01	1.36	103.52	78.78
180.14	1.37	0.89	0.77	0.11	1.36	102.74	48.42
200.06	1.91	0.88	0.73	0.01	1.36	104.30	77.53
200.08	1.92	0.89	0.75	0.11	1.36	102.74	47.95
219.90	2.81	0.87	0.71	0.01	1.36	104.30	77.53
220.03	2.82	0.88	0.73	0.09	1.36	104.30	46.39
240.25	4.19	0.87	0.68	0.02	1.48	105.74	76.44
240.29	4.22	0.89	0.71	0.13	1.48	106.52	42.16
260.10	5.90	0.84	0.66	0.01	1.73	107.05	75.35
260.05	5.93	0.87	0.68	0.23	1.60	108.74	41.70
280.05	8.18	0.85	0.64	0.02	1.98	108.37	72.84
280.17	8.23	0.88	0.66	0.14	1.85	110.05	42.03
300.06	11.05	0.85	0.61	0.01	2.35	111.12	70.19
300.07	11.10	0.84	0.62	0.21	2.72	113.09	38.12
320.15	14.59	1.02	0.57	0.03	2.85	112.96	67.85
320.11	14.83	1.02	0.58	0.32	3.10	116.62	36.58
339.97	18.95	0.97	0.53	0.00	4.09	110.94	69.10
340.20	19.17	0.97	0.54	0.20	5.22	117.62	37.23
379.90	30.19	0.87	0.47	0.11	8.80	93.73	79.71

Table A-1d. Phase equilibrium raw data of decane + ABVB (35 wt%) mixture

DATE	31-Jul-03						
System	ABVB	nC10					
Composition, wt%	35.06	64.94					
Feed, g	24.51	45.4					
Experimental Conditions		**Density for different phases(g/cm3)**			**Volume for different phases(cm3)**		
Temperature, °C	Pressure, bar	L2	L1	V	L2	L1	V
40.14	0.21		0.87	0.04		87.16	67.72
40.19	0.23		0.88	0.29		88.47	48.95
59.85	0.24		0.86	0.03		88.72	75.12
59.92	0.28		0.87	0.54		86.91	49.10
80.10	0.28		0.84	0.01		90.28	88.66

152

Temperature, °C	Pressure, bar	L2	L1	V	L2	L1	V
80.02	0.34		0.86	0.56		90.03	47.86
100.02	0.36		0.82	0.02		93.16	90.97
100.17	0.43		0.84	0.25		93.16	48.04
120.15	0.48		0.80	0.02		94.72	89.41
119.95	0.55		0.83	0.48		93.16	46.62
140.02	0.66		0.79	0.02		97.85	86.76
140.10	0.72		0.80	0.35		97.06	45.55
159.98	0.94		0.80	0.01		99.41	85.67
160.02	0.99		0.82	0.13		99.41	47.92
180.08	1.36		0.75	0.01		100.97	83.63
179.89	1.39		0.78	0.20		100.97	45.89
200.00	1.94		0.76	0.01		102.53	82.07
199.89	1.96		0.79	0.15		102.53	46.21
220.16	2.86		0.74	0.01		102.53	82.54
220.13	2.92		0.76	0.18		102.53	46.68
240.00	4.17	0.78	0.71	0.01	0.85	104.09	80.98
240.22	4.23	0.78	0.73	0.18	0.85	104.09	45.59
260.08	5.70		0.67	0.02		104.09	81.45
260.06	5.73	0.78	0.71	0.10	1.11	104.55	43.09
269.96	6.70	0.78	0.69	0.01	1.11	104.55	77.53
270.08	6.75	0.80	0.71	0.11	1.11	106.89	44.52
279.90	7.84	0.82	0.68	0.01	1.36	105.86	77.38
280.05	7.92	0.79	0.71	0.06	1.48	107.30	42.79
290.16	9.18	0.80	0.65	0.01	1.36	106.64	77.07
289.86	9.25	0.81	0.69	0.26	1.36	107.43	42.32
300.10	10.63	0.79	0.66	0.01	1.48	107.30	76.29
300.06	10.72	0.80	0.67	0.15	1.48	108.86	43.12
309.80	12.21	0.82	0.65	0.01	1.48	108.08	75.51
310.02	12.28	0.81	0.67	0.04	1.60	108.74	55.86
310.25	12.43	0.86	0.69	0.20	1.23	108.86	44.31
320.00	13.94	0.79	0.63	0.01	1.98	106.80	76.29
320.19	14.12	0.89	0.63	0.04	2.47	109.43	54.30
320.13	14.17	0.90	0.65	0.27	2.60	109.31	41.56
330.17	16.19	0.89	0.61	0.01	2.35	106.43	75.82
329.86	16.28	0.84	0.62	0.05	1.85	111.37	53.45
330.39	16.61	0.86	0.62	0.12	1.85	111.37	41.19
340.17	18.34	0.81	0.58	0.01	1.73	106.80	76.07
340.24	18.58	0.94	0.60	0.05	1.73	111.49	52.98
339.97	18.77	1.02	0.58	0.22	1.98	114.49	39.35
379.71	28.79	1.02	0.58	0.06	1.73	94.55	86.43
379.77	30.59	0.90	0.51	0.26	5.72	112.43	39.08

Table A-1e. Phase equilibrium raw data of decane + ABVB (40 wt%) mixture

DATE	2-Jul-03						
System	ABVB	nC10					
Composition, wt%	39.97	60.03					
Feed, g	28.02	42.08					
Experimental Conditions		**Density for different phases(g/cm3)**			**Volume for different phases(cm3)**		
Temperature, °C	Pressure, bar	L2	L1	V	L2	L1	V
22.97	0.17		0.93	0.07		84.57	57.10
39.94	0.20		0.91	0.04		84.82	68.65
39.95	0.22		0.91	0.08		87.69	52.56
59.99	0.25		0.89	0.02		86.38	84.54
60.00	0.30		0.91	0.15		87.69	50.20
80.05	0.31		0.87	0.01		90.82	90.48
80.12	0.37		0.88	0.21		89.25	50.06

Temperature, °C	Pressure, bar	L2	L1	V	L2	L1	V
100.03	0.40		0.87	0.01		93.16	90.97
100.09	0.46		0.89	0.27		91.60	47.71
119.95	0.52		0.84	0.01		93.94	90.19
120.10	0.61		0.87	0.37		93.16	46.62
140.00	0.70		0.83	0.01		95.50	88.63
140.03	0.77		0.85	0.08		95.50	49.94
160.04	1.00		0.81	0.02		97.06	86.12
160.05	1.06		0.85	0.18		97.06	46.49
179.90	1.40		0.79	0.01		98.50	86.10
180.03	1.44		0.83	0.15		98.50	47.41
199.99	1.96		0.79	0.01		100.19	83.94
200.04	1.99		0.81	0.15		100.06	46.32
220.09	2.95		0.76	0.01		99.41	85.19
220.25	2.99		0.80	0.13		100.19	47.14
240.02	4.32		0.76	0.01		100.06	83.12
240.00	4.40		0.78	0.24		100.19	45.25
259.93	6.00		0.74	0.01		101.63	82.50
260.06	6.12		0.77	0.13		103.19	44.61
280.07	8.21	0.84	0.72	0.01	0.73	102.45	80.00
279.98	8.32	0.85	0.73	0.37	1.23	103.64	41.98
300.12	10.92	0.86	0.70	0.00	1.23	102.08	81.76
300.03	11.09	0.86	0.71	0.24	1.11	106.77	41.34
320.01	14.31	0.89	0.68	0.01	1.23	103.52	79.85
319.94	14.67	0.89	0.70	0.17	1.36	108.08	41.67
340.03	18.41	0.85	0.66	0.02	1.73	101.46	80.00
340.46	19.10	0.88	0.67	0.28	1.36	109.64	40.10
379.99	28.59	0.87	0.63	0.08	2.85	92.53	86.86

Table A-1f. Phase equilibrium raw data of decane + ABVB (50 wt%) mixture

DATE	28-May-03						
System	ABVB	nC10					
Composition, wt%	49.81	50.19					
Feed, g	35.07	35.34					
Experimental Conditions		Density for different phases(g/cm3)			Volume for different phases(cm3)		
Temperature, °C	Pressure, bar	L2	L1	V	L2	L1	V
26.10	0.16		0.98	0.10		85.35	53.96
40.12	0.20		0.97	0.03		86.25	66.27
40.08	0.21		0.97	0.11		86.25	51.17
60.00	0.27		0.93	0.01		87.82	89.71
60.05	0.30		0.96	0.09		87.82	51.49
80.10	0.35		0.91	0.01		89.38	94.75
80.09	0.42		0.94	0.25		89.50	48.39
100.06	0.44		0.92	0.01		90.16	93.97
100.01	0.51		0.94	0.12		90.16	50.09
119.94	0.59		0.90	0.01		92.50	91.63
120.00	0.66		0.92	0.08		91.72	50.42
140.00	0.77		0.88	0.01		93.28	91.32
139.99	0.82		0.90	0.09		93.28	50.74
160.10	0.97		0.87	0.01		95.63	88.98
160.02	1.01		0.89	0.13		94.85	49.65
180.09	1.25		0.85	0.01		96.41	87.72
180.04	1.26		0.88	0.05		96.41	51.39
200.15	1.83		0.84	0.01		96.41	88.19
200.10	1.81		0.85	0.03		96.41	46.68
220.02	2.64		0.82	0.01		96.28	88.32
220.10	2.69		0.84	0.19		96.28	47.27

154

		L2	L1	V	L2	L1	V
240.00	3.88		0.82	0.03		96.03	87.62
239.94	3.93		0.84	0.18		96.03	48.94
260.10	5.47		0.79	0.01		97.60	87.48
260.11	5.54		0.81	0.06		99.16	48.64
280.04	7.57		0.77	0.00		97.60	87.95
280.08	7.70		0.79	0.08		99.94	49.28
300.02	10.20		0.76	0.01		97.60	87.95
300.01	10.28		0.77	0.10		101.50	47.71
320.02	13.20	0.87	0.74	0.02	0.86	96.74	85.12
320.20	14.05	0.87	0.75	0.40	0.86	101.42	42.22
340.00	17.04	0.87	0.72	0.01	0.86	96.74	83.23
339.80	17.77	0.94	0.72	0.24	0.86	101.42	44.10
380.08	25.91	0.98	0.71	0.02	1.36	89.58	92.25
380.12	31.81	0.91	0.72	0.22	1.11	92.71	53.04

Table A-1g. Phase equilibrium raw data of decane + ABVB (70 wt%) mixture

DATE	13-Aug-03						
System	ABVB	nC10					
Composition, wt%	69.87	30.13					
Feed, g	49.01	21.13					
Experimental Conditions		**Density for different phases(g/cm3)**			**Volume for different phases(cm3)**		
Temperature, C°	Pressure, bar	L2	L1	V	L2	L1	V
24.72	0.17		1.10	0.03		74.79	72.54
39.94	0.21		1.08	0.02		76.47	82.18
39.96	0.26		1.10	0.14		76.35	56.36
60.00	0.30		1.09	0.01		80.66	103.47
60.02	0.39		1.12	0.22		80.54	52.64
80.05	0.38		1.07	0.01		82.22	101.91
80.00	0.54		1.10	0.34		80.54	52.64
99.99	0.51		1.06	0.00		82.88	99.36
100.06	0.68		1.08	0.79		80.54	50.75
120.02	0.64		1.03	0.01		83.79	100.82
120.05	0.76		1.05	0.50		79.47	53.23
140.09	0.81		1.00	0.00		82.72	99.99
140.05	0.92		1.04	0.29		85.35	50.66
160.08	1.12		1.00	0.00		86.13	96.11
160.07	1.28		1.02	0.03		86.91	48.62
180.09	1.48		0.99	0.01		86.91	97.69
180.07	1.58		1.01	0.27		86.91	50.51
200.13	1.92		0.98	· 0.01		88.47	96.60
200.15	2.03		1.00	0.48		86.91	46.27
219.99	2.66		0.96	0.01		88.47	96.60
220.08	2.81		0.99	0.19		88.47	49.42
240.15	3.63		0.95	0.01		87.82	97.26
239.97	3.79		0.97	0.18		89.25	49.58
260.14	4.86		0.94	0.00		87.82	95.37
260.05	5.10		0.96	0.12		88.60	49.77
280.12	6.41		0.94	0.01		88.60	96.48
280.00	6.79		0.96	0.33		88.60	49.30
300.08	8.38		0.93	0.01		87.82	96.79
300.02	8.92		0.94	0.12		89.38	51.82
320.01	10.61		0.93	0.01		87.03	97.57
319.99	11.61		0.92	0.21		89.38	50.87
339.97	13.39		0.91	0.01		87.03	98.51
340.08	14.98		0.91	0.14		90.94	50.73
380.01	21.01		0.89	0.01		87.57	97.03
380.21	26.21		0.85	0.22		91.85	51.24

Table A-1h. Phase equilibrium raw data of decane + ABVB (90 wt%) mixture

DATE	18-Aug-03						
System	ABVB	nC10					
Composition, wt%	89.95	10.05					
Feed, g	63.07	7.05					
Experimental Conditions		**Density for different phases(g/cm3)**			**Volume for different phases(cm3)**		
Temperature, °C	Pressure, bar	L2	L1	V	L2	L1	V
39.98	0.21		1.26	0.03		72.48	86.65
40.10	0.23		1.27	0.13		72.48	58.81
60.18	0.28		1.22	0.01		74.41	107.83
59.92	0.35		1.26	0.13		74.29	55.58
79.92	0.39		1.21	0.01		75.85	108.28
79.95	0.54		1.24	0.16		74.29	57.00
99.96	0.43		1.20	0.01		75.97	108.16
100.10	0.61		1.23	0.18		75.60	57.10
119.97	0.47		1.19	0.01		77.16	107.44
120.05	0.66		1.21	0.09		76.63	55.13
140.30	0.61		1.18	0.01		77.16	107.44
140.29	0.81		1.19	0.22		77.41	53.88
160.41	0.74		1.15	0.01		79.76	104.85
160.24	0.97		1.18	0.38		78.97	52.31
179.95	0.94		1.14	0.00		80.66	103.94
180.31	1.14		1.16	0.27		79.88	51.41
200.09	1.24		1.12	0.01		81.32	102.81
200.00	1.37		1.15	0.58		78.97	51.84
220.05	1.56		1.11	0.01		82.10	102.97
220.03	1.66		1.14	0.41		80.66	52.04
240.00	1.94		1.10	0.01		82.10	102.50
240.17	2.07		1.13	0.58		80.66	51.10
260.03	2.30		1.08	0.01		82.22	102.85
259.99	2.48		1.11	0.19		82.22	52.37
280.03	2.79		1.09	0.01		82.22	102.38
280.10	3.07		1.11	0.30		82.22	50.48
299.91	3.46		1.08	0.01		83.00	101.60
300.08	3.88		1.08	0.13		82.22	52.37
320.46	4.25		1.06	0.01		81.57	103.51
320.49	5.38		1.09	0.47		82.22	50.95
340.12	5.23		1.06	0.01		83.13	101.47
340.02	6.83		1.06	0.23		83.13	52.88
380.05	11.08		1.01	0.01		84.69	99.91
380.46	16.72		1.01	0.17		86.25	52.58

Table A-1i. Phase equilibrium raw data of decane + ABVB (100 wt%) mixture

DATE	22-Aug-03						
System	ABVB	nC10					
Composition, wt%	100	0					
Feed, g	70	0					
Experimental Conditions		**Density for different phases(g/cm3)**			**Volume for different phases(cm3)**		
Temperature, °C	Pressure, bar	L2	L1	V	L2	L1	V
40.02	0.19		1.28	0.02		66.07	86.45
39.96	0.21		1.30	0.19		66.07	60.03

60.04	0.27	1.24	0.00		67.88	108.70
60.10	0.32	1.29	0.35		67.63	58.00
80.16	0.44	1.29	0.01		72.07	110.65
79.89	0.55	1.33	0.35		70.38	56.19
100.09	0.45	1.28	0.01		72.35	110.36
100.02	0.61	1.30	0.16		71.82	59.47
120.01	0.49	1.22	0.01		71.00	112.18
120.06	0.66	1.26	0.15		69.44	59.96
140.12	0.52	1.26	0.01		73.13	110.05
140.14	0.70	1.28	0.12		73.38	56.02
160.10	0.58	1.24	0.01		74.94	108.24
160.35	0.77	1.26	0.16		73.63	57.19
180.07	0.63	1.23	0.01		76.76	106.90
180.18	0.84	1.22	0.11		72.32	57.56
200.08	0.64	1.17	0.01		74.13	109.53
200.57	0.87	1.24	0.39		76.76	52.65
220.12	0.62	1.20	0.01		78.32	105.34
219.99	0.86	1.23	0.22		77.54	52.81
240.13	1.10	1.15	0.00		75.69	106.08
240.15	1.28	1.21	0.21		78.32	52.97
260.06	1.12	1.17	0.02		79.88	104.25
260.20	1.37	1.20	0.38		78.32	52.50
280.05	1.15	1.15	0.01		81.44	103.16
280.19	1.46	1.18	0.34		79.88	51.41
300.04	1.21	1.13	0.01		81.44	103.16
300.02	1.68	1.17	0.54		79.22	52.06
320.00	1.41	1.12	0.01		83.13	100.53
320.10	2.12	1.15	0.52		80.79	51.45
340.11	1.92	1.10	0.01		83.91	100.69
340.08	3.05	1.12	0.11		82.35	54.60
380.08	6.63	1.05	0.01		86.25	98.35
380.35	11.15	1.08	0.26		85.47	51.95

Table A-2a. Phase equilibrium raw data of decane + ABVB (10 wt%) + hydrogen (0.57 wt%) mixture

DATE	31-Aug-04						
System	ABVB	nC10	H2				
Compostion, wt%	10.04	89.96	0.560				
Feed, g	6.02	53.94	0.336				
Experimental Conditions		**Density for different phases(g/cm3)**			**Volume for different phases(cm3)**		
Temperature, °C	Pressure, bar	L2	L1	V	L2	L1	V
340.56	92.51	1.02	0.38	0.15	2.39	137.39	42.50
340.42	99.25	1.01	0.38	0.43	2.39	143.64	27.29
360.68	100.32	0.95		0.32	2.58		180.12
360.60	117.03	0.99		0.38	1.87		164.82
359.98	140.23	1.00		0.43	1.57		151.16
380.10	110.48	0.98		0.32	1.79		180.64
380.10	131.63	0.97		0.39	1.42		163.43
380.30	145.61	0.94		0.42	1.27		155.66

Table A-2b. Phase equilibrium raw data of decane + ABVB (20 wt%) + hydrogen (0.57 wt%) mixture

DATE	15-Oct-04						
System	ABVB	nC10	H2				
Compostion, wt%	20.20	79.80	0.571				
Feed, g	12.02	47.49	0.34				
Experimental Conditions		Density for different phases(g/cm3)			Volume for different phases(cm3)		
Temperature, °C	Pressure, bar	L2	L1	V	L2	L1	V
39.91	39.23		0.79	0.00	0.73	74.67	107.31
40.00	81.03		0.83	0.46	0.61	70.77	55.19
79.93	43.70		0.73	0.01	0.61	78.58	101.64
80.06	87.84		0.78	0.50	0.73	73.77	55.37
120.10	48.87	0.86	0.71	0.01	2.97	79.34	100.40
120.10	91.46	0.88	0.73	0.45	3.72	77.03	52.90
159.99	53.25	0.82	0.67	0.01	1.48	85.52	93.83
160.05	95.92	0.86	0.70	0.57	1.36	82.39	51.78
200.15	59.38	0.89	0.64	0.01	1.23	90.33	91.15
200.10	97.84	0.90	0.67	0.40	0.98	88.77	50.50
240.01	64.88	0.82	0.61	0.02	0.73	96.83	86.10
240.10	99.02	0.79	0.63	0.36	0.86	98.27	45.85
279.98	73.53	1.05	0.56	0.02	1.48	102.58	78.66
280.20	103.85	1.08	0.57	0.36	1.85	102.45	44.44
299.96	77.71	1.04	0.51	0.02	2.10	105.21	74.93
299.94	103.52	1.05	0.52	0.30	2.60	107.83	42.09
320.10	82.69	1.01	0.47	0.02	3.59	105.28	73.37
320.07	106.92	1.01	0.49	0.36	3.72	111.40	39.76
340.18	87.77	1.00	0.38	0.15	2.23	138.95	42.01
340.19	105.79	1.01	0.39	0.43	2.35	143.64	28.23
359.81	93.81	0.95		0.33	2.35		180.84
360.14	114.92	0.99		0.38	1.85		163.40
359.82	138.69	1.00		0.44	1.36		152.11
380.62	97.17	0.98		0.32	1.60		181.58
381.09	127.14	1.02		0.39	1.23		164.50
380.90	164.26	0.94		0.42	0.98		156.73

Table A-2c. Phase equilibrium raw data of decane + ABVB (30 wt%) + hydrogen (0.57 wt%) mixture

DATE	20-Oct-04						
System	ABVB	nC10	H2				
Compostion, wt%	30.01	69.99	0.563				
Feed, g	18.01	42	0.338				
Experimental Conditions		Density for different phases(g/cm3)			Volume for different phases(cm3)		
Temperature, °C	Pressure, bar	L2	L1	V	L2	L1	V
19.94	35.12	0.97	0.85	0.01	2.10	71.62	109.47
20.01	72.97	0.98	0.88	0.35	2.35	69.81	55.83
39.73	37.44	0.97	0.83	0.01	2.10	73.96	107.12
39.93	75.41	0.96	0.86	0.36	2.10	70.96	56.34
80.02	42.00		0.88	0.01	1.60	77.58	102.11
79.94	82.81		0.85	0.55	0.86	75.21	54.75
120.15	45.97		0.78	0.01	0.86	80.80	101.53
120.09	84.52		0.80	0.51	0.86	79.89	52.43
160.02	50.29		0.75	0.01	0.86	84.58	97.75
160.15	89.98		0.78	0.57	0.73	81.58	51.33

158

200.10	54.84		0.70	0.01	1.23	87.33	94.15
200.17	90.58		0.73	0.60	1.23	85.77	50.89
240.03	58.74	0.76	0.67	0.00	1.36	91.89	87.58
239.74	93.07	0.72	0.69	0.56	1.23	90.45	48.09
280.19	64.70	0.78	0.63	0.01	0.73	95.27	87.19
280.06	96.74	0.73	0.64	0.64	0.86	95.27	46.49
300.03	67.86	0.76	0.59	0.01	0.86	96.83	85.97
299.94	96.44	0.89	0.61	0.41	0.98	99.83	45.10
320.09	71.30	0.97	0.56	0.02	2.35	96.90	84.41
319.93	99.78	0.96	0.55	0.43	3.34	100.59	43.39
339.98	76.28	0.94	0.51	0.02	5.21	95.73	83.20
339.98	102.83	0.94	0.52	0.55	5.21	100.41	43.60
360.24	81.50	0.91	0.50	0.06	5.46	87.79	90.41
359.98	107.79	0.89	0.48	0.45	8.11	99.20	42.85
380.09	86.74	0.88	0.51	0.13	6.42	72.64	104.59
380.10	103.68	0.80	0.44	0.31	16.33	80.45	65.82
379.80	136.59	1.03	0.52		2.60	135.29	

Table A-2d. Phase equilibrium raw data of decane + ABVB (40 wt%) + hydrogen (0.57 wt%) mixture

DATE	26-Oct-04						
System	ABVB	nC10	H2				
Compostion, wt%	40.12	59.88	0.560				
Feed, g	23.99	35.81	0.335				
Experimental Conditions		**Density for different phases(g/cm3)**			**Volume for different phases(cm3)**		
Temperature, °C	Pressure, bar	L2	L1	V	L2	L1	V
21.33	34.63		0.91	0.01		70.47	110.83
21.38	70.72		0.93	0.16		69.69	56.88
40.02	36.39		0.90	0.01		70.47	108.94
40.08	76.37		0.93	0.40		68.91	56.72
80.13	40.94		0.88	0.01		73.60	107.23
80.07	82.80		0.90	0.44		72.03	54.54
120.04	45.52		0.85	0.01		76.72	103.16
120.10	87.57		0.87	0.30		76.72	53.62
160.06	50.57		0.81	0.01		79.84	100.51
160.02	92.80		0.83	0.36		79.84	51.92
200.17	55.65		0.78	0.02		82.97	99.27
199.97	100.23		0.80	0.53		81.41	51.30
240.10	62.43		0.75	0.02		86.09	95.21
239.90	104.46		0.76	0.52		86.09	48.97
280.05	68.44	0.78	0.68	0.01	2.82	86.49	91.61
279.96	107.34	0.81	0.71	0.46	2.38	88.55	48.06
300.27	71.59	0.83	0.68	0.02	2.15	87.24	93.02
299.88	110.03	0.84	0.69	0.47	1.85	90.49	47.44
320.10	75.67	0.82	0.65	0.02	1.93	87.37	93.50
320.00	115.32	0.82	0.67	0.52	1.74	92.30	45.88
339.88	80.60	0.83	0.65	0.02	1.81	84.37	96.62
340.00	119.55	0.84	0.64	0.45	1.74	93.86	45.73
360.09	85.56	0.79	0.63	0.05	1.59	81.49	99.75
360.04	126.14	0.88	0.62	0.49	1.80	92.05	46.47
380.10	90.41	0.81	0.64	0.10	1.47	75.24	106.12
380.07	130.05	0.96	0.58	0.45	3.02	90.81	47.54

159

Appendix IV. Sketch of the Variable Position Catalyst Holder
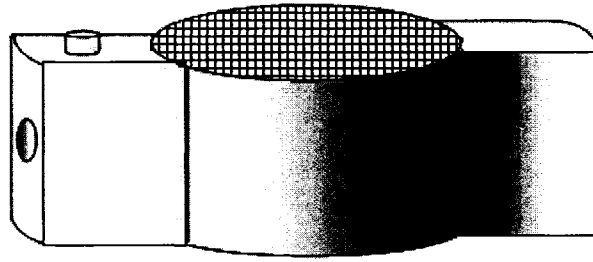

Figure A-1. Sketch of the variable position catalyst holder.

The catalyst holder is a basket with top and bottom covered with screen and supported with two wings, one of which is designed to be able to be tightened with screw and fixed at the expected position. The basket is a cylinder with a diameter of 2 cm and a height of 1 cm.

160

Appendix V. Summary of Catalyst Coking Experiments and their Repeatability

Table A-3. Raw data of catalyst coking experiments

	Run2	Run2	Run3		Run6	Run6	RH-12	RH-9	RH-15
Operation Conditions									
Composition (wt% ABVB)	30	30	30		30	30	5	10	10
Phase	L1	L2	L1+L2		L1	L2	V+L2	V+L2	V+L2
Pressure, bar	31	31	29		30	30	98	96	158
Temperature, C	380	380	380		380	380	380	380	380
Time, hrs	5	5	5		2	2	2	2	2
H2/oil	0.0000	0.0000	0.0000		0.0000	0.0000	0.0057	0.0057	0.0057
Elmental analysis									
carbon, wt%	27.64	26.126	26.435		23.318	20.741	13.013	14.598	13.075
Hydrogen, wt%	2.1516	2.0368	2.1094		1.9403	1.8161	1.5462	1.6304	1.3577
H/C (mole ratio)	0.93	0.94	0.96		1.00	1.05	1.43	1.34	1.25
sulfur, wt%	5.11	5.25	4.72		2.9	3.645	5.52	5.52	5.3
S/C	0.069	0.075	0.067		0.047	0.066	0.159	0.142	0.152
nitrogen, wt%	0.5979	0.5991	0.5765		0.4843	0.4563	0.4383	0.5037	0.4239
N/C	0.019	0.020	0.019		0.018	0.019	0.029	0.030	0.028
BET analysis			powder	pellet					
As (surface area), m2/g	112.6	113.2	126.5	125.9	157.2	165.1	203.37	181.14	156.74
Vp (pore volume), cm3/g	0.141	0.167	0.17	0.166	0.242	0.292	0.4652	0.4024	0.3622
As, m2/g cat.	160.4	157.6	177.0	176.2	210.3	213.2	238.0	216.2	183.2
Vp, cm3/g cat.	0.201	0.232	0.238	0.232	0.324	0.377	0.544	0.480	0.423
As loss, %	26.8	28.1	19.2	19.6	4.0	2.7	-8.6	1.3	16.4
Vp loss, %	65.7	60.3	59.3	60.3	44.7	35.5	6.9	17.9	27.6

Table A-3. Raw data of catalyst coking experiments (continued)

	RH-13	RH-14	RH-21	RH-21	RH-3	RH-1	RH-4	RH-2[1]	RH-2[1]
Operation Conditions									
Composition (wt% ABVB)	20	20	20	20	30	30	30	30	30
Phase	V+L2	V+L2	V	L2	L1+L2	L1+L2	L1+L2	L1	L2
Pressure, bar	109	157	112	112	89	111	138	104	104
Temperature, C	380	380	380	380	380	380	380	380	380
Time, hrs	2	2	2	2	2	2	2	2	2
H2/oil	0.0057	0.0057	0.0057	0.0057	0.0057	0.0057	0.0057	0.0057	0.0057
Elmental analysis									
carbon, wt%	14.445	13.219	13.241	15.691	14.261	14.236	13.76	14.64	16.35
hydrogen, wt%	1.5768	1.3894	2.146	2.2148	1.5423	1.4763	1.5033	1.5272	1.6678
H/C (mole ratio)	1.31	1.26	1.94	1.69	1.30	1.24	1.31	1.25	1.22
sulfur, wt%	5.93	5.97			3.94	3.26	3.95	4.68	4.83
S/C	0.154	0.169			0.104	0.086	0.108	0.120	0.111
nitrogen, wt%	0.5093	0.4847	0.7013	0.6816	0.4827	0.525	0.5142	0.5135	0.4771
N/C	0.030	0.031	0.045	0.037	0.029	0.032	0.032	0.030	0.025
BET analysis									
As (surface area), m2/g	173.15	174.19	152.09		165.89	171.91	161.09	155.49	151.33
Vp (pore volume), cm3/g	0.3599	0.3845	0.3393		0.3419	0.3613	0.354	0.3414	0.3113
As, m2/g cat.	206.2	204.0	152.1		197.0	204.0	190.1	185.5	184.6
Vp, cm3/g cat.	0.429	0.450	0.339		0.406	0.429	0.418	0.407	0.380
As loss, %	5.9	6.9	30.6		10.1	6.9	13.2	15.3	15.8
Vp loss, %	26.7	23.0	42.0		30.6	26.7	28.6	30.4	35.1

Table A-3. Raw data of catalyst coking experiments (continued)

	RH-18[1]	RH-18[1]	RH-6[1]	RH-6[1]	RH-20	RH-20	RH-10	RH-16	RH-16
Operation Conditions									
Composition(wt% ABVB)	30	30	30	30	30	30	40	40	40
Phase	L1	L2	L1	L2	L1	L2	L1+L2	L1	L2
Pressure, bar	111	111	117	117	144.5	144.5	120	124	124
Temperature, C	380	380	380	380	380	380	380	380	380
Time, hrs	2	2	2	2	2	2	2	2	2
H2/oil	0.0057	0.0057	0.0057	0.0057	0.0086	0.0086	0.0057	0.0057	0.0057
Elmental analysis									
carbon, wt%	14.425	16.316	14.35	16.405	13.915	15.571	13.865	14.271	14.561
hydrogen, wt%	1.658	1.7908	1.6454	1.7906	1.6763	1.6215	1.4717	1.4555	1.3884
H/C (mole ratio)	1.38	1.32	1.38	1.31	1.45	1.25	1.27	1.22	1.14
sulfur, wt%	5.88	5.1	6.16	5.72	5.9	5.88	5.95	5.41	5.94
S/C	0.153	0.117	0.161	0.131	0.159	0.142	0.161	0.142	0.153
nitrogen, wt%	0.4362	0.4065	0.4586	0.4473	0.4979	0.4688	0.4581	0.4645	0.4061
N/C	0.026	0.021	0.027	0.023	0.031	0.026	0.028	0.028	0.024
BET analysis									
As (surface area), m2/g	166.33	158.33	164.46	159.76	151.4	163.27	154.98	172.24	163.51
Vp (pore volume), cm3/g	0.3426	0.3165	0.3598	0.3277	0.3464	0.34	0.3487	0.3684	0.47
As, m2/g cat.	166.3	158.3	195.8	195.3	151.4	163.27	183.1	204.4	163.5
Vp, cm3/g cat.	0.343	0.317	0.428	0.401	0.3464	0.34	0.412	0.437	0.469
As loss, %	24.1	27.7	10.6	10.9	30.899	25.482	16.5	6.7	25.4
Vp loss, %	41.4	45.9	26.8	31.5	40.786	41.88	29.6	25.3	19.9

Table A-3. Raw data of catalyst coking experiments (concluded)

	RH-8	RH-11	RH-7	RH-19[2]	RH-19[2]	RH-5
Operation Conditions						
Composition(wt% ABVB)	50	60	70	80	80	100
Phase	L1	L1	L1	L1(high)	L1(low)	L1
Pressure, MPa	124	115	126	124	124	115
Temperature, C	380	380	380	380	380	380
Time, hrs	2	2	2	2	2	2
H2/oil	0.0057	0.0057	0.0057	0.0057	0.0057	0.0057
Elmental analysis						
carbon, wt%	13.293	13.66	13.489	13.574	13.537	13.663
hydrogen, wt%	1.5575	1.3661	1.5089	1.4992	1.5486	1.6431
H/C (mole ratio)	1.41	1.20	1.34	1.33	1.37	1.44
sulfur, wt%	6.13	5.92	6.19	6.26	6.14	5.85
S/C	0.173	0.163	0.172	0.173	0.170	0.161
nitrogen, wt%	0.4959	0.5136	0.4784	0.4609	0.4756	0.4095
N/C	0.032	0.032	0.030	0.029	0.030	0.026
BET analysis						
As (surface area), m2/g	173.77	171.82	176.13	171.82	179.11	173.96
Vp (pore volume), cm3/g	0.3789	0.4088	0.374	0.3702	0.3882	0.3741
As, m2/g cat.	204.1	202.2	207.2	171.82	179.11	205.4
Vp, cm3/g cat.	0.445	0.481	0.440	0.3702	0.3882	0.442
As loss, %	6.9	7.7	5.4	21.579	18.252	6.3
Vp loss, %	23.9	17.8	24.8	36.718	33.641	24.5

1. Three repeated catalyst coking experiments in L1 and L2 phases.

2. A control experiment demonstrating that holding catalysts at different elevations will not affect the catalyst coking results (within the experimental errors).

162

Table A-4. Repeatability of coking experiment results (three repeated experiments: RH-2, RH-18, RH-6; conditions: 30 wt % ABVB, H_2, in L1 and L2 phases)

L1						
	C	H	S	N	As	Vp
Mean	14.4717	1.6102	5.5733	0.4694	162.0933	0.3479
Standard Error	0.0869	0.0417	0.4539	0.0230	3.3455	0.0059
Standard Deviation	0.1505	0.0722	0.7862	0.0398	5.7946	0.0103
Sample Variance	0.0227	0.0052	0.6181	0.0016	33.5772	0.0001
Range	0.2900	0.1308	1.4800	0.0773	10.8400	0.0184
Confidence Level (95.0%)	0.3739	0.1792	1.9531	0.0988	14.3946	0.0256

L2						
	C	H	S	N	As	Vp
Mean	16.3570	1.7497	5.2167	0.4436	156.4733	0.3185
Standard Error	0.0259	0.0410	0.2635	0.0205	2.6046	0.0048
Standard Deviation	0.0449	0.0710	0.4563	0.0354	4.5113	0.0084
Sample Variance	0.0020	0.0050	0.2082	0.0013	20.3516	0.0001
Range	0.0890	0.1230	0.8900	0.0706	8.4300	0.0164
Confidence Level (95.0%)	0.1116	0.1763	1.1336	0.0880	11.2066	· 0.0208

1. The standard error of carbon elemental analysis is within 1 %. In this aspect, the repeated experiments show a reliable repeatability.

2. The standard error of catalyst surface area and pore volume is within 3%.

Table A-5. The impact of catalyst forms (oxide or sulfide) and hydrogen (with or without hydrogen) on coke deposition. (All data from batch reactor)

Catalyst form:	Oxide	Sulfide	Sulfide
H_2:	No	No	Yes
C, wt%	15.9	16.0	13.3
H, wt%	1.82	1.77	1.31
N, wt%	0.36	0.38	0.36
S, wt%	4.3	6.1	--

1. Experimental conditions: 60 wt% ABVB + decane, coked catalyst extracted by Soxhlet extraction approach.

2. The coking results between catalyst oxide and sulfide forms show no difference. But addition of hydrogen significantly reduce coke deposition.

Table A-6. The impact of extraction approaches (Soxhlet or toluene) on coke deposition. (All data from batch reactor)

Extraction	Soxhlet extraction	Toluene extraction
C, wt%	16.0	16.4
H, wt%	1.77	1.75
N, wt%	0.38	0.39
S, wt%	6.1	6.2

1. Experimental conditions: 60 wt% ABVB + decane, catalyst in sulfide form, no hydrogen.

2. Soxhlet extraction exhibits better extraction ability than toluene extraction. But the difference does not affect the interpretation of experimental results in this thesis.
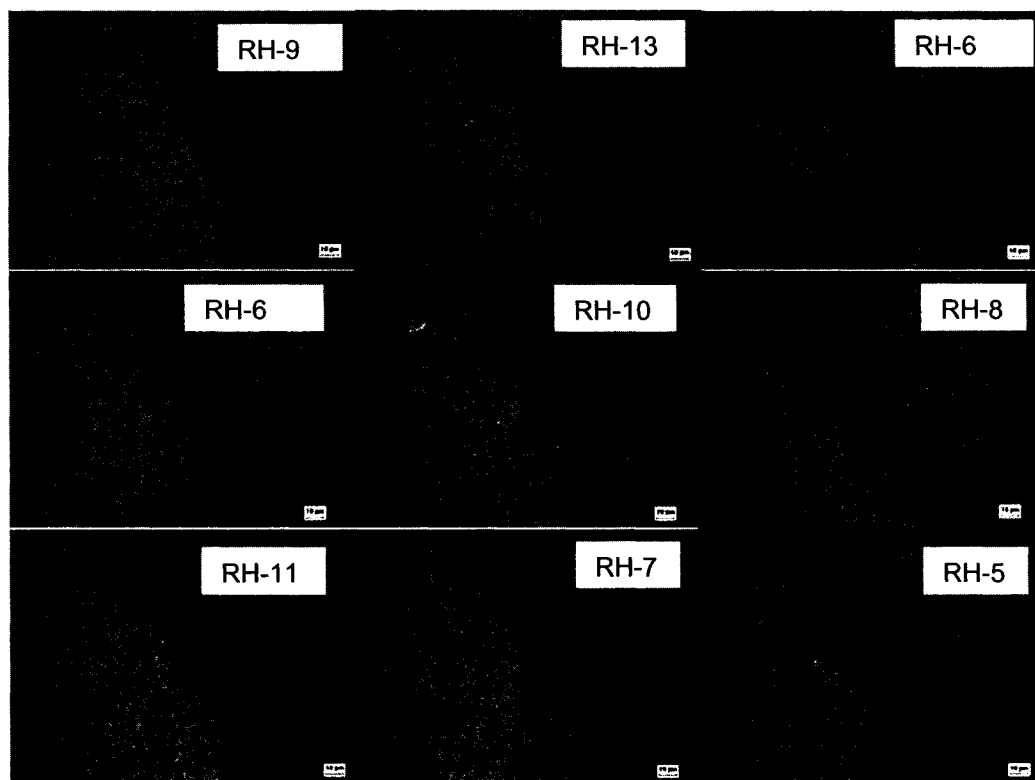

Figure A-2. Light microscopy of coked catalysts in the presence of hydrogen

164